Targeted Delivery of Biological Agents

Jenny Agnes Greig
B.Sc. (Hons)

Submitted in the fulfilment of the requirements of the degree of Doctor of Philosophy in the Faculty of Medicine, University of Glasgow

Division of Cardiovascular and Medical Sciences
Faculty of Medicine
University of Glasgow

September 2009

Author's Declaration

I declare that this thesis has been written entirely by myself and is a record of work performed by myself with the exception of Home Office licensed procedures (Dr. L.M. Work, Dr. L. Denby, Dr. D. Graham, Mrs N. Britton, Dr. S.N. Waddington and Dr. S.M.K. Buckley), echocardiography (Dr. K. Gilday), surface plasmon resonance (Dr. J.H. McVey) and electron cryomicroscopy (Dr. D. Bhella and Ms. R. Pink). This thesis has not been submitted previously for a higher degree. The research was carried out in the Division of Cardiovascular and Medical Sciences, University of Glasgow, under the supervision of Prof. A.H. Baker and Dr. L.M. Work.

Jenny A. Greig

September 2009

Acknowledgements

First and foremost I would like to thank my supervisors Prof. Andrew H. Baker and Dr. Lorraine M. Work for all their help, support, advice and guidance throughout my studies; it has been invaluable. I would also like to thank the British Heart Foundation for the support and funding of this work.

I would like to thank all the fantastic friends I have made during my time at the BHF GCRC. I would especially like to thank Dr. Alan Parker and Dr. Stuart Nicklin for teaching me the basics of gene therapy and everything after that. I would like to thank Dr. Laura Denby for answering endless questions, always providing lots of helpful information (sometimes it was even about science) and some much needed hilarity. Also I would like to thank Dr. Rachel Shirley for teaching me the joys of phage, caesium preps and for all the conversations. Thanks to Nicola Britton and Gregor Aitchison for teaching me tissue culture with infinite patience and to everyone else in the Baker group.

Most importantly, I want to thank Mónica Flores-Muñoz, Stacy Wood, Wendy Crawford and Dr. Nicole Kane. Thank you to Mónica and Stacy for listening, providing fantastic advice on everything and putting up with me every day in our lovely third floor office. Also thank you to Wendy for "dragging" me to the pub and for one infamous phrase. A huge thank you to Nicole, things have never been the same since you started but in the most amazing way! I couldn't have gotten through my PhD without the four of you.

Thank you to my friends outside the BHF GCRC and outside of science for reminding me that there was a whole wide world out there!

Last but not least; I would like to thank my family for listening, for the constant mocking and for the "inspirational" talks/texts. It meant the world to me.

Table of Contents

List of Figures

List of Tables

List of Publications

J.A. Greig, S.M.K. Buckley, S.N. Waddington, A.L. Parker, D. Bhella, R. Pink, A.A. Rahim, T. Morita, S.A. Nicklin, J.H. McVey and A.H. Baker (2009) Influence of Coagulation Factor X on *In Vitro* and *In Vivo* Gene Delivery by Adenovirus (Ad) 5, Ad35, and Chimeric Ad5/Ad35 Vectors. *Molecular Therapy*, **17**, 1683-91 [Appendix 1]

S.N. Waddington, J.H. McVey, D. Bhella, A.L. Parker, K. Barker, H. Atoda, R. Pink, S.M.K. Buckley, **J.A. Greig**, L. Denby, J. Custers, T. Morita, I.M.B. Francischetti, R.Q. Monteiro, D.H. Barouch, N. van Rooijen, C. Napoli, M.J.E. Havenga, S.A. Nicklin and A.H. Baker (2008) Adenovirus Serotype 5 Hexon Mediates Liver Gene Transfer. *Cell*, **132**, 397-409 [Appendix 2]

Abstracts:

J.A. Greig, R. Shirley, D. Graham, K. Gilday, E. Ruoslahti, L. Denby, A.F. Dominiczak, L.M. Work and A.H. Baker (2009) Targeted Anti-Oxidant Therapy in a Model of Hypertension and Stroke. *Journal of Human Hypertension*, **23**, S1

J.A. Greig, S.M.K. Buckley, S.N. Waddington, A.L. Parker, D. Bhella, R. Pink, T. Morita, J. Custers, J. Goudsmit, S.A. Nicklin, J.H. McVey and A.H. Baker (2009) Influence of Factor X on *In Vitro* and *In Vivo* Gene Delivery by Ad5 and Ad35 Vectors. *Molecular Therapy*, **17**(S1), S325

J.A. Greig, J.H. McVey, S.N. Waddington, A.L. Parker, S.M.K. Buckley, M.J.E. Havenga, S.A. Nicklin and A.H. Baker (2008) Factor X Enhances Binding and Transduction of Human Cancer Cell Lines by Adenovirus (Ad) Serotype 5 Vectors but Not by Ad35. *Human Gene Therapy*, **19**(4), 398

List of Abbreviations/Definitions

ABC	Avidin and biotinylated horseradish peroxidase complex
ACE	Angiotensin converting enzyme
Ad	Adenovirus
Ad*F	CAR binding ablated Ad5 vector
Ad35/f5	Pseudotype vector with hexon and penton of Ad35 and fiber of Ad5
Ad5/f11	Pseudotype vector with hexon and penton of Ad5 and fiber of Ad11
Ad5/f16	Pseudotype vector with hexon and penton of Ad5 and fiber of Ad16
Ad5/f17	Pseudotype vector with hexon and penton of Ad5 and fiber of Ad17
Ad5/f19p	Pseudotype vector with hexon and penton of Ad5 and fiber of Ad19p
Ad5/f19p-HIT	Ad5/f19p vector with HITSLLS peptide sequence inserted into the HI loop
Ad5/f19p-HTT	Ad5/f19p vector with HTTHREP peptide sequence inserted into the HI loop
Ad5/f24	Pseudotype vector with hexon and penton of Ad5 and fiber of Ad24
Ad5/f30	Pseudotype vector with hexon and penton of Ad5 and fiber of Ad30
Ad5/f33	Pseudotype vector with hexon and penton of Ad5 and fiber of Ad33
Ad5/f35	Pseudotype vector with hexon and penton of Ad5 and fiber of Ad35

Ad5/f45	Pseudotype vector with hexon and penton of Ad5 and fiber of Ad45
Ad5/f47	Pseudotype vector with hexon and penton of Ad5 and fiber of Ad47
Ad5/p35/f35	Pseudotype vector with hexon of Ad5 and the penton and fiber of Ad35
Ad5HVR5(Ad26)	Ad5 vector with HVR5 swapped for HVR5 of Ad26
Ad5HVR5+7(Ad26)	Ad5 vector with HVR5 and HVR7 swapped for HVR5 and HVR7 of Ad26
Ad5HVR7(Ad26)	Ad5 vector with HVR7 swapped for HVR5 of Ad26
Ad5HVR48	Ad5 vector with the HVRs swapped for those from Ad48
Ad5ΔRGD	α_v-integrin binding ablated Ad5 vector
ADA	Adenosine deaminase-deficient
AdEYH	AdKO1 vector with EYHHYNK peptide sequence inserted into the HI loop
AdHAd19	Ad5 vector with HVR5 swapped for HVR5 of Ad19
AdHAd2	Ad5 vector with HVR5 swapped for HVR5 of Ad2
AdHAd30	Ad5 vector with HVR5 swapped for HVR5 of Ad30
AdHRGD	Ad5 vector with RGD integrin binding motif inserted into HVR5
AdKO1	CAR binding ablated Ad5 vector
AdKO1PD1	CAR and α_v-integrin binding ablated Ad5 vector
AdKO1SIG	AdKO1 vector with SIGYPLP peptide sequence inserted into the HI loop
AdPD1	α_v-integrin binding ablated Ad5 vector
AdS*	Putative HSPG binding site ablated vector

ALT	Alanine aminotransferase
ANOVA	Analysis of variance
APES	3-amino-propyltriethoxysaline
APS	Ammonium persulphate
AST	Aspartate aminotransferase
AWT	Ventricular anterior wall thickness
BC-10	Human bladder cancer-associated protein
BCA	Bicinchoninic acid
BH_4	Tetrahydrobiopterin
BP	Blood pressure
BSA	Bovine serum albumin
C4BP	Complement binding protein
CAR	Coxsackie virus and adenovirus receptor
CHO	Chinese hamster ovary cells
CHO-BC1	Chinese hamster ovary cells stably expressing the BC1 isoform of human CD46
CHO-WTR	Chinese hamster ovary cells stably transfected with an empty plasmid, control for CHO-BC1
CO	Cardiac output
CPH	1-hydroxy-3-carboxy- 2,2,5,5-tetramethylpyrrolidine
CR1	Complement receptor
CRIP-2	Cysteine-rich protein 2
Cryo-EM	Electron cryomicroscopy

CuZnSOD	Copper/zinc SOD
DBP	Diastolic blood pressure
DMEM	Dulbecco's Modified Eagle Medium
DMSO	Dimethyl sulphoxide
EC	Endothelial cell
EC_{50}	Half maximal effective concentration
ECHO	Echocardiography
ECL	Enhanced luminol-based chemiluminescent
EDD	End diastolic dimension
EDRF	Endothelium-derived relaxing factor
EDTA	Ethylenediamine tetra-acetic acid
EGF	Epidermal growth factor-like domain of a blood coagulation factor
eGFP	Enhanced green fluorescent protein
eNOS	Endothelial NO synthase
EPR	Electron paramagnetic resonance
EST	Un-annotated RIKEN expressed sequence tag
EYHHYNK	VSMC targeting peptide sequence
FITC	Fluorescein
FIX	Blood coagulation factor IX
FS	Fractional shortening
FVII	Blood coagulation factor VII
FX	Blood coagulation factor X

FXI	Blood coagulation factor XI
FXII	Blood coagulation factor XII
Gla	γ-carboxylated glutamic acid domain of a blood coagulation factor
GPx	Glutathione peroxidase
H&E	Haemotoxylin and eosin
H_2O_2	Hydrogen peroxide
HAEC	Human aortic endothelial cell
HepG2	Hepatic carcinoma cell line
HIT	Kidney targeting peptide sequence HITSLLS
HIV-tat	Human immunodeficiency virus-1 transactivation tat protein
$HO^{\cdot}$	Hydroxyl radical
HR	Heart rate
HRP	Horseradish peroxidase
HSPG	Heparan sulphate proteoglycan
HSVEC	Human saphenous vein endothelial cell
HSVSMC	Human saphenous vein smooth muscle cell
HTT	Kidney targeting peptide sequence HTTHREP
HUVEC	Human umbilical vein endothelial cell
HVR	Hypervariable region
HVR3	Hypervariable region 3
HVR5	Hypervariable region 5
HVR7	Hypervariable region 7

IC_{50}	Half maximal inhibitory concentration
IgG	Immunoglobulin G
IHC	Immunohistochemistry
IL-1α	Interleukin-1α
ISWT	Interventricular septal wall thickness
IU	International unit
ka	Association rate
kd	Dissociation rate
K_D	Equilibrium dissociation constants
KKTK	Amino acid sequence of putative HSPG binding site in Ad5 fiber
LB	Luria broth
LDL	Low density lipoprotein
L-NAME	N-nitro-L-arginine methyl ester
LRP	LDL receptor-related protein
LV	Left ventricle
LVEDV	Left ventricular end diastolic volume
LVEF	Left ventricular ejection fraction
LVESV	Left ventricular end systolic volume
LVH	Left ventricular hypertrophy
LVMI	Left ventricular mass index
MAP	Mean arterial pressure
MAPK	Mitogen-activated protein kinase

MDA-MB-435	Human breast ductal carcinoma cell line
MI	Myocardial infarction
MnSOD	Manganese SOD
MOI	Multiplicity of infection
MPCII-3	Mitochondrial membrane protein integral membrane protein CII-3
NADH/NAD(P)H	Nicotinamide adenine dinucleotide (phosphate) oxidase
ng	Nanograms
NICE	National Institute for Health and Clinical Excellence
NK	Natural killer cells
NO	Nitric oxide
NOS	Nitric oxide synthase
NRP-1	Neuropilin-1 receptor
OD_{600}	Optical density of 600 nm
$ONOO^-$	Peroxynitrite
OTC	Ornithine transcarbamylase
PBS	Phosphate buffered saline
PC	Protein C
PE	Phenylephrine
PEG	Polyethylene glycol
pfu	Plaque forming unit
PMA	Phorbol myristate acetate
PMSF	Phenylmethanesulfonyl fluoride

PP	Pulse pressure
PRR	Pattern-recognition receptor
PTP-BL	Sub-membranous protein tyrosine phosphatase
qPCR	Quantitative polymerase chain reaction
QTL	Quantitative trait loci
RBC	Red blood cell
RGD	α_v-integrin binding site in the penton base
RGE	Rat glomerular endothelial cell line
RLU	Relative light units
ROS	Reactive oxygen species
RRR-AT	Natural α-tocopherol
RU	Response units
SBP	Systolic blood pressure
SCID	Severe combined immunodeficiency
SCID-X1	X-linked severe combined immunodeficiency
SCR	Short consenus repeats
SDS-PAGE	Sodium dodecyl sulphate polyacrylamide gel electrophoresis
SEM	Stardard error of the mean
SHR	Spontaneously hypertensive rat
SHRSP	Stroke-prone spontaneously hypertensive rat
SIGYPLP	Endothelial cell targeting peptide sequence
SKOV-3	Human ovary adenocarcinoma cell line

SMC	Smooth muscle cell
SO	Superoxide
SOD	Superoxide dismutase
SP	Serine protease
SPR	Surface plasmon resonance
SV	Stroke volume
T-47D	Human breast ductal carcinoma cell line
TEMED	N,N,N′,N′-tetramethylethylenediamine
TKPPR	Enhanced-tuftsin
TKPR	Tuftsin
TNF-α	Tumour necrosis factor-α
VEGF	Vascular endothelial derived growth factor
VG	Vector genomes
VP	Viral particles
VSMC	Vascular smooth muscle cell
WHO	World Health Organisation
WKY	Wistar Kyoto rat
X-bp	FX binding protein isolated from *Deinagkistrodon acutus* (the hundred pace snake)
γc	Common cytokine receptor γ chain gene

Summary

Development of selectively targeted therapeutic agents could produce more effective treatments for disease via improved efficacy and reduced toxicity. This is of particular importance in cardiovascular disease and cancer where current therapies often possess wide ranging and harmful adverse effects. Biological agents, including peptides and gene delivery systems (here recombinant adenoviral vectors), can be improved via targeting the system towards specific cell types, tissue beds and organs. This has the potential to significantly increase the therapeutic index of these agents.

In cardiovascular disease, oxidative stress is implicated in disease pathogenesis. Potential anti-oxidant therapies have shown limited effectiveness in clinical trials partly due to diverse patient populations and differences in the type and strength of the anti-oxidants used. Therefore, development of a targeted anti-oxidant therapy may potentially improve efficacy. The reactive oxygen species superoxide (SO) is produced by NAD(P)H oxidase in the vasculature and reduces nitric oxide (NO) bioavailability, leading to endothelial dysfunction. The anti-oxidant peptide gp91ds selectively inhibits assembly of NAD(P)H oxidase, thereby reducing SO production. Vascular-targeting peptides CRPPR and CSGMARTKC were previously identified by T7 phage display in mice. These peptides retained their selectivity in another species as determined in the normotensive Wistar Kyoto rat (WKY) and in a model of human essential hypertension, the stroke-prone spontaneously hypertensive rat (SHRSP). In the SHRSP, CRPPR targeted to the heart with a 17-fold increase over insert-less control phage and had a 58-fold increase in targeting to the aorta. Immunohistochemical analysis with an anti-T7 antibody showed that CRPPR-inserted phage localised to both endothelial cells and medial smooth muscle cells. CSGMARTKC selectively homed to the heart (specifically the coronary vasculature) with a 26-fold increase over control phage. Therefore, an efficacy study to assess whether linkage of gp91ds to a vascular-targeting peptide could increase the anti-oxidant effect in the SHRSP was performed.

Animals were subjected to radio-telemetry recording 10 days before peptide infusion to continuously monitor blood pressure (BP), heart rate and activity. Peptides were continuously administered at 10 mg/kg/day for 21 days by subcutaneous osmotic mini-pumps. Systolic BP was determined for one week prior to treatment, followed by three weeks of study duration before sacrifice. Systolic BP showed a progressive rise from 177.6 ± 1.1 mmHg to 200.6 ± 0.7 mmHg in those groups receiving CSGMARTKC-gp91ds, HIV-tat-gp91ds (to allow entry to all cells), gp91ds alone and the control animals. This systolic BP increase, which is characteristic of the SHRSP animal model, was completely prevented in animals receiving CRPPR-gp91ds (systolic BP 187.5 mmHg ± 5.2, * $p < 0.001$ vs. other treatment groups and control group). CRPPR-gp91ds, CSGMARTKC-gp91ds and gp91ds alone showed significantly improved NO bioavailability, determined by *ex vivo* large vessel myography, whereas HIV-tat-gp91ds treated animals continued to show impaired endothelial function, characteristic of the SHRSP. Therefore, the anti-oxidant therapy alone shows improvement in NO bioavailability. However, when the anti-oxidant peptide was targeted with CRPPR, a significant improvement in NO bioavailability and attenuation of the time-dependent and progressive increase in systolic BP in the SHRSP was observed. This demonstrates the potential of targeting biologically active peptides to defined cells *in vivo*.

A related but alternative approach to targeting was to utilise adenoviral vectors. Recently, the interaction between adenovirus (Ad) 5 and the blood coagulation factor X (FX) was shown to be pivotal for liver transduction. FX binds directly to the hexon of Ad5 and this interaction leads to hepatocyte transduction *in vivo*. Vectors based on the sub-species B Ads, including Ad35, are in development for cancer gene therapy as the Ad35 fiber uses the membrane glycoprotein CD46 as a high affinity cellular receptor instead of the coxsackie and adenovirus receptor (CAR), the primary receptor for the Ad5 fiber. CD46 is up-regulated in many cancers. Previously, it was shown that FX binds to Ad35 and, based on this, the Ad35:FX interaction was investigated in detail using Ad5, Ad35 and a range of chimeric Ad5/Ad35 vectors: the pseudotype Ad5/f35, which contains the hexon and penton of Ad5 with the Ad35 fiber (f), Ad5/p35/f35, which has the Ad5 hexon and the penton (p) and fiber of Ad35, and Ad35/f5, the reverse pseudotype. By electron cryomicroscopy at 31Å resolution, FX was observed bound to the Ad35 hexon. The

ability of the chimeric vectors and Ad35 to bind FX was analysed by surface plasmon resonance (SPR). SPR analysis revealed that Ad5, Ad35 and the chimeric Ad5/Ad35 vectors all bound to FX. Both the Ad5 and Ad35 pseudotypes have FX binding affinities akin to other vectors possessing the same hexon, with vectors containing the Ad5 hexon having an approximately ten-fold higher affinity for FX than those vectors containing the Ad35 hexon.

In CHO-CD46 cells, the presence of FX had no significant effect on binding by vectors containing Ad35 fibers (Ad5/f35, Ad5/p35/f35 and Ad35). However, the presence of FX significantly inhibited transduction by Ad5/f35, Ad5/p35/f35 and Ad35 by 2.7-, 1.9- and 2.2-fold, respectively, in CHO-CD46 cells. This inhibition of transduction by FX could be prevented by the addition of the FX binding protein, X-bp. This suggests that FX limits a post-binding or post-internalisation mechanism(s) that leads to cellular transduction by vectors containing the Ad35 fiber.

Vectors were intravenously administered to CD46 transgenic mice in the presence and absence of X-bp to assess vector targeting *in vivo*. Localisation of the luciferase expressing vectors was visualised by whole-body bioluminescence and transgene expression was quantified by luciferase assay. Vector genome (VG) accumulation was also quantified by qPCR. Ad5 selectively targeted to the liver as expected in the CD46 transgenic mice, an effect significantly inhibited by X-bp. Liver accumulation by all other vectors was substantially lower that that for Ad5 and X-bp significantly further reduced liver vector accumulation by Ad5/f35, Ad5/p35/f35, Ad35 and Ad35/f5. This suggests that FX binding to both Ad5 and Ad35 hexon mediates liver accumulation and that this can be, at least partially, reduced by inhibition of the virus:FX interaction by X-bp. In the absence of X-bp, Ad5/f35 and Ad5/p35/f35 exhibited high levels of lung vector accumulation with $5.6x10^5$ and $5.7x10^5$ VG/50ng of total DNA isolated, respectively. Ad5 demonstrated very poor lung targeting. Pre-administration of X-bp significantly reduced genome accumulation in lung by Ad5/f35 and Ad5/p35/f35 1.9- and 6.6-fold, respectively. However, lung transduction by Ad35 was significantly enhanced by 1.6-fold in the presence of X-bp. Additionally, *in vivo* Ad35 had an increased lung:liver ratio in the presence of X-bp indicating accumulation of this vector in the lung after the removal of the FX interaction. Therefore, due to its selective lung targeting ability and low

seroprevalence development of a vector based on Ad35, which had been modified to ablate the interaction with FX, would be a highly useful tool to selectively target CD46 and tumours *in vivo* by intravascular administration.

In summary, selective targeting of an anti-oxidant peptide to the vasculature has led to a significant enhancement in the efficacy of the anti-oxidant peptide gp91ds. By targeting defined cells *in vivo*, this anti-oxidant has increased potential effectiveness compared to alternative anti-oxidant therapies. Additionally, administration of a variety of Ad35-based vectors has led to increased understanding of the requirements needed for the generation of a successfully targeted Ad35 vector. Together this helps to identify the potential requirements for development of more appropriate treatments for cardiovascular disease and cancer.

CHAPTER 1

Introduction

1.1 General introduction

There is a continual need for identification and testing of new and more effective treatments for many diseases due to the lack of optimal pharmacological interventions. This is of particular importance in cardiovascular disease and cancer, due to the sheer number of patients affected by these conditions and as the developed therapies often have wide ranging and harmful adverse effects. Selective targeting of therapeutic agents is a potential method of reducing their delivery to non-target cells and organs.

Biological agents, including peptides and gene delivery systems (recombinant adenoviral vectors) have potential utility in disease treatment. However, their efficacy is limited. Therefore, optimisation by targeting such agents to specific cell types, tissue beds or organs may improve efficacy and therapeutic indices.

1.2 Cardiovascular disease

Cardiovascular disease refers to all diseases which affect the heart and circulatory system and includes hypertension, coronary heart disease, angina, myocardial infarction (MI) and stroke. Although there have been many significant advances in treatment options and medications available to help to control symptoms and reduce the risk of further problems, cardiovascular disease is the most common cause of death in the UK (www.bhf.org.uk). 29% of men and 23% of women suffer a premature death due to cardiovascular disease (www.heartstats.org.uk). This has led to the need to develop more effective treatments for specific aspects of cardiovascular disease.

Hypertension is a chronic medical condition in which the blood pressure (BP) is elevated. Hypertension can be classified as either essential (primary) or secondary hypertension. Essential hypertension has no single clear medical cause and accounts for over 90% of hypertension cases (Carretero and Oparil, 2000, Oparil *et al.*, 2003). However, there are several risk factors which have been shown to contribute to the development of essential hypertension, including smoking, obesity, high alcohol consumption, lack of exercise and high salt intake. Secondary hypertension occurs

due to another condition, such as kidney disease or tumours of the adrenal medulla and adrenal cortex, which produces hypertension due to increased secretion of catecholamines or steroids, respectively. Persistent hypertension increases the risk of stroke, MI and heart failure (Carretero and Oparil, 2000).

In the 2002 World Health Organisation (WHO) World Health Report (www.who.int/whr/2002/en/whr02_en.pdf), hypertension was identified as the second most important cause of death and disability in developed countries. In Scotland, 33% of men have a BP over 140/90 mmHg and a 20 mmHg increase in systolic BP or 10 mmHg increase in diastolic BP in patients aged 40-69 years doubles the risk of death (www.heartstats.org). Hypertension causes the smooth muscle cells (SMCs) in the media of resistance arteries to proliferate, reducing the lumen diameter and further increasing peripheral resistance. The rise in systolic BP also increases the work load of the left ventricular myocytes in the heart and this can lead to cardiac hypertrophy, where the cardiac myocytes increase in length and width in order to thicken the wall of the heart to normalise ventricular wall tension. This remodelling causes the ventricles of the heart to become stiff, leading to impaired filling and diastolic dysfunction. Over time the abnormal reduction in myocardial contractility caused by cardiac hypertrophy can predispose the individual to heart failure.

The National Institute for Health and Clinical Excellence (NICE) guidelines for the treatment of hypertension in the UK have been published (www.nice.org.uk/ nicemedia/pdf/HypertensionGuide.pdf). Hypertensive patients are commonly treated with one or more of the following antihypertensive medicines: angiotensin converting enzyme (ACE) inhibitors, angiotensin II receptor antagonists, calcium-channel blockers, diuretics and beta-blockers. ACE inhibitors reduce the formation of angiotensin II and aldosterone, which leads to reduced vascular tone and extracellular fluid volume and thus reduced BP. Angiotensin II receptor antagonists and calcium-channel blockers act as vasodilators to widen resistance arteries, reducing peripheral resistance. Diuretics increase water and salt excretion, thereby reducing extracellular fluid, blood volume and BP. Beta-blockers reduce cardiac output and hence reduce BP. However, high doses of antihypertensive drugs are often not effective during chronic administration and can cause side effects. The

adverse effects produced by antihypertensives include a dry cough produced in response to ACE inhibitors, fatigue and cold peripheries due to beta-blockers and, headaches with treatment by calcium-channel blockers.

The therapeutic benefit of the available agents for treating cardiovascular disease could be substantially enhanced by targeting them towards specific areas of the cardiovascular system. In addition, cardiovascular disease has now been shown to have a considerable genetic influence. Therefore, biological agents capable of delivering functional genes to correct mutations which lead to cardiovascular disorders could be highly effective tools at preventing the morbidity and mortality produced by cardiovascular diseases.

1.2.1 Oxidative stress

Oxidative stress is produced by an imbalance between the generation and removal of reactive oxygen species (ROS), which leads to the presence of excessive ROS. ROS are reactive chemical entities and can be classified as either free radicals or non-radical derivatives. Free radicals possess one or more unpaired electrons and these include the superoxide anion (SO or $O_2^{\cdot-}$), the hydroxyl radical ($HO^{\cdot}$) and nitric oxide (NO). Hydrogen peroxide (H_2O_2) and peroxynitrite ($ONOO^-$) are not free radicals but contribute to oxidative stress as they also have the ability to oxidise other molecules. The production of one ROS has the potential to produce many others due to radical chain reactions (Cai and Harrison, 2000). At low concentrations, ROS act as signalling molecules and are involved in many cellular processes, including cycle regulation (Harris and Levine, 2005), proliferation (Harris and Levine, 2005, Kobori *et al.*, 2007), cell growth (Frazier *et al.*, 2007), differentiation (Riou *et al.*, 2001) and apoptosis (Harris and Levine, 2005, Su *et al.*, 2006). However, at high concentrations, ROS elicit a plethora of harmful and toxic effects, in particular, ROS are key mediators that contribute to inflammation and atheroma (Cai and Harrison, 2000).

Production of ROS at levels exceeding the handling capacity of the endogenous anti-oxidant defence mechanisms leads to oxidation of biological macromolecules, including DNA, protein, carbohydrates and lipids (Cai and Harrison, 2000).

Oxidative stress has been implicated in the pathogenesis of many cardiovascular diseases, including hypertension, atherosclerosis, diabetes mellitus, MI and heart failure (Cai and Harrison, 2000, Griendling *et al.*, 2000, Neunteufl *et al.*, 2000, Schachinger *et al.*, 2000, Berry *et al.*, 2001, Heitzer *et al.*, 2001, Gokce *et al.*, 2002, Madamanchi *et al.*, 2005a, Madamanchi *et al.*, 2005b).

Possibly the most important ROS in the vasculature is SO. The major source of SO are the membrane-bound enzymes nicotinamide adenine dinucleotide (phosphate) (NADH/NAD(P)H) oxidases in vascular and cardiac tissues (Figure 1.1) (Cai and Harrison, 2000). These enzymes are thought to be responsible for the excessive generation of SO seen in many cardiovascular diseases as they primarily control the redox state of blood vessels and the myocardium (Griendling *et al.*, 2000). NAD(P)H oxidase catalyses the reduction of molecular oxygen, using NADH or NADPH as the electron donor, producing SO at the cell surface (Berry *et al.*, 2001).

$$NAD(P)H + 2O_2 \rightarrow NAD(P)^+ + H^+ + \mathbf{2O_2^-}$$

Functional NAD(P)H oxidases have been shown to be present in the endothelium (Gorlach *et al.*, 2000), vascular smooth muscle (Rajagopalan *et al.*, 1996, Laursen *et al.*, 1997) and adventitia (Rey *et al.*, 2002). In the vasculature, several isoforms of NAD(P)H oxidases are present. The membrane bound subunit $gp91^{phox}$ or Nox2 is expressed in endothelial cells (ECs) and the adventitia (Gorlach *et al.*, 2000, Rey *et al.*, 2002), Nox1 is expressed in vascular smooth muscle cells (VSMCs) (Lassegue *et al.*, 2001) and Nox4 is expressed throughout the vessel wall (Sorescu *et al.*, 2002) (Figure 1.1). In the vasculature, NAD(P)H oxidase is active during conventional metabolism to produce SO, which is used by cells as an endogenous signalling molecule at low levels. In response to endogenous agonists, for example, angiotensin II and tumour necrosis factor-α (TNF-α), activation of NAD(P)H oxidase is sustained. This continuous production of SO has been shown in both rat VSMCs (Griendling *et al.*, 1994) and in human tissues (Berry *et al.*, 2000).

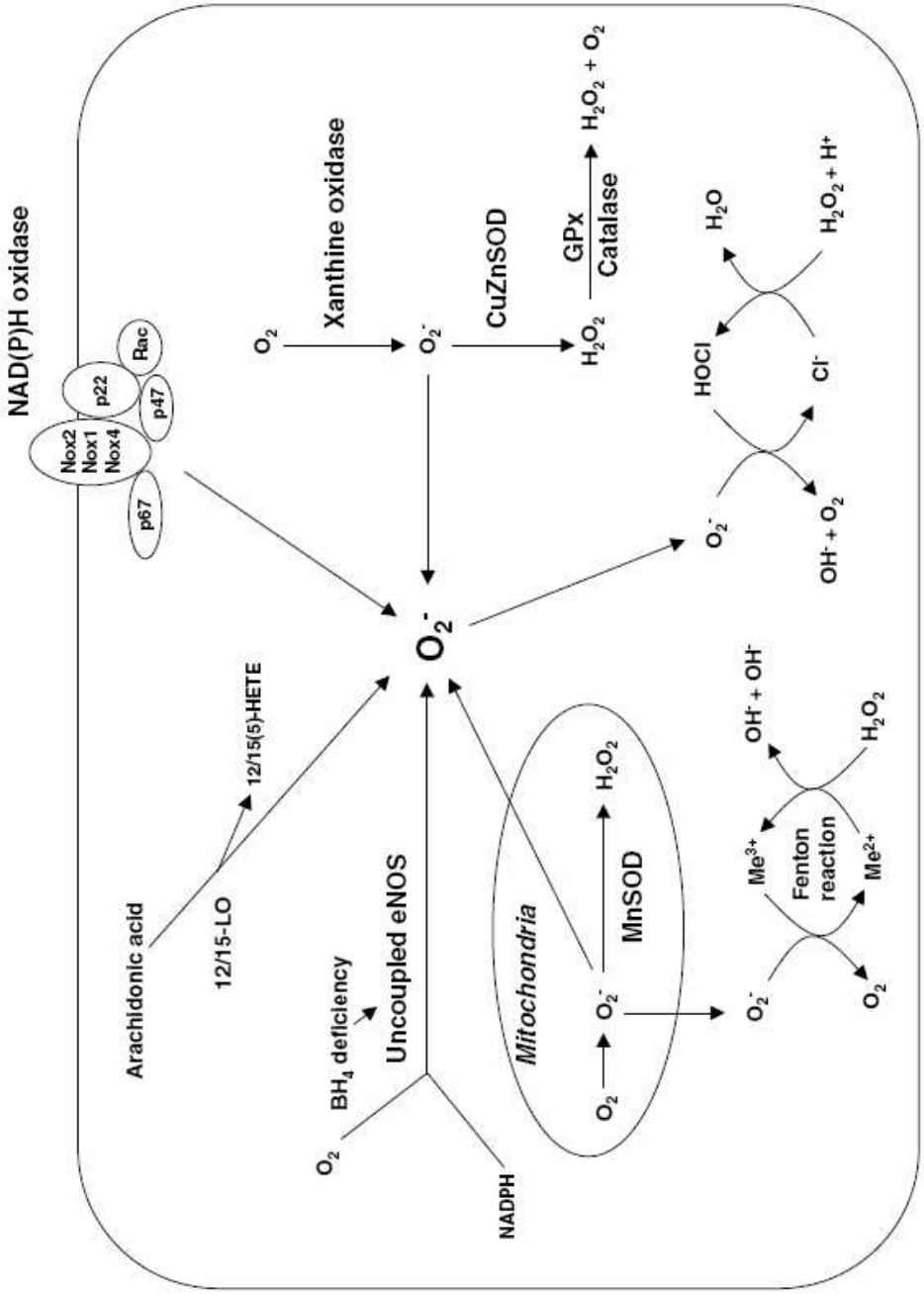

Figure 1.1 – NAD(P)H oxidase-related ROS generation and ROS degradation in the vasculature.

NAD(P)H, nicotinamide adenine dinucleotide phosphate; ROS, reactive oxygen species; SOD, superoxide dismutase; NO, nitric oxide; GPx, glutathione peroxidase; eNOS, endothelial NO synthase. Adapted from (Higashi *et al.*, 2009).

To maintain the redox balance, an endogenous anti-oxidant defence system is also present in the vasculature and this includes the enzymes superoxide dismutase (SOD), glutathione peroxidase (GPx) and catalase (Figure 1.1). There are three isoforms of SOD to scavenge any excess SO. These are; two intracellular forms, manganese SOD (MnSOD) and copper/zinc SOD (CuZnSOD), which are found in the mitochondria and cytoplasm, respectively (Figure 1.1), with a third extracellular form that is found in the extracellular space associated with heparan sulphate proteolycans (HSPGs). SOD rapidly dismutates SO into H_2O_2, which is subsequently eliminated by GPx and catalase to water (Figure 1.1).

1.2.2 Oxidative stress and endothelial dysfunction

Increased oxidative stress due to excessive production and reduced removal of ROS is associated with the development of many vascular disease states, such as hypertension (Cai and Harrison, 2000, Griendling *et al.*, 2000, Berry *et al.*, 2001, Madamanchi *et al.*, 2005a, Madamanchi *et al.*, 2005b). SO is produced by NAD(P)H oxidase in the vasculature in response to angiotensin II or increased wall stretch (Griendling *et al.*, 2000) (Figure 1.2). Under physiological conditions, SO can react with the vasodilator NO producing $ONOO^-$ (Harrison, 1997) (Figure 1.2). As the reaction between SO and NO is three times faster than the interaction of SO with SOD (Thomson *et al.*, 1995), the balance between oxidative and anti-oxidative systems can quickly change. Production of SO by NAD(P)H oxidases has been implicated in contributing to a condition called endothelial dysfunction, as the combination of SO with NO leads to reduced NO bioavailability (Rajagopalan *et al.*, 1996, Laursen *et al.*, 1997, Wang *et al.*, 1998a, Di Wang *et al.*, 1999, Gorlach *et al.*, 2000, Mollnau *et al.*, 2002, Rey *et al.*, 2002) (Figure 1.2). Endothelial dysfunction occurs when the native endothelium-dependent vasorelaxation to NO is significantly impaired (Griendling *et al.*, 2000).

Endothelial dysfunction was first shown in hypercholesterolemic rabbits (Minor *et al.*, 1990). Endothelium-dependent relaxation was severely impaired (Minor *et al.*, 1990), suggesting a lack of endothelium-derived relaxing factor (EDRF, an alternative name for NO). However, the levels of NO and NO oxidation products in the vessels were increased 3-fold (Minor *et al.*, 1990). Additionally, endothelial

nitric oxide synthase (eNOS) could be activated by acetylcholine (Minor *et al.*, 1990), indicating that the signalling pathway for producing relaxation in the vessels was intact. This effect on NO bioavailability was shown to be due to SO as treatment of hypercholesterolemic rabbits with polyethylene-glycolated-SOD enhanced endothelium-dependent vascular relaxation (Mugge *et al.*, 1991). No effect of SOD treatment was seen in control rabbits (Mugge *et al.*, 1991). Therefore, NO bioavailability is partly dependent on levels of SO, the hydroxyl radical has also been shown to possibly interact with NO (Pieper *et al.*, 1997).

The effects of SO can also be increased due to eNOS uncoupling in the vasculature (Figure 1.2). In eNOS uncoupling, lack of the substrate L-arginine or the essential cofactor and electron transfer molecule tetrahydrobiopterin (BH_4), causes eNOS to deviate from its coupled state where it produces NO. Instead, eNOS transfers electrons to molecular oxygen, reducing it and producing SO and H_2O_2. Additionally, degradation of BH_4 by ROS (including $ONOO^-$, SO and H_2O_2) can down-regulate eNOS (Kuzkaya *et al.*, 2003). Oxidation of BH_4 by $ONOO^-$ can also initiate eNOS uncoupling, further increasing endothelial dysfunction (Laursen *et al.*, 2001) (Figure 1.2). Therefore, endothelial dysfunction leads to increased endothelium-dependent vasoconstriction, increased vascular peripheral resistance and, ultimately, can lead to increased BP. If this reduction in endothelium-dependent vasodilatation occurs in the coronary circulation, it can lead to cardiovascular remodelling, increased adverse cardiovascular events and increased cardiovascular mortality (Figure 1.2) (Cai and Harrison, 2000, Schachinger *et al.*, 2000, Suwaidi *et al.*, 2000).

The generation of SO during reperfusion injury after MI exacerbates the damage produced to ischaemic areas of the heart. MI is caused by coronary artery obstruction and the resultant ischaemia produces an area of damaged or dead muscle, an infarct. When blood flow is restored to the infarct, the molecular oxygen contained within the blood is converted to SO by NAD(P)H oxidase (Bauersachs *et al.*, 1999). This burst of SO produced during reperfusion activates many intracellular signalling pathways, causing cellular damage/apoptosis and cardiac hypertrophy (Griendling *et al.*, 2000).

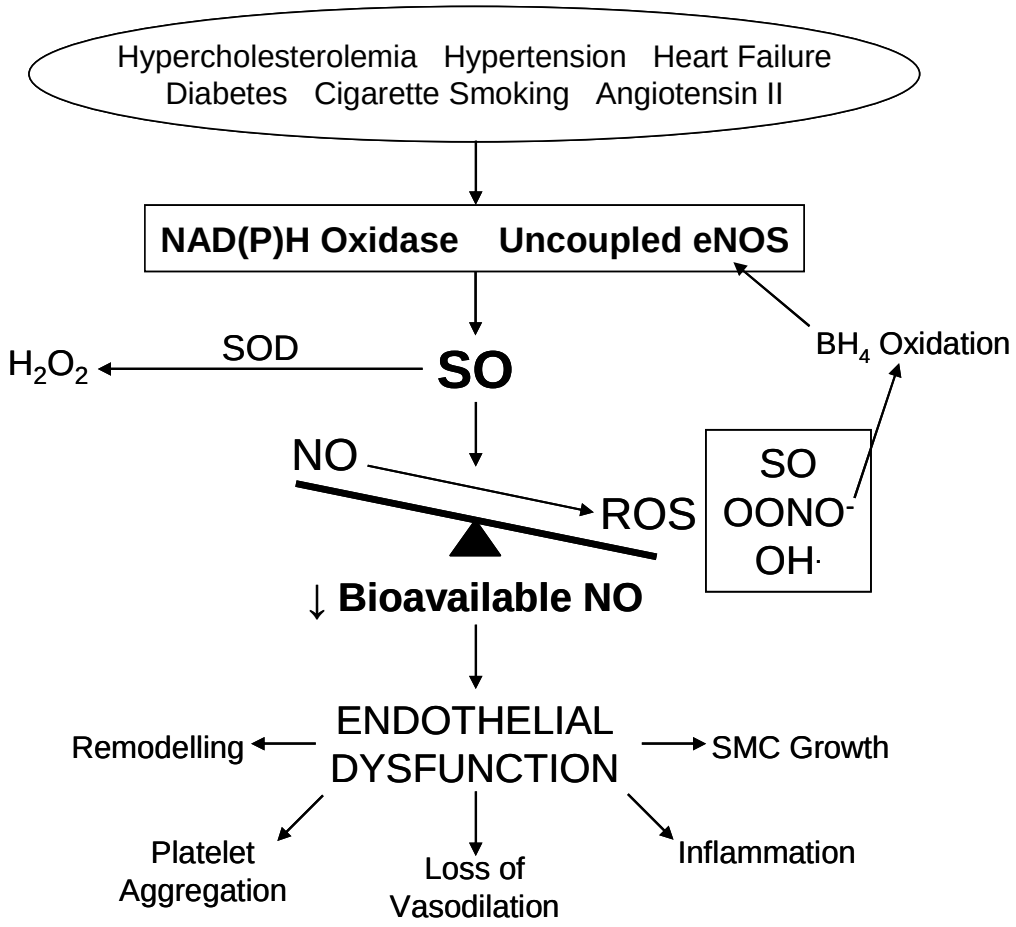

Figure 1.2 – Oxidative stress-induced endothelial dysfunction.

Adapted from Cai and Harrison (Cai and Harrison, 2000).

1.3 Clinical trials of anti-oxidants

With evidence indicating towards increased oxidative stress being responsible for a variety of human cardiovascular diseases, there has been a severe lack of effective anti-oxidants in clinical trials with respect to the primary outcomes and morbidity.

The anti-oxidant vitamin ascorbic acid (vitamin C) has been shown to increase NO bioavailability and restore endothelium-dependent vasodilatation in patients with increased oxidative stress due to coronary artery disease, essential hypertension and hypercholesterolaemia (Levine *et al.*, 1996, Ting *et al.*, 1997, Taddei *et al.*, 1998,

Gokce *et al.*, 1999, Hornig, 2002). However, other clinical trials have had mixed results. The Cambridge Heart Antioxidant Study (CHAOS) randomly assigned patients to 400 or 800 IU/day of a natural α-tocopherol (RRR-AT) or placebo (Stephens *et al.*, 1996). The RRR-AT-treated group showed a significant reduction in cardiovascular deaths and non-fatal MI (Stephens *et al.*, 1996). This study used higher doses of vitamin E than other unsuccessful clinical trials (reviewed in (Heinecke, 2001)). In the Secondary Prevention with Antioxidants of Cardiovascular Disease in End Stage Renal Disease (SPACE) study, haemodialysis patients with pre-existing cardiovascular disease were administered with either 800 IU/day of RRR-AT or a placebo (Boaz *et al.*, 2000). The treated group had a significant reduction in primary cardiovascular disease endpoints (Boaz *et al.*, 2000). However, many other anti-oxidant clinical trials have failed for a variety of reasons, including, perhaps, diverse patient populations, inappropriate clinical endpoints and the variation in the type and dose of the anti-oxidants used. Natural RRR-AT is more potent than synthetic *all rac* α-tocopherol and other natural forms of α-tocopherol (Brigelius-Flohe and Traber, 1999), potentially altering the efficacy of the trial. Additionally, the redox reactions *in vivo* are complex and occasionally treatment with anti-oxidants and can lead to a paradoxical increase in oxidant generation. The anti-oxidant β-carotene can act as an oxidant under certain conditions (Burton and Ingold, 1984), leading to an increased risk of ischemic heart disease (Rapola *et al.*, 1997). Also, high doses of vitamin C increased free radical-induced DNA damage in healthy volunteers (Podmore *et al.*, 1998). However, this does not contraindicate the role of ROS as a key mediator of vascular oxidative stress. Therefore, it is important to further increase understanding of the basic biology and pathology of ROS and develop more effective anti-oxidant therapies. Increased efficacy of anti-oxidant therapies could potentially be achieved by selectively targeting anti-oxidants *in vivo* to particular sites which are relevant in the pathogenesis of diseases related to oxidative stress.

1.4 Anti-oxidant peptide

Although there is evidence linking NAD(P)H oxidase and oxidative stress, there is a lack of effective inhibitors targeting this oxidase which do not inhibit other flavin-

containing enzymes (Riganti *et al.*, 2004). The anti-oxidant peptide gp91ds (sequence CSTRIRRQL) selectively inhibits NAD(P)H oxidase by preventing the interactions of its subunits, specifically the interaction between the membrane bound $gp91^{phox}$ subunit and the cytosolic oxidase subunit $p47^{phox}$, reducing vascular SO production (Rey *et al.*, 2001). This competitive antagonist peptide is a potent inhibitor of SO formation in cell-free human neutrophil assays with a half maximal inhibitory concentration (IC_{50}) of 3μM (DeLeo *et al.*, 1995, DeLeo and Quinn, 1996).

The anti-oxidant peptide gp91ds was linked to a peptide derived from human immunodeficiency virus-1 transactivation tat protein (HIV-tat, sequence RKKRRQRRR) (Frankel and Pabo, 1988, Green and Loewenstein, 1988). The HIV-tat peptide is derived from the viral coat of HIV and mediates cell entry of the anti-oxidant peptide, allowing it to be internalised into every cell (Fawell *et al.*, 1994). The HIV-tat system had been previously used to enable efficient delivery of conjugated, biologically active peptides after intravenous delivery (Kim *et al.*, 1997, Cardarelli *et al.*, 2007). Pre-incubation of aortic rings with the peptide gp91ds-tat (RKKRRQRRR-CSTRIRRQL) 30 minutes before angiotensin II stimulation, significantly prevented angiotensin II-induced SO production *in vitro* (Rey *et al.*, 2001). Additionally, co-infusion of angiotensin II and gp91ds-tat significantly inhibited SO production in *ex vivo* mouse aortic rings, compared to aortic rings from angiotensin II-infused animals (Rey *et al.*, 2001). Co-infusion of angiotensin II and gp91ds-tat significantly attenuated angiotensin II-induced hypertension in mice (Rey *et al.*, 2001). *In vivo* administration of the gp91ds-tat peptide into salt-induced hypertensive rats has also been shown to reduce the production of aortic SO (Zhou *et al.*, 2006). The reduced SO production in the presence of gp91ds-tat inhibited the development of endothelial dysfunction in the aorta of these inducibly-hypertensive animals but did not significantly reduce the systolic BP in the treated group (Zhou *et al.*, 2006). The gp91ds-tat peptide also did not reduce systolic BP in the normotensive Sprague-Dawley rat (Jacobson *et al.*, 2003).

The importance of the influence of the $gp91^{phox}$ subunit-containing or Nox2 form of NAD(P)H oxidase on BP has been shown as knockout mice deficient in Nox2 have a significantly reduced basal BP compared to wild-type mice (Wang *et al.*, 2001).

Infusion of angiotensin II produced similar increases in BP in both the knockout and wild-type mice but angiotensin II only increased SO production two-fold in aortic rings from wild-type mice (Wang *et al.*, 2001). This indicates an essential role *in vivo* of $gp91^{phox}$ and NAD(P)H-derived SO in both regulation of basal BP and angiotensin II-induced hypertension (Wang *et al.*, 2001). However, targeted over-expression of Nox2 in ECs did not alter the basal BP of Nox2-transgenic mice (Bendall *et al.*, 2007). There was a significant increase in total NAD(P)H oxidase activity in lysates from the left ventricle and intact aorta but this did not result in any effect on BP (Bendall *et al.*, 2007). This suggests that there are other compensatory mechanisms involved which prevent the significant increase in SO production in the endothelium from leading to a significant increase in basal BP level.

As significant evidence indicates that increased oxidative stress is responsible for a variety of human cardiovascular diseases, it is critical to develop more effective anti-oxidant therapies. The gp91ds peptide has excellent potential as a selective blocker of SO formation and, thereby, oxidative stress *in vivo*. An enhanced reduction of oxidative stress could be achieved by targeting the anti-oxidant treatments. Therefore, a vascular targeting anti-oxidant peptide was developed, the efficacy of which was compared to the non-targeted gp91ds-tat peptide in an animal model of human essential hypertension and stroke, the stroke-prone spontaneously hypertensive rat (SHRSP).

1.5 The stroke-prone spontaneously hypertensive rat (SHRSP)

The spontaneously hypertensive rat (SHR) was generated from Wistar Kyoto (WKY) rats, selectively bred for high BP without any dietary or environmental stimuli (Okamoto and Aoki, 1963). A sub-strain of the SHR with exceptionally high BP and increased susceptibility to stroke was subsequently selectively bred and designated as SHRSP. As in humans, BP in the SHRSP increases with age whilst the reference strain remains normotensive throughout its lifespan (Davidson *et al.*, 1995, Clark *et al.*, 1996). In line with human essential hypertension, there is severe concentric left ventricular hypertrophy (LVH, assessed by echocardiography with

post-mortem validation) with approximately 10-20% of male SHRSP from University of Glasgow colonies developing spontaneous strokes, either ischaemic or haemorrhagic in origin.

Research into the genetic basis of essential hypertension has been performed on the SHRSP and quantitative trait loci (QTL) have been identified linked to BP (on chromosomes 2 and 3), stroke (chromosome 5) and LVH (chromosome 14). Microarray gene expression profiling was performed for the QTLs on chromosome 2 and has identified oxidative stress related genes (McBride *et al.*, 2003, McBride *et al.*, 2005). The SHRSP has an increased infarct volume following middle cerebral artery occlusion compared to the WKY, a trait with very strong genetic determination (Jeffs *et al.*, 1997, Gratton *et al.*, 1998).

Importantly, endothelial dysfunction due to increased generation of SO and relative NO deficiency can also be reversed using both gene-based and pharmacological approaches (Alexander *et al.*, 1999, Dowell *et al.*, 1999, Alexander *et al.*, 2000, Fennell *et al.*, 2002, Miller *et al.*, 2005), thus defining oxidative stress as a key mediator of endothelial dysfunction in the SHRSP. As in man, oxidative stress and resulting endothelial dysfunction is accelerated with ageing in the SHRSP (Hamilton *et al.*, 2001).

Concentric LVH, both in the SHRSP and in human essential hypertension, is associated with increased susceptibility to MI. Moreover, it has been shown that the progression of left ventricular dysfunction is more pronounced, the greater the extent of initial LVH (Dominiczak *et al.*, 1996).

Therefore, the SHRSP is a well-characterised and well-established animal model of essential hypertension and endothelial dysfunction (McBride *et al.*, 2005). The SHRSP has greater than normal vascular SO production (Berry *et al.*, 2001) and increased levels of uncoupled eNOS. The resultant excess of SO in the SHRSP reduces NO bioavailability, impairing vascular relaxation and increasing BP (Kerr *et al.*, 1999). As the SHRSP exhibits increased SO production and hypertension, it has been chosen as the *in vivo* model for the investigation of effects of vascular targeting anti-oxidant peptides on BP and endothelial function.

1.6 Gene therapy

Gene therapy is best defined as the introduction of a gene into an organism in order to treat an inherited disorder or other disease caused by either a loss- or gain-of-function mutation in a gene. The application of gene therapy has been used in monogenic diseases, such as cystic fibrosis and Duchenne's muscular dystrophy, where replacement of a non-functional gene with the wild-type gene should restore a normal phenotype. Additionally, the potential of gene therapy to provide novel treatments for diseases currently lacking suitable therapies or cures has led to its use for the treatment of cancer. However, before the full potential of gene therapy for the treatment of wide ranging diseases and conditions can be reached, there are numerous limitations which need to be overcome. The vector chosen for each gene therapy application needs to be developed to allow efficient and selective targeting to the required cell types, to prevent gene transfer to non-target tissues and organs, thereby improving the therapeutic indices. The therapeutic gene must ideally be expressed at the correct physiological level and expressed for a suitable duration to provide a benefit to the patient, which may vary from lifelong expression to a short burst of expression. The ability to provide long-term therapeutic effects by sustained gene expression within relevant cell types has limited the clinical efficacy of many gene therapy trials performed to date.

Up to March 2009, there have been 1537 gene therapy trials approved worldwide with 12% of the trials being performed in the UK (http://www.wiley.co.uk/genetherapy/clinical/). The majority of clinical trials (66.1%) have used viral vectors (http://www.wiley.co.uk/genetherapy/clinical/). Gene therapy clinical trials have been performed for a variety of diseases, including 64.6% of trials for cancer gene therapy, 8.9% for the treatment of cardiovascular disease, 8.1% for the treatment of monogenic diseases, 7.9% for infectious diseases, 1.8% for neurological diseases and 1.1% for the treatment of ocular diseases (http://www.wiley.co.uk/genetherapy/clinical/). The first disorder to be treated by gene therapy was adenosine deaminase-deficient (ADA) severe combined immunodeficiency (SCID). This disease results in the accumulation of toxic metabolites due to the inability to metabolise purines. Patients were treated by *ex vivo* administration of a classical

retroviral vector containing the wild-type ADA gene to T-lymphocytes removed from the patient. The cells were transduced, selected and expanded *ex vivo* before being returned to the patient and expression of the wild-type ADA gene could still be detected in 20% of the lymphocytes from one patient more than 10 years later (Muul *et al.*, 2003). This demonstrates the potential of gene therapy at the clinical level.

There have also been several successful clinical trials for the treatment of X-linked SCID (SCID-X1), an inherited disorder in which patients have a loss-of-function mutation in the common cytokine receptor γ chain gene (γc), leading to defective cytokine signalling and resulting in dysfunctional B-cells and lack of T-cells and natural killer (NK) cells of the immune system. This condition is also known as "boy in the bubble" syndrome as sufferers are extremely vulnerable to infectious diseases due to a crippled adaptive immune system. Based on efficacious pre-clinical data (Candotti *et al.*, 1996, Cavazzana-Calvo *et al.*, 1996, Hacein-Bey *et al.*, 1996, Stephan *et al.*, 1996, Taylor *et al.*, 1996, Hacein-Bey *et al.*, 1998, Whitwam *et al.*, 1998, Lo *et al.*, 1999, Soudais *et al.*, 2000), clinical studies were initiated. In two clinical studies, $CD34^+$ bone marrow stem cells were removed from patients and transduced *ex vivo* by a retroviral vector, the transgene of which was the wild-type version of the mutated γc cytokine receptor gene (Cavazzana-Calvo *et al.*, 2000, Gaspar *et al.*, 2004, Cavazzana-Calvo *et al.*, 2005). After 4 months, the 18 treated infants had newly developed functional NK and T-cells, which were present within the normal ranges for the majority of the patients. Reconstitution of the immune system was variable but apparent in all patients. However, 2-6 years after gene therapy, four of the patients have developed treatment-related leukaemia due to insertional mutagenesis by the retroviral gene therapy vector, leading to expression of endogenous proto-oncogenes (Hacein-Bey-Abina *et al.*, 2003, Howe *et al.*, 2008). These studies demonstrated outstanding data but highlighted the risk involved for the patients. The risk/benefit ratio of retroviral gene therapy for patients with no match for a bone marrow donor requires careful ethical consideration until safer vectors are developed and tested.

Adenoviral-based gene therapy systems are the most commonly used vector for clinical trials with viral vectors, representing 24% of all clinical trials approved to date (http://www.wiley.co.uk/genetherapy/clinical/). These gene therapy advances

have been broadly overshadowed by the death 10 years ago of a patient in a clinical trial to treat ornithine transcarbamylase (OTC) deficiency (Raper *et al.*, 2003). OTC deficiency is an inborn error of urea synthesis, which affects the ability of the body to excrete ammonia and results in seizures and mental retardation in sufferers. A first generation adenovirus was generated carrying the functional OTC gene, a similar vector to one which corrected the metabolic defect in OTC deficient sparse fur mice (Morsy *et al.*, 1996, Ye *et al.*, 1996) and had "an acceptable safety profile" in mice and non-human primates (Yang *et al.*, 1994, Ye *et al.*, 1997, Nunes *et al.*, 1999, Raper *et al.*, 2003). The vector was administered by infusion into the right hepatic artery in a dose escalation study. Jesse Gelsinger was the most severely affected subject and was the second patient to receive the highest dose used in the clinical trial. He suffered jaundice and an altered mental status approximately 18 hrs after administration of the vector and died 98 hours after administration due to a profound and uncontrollable systemic inflammatory response syndrome, disseminated intravascular coagulation and multiple organ system failure. In fact, all 11 patients in the trial had immune responses to the vector and there was no therapeutic benefit demonstrated (Raper *et al.*, 2002).

Subsequent discussions into this trial have pointed to deaths in monkeys after administration of the vector, inadequate information given to the patients regarding the risks and benefits of the treatment and the inclusion criteria of the trial, as Jesse Gelsinger was included when he displayed high ammonia levels, as potential reasons for the unsuccessful outcome (www.fda.gov). This clinical trial highlighted the fundamental lack of understanding surrounding basic aspects of adenovirology at that point. The host:vector interaction, which determined adenoviral fate in terms of biodistribution and transduction profiles, and also the host immune response generated to adenoviral vectors required greater definition. In addition, there are significant difficulties in conducting clinical trials due to variation in patient response to new agents, relevance of animal species in pre-clinical studies and variation in levels of pre-existing immunity to Ad5 in the human population. Therefore, much of the research produced in the aftermath of the death of Jesse Gelsinger has been to increase the understanding of the gene therapy vectors themselves.

1.7 Adenoviruses

Adenoviruses (Ads) are common human pathogens of which there are 51 human serotypes divided into six sub-species (A to F) based on their phylogenic origin, haeagglutination properties in a variety of species and their oncogenicity in rodents (Figure 1.3). The sub-species are characterised by differences in their capsid structure and the primary receptor used *in vitro* (Table 1) (Wadell *et al.*, 1980, Crawford-Miksza and Schnurr, 1996, Madisch *et al.*, 2005). The sub-species B Ads can be further sub-divided into sub-species B1 and B2 Ads (Table 1 and Figure 1.3) (Wadell *et al.*, 1980, Segerman *et al.*, 2003a). Additionally, there is a degree of correlation between the sub-species of Ad and the native tissue tropism of the vector, leading to its clinical properties. Sub-species B, C and E Ads cause respiratory disease and ocular infections, sub-species B2 Ads infect the kidneys and urinary tract and sub-species F Ads produce gastroenteritis (Russell, 2009). In general, infection with Ads does not lead to severe diseases (Russell, 2009). However, Ad infection in an immune-compromised patient (for example, an allogenic bone marrow recipient) tends to be invasive and can lead to increased mortality (Hierholzer, 1992, Flomenberg *et al.*, 1994, Ljungman, 1997, Chakrabarti *et al.*, 2000, Echavarria *et al.*, 2001, La Rosa *et al.*, 2001, Legrand *et al.*, 2001, Runde *et al.*, 2001, Lankester *et al.*, 2002). There is a particularly high incidence of Ad infection in immuno-suppressed children (Hierholzer, 1992, Flomenberg *et al.*, 1994, Chakrabarti *et al.*, 2000). In one study, the peripheral blood of 132 paediatric patients undergoing allogenic stem cell transplantation for a variety of conditions was tested for the presence of Ads (Lion *et al.*, 2003). Ads were detected in the peripheral blood of 11 children, with the most prevalent being the sub-species C Ads which were detected in 78% of those infected (Lion *et al.*, 2003). There was a highly significant association between Ad infection and transplant-related mortality in the 82% of patients who died (relative risk 5.8, $p < 0.001$) (Lion *et al.*, 2003). Also, there are many Ads from other species (Jager and Ehrhardt, 2007), which are relevant to human gene therapy, especially vaccines.

Ads can infect most but not all cell types and do so independently of cell division, having evolved sophisticated mechanisms to deliver their genome to the nucleus of

host cells in the absence of cell division (Russell, 2000). Ads are under development for diverse gene therapy applications, especially for the treatment of cardiovascular disease and cancer, and for vaccination. The wide range of applications for Ads reflects the ease with which they can be genetically manipulated to produce replication deficient adenoviral vectors and their substantial tolerance to the incorporation of novel targeting ligands. The majority of gene therapy vectors used to date are based on Ad5 (a sub-species C Ad) as it can be grown to high titres and is highly efficient at transducing non-dividing cells.

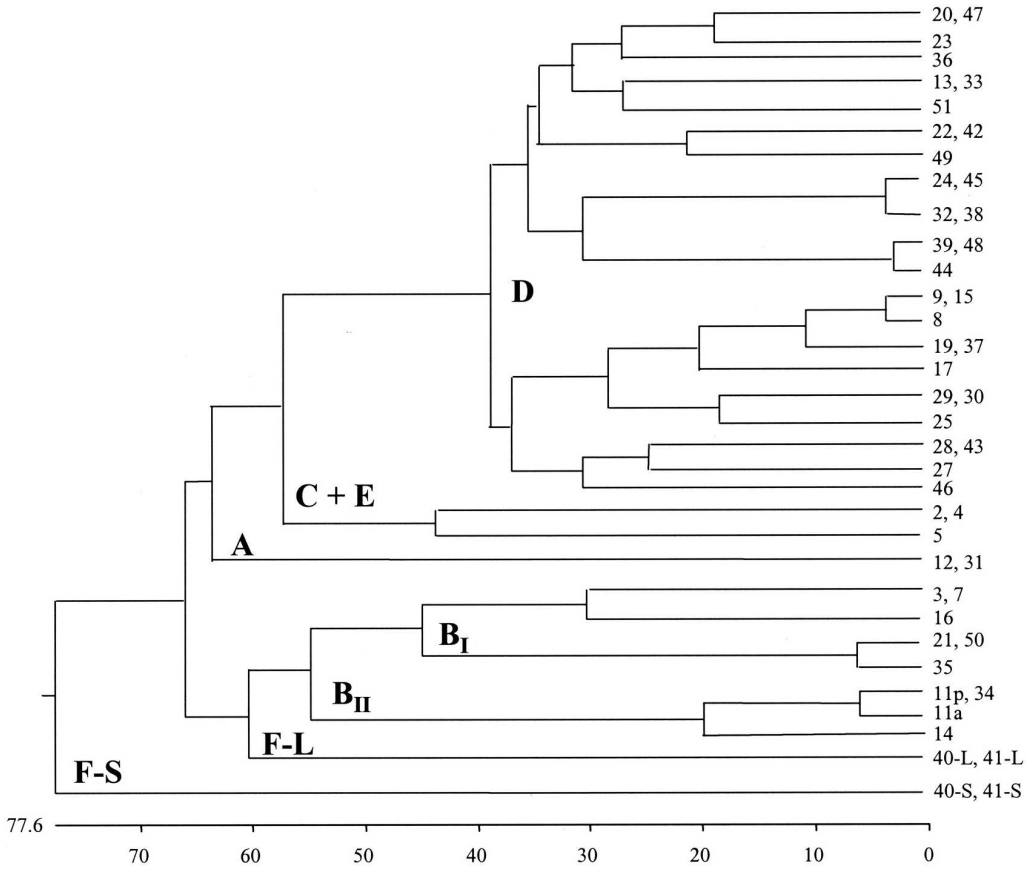

Figure 1.3 – Phylogenetic tree for human Ads.

Phylogenetic depiction of human Ads generated by parsimony analysis of fiber knob amino acid sequences. Number of each Ad is indicated on the right with sub-species designations A, B_I, B_{II}, C, D, E, F_L (long fiber of sub-species F virus) and F_S (short fiber of sub-species F virus). Amino acid diversity is shown below the tree. Adapted from Havenga *et al.* (Havenga *et al.*, 2002).

Sub-species	Serotype
A	12, 18, 31
B1	3, 7, 16, 17
B2	11, 14, 34, 35, 50
C	1, 2, 5, 6
D	8, 9, 10, 13, 15, 17, 19, 20, 22-30, 32, 33, 36-39, 42-49, 51
E	4
F	40, 41

Table 1 – Sub-species of human Ads.

1.7.1 Structure of adenoviruses

Ads are non-enveloped viruses which are 70-90 nm in diameter and have a double-stranded linear 36 kb DNA genome. The genome is enclosed within the icosahedral virion capsid which consists of three major exposed protein components – hexon, penton and fiber proteins (Figure 1.4A). The majority of the capsid consists of 240 trimeric hexon capsomers, which form 20 triangular faces, and associate with 12 pentameric penton bases. The structure of each Ad also contains 12 fiber proteins, which consists of the fiber shaft and knob. The fibers project away from the virion surface and are attached to the capsid by the penton base (Figure 1.4A). The fiber shaft of all human Ad serotypes has an N-terminal tail with a variable number of repeating sequences before the large C-terminal globular knob domain. Each repeat of the repeating sequence is encoded by 15-20 amino acids and is one of the defining characteristics between the sub-species with the sub-species B Ads having the shortest fibers (consisting of 5.5 repeats) whereas the sub-species C Ads have 22 repeats in their fibers.

The hexon proteins of the Ad capsid form into a trimeric structure and are the major site of Ad antigenicity (Norrby, 1969, Gall *et al.*, 1996). Hypervariable regions (HVRs) are present within the surface exposed area of the hexon protein and these HVRs differ between Ad sub-species and serotypes (Crawford-Miksza and Schnurr, 1996). In some, but not all, Ads the penton base of the Ad capsid contain a triple

amino acid motif (arginine-glycine-aspartic acid – RGD) on a surface exposed loop (Wickham *et al.*, 1993). The RGD motif binds to and activates cell surface integrins leading to virus uptake via clathrin-coated endocytosis, in the case of Ad5 (Wickham *et al.*, 1993, Wang *et al.*, 1998b).

1.7.2 Mechanism of human adenoviral infection in vitro

The mechanism of Ad5 infection *in vitro* is well characterised. The fiber protein of Ad5 binds to the coxsackie virus and adenovirus receptor (CAR) as its primary attachment receptor to infect cells *in vitro* (Figure 1.4B) (Bergelson *et al.*, 1997, Tomko *et al.*, 1997). CAR is a 46 kDa transmembrane glycoprotein with two extracellular immunoglobulin-like domains (D1 and D2). CAR is ubiquitously expressed (Defer *et al.*, 1990) and is a component of tight junctions. The D1 domain of CAR forms *trans* homodimers between molecules of the protein located on adjacent cells (van Raaij *et al.*, 2000) and it is through this interaction that CAR serves as a cell-cell adhesion molecule (Honda *et al.*, 2000). The mouse homologue of CAR also functions as a receptor for Ads (Bergelson *et al.*, 1998).

To investigate the interaction between sub-species C Ads and CAR, CAR-expressing cell lines were developed (Bergelson *et al.*, 1997, Tomko *et al.*, 1997). One study used CAR-negative NIH 3T3 cells for transfection with a plasmid expressing CAR (Tomko *et al.*, 1997). Ad5 transgene expression was only seen in NIH 3T3 cells transfected with CAR cDNA as control NIH 3T3 cells were completely refractory to transduction by Ad5 (Tomko *et al.*, 1997). CHO cells were also transfected with CAR cDNA and cell surface expression of CAR was detected by the anti-CAR antibody RmcB and immunoprecipitation (Bergelson *et al.*, 1997). Ad2 and isolated Ad2 fibers bound specifically to CHO-CAR cells with the same affinity and cellular attachment by the Ad2 virus was prevented in the presence of Ad2 fibers and recombinant Ad5 knob domains (Bergelson *et al.*, 1997). Transgene expression by Ad5 was increased 100-fold in CHO-CAR cells, compared to control cells (Bergelson *et al.*, 1997). These studies demonstrated that CAR is responsible for fiber-mediated attachment to cells by Ad2 and Ad5. Ad5 can also use the CAR receptor for interaction with red blood cells of some species (Nicol *et al.*, 2004, Carlisle *et al.*, 2009, Subr *et al.*, 2009).

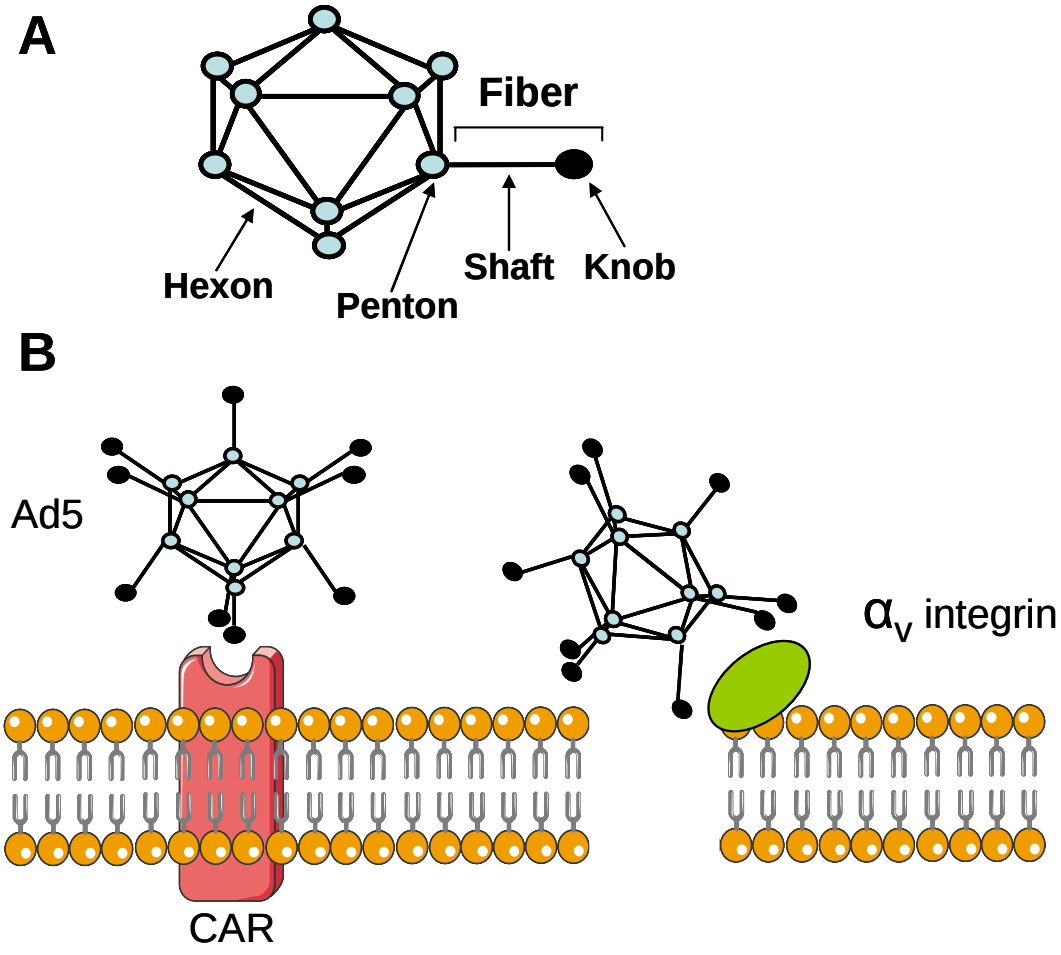

Figure 1.4 – Model of Ad5 infectivity *in vitro*.

(A) Major capsid proteins of adenovirus. (B) *In vitro* Ad5 uses the coxsackie virus and adenovirus receptor (CAR) as its primary attachment receptor to infect cells and this promotes interaction between the penton base and integrins for cell internalisation.

Ad5 binds to CAR by the knob domain as transduction by Ad5 can be efficiently inhibited by ablation of the CAR interaction by mutation of the knob, addition of anti-knob antibodies or the presence of recombinant knob protein (Henry *et al.*, 1994, Nicklin *et al.*, 2005). The interaction between the Ad5 fiber knob and soluble CAR has been shown to be a high affinity interaction with a dissociation constant of 14.8 nM (Kirby *et al.*, 2000, Kirby *et al.*, 2001). Resolution of the crystal structure of the Ad5 fiber knob bound to CAR revealed that the interface involved in the fiber knob:CAR interaction overlapped with the areas of CAR involved in CAR homodimer formation (van Raaij *et al.*, 2000). The Ad5 fiber knob binds to CAR with almost 100-fold higher affinity than the interaction between CAR molecules to form homodimers, which has a dissociation constant of 16 μM (Freimuth *et al.*, 1999, van Raaij *et al.*, 2000).

The interaction between the Ad5 fiber knob and CAR then promotes cell internalisation of the vector through engagement of $\alpha_v\beta_{3/5}$ integrins with the RGD motif in the penton base (Figure 1.4B) (Wickham *et al.*, 1993). Binding of the penton base to the integrin receptors occurs due to a flexible hinge region in the Ad5 fiber (Chiu *et al.*, 2001). Modification of the Ad5 fiber shaft to a short-shafted fiber from the sub-species B Ads hindered infection by these vectors (Shayakhmetov and Lieber, 2000), indicating that the presence of the hinge region in the Ad5 fiber shaft is crucial for cellular transduction.

CAR is a transmembrane protein with a C-terminal cytoplasmic domain and this cytoplasmic domain of the receptor contains putative phosphorylation sites, possibly indicating the potential of CAR to produce intracellular signalling. However, deletion of this cytoplasmic domain does not effect infection by Ads (Wang and Bergelson, 1999, Kirby *et al.*, 2000). Recently, the cytoplasmic tail of CAR has been shown to activate p44/42 mitogen-activated protein kinase (MAPK) (Farmer *et al.*, 2009). Activation of p44/42 MAPK was required for efficient infection by Ad5 through the CAR infection pathway as activation of this kinase enzyme, by Ad5 binding to CAR, induces CAR:CAR interaction in *cis* (in comparison to native CAR dimerisation interaction which occurs in *trans* (van Raaij *et al.*, 2000)) and clustering of CAR at the cell membrane (Farmer *et al.*, 2009). p44/42 MAPK activation also

promotes integrin activation, resulting in increased cell adhesion (Farmer *et al.*, 2009).

Following integrin engagement, the virion is internalised into endosomes by receptor-mediated endocytosis (Maxfield and McGraw, 2004). Ad5 infection was shown to be mediated by endocytosis via clathrin-coated pits by using dynamin to prevent the formation of clathrin-coated vesicles (Wang *et al.*, 1998b). Once internalised, acidification of the endocytic vessel occurs due to vacuolar H^+-ATPase activity. At pH 6.0, dissociation of the penton base and fiber from the virion occurs. Disassembly of the fiber occurs first, possibly mediated through interaction between the RGD motif in the penton and $\alpha_v\beta_{3/5}$ integrins (Wickham *et al.*, 1993). At low pH, a change in the conformation of the penton protein occurs exposing hydrophobic regions (Medina-Kauwe, 2003). Binding of the penton to integrins inside the acidified endomome (Bai *et al.*, 1993) causes dissociation of the penton base from the viral capsid to occur (Greber *et al.*, 1993, Seth, 1994a) and signals endosomal lysis by protein kinase C and a viral protease (Medina-Kauwe, 2003). This lysis of the endosomal membrane results in escape of virion into the cytosol (Seth, 1994b, Miyazawa *et al.*, 2001). Ad5 rapidly escapes into the cytosol within three to 15 minutes after internalisation (Greber *et al.*, 1993, Greber *et al.*, 1996, Leopold *et al.*, 1998, Miyazawa *et al.*, 1999). Inhibition of endosome acidification results in retention of Ad in endosomes and decreased transgene expression (Greber *et al.*, 1993, Leopold *et al.*, 1998).

Following escape from the endosome, the virion binds to microtubules for migration through the cytosol (Leopold *et al.*, 1998, Suomalainen *et al.*, 1999, Leopold *et al.*, 2000, Suomalainen *et al.*, 2001, Mabit *et al.*, 2002). Ads interact with cytoplasmic dynein, a molecular motor which drives motility along microtubule filaments towards the nucleus of the cell (Kelkar *et al.*, 2004). During this period protein IX (a capsid stabilisation protein) dissociates from the virion capsid (Greber *et al.*, 1993). Ads dissemble from the microtubles before arriving at the microtubule organising centre (Suomalainen *et al.*, 2001, Bailey *et al.*, 2003). At the nuclear membrane, interaction of the virus with nuclear pore complexes leads to hexon dissociation (Greber *et al.*, 1993, Greber *et al.*, 1997, Martin-Fernandez *et al.*, 2004). The viral genome then enters the nucleus through binding to the nuclear pore protein

CAN/Nup214 (Trotman *et al.*, 2001). Ad DNA is imported using the nuclear pore complex receptor CAN/Nup214 and histone H1 (Trotman *et al.*, 2001). The genomes of Ads do not integrate into the cellular DNA and are maintained episomally. Most Ad gene therapy vectors have deleted genes encoding early phase proteins required for the replication of viral DNA to ensure that they are replication-deficient.

1.7.3 *Mechanism of human adenoviral infection after systemic administration* in vivo

The basic mechanism of Ad5 infection *in vitro* is well established. However, the mechanism of Ad5 infection *in vivo* after systemic delivery is less clear. Following intravascular administration, a substantial proportion of the vector is rapidly cleared by Kupffer cells, resident phagocytotic macrophage cells in the liver and part of the innate (non-antigen-specific) immune system (Figure 1.5) (Lieber *et al.*, 1997, Worgall *et al.*, 1997). This interaction does not contribute to Ad5-mediated transduction (Mullbacher *et al.*, 1989, Yang *et al.*, 1994). Accumulation of Ad5 in Kupffer cells leads to rapid Kupffer cell death, within ten minutes of vector administration in mice, due to loss of membrane integrity (Manickan *et al.*, 2006). The dead Kupffer cells gradually disappear from the liver (Schiedner *et al.*, 2003, Manickan *et al.*, 2006), which results in increased transduction of the liver and other organs. The remaining Ad5 selectively accumulates within and transduces the hepatocytes of the liver (Huard *et al.*, 1995, Connelly, 1999, Parker *et al.*, 2006, Waddington *et al.*, 2007, Kalyuzhniy *et al.*, 2008, Waddington *et al.*, 2008).

Many attempts have been made to retarget Ad vectors to reduce uptake by the liver and spleen and selectively target alternative sites to allow treatment of diseased tissues. The ability to selectively target treatment sites could increase the safety and efficiency of the vectors and also increase the therapeutic index, as a reduced dose of the vector would be required. As Ads use an airborne infection mechanism naturally, the cellular interactions with the capsid and subsequent entry pathways by modified Ad vectors in the artificial blood-borne environment needs to be fully elucidated before Ads can be effectively used as gene therapy vectors.

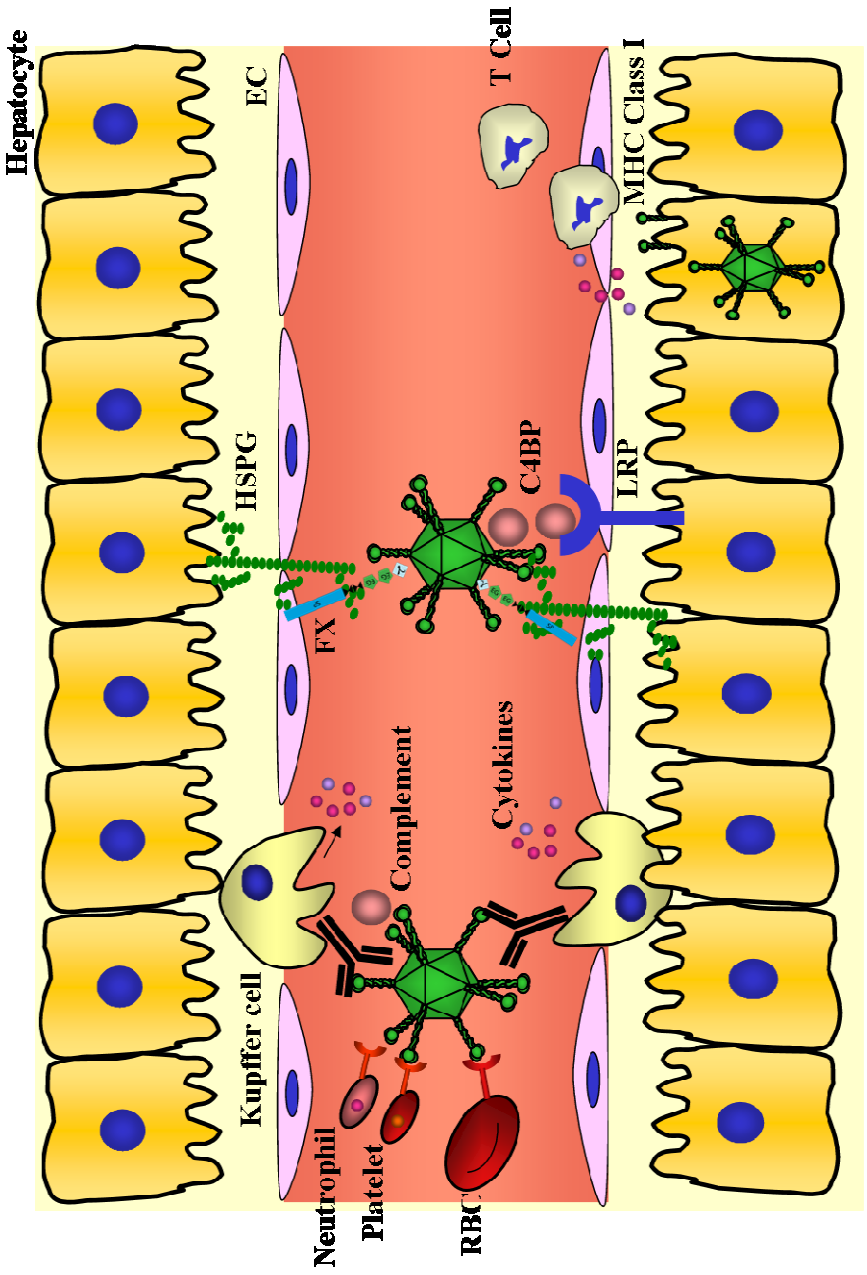

Figure 1.5 – Interactions of Ad5 after intravascular administration.

Following intravascular administration, Ad5 interacts with red blood cells (RBC), platelets, complement proteins, blood coagulation factors (including FX) and antibodies. Some of these interactions lead to subsequent binding to a variety of receptors, including HSPGs and LRP. A substantial proportion of the Ad5 is rapidly cleared by Kupffer cells. Generated by Dr. S.A. Nicklin, University of Glasgow, UK.

1.7.4 Adaptive tropism by fiber modification

The majority of attempts to retarget Ad5 away from the liver and spleen involved modification of the fiber and/or penton proteins of the viral capsid. The alterations to the fiber broadly included either mutation of the Ad5 fiber or pseudotyping (replacement of the Ad5 fiber protein with a fiber from another Ad) (reviewed by Nicklin *et al*. (Nicklin *et al.*, 2005)). Initial studies focused on residues in the fiber knob domain which had been identified as critical for binding to CAR (Bergelson *et al.*, 1997, Roelvink *et al.*, 1999). *In vitro*, a CAR-binding ablated vector (AdKO1) reduced infectivity by 99% relative to non-modified Ad5 (Jakubczak *et al.*, 2001). Modification of these residues to ablate the interaction between the fiber knob and CAR, either singularly or in combination with deletion of the RGD motif in the penton base, ablated the *in vitro* tropism of the vectors but there was no difference in liver transduction in C57BL/6 mice (Alemany and Curiel, 2001, Smith *et al.*, 2002, Martin *et al.*, 2003). There was also no difference in liver sequestration by AdKO1, AdPD1 (ablated α_v-integrin interaction) and Ad5 one hour after systemic administration of the vectors in mice (Di Paolo *et al.*, 2009b). However, other studies have shown that CAR ablation in combination with deletion of the RGD motif results in a significant reduction in liver targeting in mice (Einfeld *et al.*, 2001, Koizumi *et al.*, 2003).

Investigation into the differences between *in vitro* and *in vivo* transduction profiles by modified vectors has also been performed in rats. Five days after infusion of vectors into WKY rats pre-treated with a protocol to block Ad clearance by Kupffer cells, AdKO1 or AdPD1 did not produce different levels of liver transduction in comparison to control Ad5 (Nicol *et al.*, 2004). However, WKY rats infused with AdKO1PD1, an Ad5 vector with ablated CAR and α_v-integrin binding sites, showed a 99% reduction in liver transduction compared to Ad5 (Nicol *et al.*, 2004). In addition to the clear species differences for these vectors between mice and rats, there was also a difference between rat strains. In Brown Norway and Sprague-Dawley rats, AdKO1PD1 mediated a modest 30% reduction in liver transduction, indicating an important strain-strain variation exists (Nicol *et al.*, 2004). Although AdPD1 vectors show reduced liver targeting in some studies, the further use of

vectors with α_v-integrin binding ablated vectors (AdPD1 or Ad5ΔRGD) as a gene therapy vector is probably limited.

In vitro, Ad5ΔRGD showed a 60% reduction in internalisation at five minutes and overall significantly slower internalisation kinetics compared to Ad5 (Shayakhmetov *et al.*, 2005a). The kinetics of endosomal escape by Ad5ΔRGD was also shown to be significantly slower compared to Ad5 (Shayakhmetov *et al.*, 2005a). Therefore, Ad5 requires the ability to bind integrins for efficient internalisation and endosomal escape to produce efficient cellular transduction. Consequently, low levels of transduction are likely with AdPD1/Ad5ΔRGD and the use of this vector for gene therapy applications is limited. However, the RGD motif has been shown to partly mediate liver sequestration of intravenously administered Ad5 (Di Paolo *et al.*, 2009b). Interactions of the RGD motif and liver sinusoidal ECs and hepatocytes leads to virus retention in the space of Disse (Di Paolo *et al.*, 2009b). Recently, the RGD motif of Ad5 was also shown to be partly responsible for activation of the innate immune system in mice (Di Paolo *et al.*, 2009a). After systemic administration, Ad5 binds to β_3 integrins on splenic macrophages triggering production of interleukin-1α (IL-1α) (Di Paolo *et al.*, 2009a). Production of IL-1α was significantly reduced in mice administered with Ad5ΔRGD (Di Paolo *et al.*, 2009a). Therefore, to prevent certain aspects of the liver sequestration and the anti-viral response *in vivo*, RGD motif-deleted vectors are required but their use will reduce viral uptake and activity.

The inconsistencies in the data involving ablation of the CAR and/or α_v-integrin interaction with Ad5 outlined above led to investigation into a putative HSPG binding site in the Ad5 fiber shaft as identified by competition analysis with heparin (Dechecchi *et al.*, 2000, Dechecchi *et al.*, 2001). The HSPG-binding motif, designated by four consecutive amino acids lysine-lysine-threonine-lysine (KKTK) in position 91-94 amino acids in the fiber shaft, is only present in the sub-species C Ads. Mutation of this KKTK sequence to glycine-alanine-glycine-alanine (GAGA) significantly reduced liver transduction by 1000-fold in mice (Smith *et al.*, 2003b) and 57% in rats (Nicol *et al.*, 2004). Additionally, the mutation of the HSPG interaction significantly reduced liver infectivity in non-human primates *in vivo* (Smith *et al.*, 2003a). Moreover, liver transgene expression by a vectors with the

KKTK mutation (designated AdS*) could be significantly reduced further in combination with KO1 and KO1PD1, producing a 99% reduction in liver transduction (Nicol *et al.*, 2004). Further research into the AdS* mutant led to the conclusion that AdS* had a reduced ability to internalise and traffic to the nucleus of the infected cell (Bayo-Puxan *et al.*, 2006, Kritz *et al.*, 2007). This was due to the KKTK motif occurring in the hinge region of the Ad5 fiber and mutation of this produced an inflexible fiber. Although, the vector could still efficiently bind to the cell surface, it was unable to interact with integrins as is necessary to mediate cellular transduction and, as a result, is non-longer considered a viable gene therapy vector candidate (Bayo-Puxan *et al.*, 2006, Kritz *et al.*, 2007).

1.7.5 Adaptive tropism by modification of the HI loop

As CAR- and integrin-binding ablated vectors still displayed high levels of liver tropism, an alternative site for mutagenesis, to increase the selective targeting capacity of Ad vectors, was sought. Many vector targeting studies focussed on exosites of the knob domain, of which the HI loop of the knob domain is the most exposed. Insertion of peptide sequences into the HI loop appear not to effect the overall structure of the fiber shaft or knob domain and, as the HI loop is on the surface of the viral capsid, the inserted peptide sequence is accessible. Insertion of the integrin-binding RGD sequence into the HI loop developed a vector which transduced cells by a CAR-independent mechanism (Dmitriev *et al.*, 1998).

The combination of insertion of a targeting peptide into the HI loop of the vector and ablation of CAR binding led to the development of several Ad vectors which selectively targeted ECs (Nicklin *et al.*, 2001, Nicklin *et al.*, 2004) and VSMCs (Work *et al.*, 2004) *in vitro*. After identification of a novel human EC-binding peptide by phage display (Nicklin *et al.*, 2000), a mutant AdKO1 vector was developed with the EC targeting peptide sequence SIGYPLP inserted into the HI loop (Nicklin *et al.*, 2001). Inclusion of the SIGYPLP peptide sequence in the AdKO1 vector (AdKO1SIG), increased transduction of human umbilical vein endothelial cells (HUVECs) and human aortic endothelial cells (HAECs) by 4.7- and 8.0-fold, respectively, compared to AdKO1 (Nicklin *et al.*, 2001). Transduction by AdKO1SIG was not significantly different from AdKO1 in VSMCs and a hepatocyte

carcinoma cell line, HepG2 (Nicklin *et al.*, 2001). Therefore, SIGYPLP-mediated selective gene transfer to ECs from different vascular beds, with little tropism for other cell types. However, when AdKO1 vectors containing peptide sequences selectively targeted for HUVECs, and which produced similar levels of transduction of HUVECs as control Ad5, were administered systemically *in vivo* into mice it resulted in high levels of liver transduction equivalent to control Ad5 (Nicklin *et al.*, 2001). For one of the peptide-modified AdKO1 vectors, there was a modest increase in transduction of abdominal aorta/vena cava (Nicklin *et al.*, 2001), suggesting improved (but not efficient) retargeting of the vector.

Identification of peptides which selectively targeted VSMCs could lead to the targeting of therapeutic genes chosen to prevent late vein graft failure, which is caused by restenosis or reocclusion of the artery lumen and is a common side effect following coronary artery bypass grafting and angioplasty. VSMCs require high viral titres to achieve transduction by Ad5 due to the low expression of CAR by these cells (Havenga *et al.*, 2001). To improve the transduction efficacy by Ad vectors in VSMCs, the peptide sequence EYHHYNK was inserted into the HI loop of AdKO1 (AdEYH) (Work *et al.*, 2004). EYHHYNK selectively targets VSMCs, as identified by phage biopanning on human saphenous vein (HSV) SMCs, but did not target HSVECs (Work *et al.*, 2004). AdEYH significantly enhanced transduction of HSVSMCs and with a significant reduction in transgene expression in HSVECs compared to control Ad5 (Work *et al.*, 2004).

1.7.6 Adaptive tropism by pseudotyping

Identification of different primary cellular receptors used by Ad viruses and the variation in tropism compared to Ad5 led to the development of pseudotype Ad vectors. Fiber-pseudotype vectors have the hexon and penton from Ad5 with either the full fiber protein or only the fiber knob domain from another Ad. The fibers of the alternative serotypes showed differences to Ad5 in their lack of a CAR binding site but also had differences in the rigidity of the fiber, the length of the fiber shaft and/or the presence of the putative HSPG binding domain. It was hoped that development of pseudotype vectors with a different infection profile *in vitro* to Ad5 would display an alternative tropism *in vivo*.

The majority of research into pseudotype vectors has centred on use of the fiber from sub-species B Ads. The sub-species B Ads use the membrane glycoprotein CD46 as their cellular receptor and not CAR (Gaggar *et al.*, 2003). Therefore, cells which are relatively refractive to infection by Ad5 due to low or no CAR expression, for example SMCs, ECs and many cancer cells, should be efficiently transduced by a sub-species B pseudotype vector via CD46 engagement. This has led to the development of many novel vectors including Ad5/f35, a pseudotype vector consisting of the entire Ad5 virion but with the Ad35 fiber. This vector efficiently transduced haematopoietic cells, which are refractory to Ad5 transduction (Shayakhmetov *et al.*, 2000), thereby providing proof of principle of this technology. "Pseudotype libraries" were subsequently developed to allow screening on cell lines to determine the most efficient fiber for transduction (Havenga *et al.*, 2001, Havenga *et al.*, 2002).

Pseudotype vectors Ad5/f19p and Ad5/f37 demonstrated a striking reduction in hepatic transduction in mouse, rat and human hepatocytes *in vitro* (Denby *et al.*, 2004). These vectors which contain fibers from the sub-species D Ads Ad19p and Ad37, demonstrated less than 1% of the transgene expression achieved by Ad5 (Denby *et al.*, 2004). Both Ad5/f19p and Ad5/f37 vectors produced equivalent and significantly enhanced transduction in HUVECs and HSVSMCs, respectively, compared to Ad5 (Denby *et al.*, 2004). At one hour after systemic delivery of Ad5/f19p and Ad5/f37 in WKY rats, there was 63% and 55% reduction in liver accumulation by the vectors compared to Ad5, respectively, with no detectable vector genomes present five days post-infusion (Denby *et al.*, 2004). Ad5 genomic DNA was still present five days after delivery of the vector (Denby *et al.*, 2004). Importantly, Ad5/f19p and Ad5/f37 produced significantly less liver transduction than Ad5 (Denby *et al.*, 2004). Therefore, the markedly reduced tropism for hepatocytes demonstrated *in vitro* by Ad5/f19p and Ad5/f37 vectors remained after systemic delivery *in vivo*.

As the pseudotype Ad5/f19p demonstrated significantly reduced liver transduction (Denby *et al.*, 2004), it has been further developed to selectively retarget this vector to specific cell types. Phage display in WKY rats identified two peptides, HTTHREP (HTT) and HITSLLS (HIT), which selectively target to the kidney

(Denby *et al.*, 2007). Each of these peptides was then inserted into the HI loop of the Ad5/f19p fiber and the vectors were administered to WKY rats. The peptide-modified vectors produced a significantly higher level of kidney transduction compared to both Ad5 and the control Ad5/f19p vector, which had no peptide insertion (Denby *et al.*, 2007). Moreover, the peptide-modified vectors transduced different groups of cells within the kidney; the glomerulus was transduced by Ad5/f19p-HIT, whereas Ad5/f19p-HTT selectively transduced tubular epithelial cells (Denby *et al.*, 2007). Transduction by either vector was not detected in any non-target organ, including the liver (Denby *et al.*, 2007). Therefore, after intravenous administration, the peptide-modified Ad5/f19p vectors produced efficient and selective transduction of the kidneys. However, most pseudotype vectors showed liver transduction after systemic delivery *in vivo*, consistent with Ad5.

1.7.7 Interaction of adenoviruses with other blood components and blood cells

Human complement component C3 from plasma has been shown to bind to Ad5 (Jiang *et al.*, 2004) (Figure 1.5). In complement C3 knockout mice, a low dose Ad5 ($2.3x10^9$ virus particles(VP)/mouse) produced a 99-fold reduction in hepatocyte transduction three days after administration of the vector, in comparison to transgene expression in non-transgenic control mice (Zinn *et al.*, 2004). However, this was not reproducible at higher doses of Ad5. A dose of $1.5x10^{11}$ VP/mouse produced no significant difference in liver transduction between complement C3 knockout mice and wild-type mice (Kiang *et al.*, 2006). The acute inflammatory response to systemic delivery of Ad was significantly reduced in complement C3 knockout mice (Kiang *et al.*, 2006). The toxicity resulting from injection of Ad5 is characterised by complement activation, cytokine release with the consequent vascular damage leading to a systemic inflammatory response which can be fatal to the host (Schnell *et al.*, 2001, Lozier *et al.*, 2002, Morral *et al.*, 2002, Raper *et al.*, 2003).

The Ad5 fiber has also been shown to interact with human erythrocytes (Nicol *et al.*, 2004, Carlisle *et al.*, 2009, Subr *et al.*, 2009) and platelets (Hofherr *et al.*, 2007, Othman *et al.*, 2007, Stone *et al.*, 2007b) (Figure 1.5). Ad5 agglutinates rat and

human but not mouse erythrocytes, an effect which does not occur in CAR binding ablated vectors indicating involvement of the knob domain (Nicol *et al.*, 2004). Human erythrocytes were shown to express CAR and Ad5 bound to 90% of red blood cells suspended in phosphate buffered saline (PBS) (Carlisle *et al.*, 2009). Binding by Ad5 was prevented in the presence of excess Ad5 fiber protein or an anti-CAR antibody (Carlisle *et al.*, 2009), indicating that the interaction between erythrocytes and Ad5 is CAR-dependent. In plasma, addition of the anti-CAR antibody reduced binding of Ad5 to erythrocytes by less than 25% (Carlisle *et al.*, 2009), indicating other mechanisms of Ad5 binding occur in plasma. The complement receptor (CR1) is also present on human erythrocytes and binds Ad5 in the presence of complement and antibodies (Carlisle *et al.*, 2009). In transgenic mice which express CAR on their erythrocytes, the circulation time of Ad5 was extended and liver transduction was significantly reduced (Carlisle *et al.*, 2009). Therefore, sequestration of Ad5 by erythrocytes restricts Ad5 infection, an effect which could be seen in humans after either natural exposure to Ad5 or during its use as a gene therapy vector. Coating the Ad5 capsid with hydrophilic polymers has been shown to decrease the interaction between Ad5 and erythrocytes from 95% binding by Ad5 to 25% by Ad5 coated with the polymer (Subr *et al.*, 2009).

After intravenous delivery, Ad5 activated platelets and induced platelet-leukocyte aggregation formation in mice (Othman *et al.*, 2007). This suggests a direct interplay between Ad-platelet interaction in blood and subsequent thrombocytopenia, activation of coagulation, endothelial activation and leukocyte infiltration. In humans, 78% of platelets express CAR (Othman *et al.*, 2007), suggesting that human platelets would sequester a large number of CAR-binding Ad vector particles after systemic administration. Additionally, the interaction of Ad vectors and platelets results in vector sequestration by the hepatic reticuloendothelial system (Stone *et al.*, 2007b). Ad5 bound to over 95% of platelets in mice with subsequent accumulation in the liver sinusoids and interaction with Kupffer cells for degradation (Stone *et al.*, 2007b). This would lead to an overall reduction in the concentration of Ad5 reaching its intended target, decreased transduction of target cells and reduced circulation time (Lyons *et al.*, 2006). As higher doses may be required to produce efficacy, dose limiting toxicities would become relevant. Additionally, as Ad5 interacts with human but not murine erythrocytes (Nicol *et al.*, 2004) and 98% of Ad

genomes associated with erythrocytes taken from clinical trial patients (Lyons *et al.*, 2006), this highlights the need for utilisation of appropriate animal models which accurately and reliably predict the interaction of Ad vectors in humans.

1.7.8 Role of blood factors in liver tropism

For gene therapy applications, the goal has been delivery of the vector by minimally invasive intravenous administration with selective gene transfer to the required cell type. However, after intravenous administration Ad5 selectively transduces the liver, as discussed in Section 1.7.3. This tissue tropism does not appear to correlate with CAR expression levels and cellular localisation and cannot be redirected by the ablation of CAR binding (Smith *et al.*, 2003a, Smith *et al.*, 2003b, Nicol *et al.*, 2004, Nicklin *et al.*, 2005), indicating that the presence of or binding to CAR is not necessary for tissue transduction *in vivo*. CAR expression is also restricted to tight junctions between cells (Cohen *et al.*, 2001), which makes it difficult to correlate selective hepatocyte transduction after systemic delivery of Ad vectors *in vivo* if CAR is used as the primary receptor. Additionally, ablation of the integrin-binding RGD motif in the penton base was also largely unsuccessful (Nicklin *et al.*, 2005). This suggested that alternative pathways exist which define liver tropism *in vivo*.

The first convincing study to further investigate the mechanism of Ad5 infection *in vivo* demonstrated that factors in the blood were capable of influencing hepatocyte transduction (Shayakhmetov *et al.*, 2005b). Ad5 and a CAR-binding ablated vector, Ad*F, produced equivalent levels of liver transduction in the presence of blood *in vivo* (Shayakhmetov *et al.*, 2005b). However, when the liver was excluded from the circulation using an *in situ* perfusion model (to allow delivery of the vector in the absence of blood), there was a significant reduction in liver transduction by Ad*F but not by Ad5 (Shayakhmetov *et al.*, 2005b). This indicated that liver transduction *in vivo* was mediated by two mechanisms, one which was CAR-mediated and another CAR-independent mechanism mediated by blood factors. After injection of competing ligands (which included polymerised bovine serum albumin (BSA) to saturate the scavenger receptor SR-BI, asialofetuin to saturate the asialoglycoprotein receptor, human low density lipoprotein (LDL) to saturate the LDL receptor and lactoferrin to saturate LDL receptor-related protein (LRP) as well as HSPGs) for

cellular receptors present in the liver, it was determined that Ad vectors could use either HSPGs or LRP as receptors in the presence of blood factors as transgene expression by Ad*F was reduced 50-fold (Shayakhmetov *et al.*, 2005b) (Figure 1.5). Additionally, infusion of heparinase I (an enzyme which selectively cleaves highly sulphated polysaccharide chains preventing cell surface expression of functional HSPGs) into wild-type mice before administration of the vectors significantly reduced liver transduction by both Ad5 and Ad*F (Shayakhmetov *et al.*, 2005b). This indicates that, in the presence of blood factors, these vectors use HSPGs as their cellular receptors. Tandem mass spectrometry and slot blot assays were used to identify blood factors which bind to the fiber knob domain of Ad5. Human coagulation factor IX (FIX) and complement binding protein (C4BP) bind to the Ad5 fiber knob and addition of the physiological concentration of these proteins returns Ad*F transduction levels in cultured hepatocytes to that of Ad5 (Shayakhmetov *et al.*, 2005b). Mouse livers perfused with Ad*F in the presence of FIX, increased transduction by Ad*F to levels comparable with Ad5 and addition of coagulation factor X (FX) did not improve transgene expression by Ad*F (Shayakhmetov *et al.*, 2005b). However, there was no significant difference in liver transduction by Ad*F in wild type and FIX knockout mice (Shayakhmetov *et al.*, 2005b). This suggests that there is some influence by other blood factors for transduction by Ad5 vectors *in vivo* or possible compensatory mechanisms are activated due to the deficiency of FIX.

1.7.9 FX is responsible for liver transduction

Further work investigating the influence of the vitamin K-dependent blood coagulation factors (FVII, FIX, FX and protein C [PC]) on Ad5 liver transduction led to the finding of a direct, calcium-dependent interaction between Ad5 and FX (Parker *et al.*, 2006). FVII, FIX, FX and PC are homologous serine proteases which are synthesised in the liver and circulate in the plasma as inactive zymogens. They are activated by proteolytic cleavage as part of the coagulation cascade (Gomez and McVey, 2006). Addition of physiological concentration of FIX (5 μg/ml) or FX (8 μg/ml) significantly enhanced transduction of a hepatocyte cell line by AdKO1, a CAR-binding ablated mutant Ad5 (Parker *et al.*, 2006). However, FX was more efficient at enhancing transduction by AdKO1 as there was a substantial difference

in cellular transduction levels, particularly after a short exposure time with the vector (Parker *et al.*, 2006). Importantly, activation of FX was not required to mediate the enhancement in hepatocyte transduction since transduction was equivalent in the presence of both the latent and activated form of FX (Parker *et al.*, 2006).

Coagulation factors FVII, FIX, FX and PC all comprise of a four domain structure: a γ-carboxylated glutamic acid (Gla) domain, an epidermal growth factor-like (EGF1) domain, an EGF2 domain and a globular active site containing a serine protease (SP) domain (Gla-EGF1-EGF2-SP) (Figure 1.6). Addition of physiological concentration of FVII, FIX, FX and PC significantly enhanced transduction by AdKO1 in a hepatocyte cell line, whereas the non-homologous coagulation factors FXI and FXII did not (Parker *et al.*, 2006). This suggests a common approach is responsible for the enhancement of hepatocyte transduction in the presence of FVII, FIX, FX and PC.

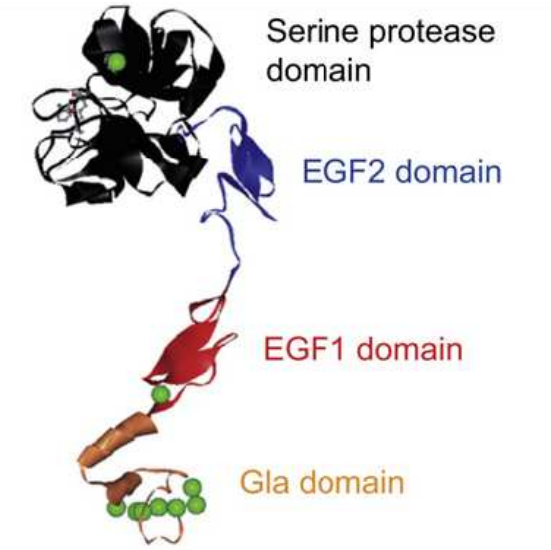

Figure 1.6 – Structure of FX.

FX shares homology with FVII, FIX, FX and PC as all comprise of a four domain structure: a γ-carboxylated glutamic acid (Gla) domain, an epidermal growth factor-like (EGF1) domain, an EGF2 domain and a serine protease (SP) domain (Gla-EGF1-EGF2-SP). Green balls indicate calcium ions. Adapted from Waddington *et al*. (Waddington *et al.*, 2008).

Surface plasmon resonance (SPR) analysis was used to determine whether FX interacts directly with the vectors Ad5 and AdKO1. Ad5 and AdKO1 were injected over a biosensor chip to which FX was covalently bound. Association and dissociation of the vectors can then be determined and kinetic analysis performed. Both Ad5 and AdKO1 bound strongly to FX and with similar affinity constants in a calcium-dependent manner as addition of 3 mM ethylenediamine tetra-acetic acid (EDTA) was required for vector dissociation (Parker *et al.*, 2006).

In an *ex vivo* liver perfusion model, designed to investigate liver transduction by vectors in the absence of blood, addition of physiological concentrations of human FX significantly increased transduction by Ad5 and AdKO1 by 25- and 250-fold, respectively, to equivalent levels of liver transgene expression (Parker *et al.*, 2006). This finding was contrary to previous reports using a similar *in situ* perfusion model (Shayakhmetov *et al.*, 2005b). To assess the effect of FX *in vivo*, a warfarin pre-treatment model was developed. Warfarin prevents the maturation and secretion of functional vitamin K-dependent coagulation factors, specifically by blocking the post-translation modification of the Gla domain by a vitamin K-dependent carboxylase enzyme. The Gla domain will then not fold properly, reducing the level of functional FX circulating in the bloodstream (Zivelin *et al.*, 1993). In mice, injection of Ad5 and AdKO1 results in highly efficient liver transduction but pre-treatment of these animals with warfarin, reduced liver transduction by several orders of magnitude due to blockade of the interaction between vitamin K-dependent coagulation factors and Ad (Parker *et al.*, 2006, Waddington *et al.*, 2007). Pre-infusion of FX into warfarin-treated mice rescued liver transduction by both Ad5 and AdKO1, thus unveiling a novel non-CAR-dependent pathway that regulates Ad5-mediated gene transfer *in vivo* (Parker *et al.*, 2006, Waddington *et al.*, 2007). However, coagulation factors do not affect Kupffer cell uptake or early Ad accumulation (Waddington *et al.*, 2007, Di Paolo *et al.*, 2009b) and warfarin pre-treatment also does not ablate Kupffer cell capacity to trap blood-borne Ad vectors (Waddington *et al.*, 2007, Di Paolo *et al.*, 2009b), indicating that coagulation factors play a pivotal role in the selective transduction of hepatocytes but are not involved in sequestration of Ad vectors by Kupffer cells.

SPR was also used to show that FX can bind directly to Ad5 vectors pseudotyped with the fibers from various sub-species D Ads (Parker *et al.*, 2007). The addition of physiological concentrations of FX significantly increased both binding and transduction by Ad5/f17, Ad5/f24, Ad5/f30, Ad5/f33, Ad5/f45 and Ad5/f47, all fibers from sub-group D Ads, in a hepatocyte cell line, HepG2 (Parker *et al.*, 2007). Transduction by these sub-species D pseudotype vectors was not significantly effected by the addition of FVII and FIX, in contrast to Ad5 and AdKO1/Ad*F, suggesting potential differences in the fiber-coagulation factor interactions (Shayakhmetov *et al.*, 2005b, Parker *et al.*, 2006, Parker *et al.*, 2007). However, consistent with Ad5 and AdKO1/Ad*F, the addition of FX seems to direct the sub-species D pseudotype vectors through HSPGs for transduction *in vitro* (Parker *et al.*, 2007). FX-mediated transduction by Ad5/f17, Ad5/f24, Ad5/f30, Ad5/f33, Ad5/f45 and Ad5/f47 was significantly reduced in the CHO-pgsA745 cell line, compared to CHO-K1 cells (wild-type CHO cells) (Parker *et al.*, 2007). CHO-pgsA745 cells have been genetically modified to be deficient in HSPG polymerisation and, therefore, have no cell surface HSPG expression. This provides further evidence that after interaction with FX, Ad5 and sub-species D pseudotyped Ads use HSPGs as their predominant cellular receptor system. However, this interaction probably does not occur using the putative HSPG binding motif KKTK (identified in the Ad5 fiber shaft), as this is not present in fibers from the sub-species D Ads and AdS* vectors, which have a mutated KKTK motif, and both these groups of vectors bind FX (Kritz *et al.*, 2007). Taken together, these data suggest the presence of a common FX binding site on the fibers from sub-species C and D Ads or the fiber protein is not responsible for binding FX.

In vivo experiments in mice also demonstrated that liver transduction by Ad5/f47 was substantially reduced by warfarin pre-treatment (Waddington *et al.*, 2007). Therefore, *in vivo* coagulation factors affect Ad vectors with sub-species D fibers (Ad5/f47) as well as those with sub-species C fibers (Ad5). These studies indicated that CAR plays little or no role in hepatocyte transduction after systemic delivery of Ad vectors (Shayakhmetov *et al.*, 2005b, Parker *et al.*, 2006, Kritz *et al.*, 2007, Parker *et al.*, 2007, Waddington *et al.*, 2007). Additionally, as coagulation factors are not responsible for the early sequestration of vectors by Kupffer cells, strategies

which deplete Kupffer cells may be required to increase the bioavailability of the vector.

1.7.10 Determination of FX binding site on adenoviral vectors

SPR analysis determined that FX did not bind to the fiber of Ad5 as Ad5 vectors with the knob domain deleted, fiber shaft deletions (Li *et al.*, 2006) or a completely fiberless Ad5 vector (Von Seggern *et al.*, 1999) all bound FX (Waddington *et al.*, 2008). Cell binding by these fiber mutant Ad5 vectors was significantly enhanced in the presence of FX (Waddington *et al.*, 2008), suggesting that FX binds to an alternative Ad5 capsid protein and not the fiber.

By use of purified Ad5 hexon protein, it was determined by SPR that FX bound to the Ad5 hexon in a direct calcium-dependent, high affinity manner (Waddington *et al.*, 2008). SPR analysis of FX mutants containing different components of the FX four domain structure (Gla-EGF1-EGF2-SP) demonstrated that the Gla domain of FX was required for binding to Ad5 (Waddington *et al.*, 2008). This was also confirmed *in vivo* as a Gla-domainless FX variant failed to rescue Ad5-mediated liver transduction in the vitamin K-dependent coagulation factor-ablated warfarin mouse model (Waddington *et al.*, 2008).

By electron cryomicroscopy (cryo-EM), it was possible to determine that FX binds within a central cavity formed by the trimeric hexon proteins of Ad5 and involves interaction with the Ad5 hexon HVRs (Kalyuzhniy *et al.*, 2008, Waddington *et al.*, 2008). A novel mutant Ad5 vector Ad5HVR48 (Roberts *et al.*, 2006), which is the complete Ad5 vector with only the amino acids in the all the HVRs swapped from Ad5 to those from Ad48, was used to ascertain the importance and relevance of this putative hexon:FX interaction. By SPR, Ad48 and Ad5HVR48 did not bind FX and FX did not enhance cellular binding or transduction by either Ad48 or Ad5HVR48 in a number of cell lines (Waddington *et al.*, 2008). *In vivo*, Ad5HVR48 produced a 600-fold reduction in liver transduction in comparison to Ad5 after systemic administration of the vectors (Waddington *et al.*, 2008). *In vivo*, fiber-dependent transduction of the Ad5HVR48 vector and Ad5 was tested by intramuscular injection

into the mouse hind limb to confirm that the Ad5HVR48 vector was viable *in vivo* (Waddington *et al.*, 2008). Transgene expression by Ad5HVR48 was not significantly different to Ad5 (Waddington *et al.*, 2008), thereby demonstrating that Ad5 can utilise alternate virion proteins for transduction when placed into different environments. This also suggests that fiber has no role in binding to FX as Ad5HVR48 has the Ad5 fiber and does not bind FX with a substantial reduction in liver tropism.

To further assess the interaction of Ad5 and FX, an inhibitor was utilised. X-bp is a 29 kDa protein isolated from *Deinagkistrodon acutus* (the hundred pace snake) which binds with high affinity to human and murine FX (Atoda *et al.*, 1998). X-bp blocks the FX-Gla domain-Ad5 interaction and pre-incubation of X-bp with FX *in vitro* totally abolished the FX-mediated enhancement in Ad5 transduction (Waddington *et al.*, 2008). Furthermore, X-bp pre-incubated with FX before administration to warfarinised mice, prevented FX rescue of liver transduction by Ad5 (Waddington *et al.*, 2008). Additionally, in non-warfarinised mice the presence of X-bp substantially reduced Ad5 liver transduction (Waddington *et al.*, 2008). The binding of FX to the Ad5 hexon proteins *in vivo* promotes the interaction of the Ad5-FX complex with cellular HSPGs via the serine protease domain of FX (Waddington *et al.*, 2008). Therefore, it is the use of HSPGs as receptors for the Ad5-FX complex, and not CAR via a direct engagement, which leads to liver transduction after systemic administration *in vivo* (Waddington *et al.*, 2008).

Investigation of the other Ad serotypes found that although the sub-species D pseudotype Ads bind FX (Parker *et al.*, 2007), the sub-species D Ads did not (Waddington *et al.*, 2008). The sub-species D pseudotype Ad5/f47 was also sensitive to warfarin pre-treatment *in vivo* (Waddington *et al.*, 2007), suggesting that binding of FX to the Ad5 hexon leads to efficient liver targeting and is dominant over any other effects produced by the fiber. The majority of previous studies to retarget the virus to alternate cells and organs have focused on fiber by creating and using pseudotype vectors (Havenga *et al.*, 2002, Parker *et al.*, 2007). However, the role of hexon in dictating Ad biodistribution is now clear and is an increasingly relevant target for Ad modification.

1.7.11 Hexon modification to prevent FX binding

Previous research into retargeting of Ad5 liver tropism by modification of the hexon protein focussed on hexon HVR 5 (HVR5) as there was low structural constraint on the insertion of proteins into this area of the capsid (Vigne *et al.*, 1999). Hexon modification to include a ligand specific for α_v integrins in HVR5 (AdHRGD) increased transduction of human VSMCs, which are naturally refractory to infection by Ad5 as they do not express CAR (Vigne *et al.*, 1999). In mice, AdHRGD produced a 98% reduction in liver transduction after systemic administration of the vector, compared to control Ad5 (Vigant *et al.*, 2008).

Ad vectors have also been generated with hexon proteins from other Ad serotypes (Ostapchuk and Hearing, 2001, Alba *et al.*, 2009). The HVR5 of Ad5 was swapped for the HVR5 of Ad2 (another sub-species C Ad, producing AdHAd2) and the sub-species D Ads Ad19 (AdHAd19) and Ad30 (AdHAd30) (Vigant *et al.*, 2008). After intravenous delivery to mice, these three HVR5 mutant vectors produced significantly reduced liver transgene expression (Vigant *et al.*, 2008). Importantly, the HVR5 swap from Ad5 to Ad2, a sub-species C vector which has strong liver tropism as a full serotype vector, did not rescue the reduction in liver transduction compared to control Ad5. AdHRGD and AdHAd2 bound FIX and FX as efficiently as control Ad5 (Vigant *et al.*, 2008). Whereas, AdHAd19 and AdHAd30 had strongly impaired binding of FIX and binding to FX was also decreased, although to a lesser degree (Vigant *et al.*, 2008). However, the addition of FX did not significantly enhance transduction *in vitro* by any of the HVR5 modified vectors (Vigant *et al.*, 2008). This suggests that HVR5 of the hexon protein is responsible for binding to FX.

Therefore, it was known that the HVRs were important in FX binding as hexon modified vectors, including Ad5HVR48 and AdHRGD, showed reduced FX binding (Vigant *et al.*, 2008, Waddington *et al.*, 2008). However, it was not known exactly which of the seven HVRs present in the hexon protein were required for the interaction with FX. Cryo-EM images at 40 Å resolution suggested that the FX density was in close proximity to HVR3, HVR5 and HVR7 of Ad5 (Kalyuzhniy *et al.*, 2008). High resolution cryo-EM images at less than 26 Å identified the HVR5

and HVR7 domains as areas potentially key for FX binding (Waddington *et al.*, 2008). Putative contact residues involved in FX binding were determined in the hexon protein and the amino acid residue glutamic acid (E) in position 451, which is conserved in all Ad serotypes that bind FX but is replaced by glutamine (Q) in Ads that do not bind to FX (Waddington *et al.*, 2008, Alba *et al.*, 2009).

For further interrogation into the precise HVRs involved in binding FX, Ad5 vectors were engineered which contained the HVRs of Ad5 exchanged for the HVRs of Ad26, a sub-species D Ad which does not bind FX (Waddington *et al.*, 2008, Alba *et al.*, 2009). Ad5 vectors were produced with the HVR5 swapped [Ad5HVR5(Ad26)], HVR7 swapped [Ad5HVR7(Ad26)] and both HVR5 and HVR7 swapped [Ad5HVR5+7(Ad26)] for that of Ad26 (Alba *et al.*, 2009). SPR analysis showed that Ad5HVR5(Ad26) had substantially reduced FX binding, whereas FX binding to Ad5HVR7(Ad26) and Ad5HVR5+7(Ad26) was completely abolished, equivalent to Ad26 (Alba *et al.*, 2009). *In vitro*, binding and transduction of SKOV-3 cells was significantly reduced by all three vectors (Alba *et al.*, 2009). The addition of physiological concentrations of FX did not affect binding and transduction by Ad5HVR7(Ad26) and Ad5HVR5+7(Ad26), whereas Ad5HVR5(Ad26) was affected by the presence of FX but this was reduced compared to control Ad5 (Alba *et al.*, 2009). *In vivo*, all vectors showed substantially reduced liver transduction in comparison to Ad5 after intravenous administration in mice (Alba *et al.*, 2009). Therefore, HVR5 and HVR7 of Ad5 are essential for FX binding. However, it was found that the Ad5HVR5(Ad26) and Ad5HVR5+7(Ad26) mutations prevented maturation of the vectors as they showed reduced capacity to transduce cells via the fiber-dependent CAR-binding pathway *in vitro* (Alba *et al.*, 2009).

To prevent alteration of the integrity of the virus capsid proteins, point mutations of the amino acid residues in HVR5 and HVR7 of the Ad5 hexon, thought to be directly involved in binding to FX, were performed. In combination with the point mutations to the HVRs and alone, the amino acid E451 (which is in HVR7) was changed to Q, the residue present in all non-FX binding serotypes (Alba *et al.*, 2009). Modification of key amino acids in HVR7 completely ablated FX binding and the E451Q mutation showed decreased binding to FX (Alba *et al.*, 2009). All point mutations demonstrated reduced *in vitro* cell binding and transduction, and

liver transduction *in vivo* was also markedly reduced compared to Ad5 (Alba *et al.*, 2009). Therefore, this study ascertained not only the regions of the Ad5 hexon which bound FX but determined specific amino acid residues responsible for this interaction.

1.7.12 Host immune reactions

After administration of Ad vectors, a variety of anti-viral host immune reactions are produced. Recognition of viral components by host pattern-recognition receptors (PRRs) induces the anti-viral innate immune response (Janeway and Medzhitov, 2002). Kupffer cells in the liver and other macrophages rapidly sequester the vectors (Lieber *et al.*, 1997, Worgall *et al.*, 1997) (Figure 1.5). Additionally, macrophages in the spleen can trigger an IL-1α-mediated response to vectors containing the RGD motif (Di Paolo *et al.*, 2009a).

There is a broad prevalence of Ad5-specific neutralising antibodies in the population (Christ *et al.*, 1997, Sprangers *et al.*, 2003, Vogels *et al.*, 2003, Sumida *et al.*, 2005, Abbink *et al.*, 2007, Parker *et al.*, 2009). These are naturally occurring antibodies associate with the virus capsid and prevent transduction *in vivo* (Kuriyama *et al.*, 1998, Stallwood *et al.*, 2000, Sprangers *et al.*, 2003). Interaction with neutralising antibodies then leads to rapid clearance of the virus (Christ *et al.*, 1997). Therefore, the adaptive immune system poses a barrier to the use of gene therapy vectors. Polyethylene glycol (PEG) and the hydrophilic polymer HPMA have been used to coat the adenoviral capsid to physically shield the vector from being recognised by both antibody-mediated and innate immune system but this has led to a reduction in the efficiency of transduction by the vector (Croyle *et al.*, 2005, Eto *et al.*, 2005, Mok *et al.*, 2005, Carlisle *et al.*, 2009). However, one study has shown that PEG modification of Ad5 prevented interaction of the vector with platelets and blood cells, attenuating the threat of thrombocytopenia, coagulation and spenomegaly seen with control Ad5, and did not show a reduction in liver transduction in mice (Hofherr *et al.*, 2007).

Ad5 also can produce an overall toxicity profile at high doses which has led to a well publicised fatality (Raper *et al.*, 2003). Activation of the immune system due to

interaction of Ad5 with both antibodies and the complement system can lead to cytokine release, resulting systemic inflammatory response syndrome which can be fatal to the host (Schnell *et al.*, 2001, Lozier *et al.*, 2002, Morral *et al.*, 2002, Raper *et al.*, 2003). Additionally, the recently terminated STEP trial, which was a vaccination study in the clinic for HIV, suggested that Ad5-based strategies may enhance infection rates in subjects with pre-existing antibodies (Perreau *et al.*, 2008). However, this has been recently refuted (Hutnick *et al.*, 2009, O'Brien *et al.*, 2009). A better understanding of the basic virus:host interactions will enable the generation of safer vectors more suited to intravenous administration with greatly improved targeting capacity and dose limiting toxicities.

1.7.13 Future of gene therapy with adenoviruses

Although the mechanism of infection by Ad5 *in vitro* and *in vivo* is now known, the effective use of Ad5 vectors is, however, severely hampered by a number of problems. Local delivery of Ad vectors often eliminate or substantially restrict the dissemination of the vector to distant, non-target sites as the vector has not been exposed to the bloodstream. However, leakage can occur and accumulation of vectors in other non-target organs, especially the liver, is an important constraint on safety (Wang *et al.*, 2003).

Therefore, the future of systemic, non-hepatic gene therapy should be based on Ad5 vectors designed to block the hexon-FX interaction or focus on Ads that offer no FX interaction and have a low seroprevalance with respect to pre-existing antibodies in the human population (Roberts *et al.*, 2006, Abbink *et al.*, 2007). This would allow intravenous administration of gene therapy vectors without liver tropism, due to the FX interaction, and with possibly reduced toxic effects. Additionally, the liver de-targeted vectors could be retargeted to selected cells and tissues, potentially realising one of the goals of gene therapy; the targeted and selective use of oncolytic Ads to eliminate metastatic disease.

1.8 Aims of thesis

The principle aim of this thesis was to investigate means of producing targeted delivery of biological agents, which includes both peptides and gene delivery systems (recombinant adenoviral vectors). This was divided into two separate studies: targeting an anti-oxidant to the vasculature to improve its potential and the investigation of the influence of blood coagulation FX on *in vivo* targeting by Ad35 and chimeric Ad5/Ad35 vectors. This was achieved through the following techniques:

- *In vitro* and *in vivo* evaluation of candidate vascular and cardiac targeting peptides through phage display for cardiac-specific endothelial markers in the stroke prone spontaneously hypertensive rat (SHRSP).

- Comparison of the benefit of vascular targeting the anti-oxidant peptide gp91ds *in vivo* in the SHRSP.

- Evaluation of the interaction between Ad35 and blood coagulation FX.

- Evaluation of the influence of FX on binding, internalisation, trafficking and transduction of Ad35 and chimeric Ad5/Ad35 vectors *in vitro*.

- Evaluation of the influence of FX on specific organ targeting by Ad35 and chimeric Ad5/Ad35 vectors *in vivo* in CD46 transgenic mice.

CHAPTER 2

Materials and Methods

2.1 Materials

2.1.1 Chemicals

All chemicals, unless otherwise stated, were obtained from Sigma-Aldrich (Poole, UK) and were of the highest grade obtainable. All cell culture reagents were obtained from Gibco (Paisley, UK) unless otherwise stated. Dulbecco's calcium and magnesium free phosphate buffered saline (PBS) was obtained from Lonza (Basal, Switzerland). Peptides were synthesised by and obtained from Peptide 2.0 (Chantilly, VA, USA).

2.2 Methods

2.2.1 Tissue culture

All tissue culture was performed in sterile conditions using biological safety class II vertical laminar flow cabinets. Cells were grown in 37°C incubators maintained at 5% CO_2, 95% air. Cell lines and media used are detailed in Table 2.

2.2.2 Maintenance of established cell lines

Cells were grown as a monolayer and media was replenished every 3-4 days. Cells were routinely passaged at approximately 80% confluence to prevent overgrowth and loss of surface contact. To passage, cells were washed twice in PBS and incubated in 3 ml of trypsin-ethylenediamine tetra-acetic acid (trypsin-EDTA, Gibco, Paisley, UK) for approximately 5 minutes at 37°C or until the majority of the cells had detached from the flask. The action of trypsin-EDTA was then prevented by the addition of 5 ml complete media. Cells were pelleted by configuration at 1500 rpm for 5 minutes and resuspended in complete media for passaging or plating. Before plating cells were counted using a haemocytometer to ensure the required seeding density.

Table 2 – Cell lines and media used.

Cell Type	Description	Composition of Cell Culture Media Used
CHO-BC1 CHO-BC2 CHO-C1 CHO-C2 CHO-WTR	Chinese hamster ovary cells stably transfected with an isoform of human CD46 or control plasmid (gift from Prof. J. Atkinson, Washington University School of Medicine, St Louis, MO, USA)	Dulbecco's Modified Eagle Medium (DMEM)/F-12 media supplemented with 10% (v/v) fetal calf serum (FCSPAA Laboratories, Yeovil, UK), 2 mM L-glutamine, 1% (v/v) penicillin, 100 µg/ml streptomycin and 500 µg/ml geneticin (G-418).
MDA-MB-435	Human breast ductal carcinoma cell line (National Institutes of Health [NIH])	RPMI 1640 media supplemented with 10% (v/v) fetal calf serum, 2 mM L-glutamine, 1% (v/v) penicillin, 100 µg/ml streptomycin, 250 µg/ml amphotericin B (fungizone) and 0.01 mg/ml gentamicin.
RGE	Rat glomerular endothelial cell line (Deutsche Sammlung von Mikrooganismen and Zellkulluren GmbH [DSMZ, Braunschweig, Germany])	DMEM supplemented with 10% (v/v) fetal calf serum, 2 mM L-glutamine, 1% (v/v) penicillin and 100 µg/ml streptomycin.
SKOV-3	Human ovary adenocarcinoma cell line (NIH)	RPMI 1640 media supplemented with 10% (v/v) fetal calf serum, 2 mM L-glutamine, 1% (v/v) penicillin, 100 µg/ml streptomycin, 250 µg/ml amphotericin B (fungizone) and 0.01 mg/ml gentamicin.
T-47D	Human breast ductal carcinoma cell line (NIH)	RPMI 1640 media supplemented with 10% (v/v) fetal calf serum, 2 mM L-glutamine, 1% (v/v) penicillin, 100 µg/ml streptomycin, 250 µg/ml amphotericin B (fungizone) and 0.01 mg/ml gentamicin.

2.2.3 Cryo-preservation and recovery of cultured cell lines

Cells were harvested as described above and resuspended in 2 ml complete media supplemented with 10% dimethyl sulphoxide (DMSO) per T-150 cell culture flask of cells (5% DMSO for cancer cell lines). 1 ml of the cell suspensions was aliquoted into cryo-preservation vials and cooled at a constant -1°C/minute to -80°C using isopropanol. Vials were then stored indefinitely in liquid nitrogen. Cryo-preserved cells were recovered by thawing at 37°C and then adding them drop-wise to 10 ml complete media. Cells were then pelleted by configuration at 1500 rpm for 5 minutes and resuspended in complete media and added to a T-25 cell culture flask. Cells were incubated overnight at 37°C and the media changed the following day.

2.3 Determination CAR and CD46 level of cell lines

The three cancer cell lines used in this study, MDA-MB-435, SKOV-3 and T-47D, were identified and obtained from the NCI60 database (http://dtp.nci.nih.gov). This database also provides information on the relative levels of molecular targets expressed by these cancer cell lines. CAR and CD46 RNA and protein expression levels were confirmed by TaqMan quantitative PCR (qPCR) and western blotting, respectively.

2.3.1 RNA extraction

Total RNA was extracted from the cancer cell lines using the RNeasy Mini Kit (QIAGEN, Crawley, UK) as per manufacture's instructions. Briefly, one T-150 cell culture flask of cells was trypsinised as described and cells were pelleted by configuration at 1500 rpm for 5 minutes. 600 µl buffer RLT was added to the cell pellet and vortexed to disrupt the cells. Buffer RLT contains guanidine isothiocyanate which immediately inactivates RNases to ensure isolation of intact RNA. To ensure complete homogenisation of the sample, it was also passed through a blunt 20-gauge needle five times. 600 µl 70% ethanol was added to the lysates to ensure ideal binding conditions. 700 µl of the lysate was loaded onto the RNeasy

Spin Column. Samples were centrifuged at 8000 x g for 15 seconds at room temperature to allow the RNA to bind to the silica-gel membrane of the spin column. This was repeated until the entire lysate had been added to the spin column. The spin column was then washed with 700 µl buffer RWT and centrifuged at 8000 x g for 15 seconds at room temperature. This was followed by two wash steps with 500 µl buffer RPE, the first wash centrifuged at 8000 x g for 15 seconds at room temperature and the second wash centrifuged at 8000 x g for 2 minutes at room temperature. Finally the RNA was eluted in 30 µl RNase-free water by centrifugation at 8000 x g for 1 minute. The eluted RNA was then passed through the spin column again to increase the RNA yield. The quantity of RNA in each sample was quantified by NanoDrop (ND-1000 spectrophotometer [Labtech International, Ringmer, UK]).

2.3.2 DNase treatment of RNA

DNase digestion is required for RNA applications which are sensitive to DNA contamination (e.g. qPCR analysis). DNase treatment of RNA samples was performed using the TURBO DNA-free™ (Ambion, TX, USA). For a 40 µl RNA sample, 4.5 µl 10 x TURBO DNase Buffer and 1 µl TURBO DNase (2 U/µl) was added. After incubation at 37°C for 30 minutes, 5 µl DNase inactivation reagent was added and incubated for 2 minutes at room temperature. The sample was then centrifuged at 13000 rpm for 2 minutes at room temperature and supernatant kept as a DNA-free RNA sample, stored at - 80°C.

2.3.3 cDNA synthesis

One µg RNA was used to synthesis cDNA using Advantage RT-for-PCR Kit (Clontech, CA, USA) as per manufacture's instructions. Briefly, 1 µg RNA samples were diluted to a total volume of 12.5 µl and 1 µl random hexamer primer was added. Samples were then incubated at 70°C for 2 minutes before placing the samples on ice. To each RNA sample, 4 µl 5 x reaction buffer, 1 µl dNTP mix (10 mM each), 0.5 µl recombinant RNase inhibitor and 1 µl MMLV reverse transcriptase was added and mixed by pipetting. The samples were incubated at 42°C for 1 hour

to allow cDNA synthesis to occur and then heated to 94°C for 5 minutes to stop the cDNA synthesis reaction and to destroy any DNase activity.

2.3.4 TaqMan qPCR

TaqMan qPCR was used to quantify the relative concentration of CAR and CD46 RNA present in each of the cancer and CHO cell lines. This quantitative measurement is based on the detection of a fluorescent signal produced proportionally during amplification of a PCR product. The amount of fluorescence released during the amplification cycle is proportional to the amount of product generated in each cycle and can be measured directly. Acquisition of data occurs when PCR amplification is in the exponential phase. The Power SYBR Green detection system (Applied Biosystems, Warrington, UK) was used. Power SYBR Green PCR master mix with 300 nM CAR or CD46 primers (CAR: forward 5'-CTCCAAAGAGCCGTACGTCC-3' and reverse 5'-AGTCTTGGAATATCCTTC-CATGTTG-3', CD46: forward 5'-TTGCTGTTGATTGTACCAAGGG-3' and reverse 5'-ACTGCTTGGCTAAGGGACTCAG-3') were used to amplify CAR or CD46 cDNA. The following conditions were used: denaturation – 95°C for 10 minutes; amplification – 95°C for 15 seconds; annealing – 60°C for 1 minute (repeated for 50 cycles); dissociation – 95°C for 15 seconds, 60°C for 15 seconds and 95°C for 15 seconds. CT values were used to ascertain the levels of CAR and CD46 present in the cell lines relative to each other.

2.3.5 Western blotting

To determine the relative expression levels of CAR and CD46 in the cancer cell lines, sodium dodecyl sulphate polyacrylamide gel electrophoresis (SDS-PAGE) and western blotting were performed. To separate the two isoforms of CD46, which are 56 and 66 kDa, respectively, and CAR, which is a 46 kDa protein, reducing conditions and a 12% polyacrylamide gel (containing 40% (v/v) polyacrylamide (30%), 11.25 mM Tris pH 8.8, 0.1% (v/v) SDS, 300 µl ammonium persulphate (APS) and 30 µl N,N,N′,N′-tetramethylethylenediamine (TEMED)) were used.

Cells were harvested and lysed in 0.2% triton X-100. Samples were also freeze/thawed and passed through a blunt 20-gauge needle five times to produce complete lysis of the cells. Protein concentration was determined by bicinchoninic acid (BCA) assay (Perbio Science, Cramlington, UK) as described below (Section 2.3.5.1). Protein samples were diluted to the same concentration in a total volume of 50 µl and mixed with 2 x reducing loading dye (125 mM Tris pH 6.8, 4% (v/v) SDS, 10% (v/v) glycerol, 0.006% (w/v) bromophenol blue and 2% (v/v) β-mercaptoethanol). The samples were then heated to 95°C for 5 minutes before loading onto the gel. 40 µl rainbow ladder (Amersham Bioscience UK Ltd, Buckingham, UK) was also added to the gel as a marker of protein size. Samples were electrophoresed at 200 V in running buffer (0.025 M Tris-HCl, 0.2 M glycine, 0.001 M SDS) for approximately 6 hours to achieve separation of the CD46 isoforms on the gel.

Proteins were transferred onto Hybond-P membrane (Amersham Bioscience UK Ltd, Buckingham, UK) overnight at 0.9 mAmps at 4°C in transfer buffer (0.025 M Tris, 0.2 M glycine, 20% (v/v) methanol, 0.01% (v/v) SDS). The membrane was then blocked in 10% (w/v) fat-free milk powder in TBS-T (150 mM NaCl, 50 mM Tris, 0.1% (v/v) Tween-20) for 2 hours with shaking. The membrane was incubated for 1 hour at room temperature with a 1:500 dilution in blocking solution of either the anti-CD46 antibody (H-294 clone; Santa Cruz Biotechnology Inc., Santa Cruz, CA, USA) or the anti-CAR antibody (RmcB clone; Upstate, Lake Placid, NY, USA). The membrane was washed by two 5 minute washes in blocking solution before addition of the secondary antibodies. A 1:2000 dilution of swine anti-rabbit horseradish peroxidase (HRP) antibody (Dako, Denmark) in blocking solution was used for the anti-CD46 membrane and a 1:1000 dilution of rabbit anti-mouse HRP antibody (Dako, Denmark) was used for the anti-CAR membrane. Both secondary antibodies were incubated with the membrane for 1 hour at room temperature. The membrane was then washed with four 15 minute washes in blocking solution with an addition two 15 minute washes with TBS-T. Proteins were visualised using enhanced luminol-based chemiluminescent (ECL) detection system (Amersham Bioscience UK Ltd, Buckingham, UK) as per the manufacture's instructions. Briefly, equal quantities of the two solutions from the ECL kit were mixed and poured onto the membrane. After one minute, the excess ECL was drained off and

films were exposed for overnight to determine the presence of the CD46 or CAR proteins.

2.3.5.1 Determination of protein concentration

Protein concentrations of the cell lysates were quantified by BCA assay (Perbio Science, Cramlington, UK) as per the manufacture's instructions. A standard curve was generated using dilution of bovine serum albumin (BSA) ranging from 2000 μg/ml to 25 μg/ml. PBS was used as the blank control. 200 μl of BCA working reagent was added to 25 μl of the cell lysate or standard in duplicate in a 96-well plate. The plate was then incubated at 37°C for 30 minutes. The absorbance was measured at 570 nm using a Wallac VICTOR^2 plate reader (Wallac, Turku, Finland).

2.4 Administration of fluorescently-labelled peptides to RGE cells

RGE cells were seeded in 96-well plates at a seeding density of 1x10^4 cells/well and incubated overnight at 37°C to produce 70-80% confluence. Peptides were added to the cells in concentrations ranging from 1 – 100 μmol/l in 300 μl of complete media. Peptides were allowed to incubate with the cells at 37°C for 10 minutes. The cells were washed with PBS and complete media was added so that images could be taken using a fluorescence microscope.

2.5 Preparation of plasmid DNA

An ampicillin containing agar plate was streaked with bacteria containing the plasmid DNA to be amplified from a glycerol stock and incubated overnight at 37°C. A single colony was then picked from the plate and used to inoculate a starter culture of 10 ml luria broth (LB) containing ampicillin. The starter culture was incubated in an orbital shaker for 8 hours at 37°C and 180 rpm. The cloudy starter culture was then added to 500 ml LB in a 2 l flask and incubated in an orbital shaker overnight at 37°C and 180 rpm. The bacterial cells were harvested by centrifugation at 6000 x g for 15 minutes at 4°C.

The plasmid DNA was extracted from the bacteria using the Plasmid Maxi Kit (QIAGEN, Crawley, UK) as per manufacture's instructions. Briefly, the bacterial pellet was re-suspended in 10 ml of the lysis Buffer P1. Buffer P1 contains Tris and EDTA. EDTA chelates divalent metals (primarily magnesium and calcium). Removal of these cations destabilises the cell membrane, producing lysis of the bacterial cells, and also inhibits DNases. In addition, Buffer P1 also contained RNase A (a ribonuclease to degrade RNA). 10 ml of Buffer P2 was added, the solution mixed thoroughly by inverting 4-6 times and incubated at room temperature for 5 minutes. Buffer P2 contains sodium hydroxide and SDS. SDS is a detergent which produces holes in the cell membranes and sodium hydroxide loosens the cell walls. This results in release of plasmid DNA and sheared cellular DNA from the cells. Sodium hydroxide also denatures the DNA, producing linearisation of cellular DNA and separation and the strands are separated. As plasmid DNA is circular, it remains topologically constrained. 10 ml of Buffer P3 was added (chilled to 4°C), the solution mixed thoroughly by inverting 4-6 times and incubated on ice for 20 minutes. Buffer P3 was a neutralisation buffer containing potassium acetate and allows precipitation of genomic DNA, proteins, cell debris and KDS (combination of acetate and SDS). The circular plasmid DNA is also allowed to renature. The solution was then centrifuged at 20000 x g for 30 minutes at 4°C and the supernatant containing the plasmid DNA was removed. A QIAGEN-tip 500 was equilibrated by addition of 10 ml Buffer QBT. The column was allowed to empty by gravity flow. The supernatant was applied to the anion-exchange QIAGEN-tip and allowed to enter the resin by gravity flow where the plasmid DNA selectively binds under low-salt and pH conditions. The QIAGEN-tip was then washed twice with 30 ml Buffer QC, which was a medium-salt wash to remove RNA, proteins, metabolites and other low-molecular-weight impurities. The plasmid DNA was then eluted from the QIAGEN-tip by addition of 15 ml Buffer QF, a high-salt buffer. As DNA is negatively charged, the addition of salt masks the charges and allows DNA to precipitate. The plasmid DNA was then concentrated and desalted by isopropanol precipitation. 10.5 ml of isopropanol was added to the plasmid DNA and centrifuged immediately at 15000 x g for 30 minutes at 4°C. The supernatant was then removed, the pellet washed by addition of 5 ml 70% (v/v) ethanol and centrifuged at 15000 x g for 10 minutes. The supernatant was removed and the

pellet air-dried for 5-10 minutes. The plasmid DNA was then re-dissolved in 200 µl TE buffer before quantification of yield by NanoDrop.

2.6 Transfection methods

Transfection of peptide receptor plasmids into RGE cells was performed using either Lipofectamine™ 2000 Transfection Reagent (Invitrogen, Carlsbad, CA, USA) or FuGENE® 6 Transfection Reagent (Roche Applied Science, Indianapolis, IN, USA) as per the manufacture's instructions and briefly described below. Transfection procedures were optimised in RGE cells using an enhanced green fluorescent protein (eGFP) expression plasmid, which would allow determination of transfected cells after viewing with a fluorescence microscope.

2.6.1 Transfection optimisation using Lipofectamine™ 2000

Lipofectamine™ 2000 reaction complexes were generated with a DNA (µg) to Lipofectamine™ 2000 (µl) ratio of 1:1, 1:2, 1:3 and 1:4 in Opti-MEM® I serum free media. 2 µg DNA was diluted in 50 µl of Opti-MEM® I serum free media and mixed gently by pipetting. In a separate Eppendorf, 2, 4, 6 or 8 µl Lipofectamine™ 2000 was diluted in 50 µl of Opti-MEM® I serum free media and incubated at room temperature for 5 minutes. The diluted DNA and diluted Lipofectamine™ 2000 were combined and incubated at room temperature for 20 minutes. Lipofectamine™ 2000 only, DNA only and no transfection complex controls were also performed.

2.6.2 Transfection optimisation using FuGENE® 6

FuGENE® 6 reaction complexes were generated with a DNA (µg) to FuGENE® 6 (µl) ratio of 1:1, 2:3, 1:2 and 2:9 in Opti-MEM® I serum free media. 2 µg DNA was diluted in 20 µl of Opti-MEM® I serum free media and mixed gently by pipetting. In an Eppendorf, 2, 3, 6 or 9 µl FuGENE® 6 was diluted in 100 µl of Opti-MEM® I serum free media and incubated at room temperature for 5 minutes. The media must be added to the tubes first to prevent interaction between the plastic tube and FuGENE® 6. The diluted DNA and diluted FuGENE® 6 were combined and

incubated at room temperature for 45 minutes. FuGENE® 6 only, DNA only and no transfection complex controls were also performed.

2.6.3 Transfection of RGE cells

RGE cells were seeded in 12-well plates at a seeding density of $1.5x10^5$ cells/well and incubated overnight at 37°C to produce 70% confluence. Transfection protocol was performed with receptor expression plasmids. Cells were washed with PBS and 500 µl Opti-MEM® I serum free media was added to each well. The transfection reagent and plasmid DNA reaction mixtures were added to individual wells and mixed by gently by rocking the plate back and forth. After 4-6 hours, 2 ml complete media was added to the cells. The cells were then left overnight before the media was changed and 48 hours after addition of transfection reagent reaction mixture the presence of transgene expression was determined. Subsequent transfection experiments were performed with a 1:1 ratio of DNA to Lipofectamine™ 2000.

2.6.3.1 Administration of fluorescent-labelled peptides to transfected RGE cells

RGE cells were seeded in 96-well plates at a seeding density of $1x10^4$ cells/well and incubated overnight at 37°C to produce 70-80% confluence. 50 µM peptides were added to the cells in 300 µl of complete media. Peptides were allowed to incubate with the cells at 37°C for 10 minutes. The cells were washed with PBS and complete media was added so that images could be taken using a fluorescence microscope.

2.7 Production of adenoviruses

2.7.1 Production of full serotype adenoviruses

Full serotype recombinant adenoviral vectors Ad5 and Ad35 were obtained from Crucell (Leiden, Netherlands) as part of a materials transfer agreement and were used to produce high titre stocks in house (Table 3). Low passage 293 cells were grown to 80-90% confluence before infection with a multiplicity of infection (MOI)

of approximately 1 plaque forming unit (pfu)/cell. After 3-4 days the cytopathic effect of the vector caused the cells to detach from the tissue culture flask. The media containing the cells was collected and the cells were harvested by centrifugation at 2000 rpm for 10 minutes at room temperature. The supernatant was discarded and the pellet resuspended in 8 ml of PBS. An equal volume of Arklone P (trichlorotrifluoroethane) was added and after inversion of the falcon tube for 10 seconds and gentle shaking for 5 seconds, the solution was centrifuged at 3000 rpm for 10 minutes at room temperature. The top aqueous layer was removed and stored at -80°C until purification by CsCl gradient

2.7.2 Production of pseudotype adenoviruses

Pseudotype recombinant adenoviral vectors Ad5/f35 and Ad5/p35/f35 were obtained from Crucell as part of a materials transfer agreement and were used to produce high titre stocks in house in the same way as above, however, with the addition of 4 µg/ml polybrene in the media (Table 3). Ad35/f5 was produced in PER.C6 cells and was obtained from Crucell as part of a materials transfer agreement (Table 3).

Virus	Transgene	Cell type and conditions for production	Original production
Ad5	Luciferase	293 cells	Crucell (Leiden, Netherlands)
Ad5.eGFP	Enhanced green fluorescent protein (eGFP)	293 cells	Crucell
Ad5/f35	Luciferase	293 cells + 4 µg/ml polybrene	Crucell
Ad5/f35.eGFP	eGFP	293 cells + 4 µg/ml polybrene	Crucell
Ad5/p35/f35	Luciferase	293 cells + 4 µg/ml polybrene	Crucell
Ad35	Luciferase	293 cells	Crucell
Ad35.eGFP	eGFP	293 cells	Crucell
Ad35/f5	Luciferase	PER.C6 cells	Crucell

Table 3 – Virus transgene and production conditions.

All viruses were originally obtained from Crucell (Leiden, Netherlands) as part of a materials transfer agreement and were used to produce high titer stocks in house.

2.8 Adenovirus purification

Centrifugation on CsCl density gradients was used to purify and concentrate crude adenoviral stocks. Ultra-clear centrifuge tubes (Beckman Coulter Ltd, Buckinghamshire, UK) were sterilised with 70% ethanol and then washed with sterile water. A CsCl gradient was produced by sequentially layering 2 ml of CsCl with a density of 1.45 g/cm^3, 3 ml of CsCl with a density of 1.32 g/cm^3 and 2 ml 40% glycerol. The crude adenoviral supernatant was then added to the top of the gradient and the remaining space was filled with PBS. The tube was loaded into a rotor and centrifuged at 25000 rpm for 1.5 hours at 4°C with maximum acceleration and zero deceleration. Following centrifugation, a band containing the complete adenovirus can be seen between the two CsCl layers. This was removed by piercing the tube below the virus band using a 21 gauge needle and removing the band in the minimum volume and taking care to prevent disruption of the other bands. Extracted virus was transferred to a Slide-A-Lyzer Dialysis Cassette (molecular weight cut-off of 10000) (Perbio Science UK Ltd., Northumberland, UK) for dialysis after hydration of the cassette for 1 minute in dialysis solution. The virus was dialysed in 2 l of 0.01 M Tris pH 8 / 0.001 M EDTA for 2 hours, after which the buffer was replaced and dialysis repeated overnight. The buffer was changed and supplemented with 10% (v/v) glycerol and dialysis was continued for a further 2 hours. The virus was then removed from the cassette, aliquoted and stored at -80°C.

2.9 Determination of adenoviral particle titres

Particle titre of all adenoviral vectors was calculated based on the protein content of the virus stock using a Micro BCA assay kit (Pierce, Rockford, IL, USA). Briefly, eight BSA standards ranging from 200 µg/ml to 0.5 µg/ml were prepared in PBS and 150 µl of each and 150 µl of PBS as the blank was pipetted in duplicate into a 96-well plate. 1, 3 and 5 µl of virus were added in duplicate and each well was made up to a total volume of 150 µl with PBS. 150 µl of BCA working reagent was added to each well and the plate incubated at 37°C for 2 hours. The absorbance was measured at 570 nm using a Wallac VICTOR^2 plate reader (Wallac, Turku, Finland). Background absorbance was subtracted from the sample and standards and the

amount of protein present in each virus was then calculated from the standard curve. The virus particle titre was then calculated using the established formula: 1 μg protein = $1x10^9$ viral particles (VP) (Von Seggern *et al.*, 1998).

2.10 Infection of cells with adenovirus

2.10.1 Adenovirus binding

Cells were seeded in 24-well plates at a seeding density of $2x10^5$ cells/well and incubated overnight at 37°C to produce 90-100% confluence. Cells were transferred to ice-cold serum-free media ± 8 μg/ml FX (1 IU/ml, Cambridge Biosciences, Cambridge, UK) or serum-free media + FX and FX binding protein, X-bp (15 μg/ml). X-bp was pre-incubated with FX for 30 min before adding to cells. Virus was diluted in PBS and added at 1000 VP/cell in triplicate and cells were incubated at 4°C for 1 hour. The cells were then washed in ice-cold PBS and the wells were scraped to remove the cells in 500 μl PBS into a 1.5 ml Eppendorf. The cell suspension was then centrifuged at 13000 rpm for 5 minutes at room temperature to allow the cells to pellet. Supernatant was then removed and the pellet was resuspended in 200 μl PBS.

2.10.1.1 DNA extractions

Viral and total genomic DNA was isolated from each well of the adenoviral cell binding experiment using the QIAamp DNA Mini Kit (QIAGEN, Crawley, UK) as per manufacturer's instructions. Briefly, 20 μl proteinase K and 200 μl buffer AL was added to each of the 200 μl resuspended cell samples and vortexed. Buffer AL contains chaotropic salts which allow the nucleic acids to be adsorbed onto the silica-gel membrane of the QIAamp Spin Column as the chaotropic salts remove water from hydrated molecules in solution. Polysaccharides and proteins do not adsorb and are removed. Samples were incubated at 56°C for 10 minutes. 200 μl 100% ethanol was added to the samples, mixed and then the complete sample was loaded onto a QIAamp Spin Column. Samples were centrifuged at 6000 x g for 1 minute at room temperature to allow the DNA to adsorb onto the silica-gel membrane of the spin column. The spin column was then washed with 500 μl buffer

AW1 and centrifuged at 6000 x g for 1 minute at room temperature, followed by a second wash step with 500 µl buffer AW2 and centrifuged at 16000 x g for 3 minutes at room temperature. Finally the DNA was eluted in 50 µl nuclease-free deionised water by centrifugation at 6000 x g for 1 minute. The quantity of DNA in each sample was quantified by NanoDrop (ND-1000 spectrophotometer [Labtech International, Ringmer, UK]).

2.10.1.2 TaqMan qPCR

TaqMan qPCR was used to quantify the number of virus genome particles remaining bound to the cells from the cell-binding experiment. The Power SYBR Green detection system (Applied Biosystems, Warrington, UK) was used. Power SYBR Green PCR master mix with 300 nM luciferase primers, forward (5'-GCCCGCGAACGACATTTATAA3') and reverse (5'-CGCAGTATCCGGAATGATTTG-3'), were used to amplify luciferase DNA. The conditions used were described previously (Section 2.3.4). A luciferase quantification standard curve was produced from serial dilutions of Ad5 (10^2-10^7 VP). 50 or 100 nanograms (ng) total DNA was used in each reaction and total adenoviral genomes were calculated using the SDS 2.3 software.

2.10.2 Adenovirus internalisation

Cells were seeded in 24-well plates at a seeding density of $2x10^5$ cells/well and incubated overnight at 37°C to produce 90-100% confluence. Cells were transferred to ice-cold serum-free media ± FX. Virus was diluted in PBS and added at 1000 VP/cell in triplicate and cells were incubated at 4°C for 1 hour. Cells were then incubated at 37°C for 1 hour to allow internalisation of the vectors. The cells were then washed in glycine (0.2 M glycine, pH 2.2) for 10 min of ice, which was neutralised with 1 M Tris, pH 8. The cells were then washed in ice-cold PBS and the wells were scraped to remove the cells in 500 µl PBS into a 1.5 ml Eppendorf. The cell suspension was then centrifuged at 13000 rpm for 5 minutes at room temperature to allow the cells to pellet. Supernatant was then removed and the pellet was resuspended in 200 µl PBS. Viral and total genomic DNA was isolated as described above and qPCR was preformed.

2.10.3 Adenovirus transduction

Cells were seeded in 96-well plates at a seeding density of $4x10^4$ cells/well and incubated overnight at 37°C to produce 70-80% confluence. Cells were transferred to serum-free media ± 8 μg/ml FX or serum-free media + FX and 15 μg/ml X-bp. X-bp was pre-incubated with FX for 30 min before adding to cells. Virus was diluted in PBS and added at 1000 VP/cell in triplicate and cells were incubated at 37°C for 3 hours. The cells were washed with PBS and complete media was added. Cells were incubated at 37°C for 72 hours.

2.10.3.1 Transgene quantification

Expression of luciferase transgene was quantified using Luciferase Assay System (Promega, Madison, WI, USA) and recombinant luciferase protein (Promega, Madison, WI, USA) was used a standard. Briefly, cells were washed with PBS and 50 μl 1 x Reporter Lysis Buffer (5 x Reporter Lysis Buffer stock solution, Promega, Madison, WI, USA) was added. To ensure complete lysis of the cells, the plate was also freeze/thawed. 10 μl of each sample was transferred to a white 96-well plate and 90 μl 1 x Reporter Lysis Buffer was added to each well. Standard curves of recombinant luciferase ranging from 0-100 pg/ml and 0-1 pg/ml were produced and 100 μl of each dilution was added in duplicate. Luciferase Assay Buffer was added to Luciferase Assay substrate and 100 μl was then added to each well. Luminescence was measured using a Wallac VICTOR^2 plate reader. Luciferase activity was then normalised to total protein content of the samples determined by BCA assay producing relative light units per milligram protein (RLU/mg protein).

2.10.3.2 Transduction in the presence of anti-CD46 antibody

Cells were seeded in 96-well plates at a seeding density of $4x10^4$ cells/well and incubated overnight at 37°C to produce 70-80% confluence. Cells were transferred to serum-free media ± either 1 μg/ml MEM258 mouse anti-human CD46 antibody (AbD Serotec, Oxford, UK) or 100 μg/ml mouse immunoglobulin G (IgG) 1 control (Dako, Denmark) 30 min before addition of the virus. Virus was diluted in PBS and added at 1000 VP/cell in triplicate and cells were incubated at 37°C for 3 hours. The

cells were washed with PBS and complete media was added. Cells were incubated at 37°C for 72 hours. Expression of the luciferase transgene was then quantified and normalised to total protein content.

2.10.4 Labelled vectors

Labelled adenoviral vectors were produced using the Alexa Fluor® 488 Microscale Protein Labeling Kit (Invitrogen, Carlsbad, CA, USA) as per manufacture's instructions. Briefly, the quantity of vector required was determined by the following calculation, where MW is the molecular weight:

$$\frac{([(\mu g \text{ protein}/\text{protein MW}) \times 1000] \times \text{dye:protein molar ratio})}{\text{Concentration of the dye provided in the kit (11.3 nmol/}\mu L)} = \mu l \text{ of dye required}$$

The molecular weight of an Ad is $150x10^6$ Da and the volume of the dye provided in the kit was 9 µl. To produce a sufficient percentage of labelled to non-labelled vectors, the dye:protein molar ratio attempted was 100%. After calculation, this meant that 152550 µg of protein was required for the labelling reaction. As 1 µg protein = $1x10^9$ VP using the established formula (Von Seggern *et al.*, 1998), this meant that $6.1x10^{14}$ VP were required for each labelling reaction. The volume of each vector required for addition to the labelling reaction was then calculated by:

$6.1x10^{14}$/viral titre per µl

The calculated volume of vector, including a 20% excess, was transferred to a Slide-A-Lyzer Dialysis Cassette (molecular weight cut-off of 10000) (Perbio Science UK Ltd., Northumberland, UK) for dialysis after hydration of the cassette for 1 minute in dialysis solution. The virus was dialysed in 2 l of PBS pH 7.4 overnight to remove the glycerol in which the vector was stored. The vector was removed from the cassette and the calculated volume of vector was added to the reaction tube (Component C) supplied by the kit. A 1 M sodium bicarbonate solution (pH 8.3) was prepared by addition of 1 ml of deionised water was added to the vial of sodium bicarbonate (Component B). A 1/10 volume of 1 M sodium bicarbonate was added to the reaction tube and mixed by pipetting up and down several times. Immediately before use, 10 µl of deionised water was added to one vial of Alexa Fluor® 488 TFP

ester (Component A) and pipetted up and down to ensure the contents of the vial were completely dissolved. 9 µl of the reactive dye solution was added to the reaction tube and was mixed thoroughly by pipetting up and down several times. The reaction mixture was incubated at room temperature for 15 minutes in the dark.

The labelled vector was then transferred to a new dialysis cassette (molecular weight cut-off of 10000) for dialysis after hydration of the cassette for 1 minute in dialysis solution. The virus was dialysed in 2 l of 0.01 M Tris pH 8 / 0.001 M EDTA for 2 hours, then the buffer was changed and supplemented with 10% (v/v) glycerol and dialysis was continued for a further 2 hours. The dialysis was performed in the dark. The virus was then removed from the cassette, aliquoted and stored at - 80°C wrapped in tin foil to protect from the light.

2.10.4.1 Cell trafficking with labelled vectors

SKOV-3 cells were seeded in 6 well plates at $5x10^5$ cells/well on coverslips and incubated overnight at 37°C to produce approximately 50% confluence. Cells were transferred to serum-free media ± 8 µg/ml FX. Virus was diluted in PBS and added at 10000 VP/cell in duplicate and cells were incubated at 4°C for one hour. The cells were then either immediately washed in PBS and fixed in 4% paraformaldehyde for 5 minutes at room temperature or fixed after incubation at 37°C for 15 minutes, one hour or three hours. The coverslips were then removed from the plates and mounted cell side down on slides in ProLong® Gold Antifade Reagent with DAPI to counterstain the nuclei of the cells. The mounting agent was allowed to set overnight before viewing on the confocal microscope.

2.11 Surface plasmon resonance (SPR)

SPR analysis was performed using a Biacore T100 (GE Healthcare, Little Chalfont, UK) as described (Parker *et al.*, 2006). Briefly, virus was biotinylated using sulfo-NHS-LC-biotin (Pierce, Rockford IL) according to the manufacturer's instructions. Virus was covalently immobilized onto the flowcell of a streptavidin biosensor chip (SA, Biacore) according to the manufacturer's instructions. Immobilisation of the virus by biotinylation was chosen as it can be controlled to give a very low

incorporation of biotin, with hopefully only 1-2 molecules per virus particle. The immobilisation densities of the viruses were: Ad5 – 400 response units (RU), Ad5/f35 – 132 RU, Ad5/p35/f35 – 198 RU, Ad35 – 198 RU and Ad35/f5 – 310 RU.

FX in 10 mM HEPES pH 7.4; 150 mM NaCl; 5 mM $CaCl_2$; 0.005% Tween 20 was passed over the chip at a flow rate of 30 µl/min. Sensorchips were regenerated between FX application by injection of 10 mM HEPES pH 7.4; 150 mM NaCl; 3 mM EDTA; 0.005% Tween 20. Kinetic analysis was performed in triplicate using FX concentrations in the range 108 to 0.05 µg/mL and analysed using Biacore T100 Evaluation software using either a 1:1 or heterogenous ligand model. Non-specific binding was determined by examination of FX binding to a flow cell with no virus immobilised. FX showed no non-specific binding to the flow cell over the range of FX concentrations used.

Immobilisation of FX on the chip, instead of immobilisation of the virus, was attempted but this method only yielded binding data due to the 240 binding sites for FX on the virus particle. The avidity of this interaction is so tight that no dissociation of FX from the virus particle was detected. Therefore, for determination of association rate, dissociation rate and equilibrium dissociation constants the virus particle was immobilised on the chip.

2.12 Phage methods

Phage experiments were carried out using T7Select415-b phage display system (Novagen, EMD Biosciences, Darmstadl, Germany), which used the T7 capsid protein to display peptides on the surface of the phage. All candidate peptide-phage and a non-recombinant control phage (with no peptide insertion) were obtained as a gift from Professor E. Ruoslahti (Burnham Institute, Santa Barbara, CA, USA). Candidate peptides had been isolated by three rounds of selection on *ex vivo* murine heart cells, followed by three rounds of selection *in vivo* (Zhang *et al.*, 2005). All phage amplification and titration was performed using *Escherichia coli* strain BL21 (Novagen, EMD Biosciences, Darmstadl, Germany).

2.12.1 Amplification of phage

Phage were amplified using the liquid lysate amplification protocol as described in the Novagen T7 Select system manual. Briefly, a single BL21 colony was picked from a freshly streaked plate and amplified overnight in 25 ml M9LB (1.25 ml 20x M9 salts [20 g/l NH_4Cl, 60 g/l KH_2PO_4, 120 g/l $NaH_2PO_4.7H_2O$], 0.5 ml 20% glucose, 25 µl 1M $MgSO_4$, 25 ml LB) in an orbital shaker at 37°C and 180 rpm. 5 ml of the overnight culture was added to 500 ml LB in a 2 l flask and incubated for approximately 3 hours at 37°C in an orbital shaker at 180 rpm. The absorbance of the culture was read at intervals until the optical density reached 600 nm (OD_{600}) 0.5-1.0. Separately, 50 µl phage was added to 5 ml of the overnight culture and grown until lysis had occurred. This was then added to the 500 ml culture and was incubated with shaking at 37°C for 1-3 hours until cell lysis had occurred as determined by an OD_{600} of less than 0.5. 10% (v/v) 5 M NaCl was added to the culture, which was then centrifuged at 8000 x g for 10 minutes to remove cell debris. The supernatant was transferred to a sterile bottle for polyethylene glycol (PEG-8000) precipitation.

2.12.2 Purification of phage

$1/6^{th}$ volume of 50% (v/v) PEG-8000 was added to the supernatant and thoroughly mixed before incubating at 4°C overnight. The supernatant was then centrifuged at 3185 x g for 30 minutes at 4°C. The pellet was resuspended in 2 ml TBS and transferred to microcentrifuge tubes where $1/6^{th}$ volume of 20% PEG-8000/2.5M NaCl was added to the phage and left overnight at 4°C. The phage was centrifuged for 30 minutes at 12600 x g and 4°C and the pellet resuspended in 1 ml TBS and left on ice for 1 hour prior to centrifugation for 10 minutes at 12600 x g and 4°C. The pellet was resuspended in 1 ml 0.02% NaN_3 and left at room temperature for 20 minutes before a further centrifugation of 10 minutes at 12600 x g and 4°C. Supernatants were then pulled and stored at 4°C.

2.12.3 Determination of phage titre

To determine the titre of the phage stocks produced, a single BL21 colony was picked from a freshly streaked plate and amplified overnight in 25 ml LB supplemented with 5 ml M9 salts, 2 ml 20% glucose and 0.1 ml 1 M $MgSO_4$ in an orbital shaker at 37°C and 180 rpm. The culture was diluted to an OD_{600} of approximately 1. LB plates were pre-warmed in a 37°C incubator and serial dilutions of phage were made in LB (10^{-6} to 10^{-9}). Agar tops (10 g/l bactrotyptone, 5 g/l yeast extract, 1 g/l $MgCl.6H_2O$, 7 g/l agarose) were melted and 3 ml aliquots made and placed in a 50°C water bath. 250 µl of culture was added to 20 µl of each dilution of phage and incubated together for 10 minutes at room temperature. This was then added to an aliquot of agar top and poured onto an LB plate. Once set plates were inverted and left at room temperature overnight. The number of plaques at each dilution were counted and used to calculate an average titre for the phage stock using the formula:

Phage titer (pfu/ml) = Number of plaques x dilution factor x 50

2.12.4 Extraction of phage from tissues

Phage was also extracted from approximately 25 mg of tissue from selected organs. Tissues were placed into 2 ml microcentrifuge tubes containing 1 ml ice cold DMEM-PI (DMEM supplemented with 1% (w/v) BSA, 1 mM phenylmethanesulfonyl fluoride (PMSF), 1 µg/ml leupeptin, 2 µg/ml aprotinin). Tissues were homogenised in a Tissuelyser (QIAGEN, Crawley, UK) by performing two 3 minutes runs at 25 Hz. Leupeptin, PMSF and aprotinin inhibit proteases, serine proteases and trypsin, respectively, preventing degradation of proteins in the homogenate. 66 µl of 1% non-ident P40 (NP40) was added to each homogenate and incubated on ice for 5 minutes to disrupt the cyotplasmic membrane of the cells. This was followed by the addition of 20 µl 1% NaN_3 and samples were stored at 4°C for up to 5 days before titration.

2.13 Preparation of osmotic mini-pumps

The 2ML4 osmotic mini-pumps (Alzet, CA, USA) were filled as per manufacture's instructions. Briefly, the reservoir of the mini-pumps was required to be 90% filled to ensure optimum operating efficiency and the concentration of the peptide solution depended on the weight of the rat and the release rate of the mini-pump. Animals were administered 10 mg/kg/day peptide and the pumps were filled with enough peptide for 29 days of administration to ensure over 90% filling. Peptides were diluted to a 350 mg/ml stock solution in DMSO for storage and the required further dilution with deionised water was calculated from the formula:

Mass delivery rate (μg/hour) = concentration of peptide (μg/μl) x volume delivery rate (μl/hour)

Therefore, for a 225 g rat, required administration rate = 2.25 mg/day

(2.25 mg/day x 29 days) / 350 mg/ml = 186.4 μl peptide + 1658 μl dH_20

Mini-pumps were filled the day before implantation and incubated overnight at 37°C in isotonic saline to ensure that the pumping rate had reached a steady state before implantation.

2.14 Animal models

All animals were housed under controlled environmental conditions. Temperature was maintained at ambient temperature with 12 hours light/dark cycles. Mice and rats were fed standard chow (rat and mouse No.1 maintenance diet, Special Diet Services) and water was provided *ad libitum*. All experiments were carried out in accordance with the Animals (Scientific Procedure) Act, 1986. Administration of Ad vectors into mice was performed under the project license held by Dr. S.N. Waddington (Royal Free and University College Medical School, London, UK), Licence No. 70/6906. Administration of phage and peptides into rats was performed under the project license held by Prof. A.F. Dominiczak (University of Glasgow, UK), Licence No. 60/2874. CD46 transgenic mice were generated by back-crossing

an established CD46 transgenic line onto white MF1 mice. Both CD46 transgenic mice and control MF1 mice were used for the *in vivo* experiments. Male SHRSP were obtained from the Glasgow colony by brother-sister mating (Dominiczak *et al.*, 1993)

2.14.1 Administration of adenovirus

In vivo adenoviral work was performed in CD46 transgenic mice 25-30 g. Mice were anaesthetised and injected with $5x10^{10}$ VP/mouse via lateral tail vein injection. X-bp treated animals were injected with 4.8 mg/kg X-bp 30 minutes before injection of Ad.

2.14.1.1 Quantification of adenoviral accumulation and transgene expression

Mice were subject to whole body bioluminescence quantification (IVIS Spectrum; Caliper Life Sciences, Hopkinton, MA, USA) 48 hours post-Ad administration and were sacrificed after 72 hours for tissue analysis. Tissue homogenates were produced from 25 mg tissue (10 mg spleen) using TissueLyser II (QIAGEN, Crawley, UK). Luciferase expression analysis was then performed on the tissue homogenates and normalised to total protein content. DNA was also isolated from tissue homogenates using QIAamp DNA mini kit (QIAGEN, Crawley, UK). 50 ng of total DNA was subject to qPCR analysis as described above.

2.14.2 Administration of phage

In vivo phage work was performed in 12-week male SHRSP rats. Rats were anaesthetised by isofluorane (3%). All rats received $5x10^{10}$ pfu phage via femoral vein injection which was left to circulate for 5 minutes. Blood samples were taken by cardiac puncture before rats were perfused through the heart with heparinised saline and organs were removed and snap frozen.

2.14.3 Administration of peptides

For the *in vivo* anti-oxidant study, rats were implanted with radio-telemetry probes under isofluorane anaesthesia at 10 weeks of age. Under isofluorane anaesthesia, animals were implanted with 2ML4 osmotic mini-pumps at 12 weeks of age to deliver the peptides continuously for 3 weeks. At 15 weeks of age, the animals were sacrificed under terminal isofluorane anaesthesia; blood was immediately drawn from the heart and stored in EDTA before being snap frozen in liquid NO_2 for SO measurement by EPR. The descending thoracic aorta was isolated and removed to study endothelial function. Internal carotid arteries and selected organs were taken for further study. Throughout procedures and subsequent analysis, animal breeding numbers were used to identify SHRSP, and not treatment groups, to ensure a blinded study.

2.15 Determination of blood pressure changes

Radio-Telemetry Monitoring of Blood Pressure and Heart Rate The Dataquest IV telemetry system (Data Sciences International) was used for measurement of systolic pressure, diastolic pressure, mean arterial pressure, heart rate, and motor activity, as previously described (Davidson *et al.*, 1995). Briefly, the monitoring system consists of a transmitter (radio frequency transducer model TA11PA), receiver panel, consolidation matrix, and personal computer with accompanying software. Before the device was implanted, calibrations were verified to be accurate within 3 mm Hg. SHRSP rats at 10 weeks of age were anesthetised with isofluorane and the flexible catheter of the transmitter was surgically secured in the abdominal aorta just below the renal arteries and pointing upstream (against the flow). The transmitter was sutured to the abdominal wall. Rats were housed in individual cages after the operation. Each cage was placed over the receiver panel which was connected to the computer for data acquisition. The rats were unrestrained and free to move within their cages. Haemodynamic data were sampled every 5 minutes for 10 seconds. Blood pressure and heart rate takes up to 7 days to stabilise post-operatively (Davidson *et al.*, 1995). Therefore, mini-pumps were implanted two weeks later and

telemetry data were collected for one week prior to implantation of the mini-pumps and for the 21 days on treatment.

2.16 Echocardiography (ECHO)

Trans-thoracic ECHO was carried out by Dr. K. Gilday (University of Glasgow, UK). Briefly, it was performed using an ACUSON Sequoia C512 ultrasound system (Siemens, Germany) with a linear array transducer at a frequency of 15 MHz. Echocardiography was performed on a lightly anesthetized animal (1.25% to 1.5% isoflurane in 1.5 litres/min O_2) placed in the left lateral decubitus position on a heated pad. Non-invasive acquisitions of 2-D guided M-mode images at a depth of 20 mm were recorded at the tip of the papillary muscles. The thickness of the posterior and anterior walls of the left ventricle (LV) chamber and the LV chamber diameter during systole and diastole were measured in a short axis view using the leading edge to leading edge convention. All parameters were measured over at least three consecutive cardiac cycles. Pulse-wave velocity was used to measure the velocity of blood through the mitral valve and to qualitatively examine the valve for evidence of mitral valve regurgitation.

2.16.1 Formulae used in ECHO assessments

Ejection fraction was defined as follows: EF = [(LVEDV - LVESV) / LVESD x 100], where LVEDV is left ventricular end diastolic volume and LVESV is left ventricular end systolic volume. Fractional shortening was derived from: FS = [(LVEDD - LVESD) / LVEDD x 100], where LVEDD is left ventricular end diastolic diameter and LVESD is left ventricular end systolic diameter. Cardiac output was derived from: CO = [(ESV - EDV) x HR], where HR is heart rate. Change in interventricular septal wall thickness (ISWT) was measured using the formula [(AWTs - AWTd) / AWTs x 100], where AWT is anterior wall thickness, s is systole and d is diastole.

2.17 Myography

2.17.1 Large vessel myography

Thoracic aorta was cleaned of connective tissue and cut into 2 mm rings, which were mounted in large vessel 5 ml myograph baths containing Krebs buffer maintained at 37°C and oxygenated with 95% O_2, 5% CO_2. After pre-treatment with potassium-buffered Krebs and stimulatory dose of phenylephrine (PE), cumulative concentration-response curves to PE (1 nmol/l to 10 μmol/l) were constructed, first in the absence and again after washout in the presence of 100 μmol/l N-nitro-L-arginine methyl ester (L-NAME) to inhibit eNOS. Response to PE was expressed as percentage of maximum contraction produced during the first PE curve. The increase in tension in the presence of L-NAME provided a measure of the effect of NO on basal tone.

Other sections of the thoracic aorta were also used to perform cumulative concentration-response curves to apocynin (10 μmol/l to 1 mmol/l) directly after a cumulative concentration-response curve to PE (1 nmol/l to 10 μmol/l) was constructed. Apocynin (also known as 4′-Hydroxy-3′-methoxyacetophenone or acetovanillone) inhibits NAD(P)H oxidase and can act an anti-oxidant. Response to apocynin was expressed as percentage of maximum contraction produced during the first PE curve.

2.17.2 Small vessel myography

Third order mesenteric resistance arteries were dissected from connective tissue and stored overnight at 4°C before use. Segments (approximately 2 mm in length) were mounted as ring preparations in Krebs buffer maintained at 37°C and oxygenated with 95% O_2, 5% CO_2 on two stainless steel wires on a four-channel small vessel myograph (Danish MyoTechnology, Aarhus, Denmark). One wire was attached to a force transducer and the other to a micrometer. Following a 30 minute rest period, vessels were set to a normalised internal diameter (L1) to achieve optimal contraction. Internal diameter was calculated using the following equation: L1=0.0*L100, (where L100 was determined using the LaPlace equation, P=T/r (P is

effective pressure, T is wall tension and r is the internal radius). After further 60 min, contractile responses to 10 μmol/l KCl were examined, followed by washout. A cumulative concentration response curve to PE (1 nmol/l to 30 μmol/l) was performed first in the absence and again after washout, in the presence of 100 μmol/l L-NAME. The increase in tension in the presence of L-NAME provided a measure of the effect of NO on basal tone.

2.18 Electron paramagnetic resonance (EPR)

Oxidative stress status was assessed by analysing SO release from heparinised whole blood taken by cardiac puncture at sacrifice. Blood was kept on ice and processed within one hour. SO levels were detected by EPR (e-scan R; Bruker BioSpin GmbH, Rheinstetten Germany) with the spin probe 1-hydroxy-3-carboxy- 2,2,5,5-tetramethylpyrrolidine (CPH; Noxygen, Elzach, Germany) added to a final concentration of 500 μmol/l. Blood was then incubated at 37°C for 30 minutes before being snap frozen in liquid nitrogen. SO levels were then measured in the snap frozen samples and the rate of SO production was calculated as counts per minute. Instrument settings were: centre field of 3392 G, modulation amplitude of 5.08 G, sweep time of 10.49 s, sweep width of 120 G and 10 scans.

2.19 Histology

Tissues were excised and immediately fixed in 10% formalin overnight and then transferred to PBS. Tissues were then paraffin embedded and single tissue sections of 6 μm thickness mounted onto a salinised glass slide, which were heated for 3 hours at 65°C, then overnight at 40°C.

2.19.1 Slide salinisation

Blank glass slides were placed in a solution of 2% 3-amino-propyltriethoxysaline (APES) in 100% acetone for 30-60 seconds. Slides were then rinsed twice in 100% acetone, followed by two rinses in deionised water before being left to air dry in an oven overnight at 37°C.

2.19.2 Immunohistochemistry

Paraffin was removed from the sections by two 7 minute washes in Histoclear (Thermo Fisher Scientific, UK). Sections were rehydrated by passing through an alcohol gradient 100%, 95% and 70% ethanol for 7 minutes each. After washing slides in deionised water for 5 minutes, endogenous peroxide activity was quenched by incubating slides in 0.3% (v/v) methanol-hydrogen peroxide for 30 minutes at room temperature. Slides were then washed twice in deionised water for 5 minutes. Antigen unmasking was then performed in 10 mM sodium citrate, pH 6.0 for 15 minutes at 95-100°C. Slides were then washed twice in deionised water for 5 minutes. Immunohistochemistry was performed using Vectastain avidin and biotinylated horseradish peroxidase complex (ABC) rabbit IgG kit (Vector Laboratories, UK). Sections were incubated in blocking solution (goat serum) for 1 hour at room temperature in a humidified chamber. The primary anti-T7 antibody (Chemicon, CA, USA) and the negative control rabbit IgG antibody (Dako, Denmark) were diluted to 0.01 mg/ml in blocking solution. Antibodies were incubated on the sections overnight at room temperature in a humidified chamber. Slides were washed three times in PBS for 5 minutes each. The secondary Vectastain avidin and biotinylated goat anti-rabbit IgG antibody was diluted 1:200 in blocking solution and incubated on the slides for 30 minutes at room temperature. Slides were then washed three times in PBS for 5 minutes each. The avidin and biotinylated horseradish peroxidase complex (ABC) was then incubated on the slides for 30 minutes at room temperature, followed by three washes in PBS of 5 minutes each. Slides were then incubated with DAB chromagen solution (3,3-diaminobenzidine, hydrogen peroxide and nickel solution) (Vector Laboratories, UK) for 5 minutes. Slides were washed in deionised water for 5 minutes then nuclei were counterstained by incubation with Harris haematoxylin for 30 seconds. Slides were washed in running water and dehydrated by incubation in 70%, 95% and 100% ethanol, followed by Histoclear for 7 minutes each. Finally, slides were mounted using Histomount (National Diagnostics, GA, USA). Nuclei appeared blue/purple and areas to which the primary antibodies bound appear brown.

2.19.3 Immunofluorescence

After the removal of paraffin and rehydration of slides as described above, endogenous peroxide activity was quenched by incubating slides in 0.3% (v/v) methanol-hydrogen peroxide for 30 minutes at room temperature. Slides were then washed twice in deionised water for 10 minutes. Antigen unmasking was performed by incubating the sections in proteinase K solution (20 μg/ml proteinase K [Roche Applied Science, Indianapolis, IN, USA], 2.5 mM Tris pH 8.0 / 0.05 mM EDTA) for 20 minutes at 37°C. Slides were then removed from the incubator and left for 20 minutes at room temperature. Slides were washed twice in PBS for 5 minutes and then washed twice in TBS (150 nM NaCl, 50 nM Tris pH 7.4) 0.0025% (v/v) Triton X-100. Sections were incubated in 10% goat serum in TBS for 30 minutes at room temperature in a humidified chamber. The primary anti-GFP antibody (Abcam, Cambridge, UK) and the negative control rabbit IgG antibody (Invitrogen, Carlsbad, CA, USA) were diluted to 0.5 μg/ml in 1% goat serum in TBS. Antibodies were incubated on the sections for one hour at room temperature. Slides were washed twice in TBS 0.0025% (v/v) Triton X-100 for 5 minutes each. The fluorescent Alexa Fluor® 488 secondary goat anti-rabbit IgG antibody (Invitrogen, Carlsbad, CA, USA) was diluted 1:750 in 1% goat serum in TBS and incubated on the slides for 30 minutes at room temperature. Slides were then washed three times in TBS for 5 minutes each and mounted in ProLong® Gold Antifade Reagent with DAPI to counterstain the nuclei of the cells. The mounting agent was allowed to set overnight before viewing on the confocal microscope.

2.19.4 Haemotoxylin and eosin (H&E) staining

After the removal of paraffin and rehydration of slides as described above, slides were stained in Harris haemotoxylin for 2 minutes. Slides were washed in running water for 5 minutes and then placed in eosin for two minutes, before a further 5 minutes wash in running water. Slides were dehydrated and then mounted in Histomount. Nuclei appeared blue/purple whereas cytoplasm was stained pink.

2.19.5 Picro-sirius red staining

After the removal of paraffin and rehydration of slides as described above, slides were incubated in Sirius red F3B dissolved in 0.1% (w/v) saturated picric acid for 90 minutes at room temperature in the dark. Slides were washed twice with 0.01 N HCl for 3 minutes each, followed by two washes in deionised water for 3 minutes each. Slides were dehydrated and then mounted in Histomount. Collagen was stained various shades of red.

2.19.6 Masson's trichrome staining

Masson's Trichrome staining was performed using the kit obtained from Sigma-Aldrich (Poole, UK). Briefly, after the removal of paraffin and rehydration of slides as described above, slides were incubated in Bouin's solution overnight at room temperature. Slides were washed under running water until the yellow colour was removed. Sections were stained for 5 minutes in Weigert's Iron Haematoxylin solution (Weigert's Iron Haematoxylin solution was prepared by mixing equal parts of Solution A (1% haematoxylin in ethanol) and Solution B (1.2% (w/v) ferric chloride and 1% (v/v) hydrochloric acid)). Slides were then washed in running water for 5 minutes. Slides were stained in Biebrich Scarlet-Acid Fuchsin (0.9% Biebrich scarlet, 0.1% acid fuchsin, 0.1% acetic acid) for 5 minutes and then rinsed in deionised water. Slides were placed in Working Phosphotungstic/Phospho-molybdic Acid Solution (1 volume 10% Phosphotungstic Acid, 1 volume 10% Phosphomolybdic Acid with two volumes deionised water) for 5 minutes and then in Aniline Blue Solution (2.4% Aniline Blue and 2% acetic acid) for 5 minutes. Sections were washed in 1% acetic acid for two minutes before they were dehydrated and mounted in Histomount. Cell nuclei appear black, cytoplasm and muscle fibres appear red and collagen was stained blue.

2.20 Statistical analysis

All results are expressed as mean ± stardard error of the mean (SEM). *In vitro* experiments were performed in triplicate on at least three independent occasions and analysis was by unpaired Student's t test. Comparisons between myography curves

in the individual groups were performed using an unpaired Student's t test for the area under the curve. Comparison between EPR blood SO production by the different groups was performed using an unpaired Student's t test.

2.20.1 In vivo *statistical analysis*

In vivo experiments were performed with at least four mice per group in the Ad study and six SHRSP per group for the anti-oxidant study. Comparison between groups for the radio-telemetry data was performed by repeated measures analysis of variance (ANOVA), as described previously (Davidson *et al.*, 1995). Comparison between treatment groups and control animals for the ECHO data was performed by one-way ANOVA with a Dunnett's post-test.

CHAPTER 3

In Vitro and *In Vivo* Characterisation of Vascular-Targeting Anti-Oxidant Therapy

3.1 Introduction

Evidence indicates that increased oxidative stress is responsible for a variety of human cardiovascular diseases. Therefore, it is critical to develop more effective anti-oxidant therapies. Enhanced reduction of oxidative stress could be achieved by using targeted anti-oxidant treatments. Specific proteins have been found to be restricted to highly defined regions of the vasculature, particularly within organs. Previously ECs have been shown to differentially express markers in various organs and disease states (Garlanda and Dejana, 1997, Ghitescu *et al.*, 1997, Thorin and Shreeve, 1998, Ruoslahti and Rajotte, 2000, Ribatti *et al.*, 2002, Oh *et al.*, 2004). Exploitation of this differential expression of proteins on the cell surface of ECs has led to the identification of peptides that selectively target specific areas of the vasculature.

Screening with phage-displayed peptide libraries and cDNA libraries has previously led to the discovery of tissue-specific peptides, including peptides that target the heart (Zhang *et al.*, 2005), brain, kidneys, lungs, breast, prostate (Rajotte and Ruoslahti, 1999, Ruoslahti and Rajotte, 2000, Essler and Ruoslahti, 2002), muscle (Samoylova and Smith, 1999), fat (Kolonin *et al.*, 2004) and venous circulation (Nicklin *et al.*, 2000). Both *ex vivo* and *in vivo* phage display was performed to identify peptides which selectively targeted ECs of the coronary vasculature and chambers of the heart (Zhang *et al.*, 2005). Three rounds of *ex vivo* phage display were performed on ECs isolated from murine heart cell suspensions, increasing binding by peptide-inserted phage 230-fold over non-recombinant control phage (Zhang *et al.*, 2005). The *ex vivo* selected phage were then subject to selection *in vivo* in BALB/c mice based on their heart-homing capacity. After three rounds of *in vivo* screening the heart-targeting capacity of the phage had increased to 200-fold greater than the control phage with low levels of phage bound in other non-target organs (Zhang *et al.*, 2005).

Following sequencing to identify the peptide inserts in the heart-targeted phage, the peptides were matched against a heart cDNA library expressed in a bacterial 2-hybrid system (Zhang *et al.*, 2005). After exclusion of abundant cardiac muscle proteins (including myosin and myoglobin), six membrane or cell-surface proteins

were identified producing putative peptide-receptor combinations (Zhang *et al.*, 2005). Cysteine-rich protein 2 (CRIP-2) was identified as the receptor for two of the peptide sequences, CRPPR and CGRKSKTVC, and is expressed in the vascular endothelium of the heart (Yu *et al.*, 2002). Phage displaying peptide insert sequences CRPPR and CGRKSKTVC targeted to the heart with 310- and 46-fold selectivity compared to the non-recombinant control phage, respectively (Zhang *et al.*, 2005). CPKRPR-inserted phage demonstrated 35-fold heart selectivity and bound to an un-annotated RIKEN expressed sequence tag (EST) (Zhang *et al.*, 2005). CRSTRANPC binds to an "un-named" protein product similar to the mitochondrial membrane protein integral membrane protein CII-3 (MPCII-3) (Zhang *et al.*, 2005). CRSTRANPC was 22-fold more selective for the heart than the non-recombinant control phage (Zhang *et al.*, 2005). The final receptor identified for peptides CPKTRRVPC and CSGMARTKC was the mouse homologue of the human bladder cancer-associated protein BC-10, a protein which is down-regulated as cancer develops from pre-malignant lesions in the bladder (Gromova *et al.*, 2002). The peptides CPKTRRVPC and CSGMARTKC targeted the heart with a 62- and 14-fold increase, respectively, relative to the control phage (Zhang *et al.*, 2005). Receptor expression analysis by qPCR showed that CRIP-2, MPCII-3 and BC-10 were expressed at the highest level in the heart, with much lower levels of the receptors present in other tissues (Zhang *et al.*, 2005).

Co-injection of selected phage displaying the heart-targeted peptide sequences (including the peptide sequences CRPPR, CRSTRANPC and CPKTRRVPC) into mice with fluorescein-conjugated tomato lectin to stain blood vessels identified that the phage were bound to the endothelium of the heart (Zhang *et al.*, 2005). Importantly, none of the phage were seen to bind to the endothelium of other tissues (Zhang *et al.*, 2005). Additionally, using fluorescein-conjugated CRPPR peptide, it was shown that this peptide extensively co-localised with an anti-CRIP-2 antibody and the endothelial marker CD31 in coronary arteries, capillaries and the endocardium (Figure 3.1) (Zhang *et al.*, 2005). Therefore, heart-targeting peptides and their receptors in the endothelium of the cardiac vasculature are known and can be exploited to develop an anti-oxidant therapy that selectively targets to the areas of oxidative stress.

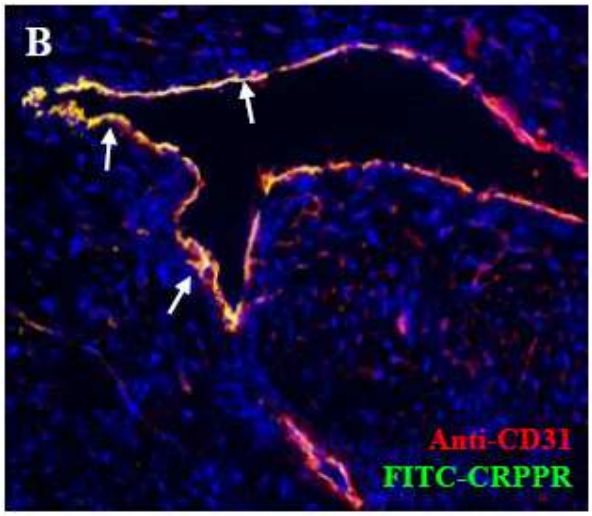

Figure 3.1 – CRPPR peptide co-localises with CD31 in mouse endocardium.

Fluorescein-conjugated CRPPR peptide (green) co-localises with anti-CD31 antibody (red) in the endocardium of the heart after intravenous administration in mice. CD31 is an endothelial cell marker. Adapted from Zhang *et al*. (Zhang *et al.*, 2005).

The heart-targeting capability of CRPPR was tested in three mouse strains (BALB/c, FVB and C57BL/6), with a similar degree of specific cardiac homing seen in the different strains (Zhang *et al.*, 2005). Phage inserted with the peptide sequences CGRKSKTVC, CPKRPR, CPKTRRVPC, CRPPR, CRSTRANPC and CSGMARTKC have been previously administered to the normotensive WKY rat to investigate whether the efficiency and selectivity of the peptides extended across species (Shirley, 2008). Phage recovery analysis from the major organs showed enhanced recovery of all six peptides from rat heart homogenates, compared to control insert-less phage (Shirley, 2008). However, three of the peptides, CGRKSKTVC, CPKRPR and CPKTRRVPC, did not show strong selectivity for the heart (Shirley, 2008). CRPPR, CRSTRANPC and CSGMARTKC retained their strong heart-targeting capacity with high selectivity (Shirley, 2008). CRPPR,

CRSTRANPC and CSGMARTKC all demonstrated enhanced cardiac selectivity of over 400-fold, 2000-fold and 80-fold, respectively (Shirley, 2008). Immunohistochemical analysis using an anti-T7 phage antibody confirmed the cardiac targeting of CRPPR, CRSTRANPC and CSGMARTKC. The histology also revealed that CSGMARTKC was found to primarily target the vascular endothelial cells, whereas T7 phage displaying the peptides CRPPR and CRSTRANPC were also found throughout the myocardium (Shirley, 2008).

The phage inserted with the most selective and effective heart-targeting peptide sequences in the WKY rat (CRPPR, CRSTRANPC and CSGMARTKC) were tested in the SHRSP, a disease model of human essential hypertension. The peptides which remained selective for the cardiac vasculature in the SHRSP (CRPPR and CSGMARTKC) were linked to the anti-oxidant peptide gp91ds (Rey *et al.*, 2001) to develop a novel vascular-targeting anti-oxidant peptide. The effect of this vascular-targeting anti-oxidant therapy on BP and endothelial function in the SHRSP was then assessed.

3.2 Results

3.2.1 In vitro *internalisation of targeting peptides in a rat endothelial cell line*

The ability of the peptides to bind to and internalise into cells *in vitro* was assessed using a rat glomerular endothelial (RGE) cell line. RGE cells provide a model of rat endothelial cells and have been used previously with success (Nicol *et al.*, 2009). The heart-targeting peptides CRPPR, CSGMARTKC and CRSTRANPC were previously identified by *ex vivo* and *in vivo* phage display (Zhang *et al.*, 2005) and their selectivity for the cardiac vasculature was maintained in WKY rats (Shirley, 2008). The targeting peptides and the HIV-tat peptide were linked to a fluorescein (FITC) label to allow visualisation by fluorescence microscopy. 1 – 100 μmol/l of the peptides were added to $1x10^4$ RGE cells/well and internalisation of the peptides by the cells was determined by the presence of the green FITC-labelled peptide after the cells were washed.

At 1-10 μmol/l of the peptides, there was no clear internalisation observed by any of the heart-targeting peptides (Figure 3.2). However, the HIV-tat peptide internalised into a small number of RGE cells (Figure 3.2). CRSTRANPC and HIV-tat peptides both effectively internalised at 50 μmol/l, with the HIV-tat peptide present in a greater number of the cells (Figure 3.2). CRPPR and CSGMARTKC were also internalised by the RGE cells at 50 μmol/l concentration but at a lower level (Figure 3.2). At 100 μmol/l of the peptides, there was considerable internalisation by all four peptides, with the HIV-tat peptide again producing the highest level of internalisation (Figure 3.2). However, 100 μmol/l of peptide also produced cell death, resulting in reduced cell numbers at this concentration (Figure 3.2). As the targeting peptides can internalise into the RGE cells, this suggests that there was some expression of their receptors. The visually most effective peptide internalisation at each of the concentrations was produced by the HIV-tat peptide (Figure 3.2). For further experiments, 50 μmol/l of the peptides was used as this concentration of peptide produced internalisation into the RGE cells without high levels of cell death.

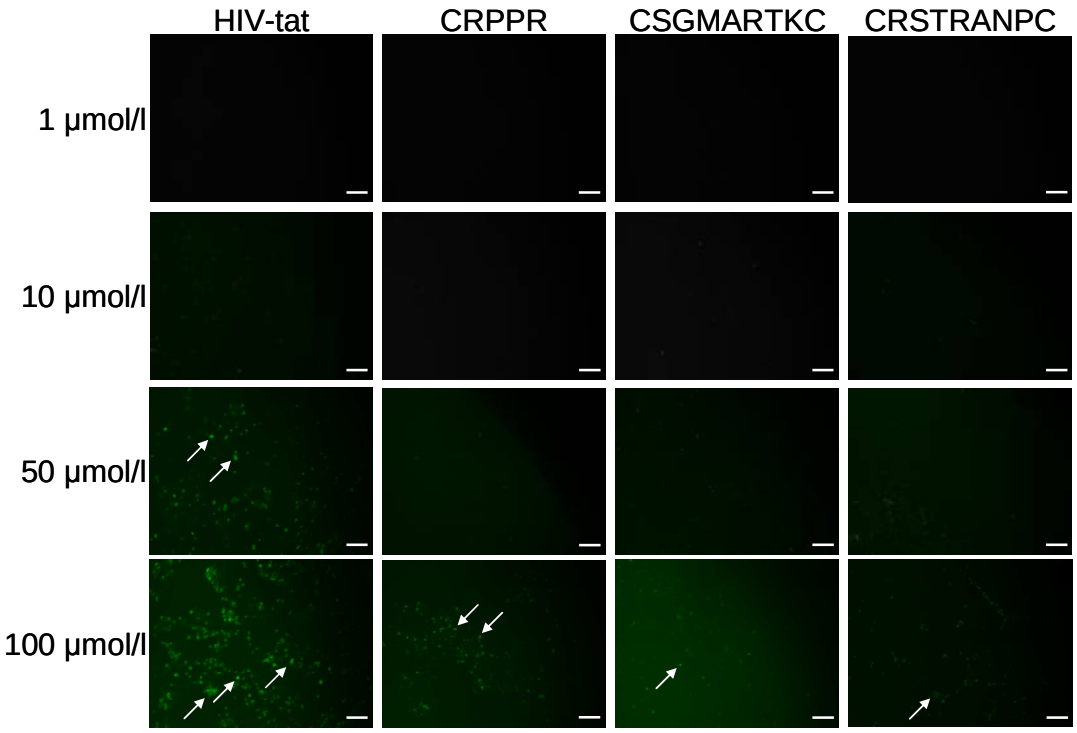

Figure 3.2 – Internalisation of peptides in RGE cells.

Peptides were added to $1x10^4$ RGE cells/well in concentrations ranging from 1 – 100 µmol/l. Peptides were incubated with the cells at 37°C for 10 minutes. The cells were then washed and internalisation of the peptides by the cells was determined by the presence of the green FITC-labelled peptide after the cells were washed. Visualisation of the FITC-label was ascertained by fluorescence microscopy and arrows indicate cells with internalised peptides. Scale bar = 50 µm, magnification x 10.

3.2.2 Transfection of RGE cells with plasmids containing the putative receptors for each peptide

To attempt to increase internalisation of the peptides in RGE cells, cells were transfected with the putative receptors for each peptide (discussed in Section 3.1). RGE cells are derived from the glomerular endothelium and, therefore, may not express the necessary receptors for the heart-targeting peptides. However, Figure 3.2 does suggest some presence of receptors for two of the peptides. The transfection procedure was optimised in RGE cells using an eGFP expression plasmid and two transfection reagents, Lipofectamine™ 2000 and FuGENE® 6. The ratio of transfected to non-transfected cells in each condition was determined by fluorescence microscopy.

Lipofectamine™ 2000 reaction complexes were generated with a DNA (μg) to Lipofectamine™ 2000 (μl) ratio of 1:1, 1:2, 1:3 and 1:4 in Opti-MEM® I serum free media, with 2 μg DNA being used for each complex. Complexes were incubated with the RGE cells for 4-6 hours and 48 hours after transfection images were taken (Figure 3.3). Over 90% of the cells transfected with a 1:1 ratio of Lipofectamine™ 2000 and DNA expressed eGFP (Figure 3.3). Increasing concentrations of Lipofectamine™ 2000 increased the transfection efficiency slightly but substantially increased cell death as Lipofectamine™ 2000 was toxic to the RGE cells (Figure 3.3).

A similar optimisation experiment was performed with FuGENE® 6, with reaction complexes with a DNA (μg) to FuGENE® 6 (μl) ratio of 1:1, 2:3, 1:2 and 2:9 in Opti-MEM® I serum free media. Approximately 10% of RGE cells were transfected with a 1:1 FuGENE® 6 to DNA ratio (Figure 3.4). Increasing the ratio to 2:3 and 1:2, significantly increased the transfection efficiency but the toxicity of the transfection reagent was producing some cell death at these concentrations (Figure 3.4). At the highest concentration of FuGENE® 6 (ratio 2:9), over 70% cell death was observed with no transfection of the remaining cells (Figure 3.4).

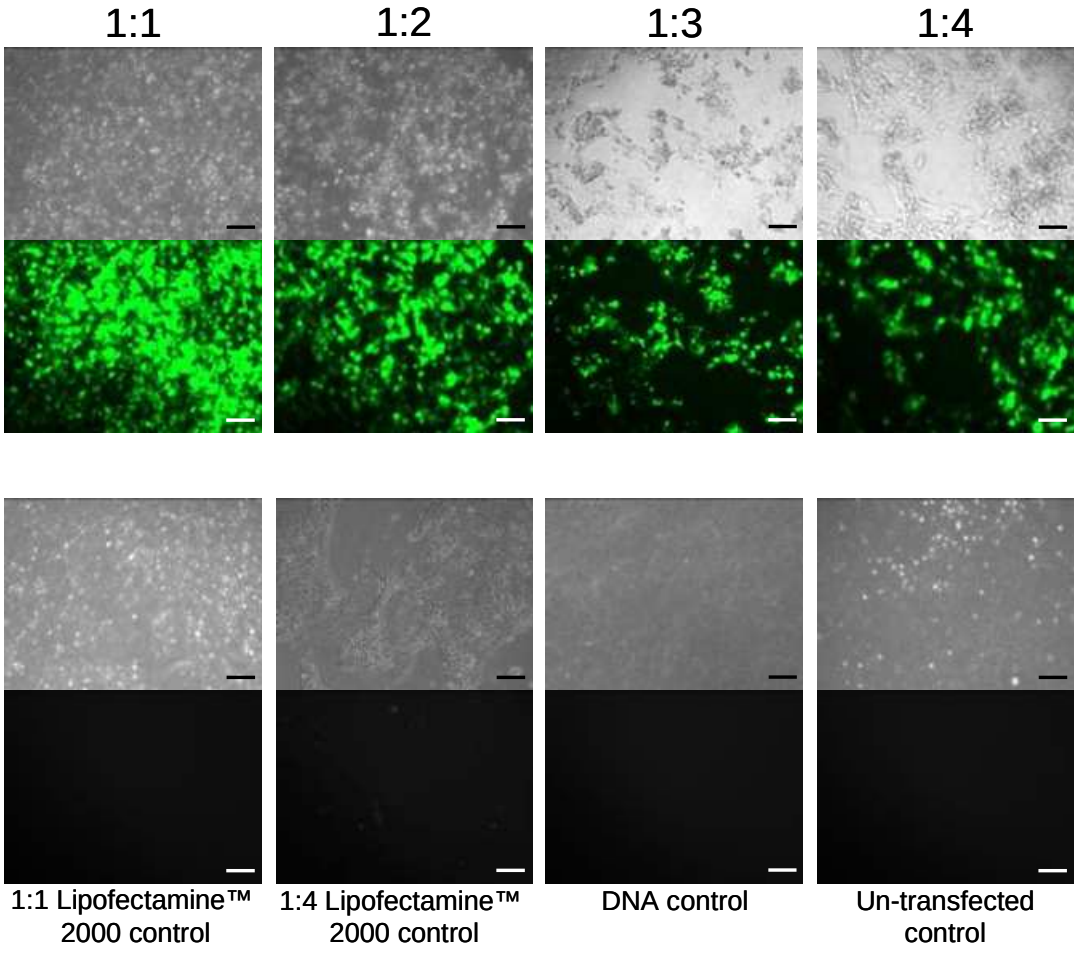

Figure 3.3 – Transfection optimisation using Lipofectamine™ 2000.

Transfection was optimised in RGE cells using an eGFP expression plasmid to allow determination of transfected cells after viewing by fluorescence microscopy. Lipofectamine™ 2000 reaction complexes were generated with a DNA (μg) to Lipofectamine™ 2000 (μl) ratio of 1:1, 1:2, 1:3 and 1:4 in Opti-MEM® I serum free media. Lipofectamine™ 2000 and DNA only controls were produced, in addition to a complete un-transfected control. Images were taken 48 hours after transfection and light-field images show the presence of cells (top) with the presence of eGFP expression shown below. Scale bar = 50 μm, magnification x 10.

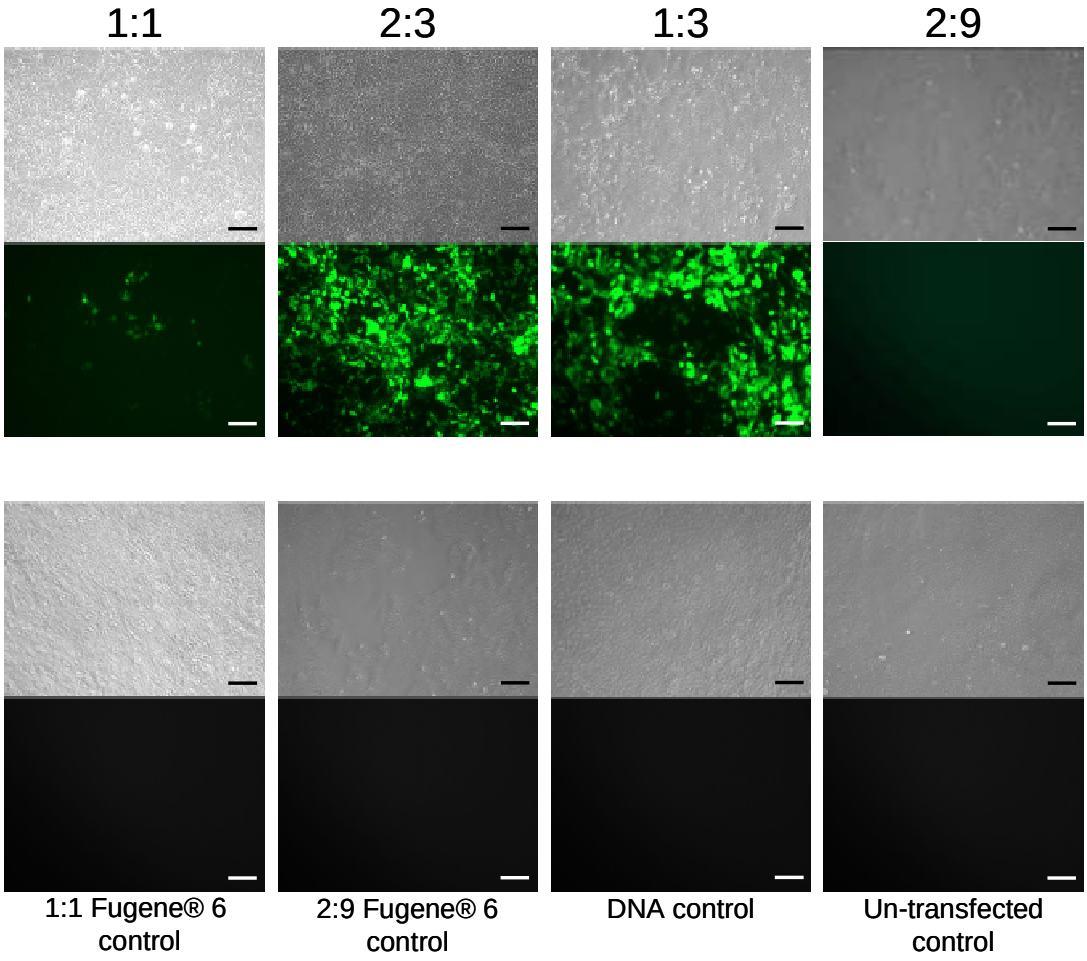

Figure 3.4 – Transfection optimisation using FuGENE® 6.

Transfection was optimised in RGE cells using an eGFP expression plasmid to allow determination of transfected cells after viewing by fluorescence microscopy. FuGENE® 6 reaction complexes were generated with a DNA (μg) to FuGENE® 6 (μl) ratio of 1:1, 2:3, 1:2 and 2:9 in Opti-MEM® I serum free media. FuGENE® 6 and DNA only controls were produced, in addition to a complete un-transfected control. Images were taken 48 hours after transfection and light-field images show the presence of cells (top) with the presence of eGFP expression shown below. Scale bar = 50 μm, magnification x 10.

Subsequent transfection experiments were performed with a 1:1 ratio of DNA to Lipofectamine™ 2000. The lowest dilution of this transfection reagent produced greater than 90% transfection of the RGE cells in the absence of visual cell death. Expression plasmids containing the sequences for the putative receptors for CRPPR, CSGMARTKC and CRSTRANPC, called CRIP-2, BC-10 and MPCII-3 respectively, were transfected into RGE cells. After the cells were incubated for 48 hours to allow expression of the transfected receptors to occur, 50 μmol/l of each of the peptides were added and incubated with the cells at 37°C for 10 minutes after which images were taken by fluorescence microscopy to visualise internalisation of the FITC-labelled peptides by transfected and control cells.

RGE cells were transfected with the expression plasmid for the putative receptor for the peptide CRPPR, CRIP-2 (Zhang *et al.*, 2005) (Figure 3.5) . The HIV-tat peptide effectively internalised into the transfected cells, however, lower levels of internalisation were observed for the other peptides (Figure 3.5). Transfection with the CRIP-2 expression plasmid did not enhance internalisation by the CRPPR peptide (Figure 3.5). RGE cells were also transfected with a BC-10 expression plasmid, the putative receptor for the CSGMARTKC peptide (Zhang *et al.*, 2005) (Figure 3.6). HIV-tat effectively internalised and CRSTRANPC also internalised into the transfected RGE cells (Figure 3.6), similar to the levels of internalisation seen in the non-transfected cells (Figure 3.2). Transfection of the BC-10 expression plasmid into the RGE cells did not enhance internalisation by CSGMARTKC (Figure 3.6). Finally, RGE cells were transfected with the MPCII-3 expression plasmid, the putative receptor for the peptide CRSTRANPC (Zhang *et al.*, 2005) (Figure 3.7). Again, HIV-tat produced high levels of internalisation in the transfected RGE cells; whereas the other peptides produced internalisation only in a few transfected cells (Figure 3.7).

Taken together, these data suggest that transfection of RGE cells with the expression plasmids for the putative receptors for the heart-targeted peptides did not significantly enhance internalisation of the peptides. The peptides did achieve low levels of internalisation into RGE cells, either transfected or non-transfected, but in all cases, the highest level of internalisation was produced by the HIV-tat peptide.

Based on this, it was concluded that RGE cells were not a suitable model system and consequently, *in vivo* experiments were progressed.

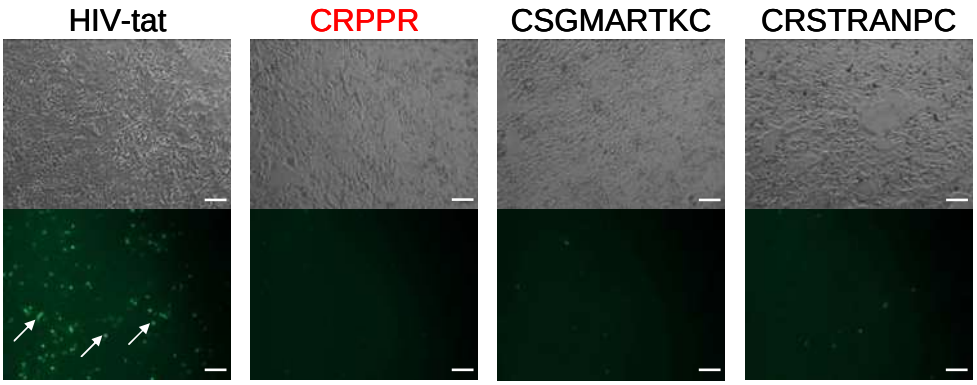

Figure 3.5 – Transfection of RGE cells with CRIP-2 expression plasmid.
RGE cells transfected with the CRIP-II expression plasmid, the putative receptor for the peptide CRPPR. Transfected cells were incubated with 50 μmol/l peptide at 37°C for 10 minutes. The cells were then washed and internalisation of the peptides by the cells was determined by the presence of the green FITC-labelled peptide after the cells were washed. Visualisation of the FITC-label was ascertained by fluorescence microscopy and arrows indicate cells with internalised peptides. Scale bar = 50 μm, magnification x 10.

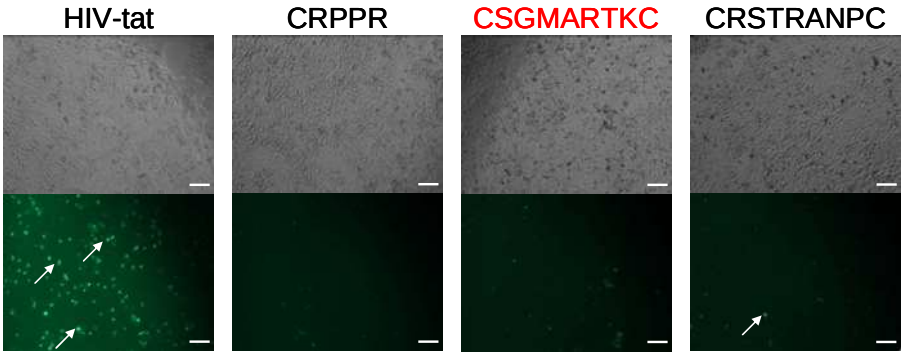

Figure 3.6 – Transfection of RGE cells with BC-10 expression plasmid.
RGE cells transfected with the BC-10 expression plasmid, the putative receptor for the peptide CSGMARTKC. Transfected cells were incubated with 50 µmol/l peptide at 37°C for 10 minutes. The cells were then washed and internalisation of the peptides by the cells was determined by the presence of the green FITC-labelled peptide after the cells were washed. Visualisation of the FITC-label was ascertained by fluorescence microscopy and arrows indicate cells with internalised peptides. Scale bar = 50 µm, magnification x 10.

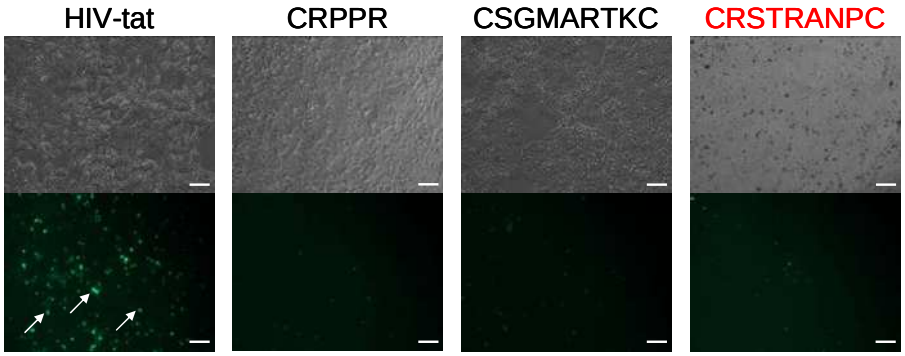

Figure 3.7 – Transfection of RGE cells with MPCII-3 expression plasmid.
RGE cells transfected with the MPCII-3 expression plasmid, the putative receptor for the peptide CRSTRANPC. Transfected cells were incubated with 50 µmol/l peptide at 37°C for 10 minutes. The cells were then washed and internalisation of the peptides by the cells was determined by the presence of the green FITC-labelled peptide after the cells were washed. Visualisation of the FITC-label was ascertained by fluorescence microscopy and arrows indicate cells with internalised peptides. Scale bar = 50 µm, magnification x 10.

3.2.3 *Assessment of phage displaying peptides after* in vivo *administration in the SHRSP*

As discussed above, peptide sequences which targeted the cardiac vasculature were identified in the mouse by phage display technology (Zhang *et al.*, 2005). Six phage inserted with the peptide sequences CGRKSKTVC, CPKRPR, CPKTRRVPC, CRPPR, CRSTRANPC and CSGMARTKC have been previously administered to the normotensive WKY rat to confirm the efficiency and selectivity of the peptides extended across species (Shirley, 2008). Phage recovery analysis from the major organs showed enhanced recovery of all six peptides from rat heart homogenates compared to control insert-less phage (Shirley, 2008). However, three of the peptides did not show strong selectivity for the heart, whereas CRPPR, CRSTRANPC and CSGMARTKC showed strong heart targeting with high selectivity (Shirley, 2008). Therefore, the phage with the most selective and effective heart-targeting peptide sequences (CRPPR, CRSTRANPC and CSGMARTKC) were tested in the SHRSP, a disease model of human essential hypertension. Co-localisation of phage in the heart and non-target organs was determined in the SHRSP, which included the aorta. Animals were intravascularly infused with $5x10^{10}$ pfu and the major organs recovered (n = 3 per group). Phage containing the peptide sequence CRSTRANPC showed no selective targeting to the heart in the SHRSP (Figure 3.8A). CRPPR targeted to the heart with a 17-fold increase over the control phage and further showed a 58-fold increase in targeting to the aorta (Figure 3.8B). CSGMARTKC displayed selective targeting for the heart with 26-fold greater homing to the heart than the control phage (Figure 3.8C).

Immunohistochemical analysis of major organs was performed with an anti-T7 antibody to determine the cell specific targeting within organs by the phage displaying each of the peptide sequences. Antibody detection was performed using DAB chromagen solution and sections were counterstained with Harris haematoxylin. Therefore, the nuclei appear blue/purple and areas to which the primary antibodies bound appear brown (Figure 3.9).

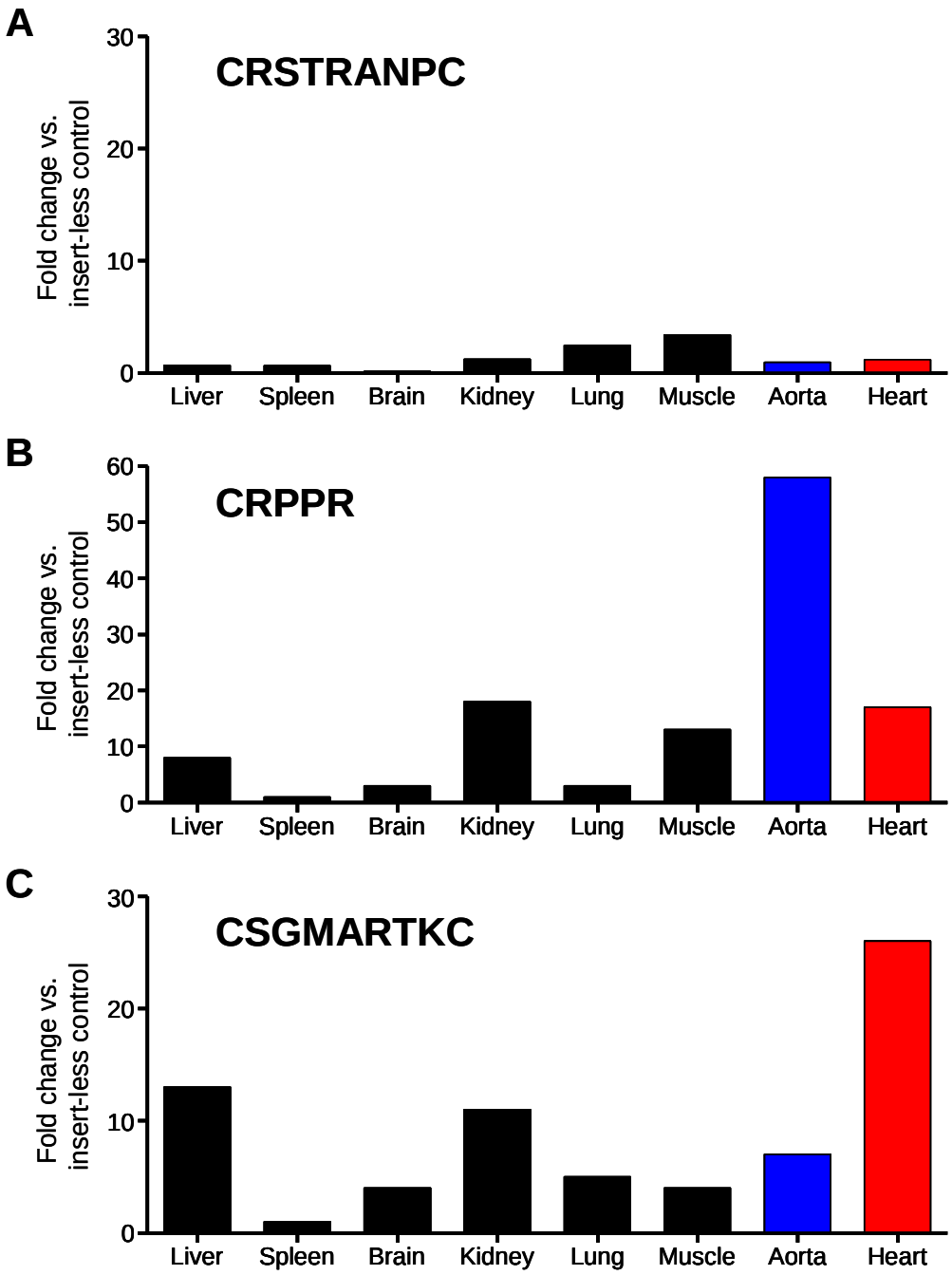

Figure 3.8 – Targeting capacity of peptide-inserted phage in SHRSP.

Recovery of T7 phage which displayed the cardiac endothelial homing peptides CRSTRANPC (A), CRPPR (B) and CSGMARTKC (C) from SHRSP animals intravenously infused with $5x10^{10}$ pfu of indicated phage. Data represented as fold change in comparison to control insert-less phage in liver, spleen, brain, kidney, lung, muscle, aorta and heart (n = 3/group).

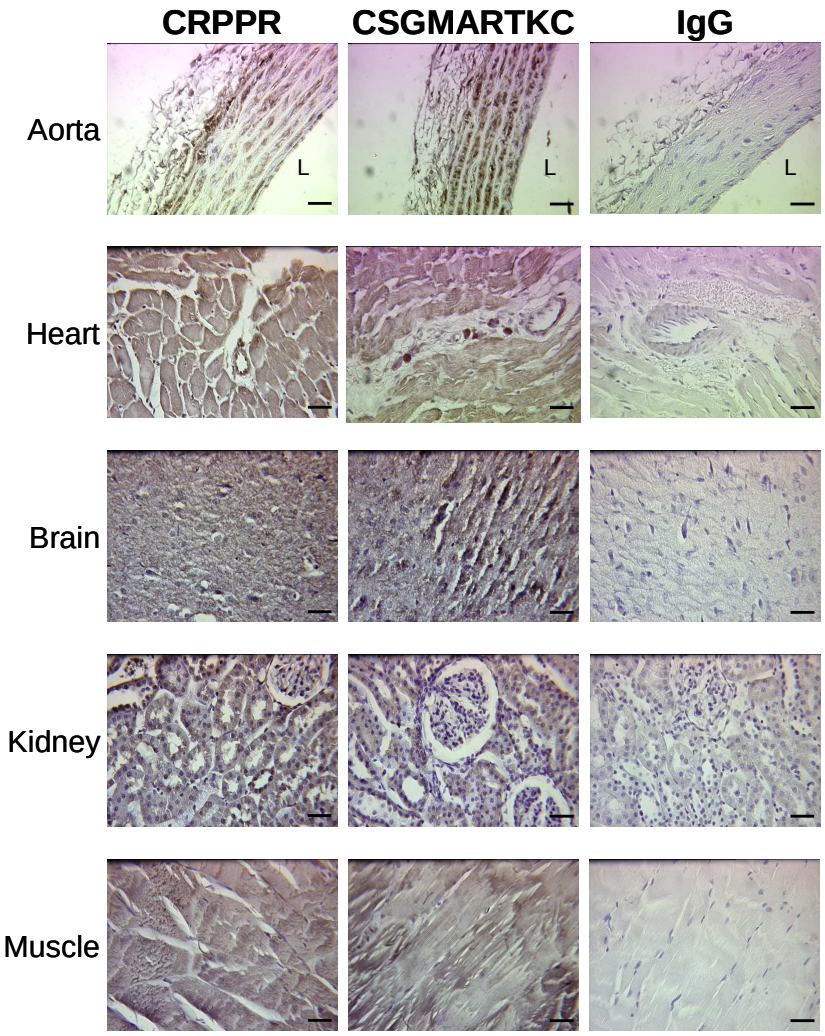

Figure 3.9 – Immunohistological analysis of targeting capacity of peptide-inserted phage in SHRSP.

Immunohistological analysis of vascular targeting with an anti-T7 antibody or IgG control antibody was performed on sections of heart, aorta, muscle, brain and kidney from SHRSP intravenously infused with $5x10^{10}$ pfu of peptide-inserted T7 phage. Binding by the anti-T7 and IgG antibodies was detected using DAB chromagen (areas to which the primary antibody bound appear brown) and followed by incubation with Harris haematoxylin (nuclei appear blue/purple). The IgG antibody provides a negative control to test for non-specific binding of the primary antibody, as the sections incubated with IgG show no brown staining the binding of the primary antibody is specific. L indicates luminal side of aorta. Scale bar = 100 µm, magnification × 40.

Phage containing the peptide sequence CRPPR localised to both ECs and SMCs in the aorta (Figure 3.9). There was a high degree of staining in the aorta from animals infused with phage inserted with the peptide sequence CSGMARTKC but this was diffuse and non-specific (Figure 3.9). Phage inserted with CSGMARTKC selectively bound to the coronary vessels of the heart (Figure 3.9). In the brain, kidney and muscle, the staining was non-specific, indicating little binding by the phage in these non-target organs (Figure 3.9).

Taken together, phage inserted with the CRPPR peptide selectively target both the endothelial and smooth muscle layers of the aorta and CSGMARTKC-containing phage target the coronary vasculature in the SHRSP. Therefore, these peptide sequences may enhance the efficacy of an anti-oxidant therapy by selectively targeting specifically to the vasculature.

3.2.4 Administration of peptides into SHRSP

To investigate the effect of targeting the anti-oxidant peptide gp91ds (Rey *et al.*, 2001) with either the CRPPR or CSGMARTKC peptides *in vivo*, an *in vivo* protocol was designed in the SHRSP (Figure 3.10A). Animals underwent baseline, 7 day and terminal ECHOs to monitor heart function and were placed on radio-telemetry 10 days before the start of the experiment. Telemetry was used to monitor BP, heart rate (HR) and activity of the animals from one week prior to administration of the peptides and for the three weeks of study duration. Peptides were continuously administered at 10 mg/kg/day for 21 days by subcutaneous osmotic mini-pumps. BP and HR takes up to 7 days to stabilise post-operatively (Davidson *et al.*, 1995), therefore, mini-pumps were implanted two weeks after telemetry implantation and telemetry data were collected for one week prior to implantation of the mini-pumps and for the 21 days on treatment.

There were four treatment groups in the *in vivo* study, in addition to a control group which only received vehicle by mini-pump. Four groups of animals were continuously administered with a peptide: the two heart-targeting peptides (CRPPR and CSGMARTKC) linked to the anti-oxidant peptide, the HIV-tat peptide linked to the anti-oxidant peptide as a positive control to allow entry to all cells and the anti-

oxidant peptide alone as a negative control, to allow determination of the effect produced by targeting the anti-oxidant peptide (Figure 3.10B).

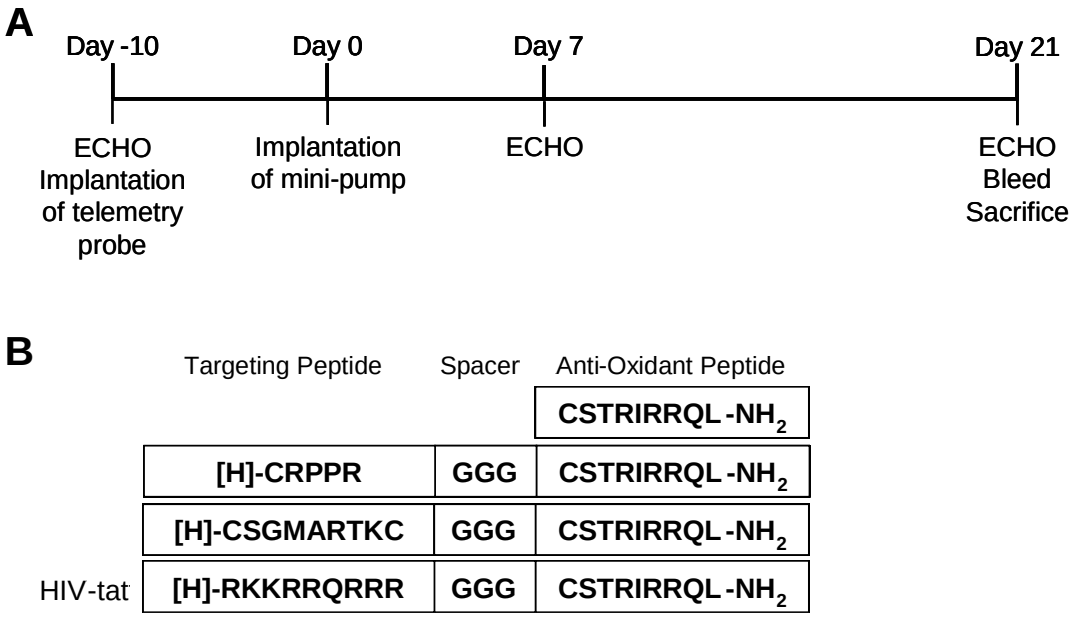

Figure 3.10 – Animal protocol and design of vascular targeting anti-oxidant peptides.

(A) *In vivo* animal protocol used for administration of vascular targeting anti-oxidant peptides in the SHRSP. Day 0 indicates the start of the continuous infusion of peptides by subcutaneous osmotic mini-pump. Peptides were administered at 10 mg/kg/day for 21 days. (B) Sequence of anti-oxidant peptide gp91ds (Rey *et al.*, 2001), the anti-oxidant peptide targeted with either CRPPR or CSGMARTKC peptides and non-targeted anti-oxidant peptide linked to the HIV-tat peptide.

3.2.5 Effect of vascular targeting anti-oxidant peptide on BP

BP in the SHRSP was determined by radio-telemetry for one week at baseline prior to mini-pump implantation, followed by three weeks of study duration before sacrifice (Figures 3.11, 3.12, 3.13). Systolic BP showed a progressive and time-dependent rise in animals receiving the anti-oxidant peptide gp91ds alone, HIV-tat-gp91ds, CSGMARTKC-gp91ds and control animals from 177.6 ± 1.1 mmHg to 200.6 ± 0.7 mmHg (Figure 3.11), characteristic of the SHRSP (Davidson *et al.*, 1995, Clark *et al.*, 1996). However, this increase in systolic BP was significantly attenuated in animals receiving CRPPR-linked to the anti-oxidant peptide with the maximum systolic BP only reaching 187.5 ± 5.2 mmHg (Figure 3.11). Diastolic BP in animals treated with CSGMARTKC-gp91ds, HIV-tat-gp91ds and gp91ds alone also showed a progressive rise over the three weeks of the study (Figure 3.12). There was also a significant attenuation in the rise in diastolic BP in animals treated with CRPPR-gp91ds (Figure 3.12). However, the average diastolic BP of animals in the control group was highly variable and not significantly different for the animals which received CRPPR-gp91ds (Figure 3.12).

Mean arterial pressure (MAP) was also calculated by the telemetry equipment using the following formula:

MAP = DBP + 1/3 PP (where DBP is diastolic BP and PP is pulse pressure, defined by the difference between systolic and diastolic BP (SBP-DBP))

MAP showed a progressive rise in animals receiving CSGMARTKC-gp91ds, HIV-tat-gp91ds, gp91ds alone and control animals from 163.6 ± 1.1 mmHg to 170.5 ± 0.8 (Figure 3.13). This increase in MAP was significantly attenuated in animals receiving CRPPR-gp91ds as the maximum MAP only reached 160.0 ± 5.0 mmHg (Figure 3.13). Taken together these data suggest that only when the anti-oxidant peptide was targeted by the CRPPR peptide could it produce a significant reduction in systolic BP and MAP in the SHRSP.

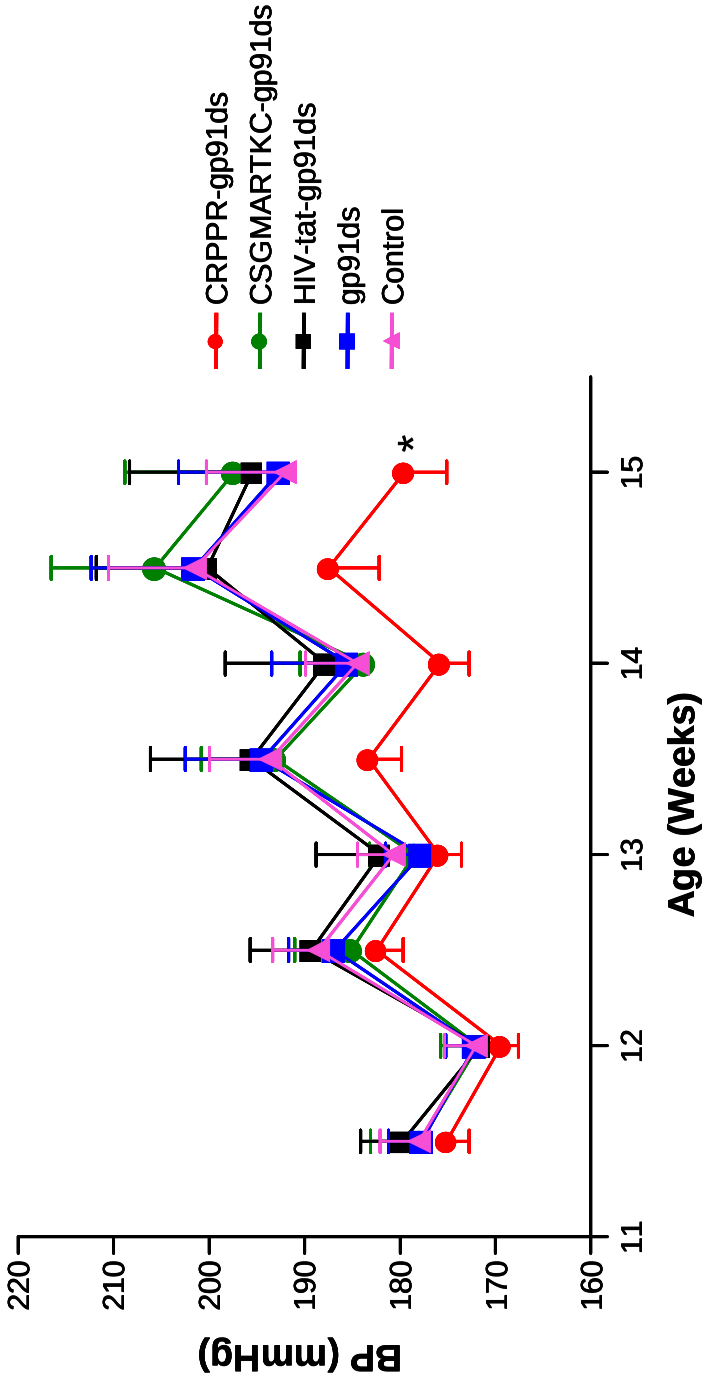

Figure 3.11 – Effect of vascular targeting anti-oxidant peptide on systolic BP.

Systolic BP in SHRSP was determined for one week at baseline prior to mini-pump implantation, followed by three weeks of study duration before sacrifice. Error bars represent SEM (* $p < 0.001$ vs. all other groups, n = 6/group).

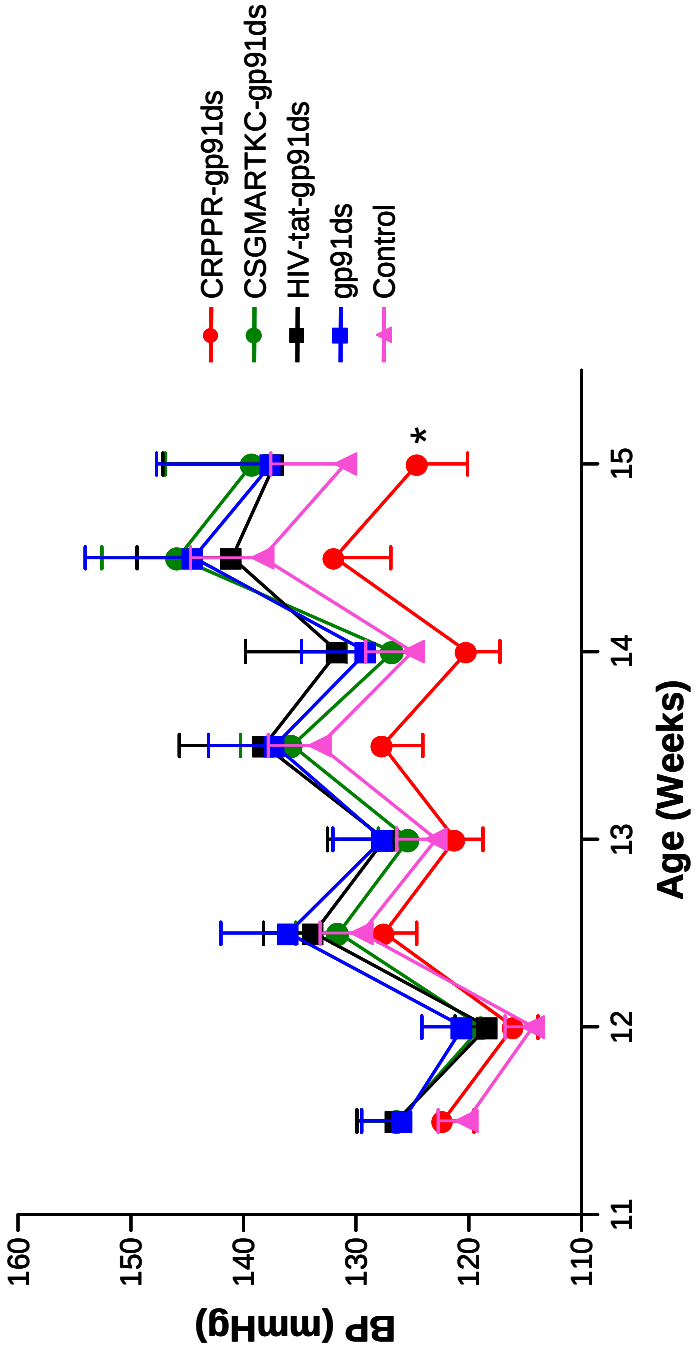

Figure 3.12 – Effect of vascular targeting anti-oxidant peptide on diastolic BP.

Diastolic BP in SHRSP was determined for one week at baseline prior to mini-pump implantation, followed by three weeks of study duration before sacrifice. Error bars represent SEM (* $p < 0.001$ vs. CSGMARTKC-gp91ds, HIV-tat-gp91ds and gp91ds, n = 6/group).

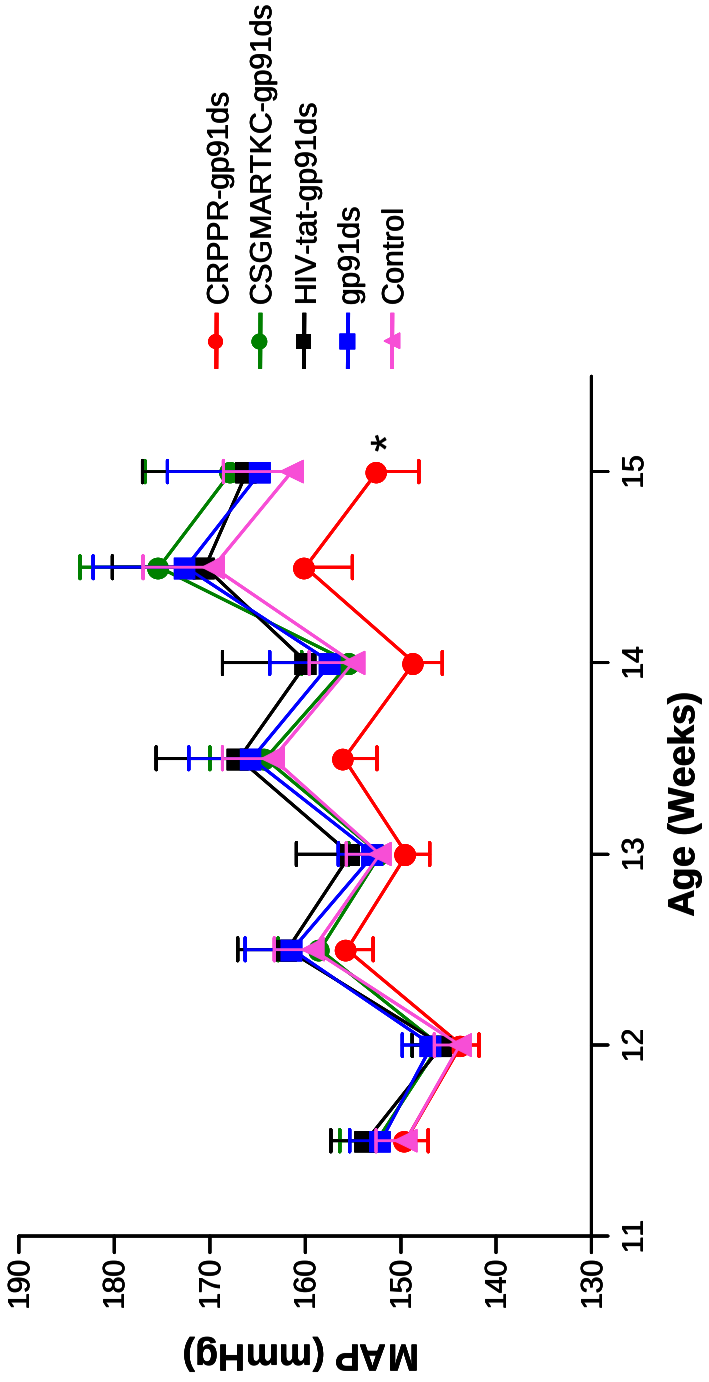

Figure 3.13 – Effect of vascular targeting anti-oxidant peptide on mean arterial pressure (MAP).

MAP in SHRSP was determined for one week at baseline prior to mini-pump implantation, followed by three weeks of study duration before sacrifice. Error bars represent SEM (* $p < 0.01$ vs. all other groups, gp91ds, n = 6/group).

3.2.6 Effect of vascular targeting anti-oxidant peptide on cardiac function

Animals underwent baseline (at 10 weeks of age), 7 day (at 13 weeks of age) and terminal (at 15 weeks of age) trans-thoracic left ventricular M-mode ECHO to monitor heart function performed by Dr. K. Gilday (University of Glasgow, UK). ECHOs allow measurement of cardiac function parameters including stroke volume (SV), left ventricular ejection fraction (LVEF) and left ventricular mass index (LVMI). Also, in combination with the heart rate (HR) data obtained by telemetry, the cardiac output (CO) can also be calculated. ECHO parameters were compared to control animals at the corresponding time point.

Heart rate significantly decreased over the time period of the study, consistent with growth of the animal, and there was no significant difference between the groups (Figure 3.14). The stroke volume (the volume of blood pumped from the left ventricle per beat) in the control group increased progressively over time (Figure 3.15). At 13 weeks, there was a significant difference between the stroke volume of the control animals and animals treated with CSGMARTKC-gp91ds, HIV-tat-gp91ds and the anti-oxidant gp91ds peptide alone (Figure 3.15). At 15 weeks, the stroke volume of the control group had increased to 0.76 ± 0.03 ml and was significantly higher than animals treated with HIV-tat-gp91ds and gp91ds alone at the same time point (Figure 3.15, Table 4). As cardiac output is a function of heart rate and stroke volume, cardiac output also progressively increased in the control animals from 203.5 ± 16.0 ml/min to 315.7 ± 30.6 ml/min between 10 and 15 weeks of age (Figure 3.16, Table 4). The cardiac output of the control animals was significantly increased compared to CSGMARTKC-gp91ds, HIV-tat-gp91ds and the gp91ds peptide alone at 13 weeks and compared to all treatment groups at 15 weeks (Figure 3.16).

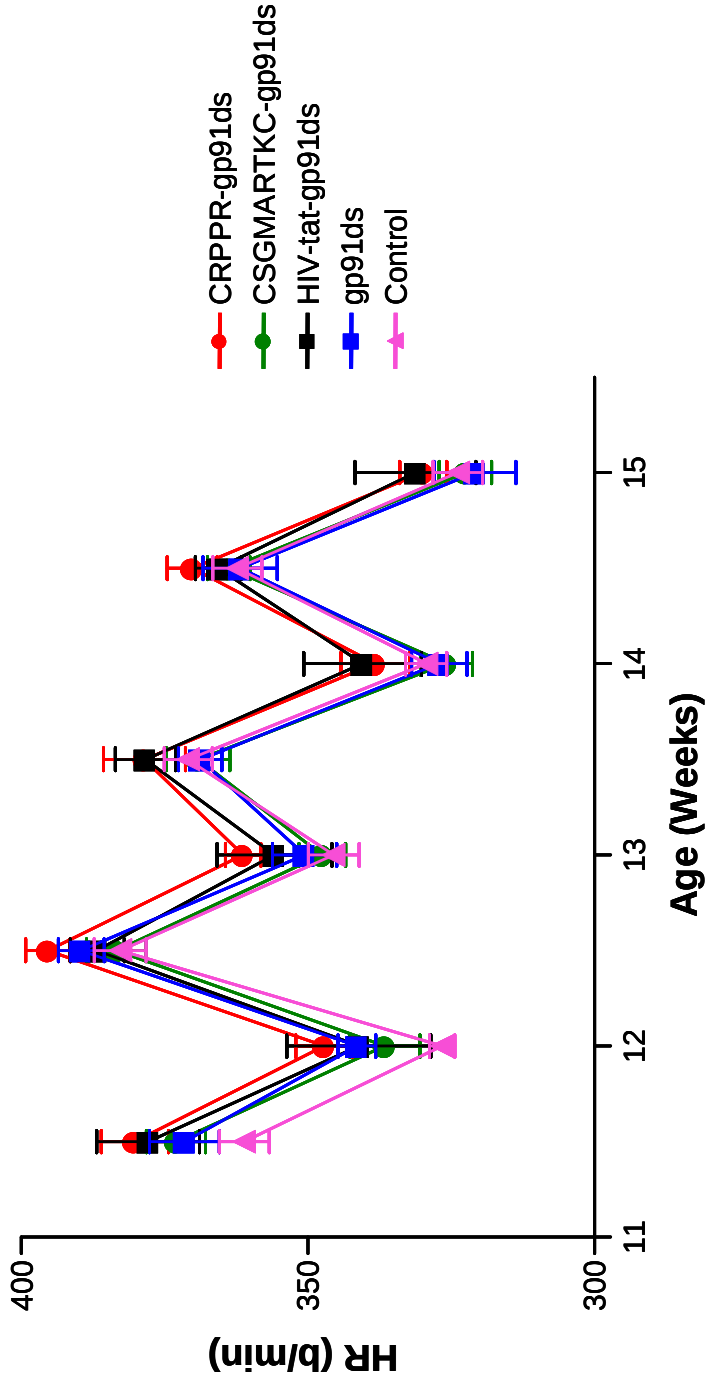

Figure 3.14 – Effect of vascular targeting anti-oxidant peptide on HR.

HR in SHRSP was determined for one week at baseline prior to mini-pump implantation, followed by three weeks of study duration before sacrifice. Error bars represent SEM (no statistically significant difference between the groups by repeated measures ANOVA, n = 6/group). b/min, beats per minute.

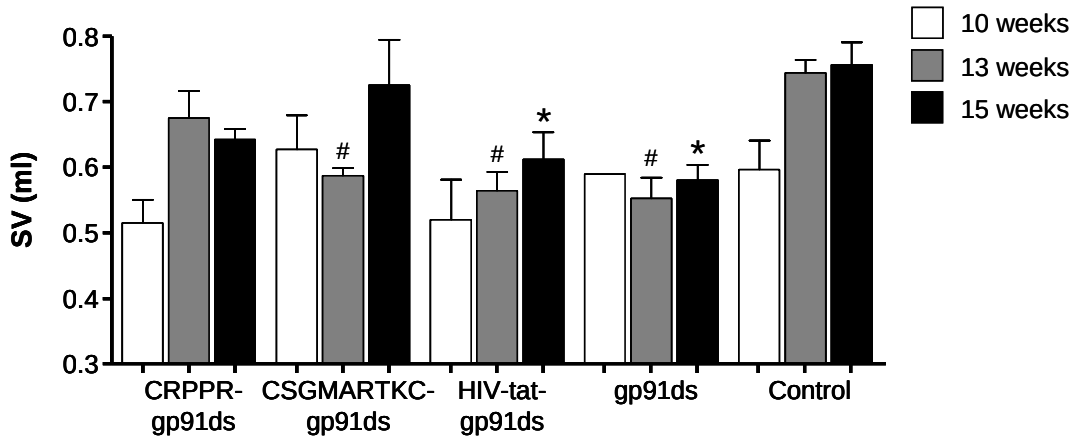

Figure 3.15 – Effect of vascular targeting anti-oxidant peptide on stroke volume.

Animals underwent baseline, 7 day and terminal trans-thoracic ECHOs to determine stroke volume (SV). Error bars represent SEM (# $p < 0.05$ vs. control at 13 weeks, * $p < 0.05$ vs. control at 15 weeks, n = 6/group).

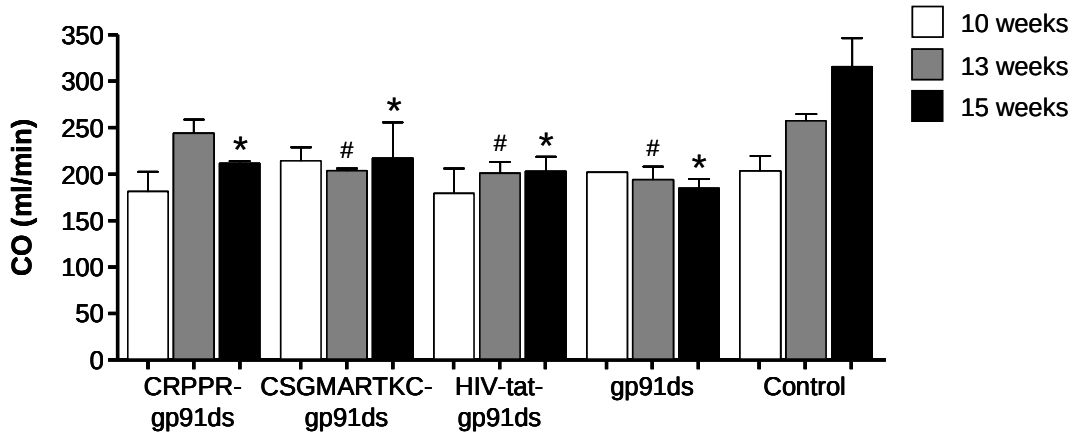

Figure 3.16 – Effect of vascular targeting anti-oxidant peptide on cardiac output.

Animals underwent baseline, 7 day and terminal trans-thoracic ECHOs. By determination of stroke volume by ECHO and heart rate by telemetry, cardiac output (CO) was calculated. Error bars represent SEM (# $p < 0.05$ vs. control at 13 weeks, * $p < 0.05$ vs. control at 15 weeks, n = 6/group).

The left ventricular ejection fraction (LVEF), the percentage of blood pumped out of the left ventricle with each beat, decreased over time in the control animals and animals treated with gp91ds alone (Figure 3.17). However, in animals treated with CRPPR-gp91ds, the LVEF increased from 87.2 ± 4.8% to 89.5 ± 1.0% (Figure 3.17, Table 4). The LVMI of control animals and animals treated with CSGMARTKC-gp91ds and the anti-oxidant peptide alone increased progressively over time from 10 to 15 weeks of age, consistent with growth of the animal (Figure 3.18). Animals treated with CRPPR-gp91ds and HIV-tat-gp91ds did not show an increase in LVMI over time (Figure 3.18).

Treatment Group	HR (b/min)	SV (ml)	CO (ml/min)	LVEF (%)	LVMI (g/mm)
CRPPR-gp91ds	329.6 ± 5.3	0.64 ± 0.02	211.5 ± 2.3 *	89.5 ± 1.0	1.70 ± 0.09
CSGMARTKC-gp91ds	324.4 ± 5.4	0.73 ± 0.07	217.2 ± 38.4 *	86.0 ± 1.1	1.92 ± 0.10
HIV-tat-gp91ds	331.2 ± 10.5	0.61 ± 0.04 *	203.0 ± 15.8 *	85.1 ± 2.3	1.67 ± 0.06
gp91ds	318.4 ± 8.7	0.58 ± 0.02 *	184.8 ± 9.8 *	85.7 ± 3.2	1.88 ± 0.08
Control	323.2 ± 5.1	0.76 ± 0.03	315.7 ± 30.6	85.5 ± 0.8	1.85 ± 0.05

Table 4 – Effect of vascular targeting anti-oxidant peptide on ECHO parameters at 15 weeks.

Animals underwent terminal trans-thoracic ECHOs at 15 weeks of age to determine stroke volume (SV), left ventricular ejection fraction (LVEF) and left ventricular mass index (LVMI). Heart rate (HR) was measured by telemetry and cardiac output (CO) was calculated. Value ± SEM (* $p < 0.05$ vs. control).

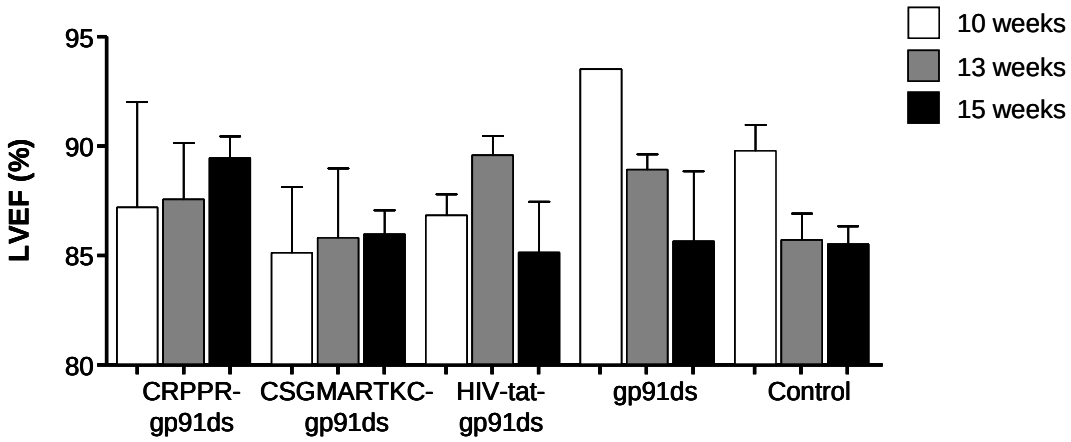

Figure 3.17 – Effect of vascular targeting anti-oxidant peptide on LVEF.

Animals underwent baseline, 7 day and terminal trans-thoracic ECHOs to determine left ventricular ejection fraction (LVEF). Error bars represent SEM (no statistically significant differences between the treatment groups and control animals at 13 and 15 weeks by one-way ANOVA, n = 6/group).

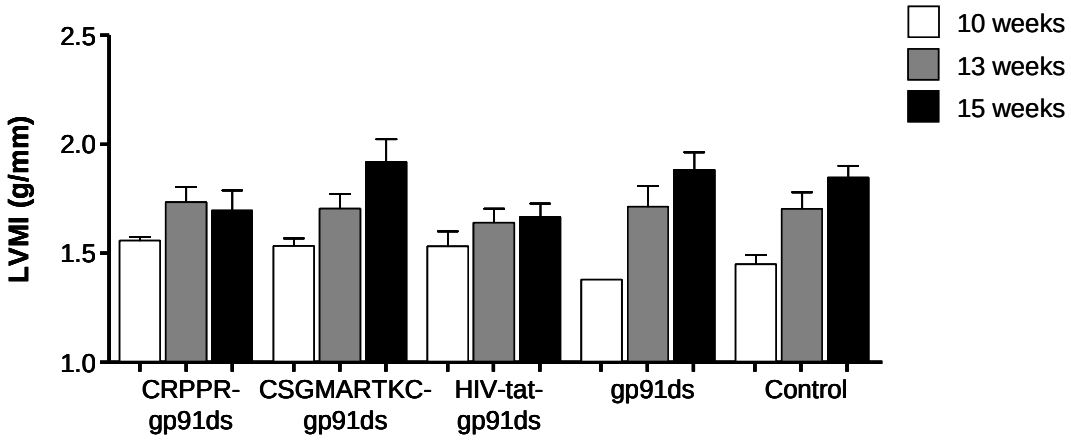

Figure 3.18 – Effect of vascular targeting anti-oxidant peptide on LVMI.

Animals underwent baseline, 7 day and terminal trans-thoracic ECHOs to determine LVMI. Error bars represent SEM (no statistically significant differences between the treatment groups and control animals at 13 and 15 weeks by one-way ANOVA, n = 6/group).

3.2.7 Effect of vascular targeting anti-oxidant peptide on NO bioavailability

At sacrifice, the thoracic aorta of all animals (n = 6/group) and the third order mesenteric arteries of three animals from each group were removed for functional studies by large vessel and small vessel myography, respectively.

3.2.7.1 Large vessel myography

At sacrifice, the thoracic aorta of all animals (n = 6/group) was removed for functional studies by large vessel myography to determine NO bioavailability. Cumulative concentration-response curves to phenylephrine (PE) were performed (1 nmol/l to 10 μmol/l) and subsequently repeated in the presence of 100 μmol/l N-nitro-L-arginine methyl ester (L-NAME) to competitively inhibit eNOS. The response to PE was expressed as the percentage of the maximum contraction produced during the first PE curve and the difference between the two curves indicates the degree of NO bioavailability (Figure 3.19). PE produces vasoconstriction by activation of α_1-adrenoceptors and an increased contraction to an equivalent concentration of PE in the presence of L-NAME would indicate a degree of basal release of NO in the aorta. However, if the PE concentration-response curve was comparable in the presence and absence of L-NAME, this would indicate no basal NO release was present, indicative of endothelial dysfunction.

There was no difference between the two curves for animals treated with the HIV-tat peptide linked to anti-oxidant peptide, which indicates impaired endothelial function characteristic of the SHRSP and consistent with previous studies (Kerr *et al.*, 1999, Hamilton *et al.*, 2002) (Figure 3.19C). CRPPR-gp91ds (Figure 3.19A), CSGMARTKC-gp91ds (Figure 3.19B) and the anti-oxidant peptide gp91ds alone (Figure 3.19D) showed significantly improved NO bioavailability. The greatest difference between the two curves in the presence and absence of L-NAME occurred in those animals treated with CRPPR linked to the anti-oxidant peptide (Figure 3.20). This indicates that targeting the anti-oxidant peptide to the vasculature by the CRPPR peptide enhances the ability of the anti-oxidant peptide to increase NO bioavailability.

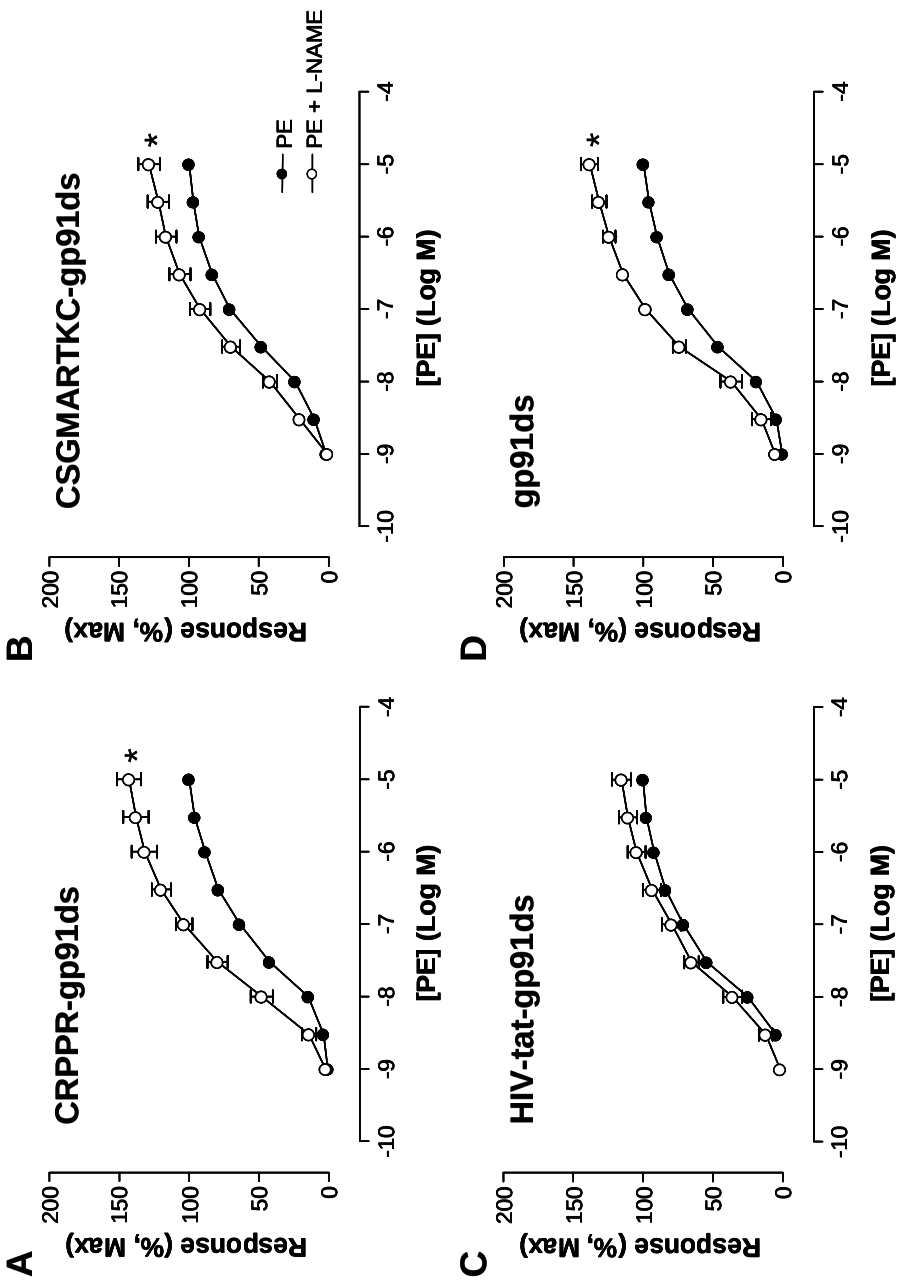

Figure 3.19 – Effect of vascular targeting anti-oxidant peptide on NO bioavailability in the aorta.

Concentration-response curve to phenylephrine (PE) produced by large vessel myography on the thoracic aorta, repeated in the presence of 100 μmol/l L-NAME. Response to PE was expressed as percentage of maximum contraction produced during the first PE curve. Error bars represent SEM (* $p < 0.001$ vs. PE curve, n = 6/group).

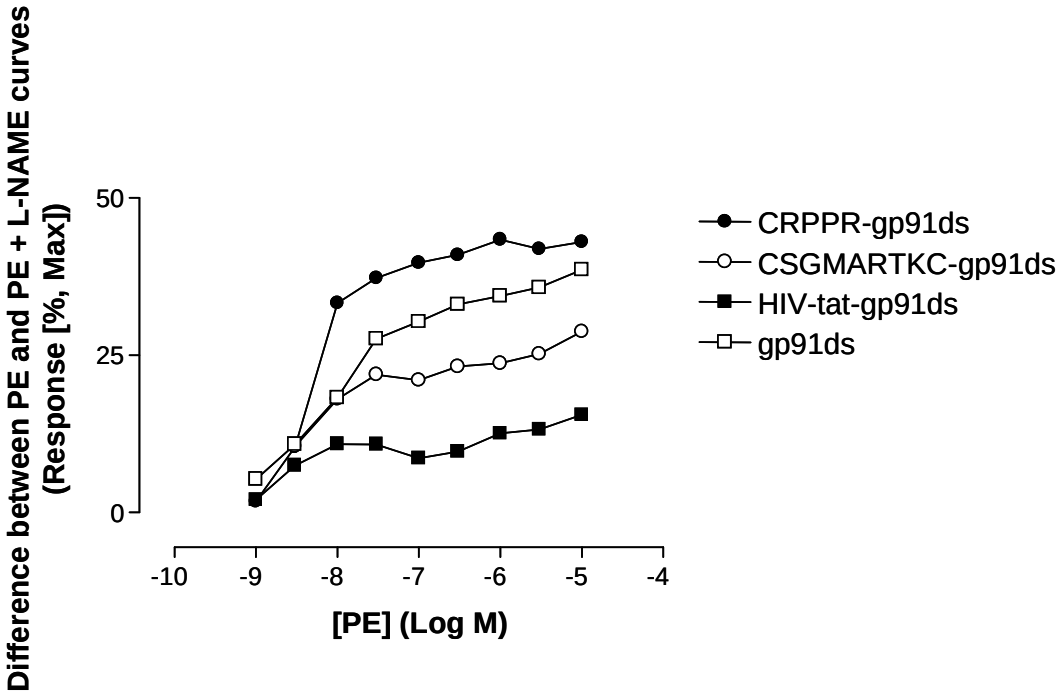

Figure 3.20 – Differential effect of vascular targeting anti-oxidant peptide on NO bioavailability in the aorta.

Calculated difference between concentration-response curve to PE and PE curve repeated in the presence L-NAME for each treatment group.

Peptide	$LogEC_{50}$ (M)	EC_{50}	
		Mean (µmol/l)	SEM (µmol/l)
CRPPR-gp91ds	-3.56	272.6	54.4
CSGMARTKC-gp91ds	-3.56	277.4	46.8
HIV-tat-gp91ds	-3.47	339.7	57.4
gp91ds	-3.53	293.9	37.0

Table 5 – $LogEC_{50}$ and EC_{50} values for apocynin concentration-response curves.

$LogEC_{50}$ and EC_{50} values calculated from concentration-response curves to apocynin produced by large vessel myography on the thoracic aorta. SEM, standard error of the mean.

In addition, other sections of the thoracic aorta were used to perform cumulative concentration-response curves to apocynin (10 μmol/l to 1 mmol/l) directly after a cumulative concentration-response curve to PE was constructed (n = 6/group). Response to apocynin was expressed as the percentage of the maximum contraction produced during the first PE curve (Figure 3.21). Apocynin was first characterised as a reversible inhibitor of NAD(P)H oxidase (Simons *et al.*, 1990) and as such has been used for numerous studies investigating the action of vascular oxidases. However, recently apocynin has been shown to also act an anti-oxidant (Heumuller *et al.*, 2008).

Increasing concentrations of apocynin increased relaxation by the vessel for all treatment groups (Figure 3.21). Only aorta taken from animals treated with CRPPR-gp91ds achieved a complete relaxation in the presence of apocynin (Figure 3.21A). In addition, the EC_{50} value was calculated for the apocynin concentration-response curves to determine half maximal effective concentration of apocynin in each treatment group (Table 5). The targeting peptides CRPPR and CSGMARTKC linked to the anti-oxidant peptide had substantially lower EC_{50} values (272.6 μmol/l and 277.4 μmol/l, respectively) compared to HIV-tat-gp91ds and gp91ds alone, EC_{50} values of 339.7 μmol/l and 293.9 μmol/l, respectively (Table 5). Therefore, apocynin had a greater efficacy in animals treated with the targeting peptides linked to the anti-oxidant peptide, in particular CRPPR-gp91ds.

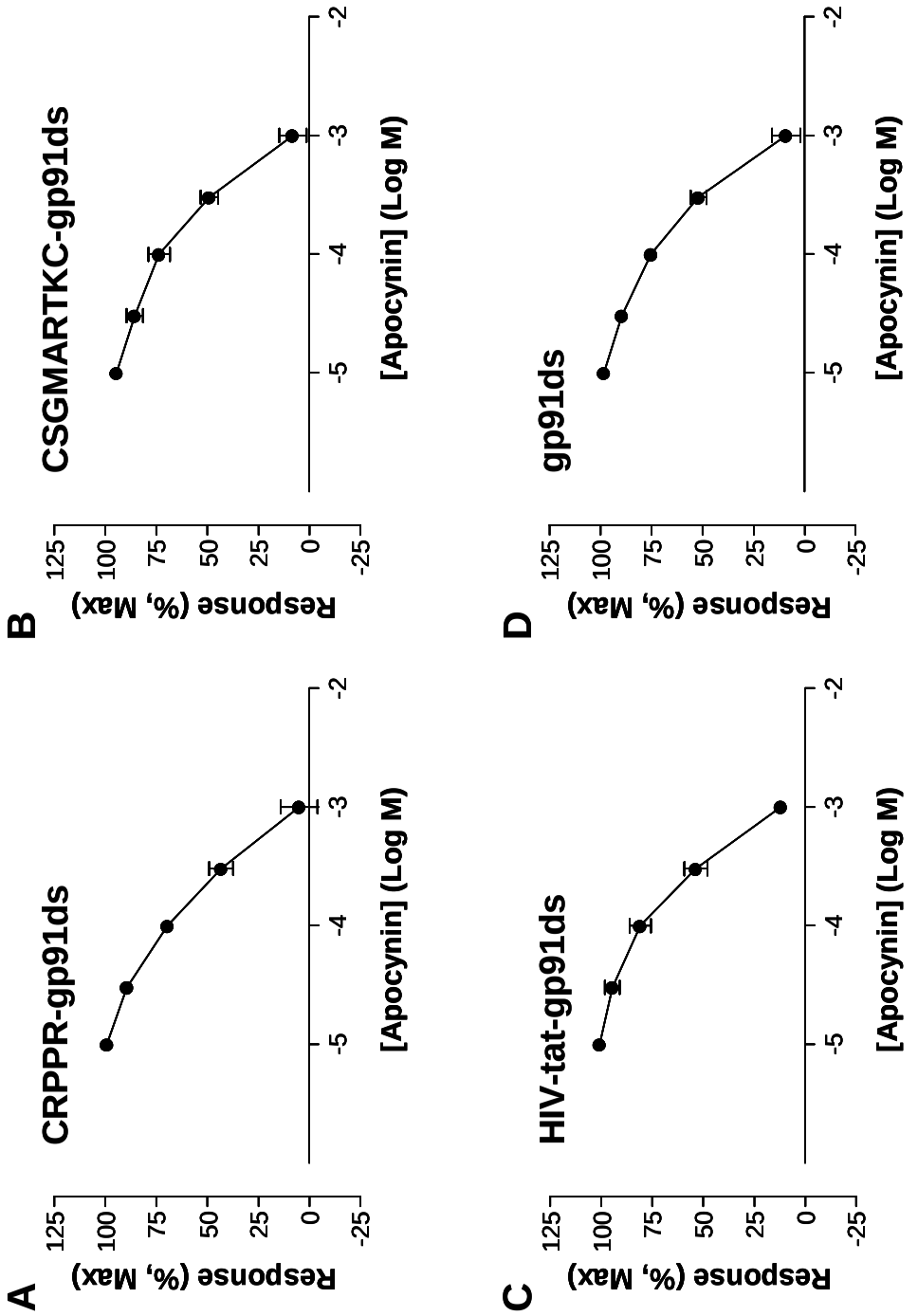

Figure 3.21 – Effect of vascular targeting anti-oxidant peptide on NAD(P)H oxidase activity in the aorta.

Concentration-response curve to apocynin produced by large vessel myography on the thoracic aorta and expressed as percentage of maximum contraction produced during the third PE curve. Error bars represent SEM (n = 6/group).

3.2.7.2 Small vessel myography

In addition to large vessel myography on the thoracic aorta, small vessel myography was also performed on third order mesenteric arteries to determine the NO bioavailability of resistance vessels. Vessels were removed at sacrifice from three animals from each group, dissected from connective tissue and segments (approximately 2 mm in length) were mounted as ring preparations on two stainless steel wires on a small vessel myograph. Following an internal diameter normalisation period, a cumulative concentration-response curve to PE (1 nmol/l to 30 μmol/l) was performed in the absence and presence of 100 μmol/l L-NAME. The difference between the two curves indicates the degree of NO bioavailability (Figure 3.22).

There was no significant difference between the two curves for animals treated with CRPPR-gp91ds (Figure 3.22A). However, there was a clear difference between the straight sections of the sigmoid curve indicating an enhanced efficacy of PE in the presence of L-NAME (Figure 3.22). CSGMARTKC-gp91ds (Figure 3.22B), HIV-tat-gp91ds (Figure 3.22C) and the anti-oxidant peptide gp91ds alone (Figure 3.22D) showed significantly improved NO bioavailability. Therefore, this suggests that all the peptides are producing an effect on NO bioavailability in resistance arteries.

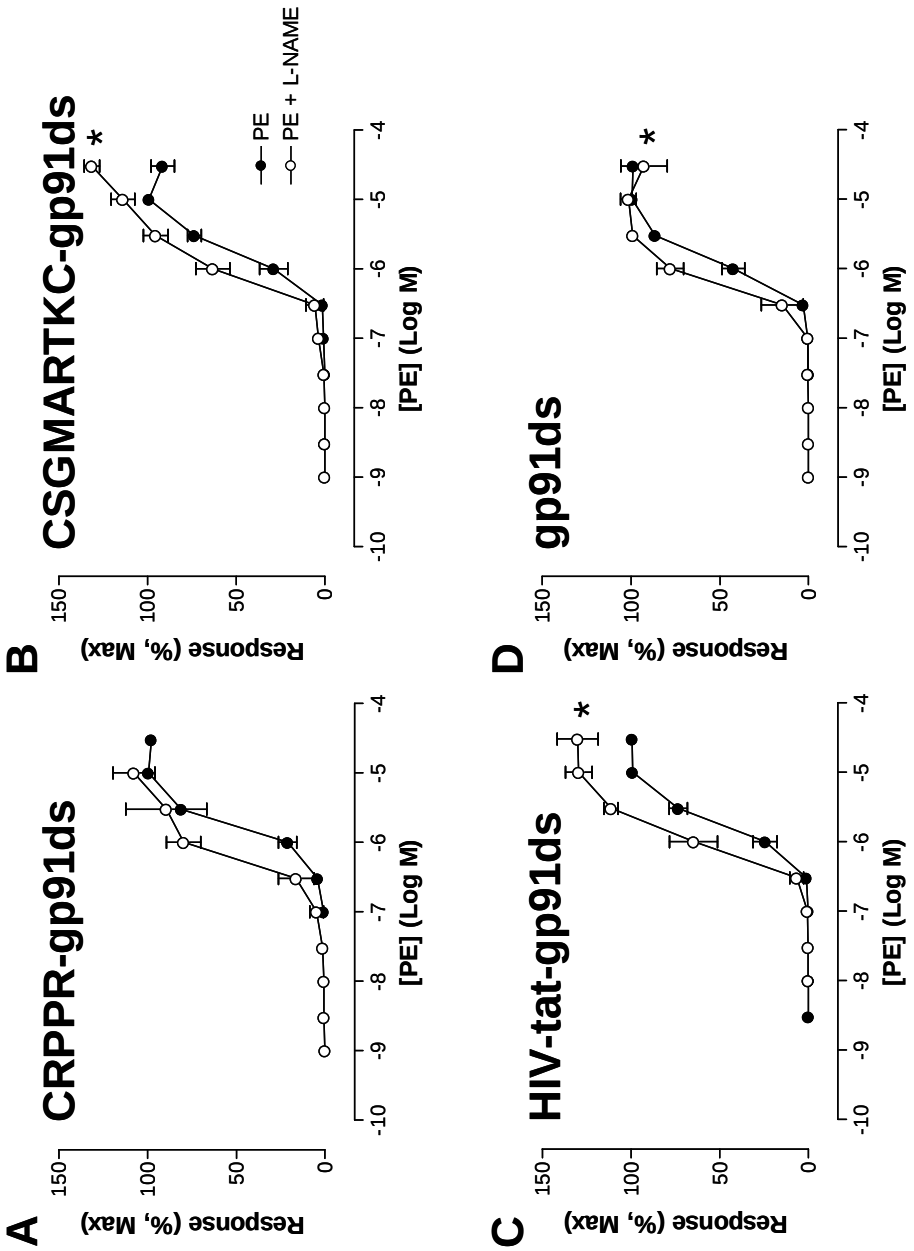

Figure 3.22 – Effect of vascular targeting anti-oxidant peptide on NO bioavailability in resistance arteries.

Concentration-response curve to phenylephrine (PE) produced by small vessel myography on third order mesenteric arteries, repeated in the presence of 100 μmol/l L-NAME. Response to PE was expressed as percentage of maximum contraction produced during the first PE curve. Error bars represent SEM (* $p < 0.01$ vs. PE curve, n = 3/group).

3.2.8 Effect of vascular targeting anti-oxidant peptide on cardiac histology

Due to the differences in some relevant cardiac parameters between the groups, the structure of the heart was investigated by histology. After the removal of paraffin and rehydration, sections were stained with haemotoxylin and eosin (H&E), which stains nuclei blue/purple and the cytoplasm of cells pink (Figure 3.23). For investigation into differences in collagen deposition, picro-sirius red and Masson's trichrome staining were used. Picro-sirius red stains collagen red on a pale yellow background (Figure 3.24) Masson's trichrome staining produces black cell nuclei, red cytoplasm and muscle fibres and collagen was stained blue (Figure 3.25). There were no differences observed between the sections of heart taken from animals from each treatment group.

3.2.9 Effect of vascular targeting anti-oxidant peptide on oxidative stress status

Overall oxidative stress status was assessed by SO release from heparinised whole blood by electron paramagnetic resonance (EPR). Blood samples were taken by cardiac puncture at sacrifice and incubated for 30 minutes at 37°C with 500 μmol/l of CPH spin probe before being snap frozen in liquid nitrogen. The rate of SO production by the frozen samples was calculated as counts per minute by EPR. There was a significant difference in SO production levels between control animals and animals treated with CRPPR-gp91ds and HIV-tat-gp91ds (Figure 3.26). In addition, there was a significant reduction in SO production in HIV-tat-gp91ds treated animals compared to animals treated with CRPPR-gp91ds (Figure 3.26).

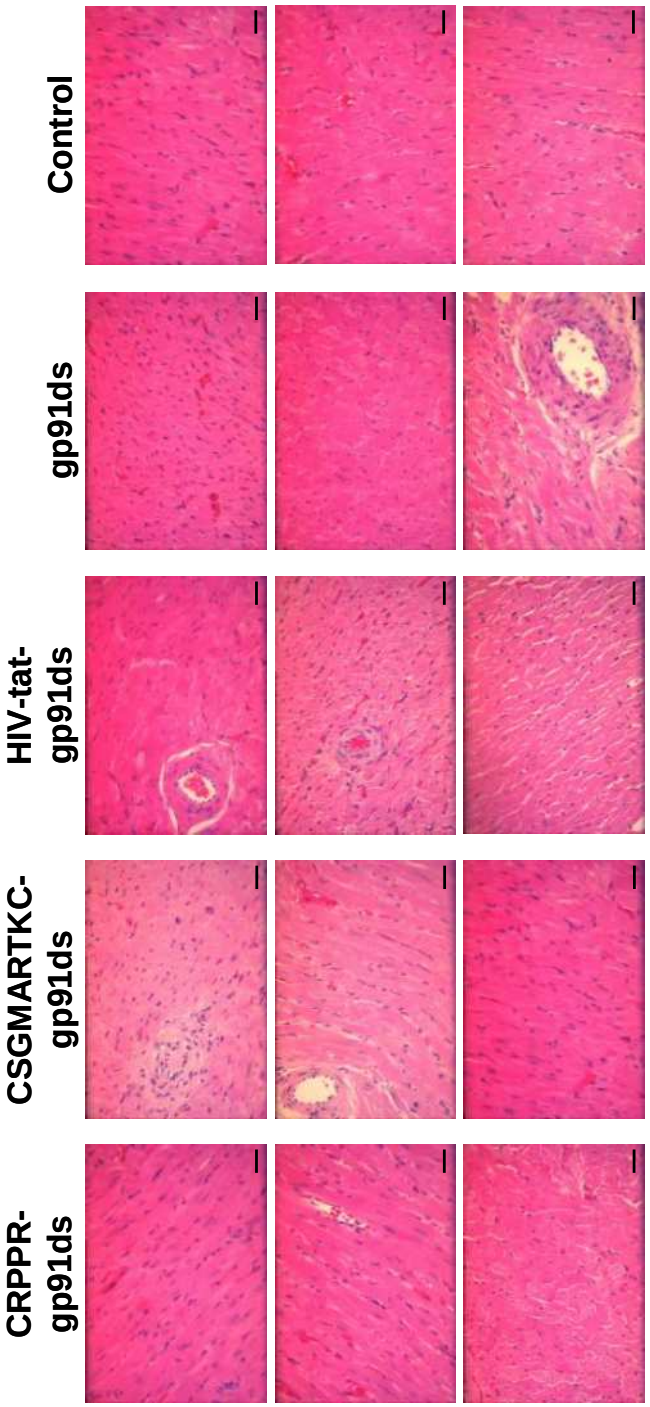

Figure 3.23 – Effect of vascular targeting anti-oxidant peptide on the heart by H&E staining.

Histological analysis of sections of the heart from control and treated animals by H&E staining. H&E stains nuclei blue/purple and the cytoplasm of the cells pink. Images are from three animals per group. Scale bar = 100 µm, magnification × 40.

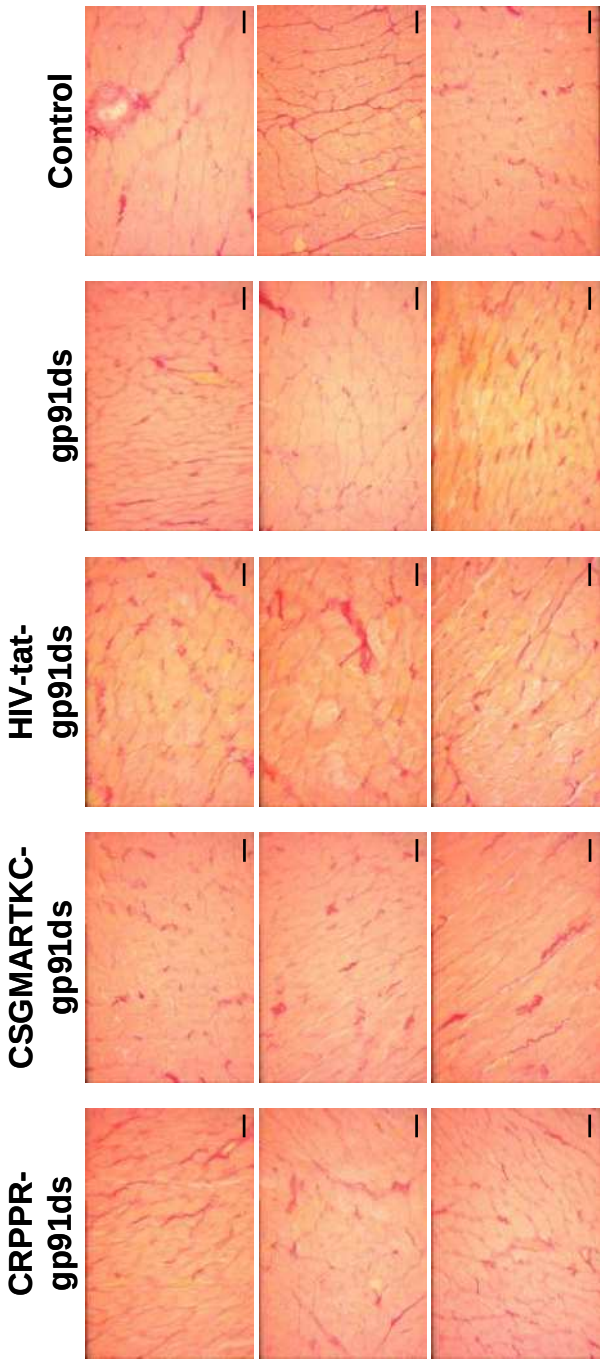

Figure 3.24 – Effect of vascular targeting anti-oxidant peptide on collagen deposition in the heart by picro-sirius red staining.

Histological analysis of collagen deposition in sections of the heart from control and treated animals by picro-sirius red staining. Picro-sirius red stains collagen red on a pale yellow background. Images are from three animals per group. Scale bar = 100 µm, magnification × 40.

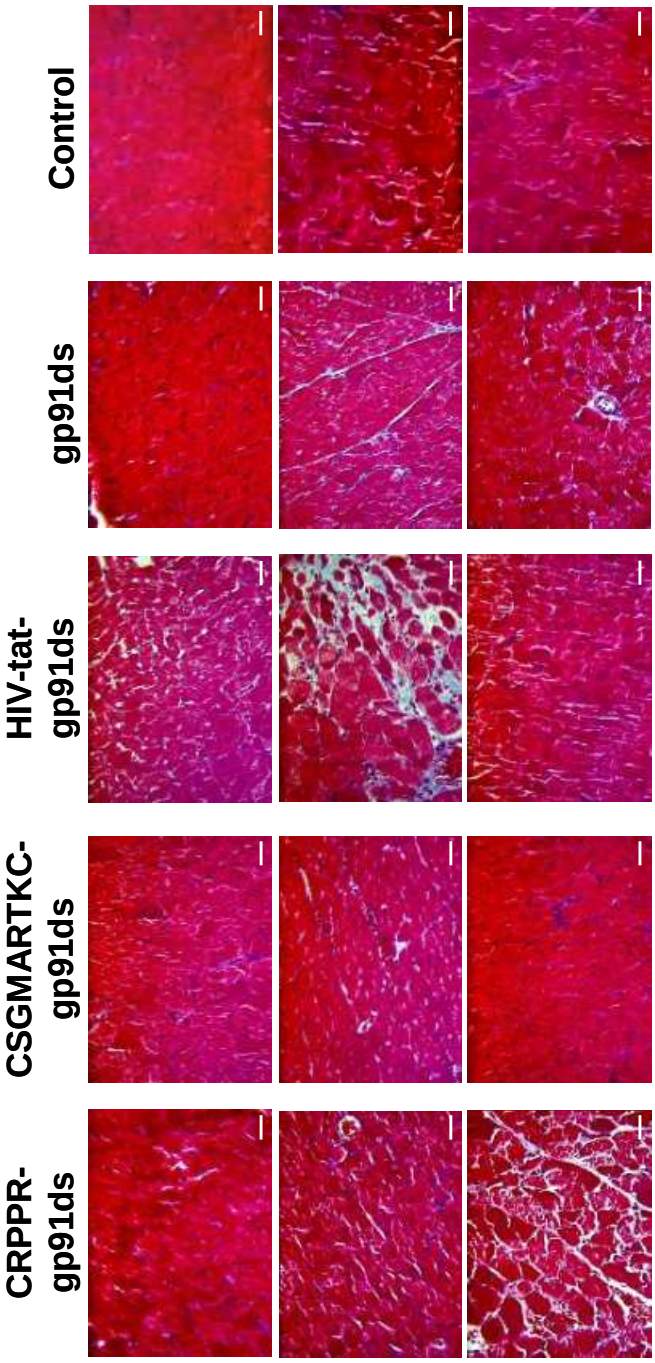

Figure 3.25 – Effect of vascular targeting anti-oxidant peptide on collagen deposition in the heart by Masson's trichrome staining.

Histological analysis of collagen deposition in sections of the heart from control and treated animals by Masson's trichrome staining. Masson's trichrome staining produces black cell nuclei, red cytoplasm and muscle fibres and collagen was stained blue. Scale bar = 100 µm, magnification × 40.

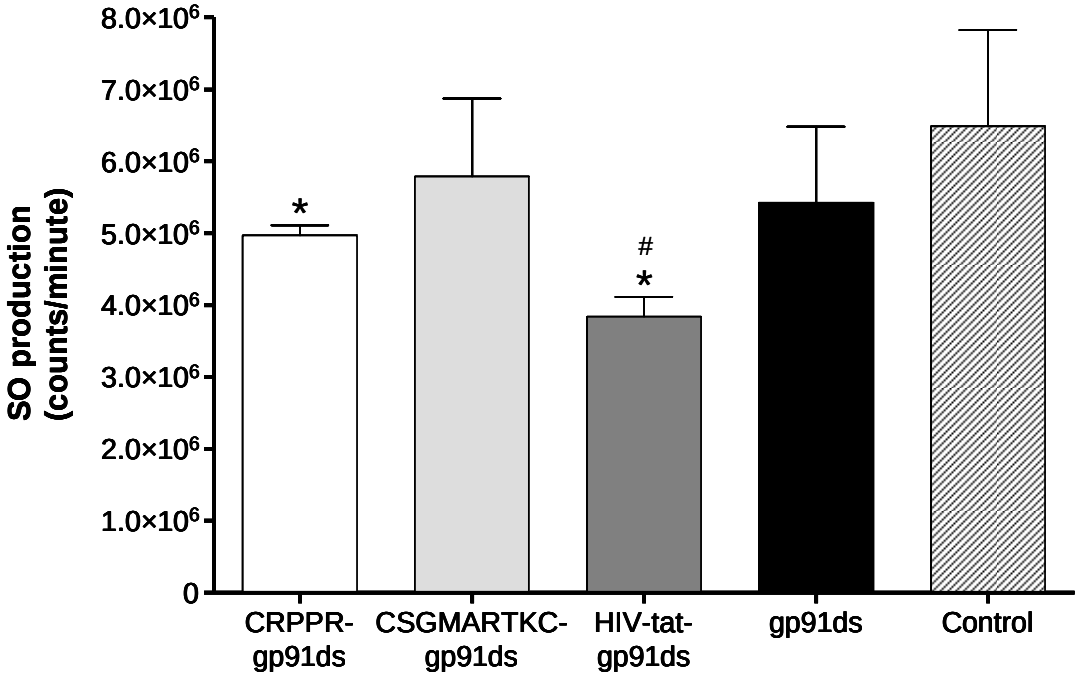

Figure 3.26 – Effect of vascular targeting anti-oxidant on SO production in whole blood.

SO production from heparinised whole blood samples by EPR. Blood samples were taken by cardiac puncture at sacrifice and incubated for 30 minutes at 37°C with 500 μmol/l of CPH spin probe before being snap frozen in liquid nitrogen. The rate of SO production by the frozen samples was calculated as counts per minute by EPR. Error bars represent SEM (* $p < 0.05$ vs. control, # $p < 0.05$ vs. CRPPR-gp91ds treated animals, n = 6/group).

3.3 Discussion

This study has determined the efficacy produced by targeting an anti-oxidant peptide selectively to the vasculature. Six selectively heart-homing peptides were originally determined by *ex vivo* and *in vivo* phage display in BALB/c mice (CGRKSKTVC, CPKRPR, CPKTRRVPC, CRPPR, CRSTRANPC and CSGMARTKC) (Zhang *et al.*, 2005). The heart-targeting capability of CRPPR was further tested in an additional two mouse strains (FVB and C57BL/6) with a similar degree of specific cardiac homing seen in the different strains (Zhang *et al.*, 2005). Three out of the six cardiac targeting peptides (CRPPR, CRSTRANPC and CSGMARTKC), retained their selectivity for the heart when they where taken across species into the WKY rat (Shirley, 2008). This indicates that there are similarities and significant differences between the proteins expressed on the EC surface of these two different species. Furthermore, only two of the peptide sequences (CRPPR and CSGMARTKC) could produce a degree of selectivity to one organ or vessel in the SHRSP, a model of human essential hypertension. Therefore, careful selection and testing of targeting peptide sequences is required before they can be used effectively in the model of choice.

The anti-oxidant peptide gp91ds selectively inhibits production of SO by NAD(P)H oxidase (Rey *et al.*, 2001). In the SHRSP, which has endothelial dysfunction due to increased generation of SO and relative NO deficiency (Kerr *et al.*, 1999, Hamilton *et al.*, 2002), gp91ds either alone or targeted by CRPPR and CSGMARTKC significantly enhanced NO bioavailability, as determined by large vessel myography on the thoracic aorta. Animals treated with CRPPR-gp91ds showed the greatest improvement in NO bioavailability, suggesting that targeting the anti-oxidant peptide to the vasculature increases the efficacy of the anti-oxidant peptide to improve endothelial function. Small vessel myography performed on third order mesenteric resistance arteries suggested that all the peptides were increasing NO bioavailability. This further indicates the differences produced by targeting the anti-oxidant peptide, when gp91ds was targeted to the aorta by CRPPR it produced the greatest increase in NO bioavailability.

During myography experiments, the aorta was also exposed to apocynin. Increasing concentrations of apocynin increased relaxation by the vessel for all treatment groups but only in the CRPPR-gp91ds treated group did complete relaxation occur in the presence of apocynin. The targeting peptides CRPPR and CSGMARTKC linked to the anti-oxidant peptide had substantially lower EC_{50} values compared to HIV-tat-gp91ds and gp91ds alone. This suggests that apocynin had a greater efficacy in animals treated with the targeting peptides linked to the anti-oxidant peptide, in particular CRPPR-gp91ds, than the non-targeted anti-oxidant peptide. However, the mechanism of action of apocynin in these experiments is unclear. If apocynin was acting as an anti-oxidant (Heumuller *et al.*, 2008), then it would prevent any SO released from the vessels interacting with NO, increasing NO bioavailability. This would be consistent with the findings in the presence of L-NAME, whereby CRPPR-gp91ds has the greatest effect on NO bioavailability. Conversely, if apocynin was inhibiting NAD(P)H oxidase (Simons *et al.*, 1990), the greater relaxation response to apocynin by aorta from CRPPR-gp91ds-treated animals could suggest increased SO was present in these vessels due to either increased NAD(P)H oxidase activity or increased expression of the enzyme. The highly effective inhibition of NAD(P)H oxidase by the CRPPR-gp91ds could lead to an up-regulation in expression of NAD(P)H oxidase. When the anti-oxidant peptide targeted by CRPPR was washed off in the myograph bath, the increased SO production by increased levels of NAD(P)H oxidase could possibly enable a greater relaxation of the vessel to be produced in the presence of increasing concentrations of apocynin.

The increase in NO bioavailability produced by CRPPR-gp91ds, CSGMARTKC-gp91ds and gp91ds alone treated animals was only considerable enough in animals treated with CRPPR-gp91ds to produce a significant reduction in systolic BP. The anti-oxidant peptide by inhibition of NAD(P)H oxidase has been previously shown to reduce SO production in angiotensin II- and salt-induced hypertension (Rey *et al.*, 2001, Zhou *et al.*, 2006). Here it has been shown that only when gp91ds was targeted to the vasculature could it reduce systolic BP in a disease model, the SHRSP. The rise in systolic BP was progressive and time-dependent in the control animals and in animals treated with CSGMARTKC-gp91ds, HIV-gp91ds and gp91ds alone, characteristic of the SHRSP (Davidson *et al.*, 1995, Clark *et al.*, 1996).

Animals were treated with the HIV-tat peptide linked to the anti-oxidant peptide as a positive control but this treatment provided no benefit in NO bioavailability or reduction in systolic BP. After investigation of the SO production in whole blood samples taken from this group by EPR, it was shown that animals treated with HIV-tat-gp91ds had significantly reduced SO production in the blood compared to CRPPR-gp91ds treated animals. This suggests that the HIV-tat peptide was enabling delivery of the anti-oxidant peptide to blood components, most likely mononuclear white blood cells, and this resulted in reduced SO production in the whole blood sample from these animals. Previously, gp91ds-tat has been shown to inhibit phorbol myristate acetate (PMA)-induced SO production in neutrophils by 35% (Rey *et al.*, 2001). This interaction with the blood would, thereby, reduce the overall bioavailability of the HIV-tat-gp91ds peptide, possibly preventing it producing the effects on BP seen in other studies (Rey *et al.*, 2001). Therefore, HIV-tat was effective at delivering the anti-oxidant peptide but the lack of selective targeting by this peptide means that it was not successful in conveying the anti-oxidant peptide to sites of oxidative stress where it would produce significant effects on BP.

The receptor for CRPPR was previously identified as CRIP-2 (Zhang *et al.*, 2005). CRIP-2 was expressed at the highest level in the heart of mice, with much lower levels of this receptor present in other tissues (Zhang *et al.*, 2005). Fluorescein-conjugated CRPPR peptide extensively co-localised with an anti-CRIP-2 antibody and the endothelial marker CD31 in coronary arteries, capillaries and the endocardium (Zhang *et al.*, 2005). However, CRIP-2 has no discernible membrane-spanning domain and has been previously shown to be a binding partner of sub-membranous protein tyrosine phosphatase (PTP-BL) (van Ham *et al.*, 2003). Therefore, it is possible that the CRIP-2 protein was expressed on the surface of ECs, allowing binding by CRPPR. Recently, a study has shown that the vascular targeting capacity of, in particular the CRPPR peptide, was possibly due to the presence of a C-terminal arginine residue (R by amino acid single letter code) (Teesalu *et al.*, 2009). It was further shown that a tandem RXXR motif was highly efficient at promoting initial phage binding (Teesalu *et al.*, 2009). Phage inserted with peptide sequences containing RXXR demonstrated greater than 1000-fold increase in binding over control phage (Teesalu *et al.*, 2009). Indeed, addition of further basic amino acids to the peptide sequence increased binding in a dose-

dependent manner, contributing to subsequent internalisation (Teesalu *et al.*, 2009), possibly due to the increased similarity to the HIV-tat peptide (sequence RKKRRQRRR). The mechanism of internalisation by peptide containing the RXXR motif was investigated using the inhibitors of various endocytosis pathways but this mechanism of cell entry was not used (Teesalu *et al.*, 2009). This was expected at least for the CRPPR peptide as a putative receptor had been previously identified for this peptide (Zhang *et al.*, 2005). The putative receptor for internalisation of peptides with a C-terminal R, neuropilin-1 (NRP-1), was not identified in the previous peptide receptor screen for the receptor for CRPPR (Zhang *et al.*, 2005). Also, CRPPR bound to HCAECs more strongly than to HUVECs (Zhang *et al.*, 2005), suggesting specific targeting to the arterial vasculature and not generic endothelial targeting.

When the C-terminal R was capped in peptides containing the RXXR motif with an additional non-basic amino acid, it abolished cellular binding by the phage inserted with this peptide sequence (Teesalu *et al.*, 2009). This has important implications as the CRPPR peptide was linked to the anti-oxidant peptide through the terminal R residue (CRPPR-gp91ds sequence was CRPPR-GGG-CSTRIRRQL). Although it was shown that trypsin, through cleavage of the targeting peptide at basic residues, could activate a peptide with a "cryptic binding site" by proteolytic cleavage (Teesalu *et al.*, 2009). It is possible that the binding site for C-terminal R peptides in the NRP-1 receptor is small and the presence of the GGG linker sequence in the CRPPR-gp91ds peptide allows the anti-oxidant peptide to bend away from the receptor, producing interaction between CRPPR and NRP-1. Indeed the binding site of NRP-1 probably requires five amino acids as the conversion from tuftsin (TKPR) to enhanced-tuftsin (TKPPR) increased binding to endothelial cells by 20-fold (von Wronski *et al.*, 2006). Vascular endothelial derived growth factor (VEGF) binds to NRP-1 to increase vascular permeability (Becker *et al.*, 2005, Mamluk *et al.*, 2005, Acevedo *et al.*, 2008). VEGF binds to the same site of NRP-1 as the HIV-tat peptide (Jia *et al.*, 2001). A peptide with the RXXR motif was shown to significantly increase vascular leakage (Teesalu *et al.*, 2009). This increased vascular permeability produced by the presence of the CRPPR peptide could have produced the increased effectiveness of the anti-oxidant peptide by increasing delivery to VSMCs.

The SHRSP has been used in this study as a model of human essential hypertension as BP in these animals increases with age (Davidson *et al.*, 1995, Clark *et al.*, 1996). Additionally, as the SHRSP has endothelial dysfunction due to oxidative stress, which has been previously reversed (Alexander *et al.*, 1999, Dowell *et al.*, 1999, Alexander *et al.*, 2000, Fennell *et al.*, 2002, Miller *et al.*, 2005, Graham *et al.*, 2009), it was an excellent model for the study of a novel anti-oxidant therapy. The anti-oxidant peptide gp91ds was targeted to the vasculature and the effect on BP and endothelial function in the SHRSP was then assessed. The anti-oxidant therapy alone shows improvement in NO bioavailability but only when it was targeted with CRPPR was a significant improvement in NO bioavailability and an attenuation of the time-dependent and progressive increase in systolic BP observed in the SHRSP.

CHAPTER 4

Influence of Coagulation FX on *In Vitro* and *In Vivo* Gene Delivery by Ad35 and Chimeric Ad5/Ad35 Vectors

4.1 Introduction

There are significant hindrances in the deployment of Ad5-based gene therapy vectors, including extensive liver and spleen accumulation (Huard *et al.*, 1995, Connelly, 1999, Parker *et al.*, 2006, Waddington *et al.*, 2007, Kalyuzhniy *et al.*, 2008, Waddington *et al.*, 2008), broad seroprevalence of neutralising antibodies (Christ *et al.*, 1997, Sprangers *et al.*, 2003, Vogels *et al.*, 2003, Sumida *et al.*, 2005, Abbink *et al.*, 2007, Parker *et al.*, 2009) as well as interactions with erythrocytes (Nicol *et al.*, 2004, Carlisle *et al.*, 2009, Subr *et al.*, 2009) and platelets (Hofherr *et al.*, 2007, Othman *et al.*, 2007, Stone *et al.*, 2007b) which all serve to limit efficacy. Consequently, research has been undertaken to find an alternative gene therapy vector with one possible solution being to develop alternative serotype Ad vectors which circumvent some of the negative aspects of Ad5. Sub-species B Ads are a relatively well characterised sub-species of Ad with many potentially favourable differences to Ad5 due to alternative receptors and lower seroprevalence.

4.1.1 Sub-species B Ads

The sub-species B Ads include Ad3, 7, 11, 16, 35 and 50. Relative to sub-species C Ads, sub-species B Ad fibers are short-shafted, consisting of 5.5 repeats in comparison to the 22 repeats in the sub-species C Ads (Ad2 and Ad5). The sub-species B Ads form two genetic clusters, B1 (Ad3, Ad7, Ad16, Ad21, and Ad50) and B2 (Ad11, Ad14, Ad34, and Ad35) (Wadell *et al.*, 1980) (Figure 1.3). The sub-species B Ads were originally shown to use CD46 as their high affinity cellular receptor (Gaggar *et al.*, 2003, Segerman *et al.*, 2003b, Sirena *et al.*, 2004). The high affinity interaction between the Ad35 fiber knob and CD46 has a dissociation constant of 14.64 nM (Wang *et al.*, 2008b), which is similar to the affinity of the Ad5 fiber knob:CAR interaction (Kirby *et al.*, 2000, Kirby *et al.*, 2001). Short consensus repeats 1 and 2, two distal extracellular domains of CD46, are involved in Ad35 binding (Gaggar *et al.*, 2003, Fleischli *et al.*, 2005, Sakurai *et al.*, 2006b) (Figure 4.1).

CD46 is a 56-66 kDa membrane glycoprotein which protects cells from complement-mediated damage and is usually present on all human nucleated cells at

a relatively low level. There are four major isoforms of CD46 (BC1, BC2, C1 and C2, Figure 4.1) produced by alternative splicing of a region encoding an extracellular domain and the choice between one of two cytoplasmic tails, Cyt-1 and Cyt-2. The use of CD46 as a virus receptor allows the sub-species B Ads to produce more efficient transduction of both VSMCs and ECs, in comparison to other sub-species due to the low CAR expression of these cells (Havenga *et al.*, 2001, Havenga *et al.*, 2002).

Several of the sub-species B Ads also use an unidentified receptor for the infection of human cells, named receptor X (Tuve *et al.*, 2006). By using soluble CD46 and an anti-CD46 antibody, three sub-groups of the sub-species B Ads were determined (Tuve *et al.*, 2006). Ad16, Ad21, Ad35 and Ad50 nearly exclusively use CD46 as their receptor, Ad3, Ad7p and Ad14 use receptor X and not CD46 and Ad11p utilises both CD46 and receptor X (Tuve *et al.*, 2006). Competition studies with recombinant fiber knob protein showed that the interaction of Ad3, Ad7p, Ad11p and Ad14 with receptor X was mediated through the fiber knob (Tuve *et al.*, 2006). Further analysis demonstrated that receptor X is likely to be an abundantly expressed glycoprotein, present on a variety of cancer and primary cells (Tuve *et al.*, 2006). Ad3, Ad7p, Ad11p and Ad14 bind to receptor X with low affinity in a calcium-dependent manner (Tuve *et al.*, 2006).

Many previous studies have focused on chimeric vectors, where the fiber of sub-species B Ads is “pseudotyped” onto the Ad5 capsid through swapping of either the knob domain (Shayakhmetov and Lieber, 2000, Gaggar *et al.*, 2003, Shayakhmetov *et al.*, 2004, Shayakhmetov *et al.*, 2005a, Wang *et al.*, 2008a) or the full length fiber (Shayakhmetov *et al.*, 2000, Havenga *et al.*, 2001, Shayakhmetov *et al.*, 2002, Sakurai *et al.*, 2003a, Sakurai *et al.*, 2003b, Shayakhmetov *et al.*, 2004, Di Paolo *et al.*, 2006, Ni *et al.*, 2006, Shinozaki *et al.*, 2006, Tuve *et al.*, 2006, Brouwer *et al.*, 2007, Stone *et al.*, 2007a). *In vitro* this strategy was effective at improving delivery through CD46 (Di Paolo *et al.*, 2006, Ni *et al.*, 2006, Brouwer *et al.*, 2007).

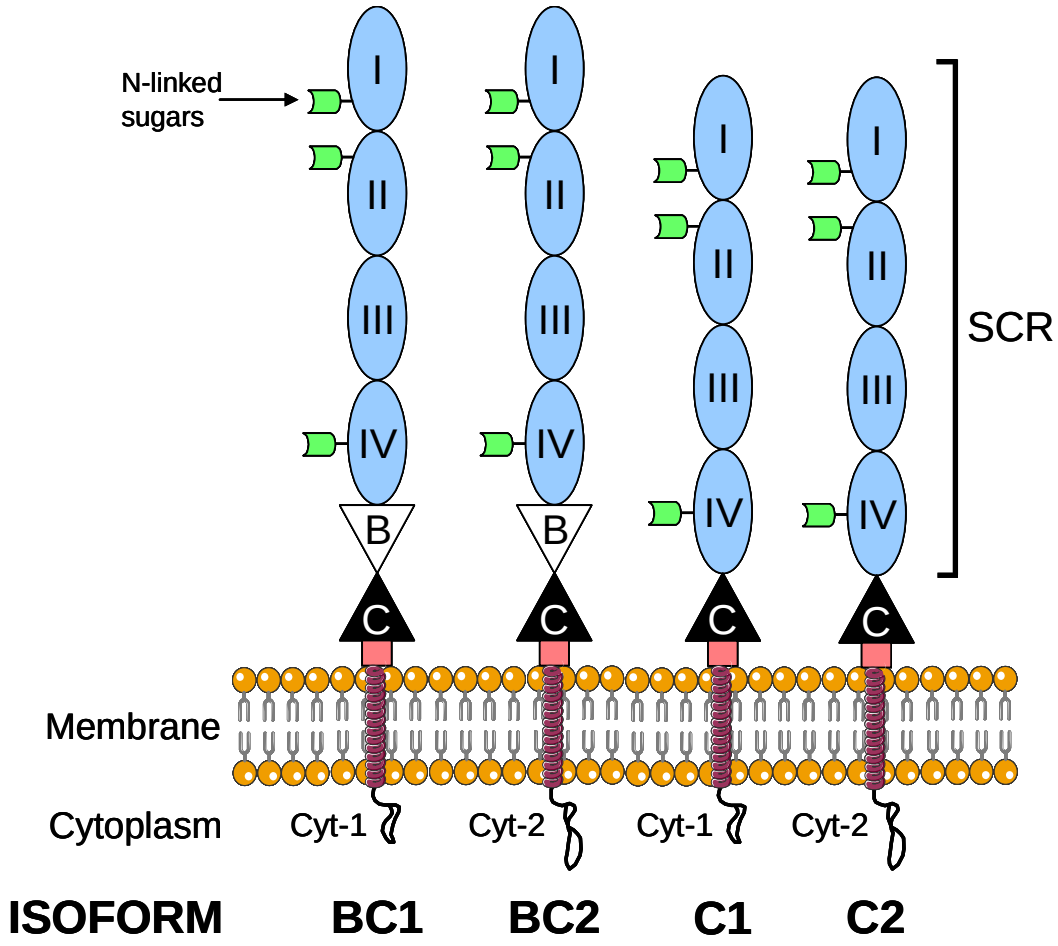

Figure 4.1 – Structure of CD46 isoforms.

There are four major isoforms of CD46 (BC1, BC2, C1 and C2) produced by alternative splicing of a region encoding an extracellular domain and the choice between one of two cytoplasmic tails, Cyt-1 and Cyt-2. Short consensus repeats (SCR) I and II are crucial for Ad35 binding. Adapted from Manchester *et al.* (Manchester *et al.*, 1994).

4.1.2 Sub-species B pseudotype vectors

The first studies using a sub-species B pseudotype vector, Ad5/f35 (a vector consisting of the hexon and penton of Ad5 and the Ad35 fiber) showed that Ad5/f35 could efficiently transduce haematopoietic $CD34^+$ cells (Shayakhmetov *et al.*, 2000, Di Paolo *et al.*, 2006). Ad5/f35 transduced 54% of $CD34^+$ cells, whereas transduction by Ad5 was restricted to the 25% of $CD34^+$ cells which expressed α_v-integrins (Shayakhmetov *et al.*, 2000). The remaining $CD34^+$ cells were refractory to Ad5 transduction as they did not express CAR or α_v-integrins (Shayakhmetov *et al.*, 2000). In addition, studies investigating alternative human serotypes for cardiovascular gene therapy utilised a "pseudotype library" for screening on cell lines to determine the most efficient fiber for transduction (Havenga *et al.*, 2001, Havenga *et al.*, 2002). The sub-species B pseudotype Ad5/f16 was found to increase transduction of human ECs and SMCs by 8- and 64-fold, respectively, compared to the Ad5 control (Havenga *et al.*, 2001). When other sub-species B pseudotype vectors were tested, namely Ad5/f11 and Ad5/f35, they both increased transduction efficiency compared to Ad5 but not to the same efficiency as Ad5/f16 (Havenga *et al.*, 2001). These data in ECs were corroborated in another study where Ad5/f35 transduced 95-100% of both HUVECs and HAECs, whereas Ad5 transduced less than 10% of both cell types (Shinozaki *et al.*, 2006). This was due to the relatively low level of CAR expression by SMCs and ECs (Havenga *et al.*, 2001). Therefore, as the sub-species B vectors use CD46 and not CAR as their cellular receptor, which is expressed at high levels on SMCs and ECs (Shinozaki *et al.*, 2006), they are able to efficiently transduce SMCs and ECs. Whilst SMCs can be transduced by Ad5, it requires a very high multiplicity of infection of Ad5 per cell and this has implications for toxicity (Havenga *et al.*, 2001, Work *et al.*, 2004).

The sub-species B pseudotype vectors also demonstrate increased infectivity of many cancer cell lines compared to Ad5 (Havenga *et al.*, 2002, Shayakhmetov *et al.*, 2002, Brouwer *et al.*, 2007), likely due to CD46 being up-regulated in many human cancers (Kinugasa *et al.*, 1999, Murray *et al.*, 2000, Ni *et al.*, 2006). In addition, expression of CAR correlates negatively with tumour malignancy *in vivo* (Miller *et al.*, 1998, Li *et al.*, 1999, Okegawa *et al.*, 2000, Ni *et al.*, 2006), indicating that vectors using a CAR-dependent pathway for infection would be largely ineffective at

transducing the most aggressive forms of cancer. *In vitro*, the cancer cell line MDA-MB-435 was efficiently transduced by Ad5/f35, whereas this cell line was refractory to Ad5 transduction due to very low CAR expression by these cells (Shayakhmetov *et al.*, 2002). There was a strong correlation between transduction efficiency of primary cancer cells *in vitro* by Ad5 and Ad5/f35 and the CAR and CD46 expression levels (Ni *et al.*, 2006, Suominen *et al.*, 2006, Brouwer *et al.*, 2007).

Pseudotype vectors from the sub-species B Ads have been shown to significantly enhance transduction of primary glioma cells taken from patients with brain tumours, compared to Ad5 (Brouwer *et al.*, 2007). Transduction was enhanced by the presence of the sub-species B fiber due to the low level of CAR expression by the cells and the primary glioma cell suspensions readily expressed the BC1 isoform of CD46 (Brouwer *et al.*, 2007). Transgene expression by the Ad35 vector was significantly enhanced in the primary glioma cells compared to Ad5 (Brouwer *et al.*, 2007). However, there was no direct comparison made between the Ad35 vector and the pseudotype Ad5/f35 vector.

The properties displayed by the Ad5/f35 pseudotype vector are maintained in the Ad35 vector. Ad35 displays a higher transduction efficiency into human $CD34^+$ cells compared to both Ad5 and Ad5/f35 (Sakurai *et al.*, 2003a). In CAR expressing cell lines, Ad35 produced similar or lower levels of transduction compared to Ad5 and Ad5/f35 (Sakurai *et al.*, 2003b). Furthermore, in cell lines which did not express CAR, transduction by Ad35 was significantly enhanced compared to Ad5, as expected (Sakurai *et al.*, 2003b).

Therefore, *in vitro* studies suggest that it would be possible to selectively target and effectively transduce cancer cells, possibly either as part of a solid tumour or ideally disseminated metastases, by systemic administration of vectors based on the sub-species B Ads as this sub-species also shows reduced hepatocyte transduction (compared to Ad5) but efficient cancer cell transduction. Indeed, Ad5/f35 has been approved in the UK for a cancer gene therapy phase I clinical trial (http://www.dh.gov.uk/ab/GTAC/index.htm).

4.1.3 *Animal models for* in vivo *study of the tropism of sub-species B Ads*

Many of the *in vivo* studies into the efficacy and safety of vectors based on the sub-species B Ads have produced variable results. In many cases, this could be due to the use of wild-type mice, rather than CD46 transgenic mice. Although humans ubiquitously express CD46, expression in rodents is restricted to the testes (Inoue *et al.*, 2003). In addition, there is no homology between the mouse and human cytoplasmic domains of CD46. When non-transgenic mice are used for the *in vivo* studies, the sub-species B Ad vectors showed no retargeting away from the liver (Shayakhmetov *et al.*, 2002). This was entirely expected based on the lack of expression of CD46. However, the sub-species B Ads did demonstrate reduced liver transduction in comparison to Ad5 (Shayakhmetov *et al.*, 2002).

The difficulties in using animal models to translate the tropism of sub-species B Ad vectors to humans were first highlighted by the differences in Ad5/f16 transduction of human SMCs to those taken from rats, pigs and rhesus monkeys (Havenga *et al.*, 2001). In human SMCs, Ad5/f16 produced a 64-fold increase in transduction in comparison to Ad5 (Havenga *et al.*, 2001). This increase in transduction efficiency was also seen in rhesus monkey SMCs, where Ad5/f16 increased transduction by 5-fold compared to Ad5 (Havenga *et al.*, 2001). However, in pig and rat SMCs, transduction by Ad5/f16 was reduced 10- and 100-fold, respectively, compared to Ad5 (Havenga *et al.*, 2001). This was later explained when it was found that rodents only express CD46 in the testes (Inoue *et al.*, 2003). Therefore, rat SMCs would not express CD46 preventing efficient transduction by a sub-species B pseudotype vector. This also suggests that porcine SMCs express CD46 at a moderate level (lower than human SMC CD46 expression) as, although transduction by Ad5/f16 was reduced in cells taken from the pig, transduction was not attenuated. Therefore, the pig is also a poor animal model for studies into the *in vivo* tropism of sub-species B Ad vectors.

4.1.3.1 Studies in non-CD46 transgenic mice

Although non-CD46 transgenic mice do not provide a good animal model for the use of sub-species B Ads in humans, studies in these animals have provided useful data on the selective targeting capacity of these vectors. *In vivo* studies in immuno-deficient CB17/SCID mice demonstrated attenuated liver transduction by Ad5/f35 compared to Ad5 (Shayakhmetov *et al.*, 2002), indicating that Ad5/f35 had a reduced liver tropism. Therefore, it was hoped that due to the reduced liver tropism of Ad5/f35 and the enhanced transduction of cancer cell lines by this vector, Ad5/f35 would be an effective vector for potentially targeting metastases after intravenous administration. In a xenograft model of liver metastases produced by transplantation of a human breast carcinoma cell line (MDA-MB-435) into the portal vein of immuno-deficient CB17/SCID mice, Ad5/f35 transduced 8% of liver metastases (Shayakhmetov *et al.*, 2002). Due to the up-regulation of CD46 in many human cancer cell lines and the lack of native CD46 expression in the mouse, Ad5/f35 should selectively and efficiently transduce the cancer cells. Another similar study did find that Ad5/f35 could selectively target a transplanted human cancer cell line (Bernt *et al.*, 2003). Immuno-deficient CB17/SCID mice were transplanted with a human carcinoma cells (HeLa) via portal vein injection and Ad5 selectively transduced mouse hepatocytes (Bernt *et al.*, 2003). Transduction by Ad5/f35 was selectively restricted to liver metastases with no obvious transduction of hepatocytes (Bernt *et al.*, 2003). The reason behind the difference between these two studies is unclear, possibly due to CD46 expression levels on the different human cancer cell lines used to produce the liver metastases.

There are also differences between Ad5 and Ad5/f35 transduction after local delivery *in vivo*. In an *in vivo* model of head and neck cancer, created by subcutaneous injection of a human squamous cell carcinoma cell line into immunodeficient SCID knockout mice, Ad5/f35 transgene expression was detected uniformly across 60% of the tumour (Suominen *et al.*, 2006). However, administration of Ad5 by the same route resulted in transduction of only those cells directly surrounding the injection site (Suominen *et al.*, 2006). The dispersion by the Ad5/f35 vector, allowing transduction of cells not immediately adjacent to the site of injection, suggests that administration of Ad5/f35 by a single intra-tumoural

injection is a therapeutically relevant route of administration and may be clinically relevant.

The pseudotype vector Ad5/f35 has also been used in a rat hepatic tumour model (Shinozaki *et al.*, 2006). Cancer cells (McA-RH7777) were implanted into non-transgenic rats 14 days before administration of either Ad5 or Ad5/f35 into the hepatic artery (Shinozaki *et al.*, 2006). Ad5 transgene expression was detected primarily in the liver parenchyma with transduction occurring in only a few tumour cells (Shinozaki *et al.*, 2006). However, Ad5/f35 selectively targeted the rim of the hepatic tumour, co-localising with the endothelial cell markers CD31 and Flk-1, indicating transduction of endothelial cells *in vivo* (Shinozaki *et al.*, 2006). Additionally, Ad5/f35 produced very little transduction of normal liver tissue (Shinozaki *et al.*, 2006), suggesting that Ad5/f35 could be used to deliver genes via the hepatic artery to sites of neoangiogensis associated with liver tumours. However, this study was performed in the rat which does not share the CD46 expression pattern of humans and it is difficult to correlate the observed vector distribution with this receptor expression.

The Ad35 vector behaves similarly to the pseudotype Ad5/f35 vector *in vivo* in non-transgenic mice. Ad5/f35 and Ad35 produced their highest levels of organ transduction in the liver but transduction by these vectors was 3 and 4 log orders, respectively, lower than transgene expression mediated by Ad5 (Sakurai *et al.*, 2003b). In other organs, including spleen, kidney, heart and lung, transduction by Ad35 was lower than transduction by Ad5/f35 (Sakurai *et al.*, 2003b). To investigate why there was a difference in the transduction efficiency by Ad35 and the pseudotype Ad35 vectors, the blood clearance kinetics of Ad5 and Ad35 were determined (Sakurai *et al.*, 2003b). The clearance of Ad5 and Ad35 from the blood was rapid for both vectors and not significantly different to each other; both had a half-life in the blood of approximately three minutes (Sakurai *et al.*, 2003b). The blood clearance kinetics of Ad5/f35 was not reported. Therefore, the rate of clearance from the animal was not involved in producing the overall reduced transduction efficiency by Ad35. One hour post intravenous infusion of the vector into non-transgenic mice, the majority of the viral dose accumulated in the liver due to the action of Kupffer cells (Sakurai *et al.*, 2003b). However, 48 hours after

administration of the vectors, 43% of the Ad5 dose remained in the liver due to transduced hepatocytes, whereas no Ad35 DNA was detected (Sakurai *et al.*, 2003b). This was likely due to the absence of CD46 in the non-transgenic mice.

In the same study, non-transgenic mice were given Ad5, Ad5/f35 and Ad35 vectors by intramuscular injection (Sakurai *et al.*, 2003b). Although, skeletal muscle cells express low levels of CAR (Tomko *et al.*, 1997, Bergelson *et al.*, 1998, Nalbantoglu *et al.*, 1999), Ad5 produced the highest level of transgene expression but this was not significantly different to Ad5/f35 and Ad35 (Sakurai *et al.*, 2003b). This suggests that the efficacy of the Ad5/f35 and Ad35 vectors to infect skeletal muscle cells was poor. Additionally, the hepatotoxicity produced by Ad5 and Ad35 vectors was significantly different. The level of the liver enzyme aspartate aminotransferase (AST) was used as a measure of hepatotoxicity, as release of this enzyme into the bloodstream occurs after acute damage to the liver. One day after administration, Ad35 and Ad5 produced a 2- and 5-fold increase in AST levels, respectively (Seshidhar Reddy *et al.*, 2003). In mice injected with Ad35, the AST level returned to baseline four days after delivery of the vector. However, four days after administration of Ad5, the level of AST had increased by 40-fold (Seshidhar Reddy *et al.*, 2003). These data suggest that Ad35 may be less toxic to the liver than Ad5 but, as these experiments were performed in non-transgenic mice, it does not predict the immune reactions to administration of an Ad35 vector in humans.

4.1.3.2 Studies in CD46 transgenic mice

Transgenic mice with different expression profiles of human CD46 were used to evaluate Ad35 transduction *in vivo*. However, there were some distinct differences between transgenic strains, for example, CD46 was not detected on the erythrocytes of some CD46 transgenic mice (Sakurai *et al.*, 2006a) but other studies have shown this (Oldstone *et al.*, 1999, Kemper *et al.*, 2001). The reason for the differential expression of CD46 on erythrocytes is likely due to the method of production of the CD46 transgenic mice strains. Transgenic mice produced using a yeast artificial chromosome under the control of a β-actin promoter to transfer DNA encoding CD46, expressed CD46 on their red blood cells (Oldstone *et al.*, 1999). Whereas erythrocytes did not express CD46 when a bacterial artificial chromosome was used,

driven by the human CD46 promoter (Sakurai *et al.*, 2006a). This produced an expression profile similar to that in humans (Mrkic *et al.*, 1998, Oldstone *et al.*, 1999, Kemper *et al.*, 2001).

There are distinct differences in the transduction properties of sub-species B Ad vectors after local delivery in CD46 transgenic and non-transgenic mice. After intramuscular injection, Ad5/f35 selectively transduced myocytes surrounding the injection site in CD46 transgenic mice but this did not occur in non-transgenic mice (Di Paolo *et al.*, 2006). Intramuscular injections led to leakage of a proportion of the delivered vector into the bloodstream and resulted in liver transduction (Di Paolo *et al.*, 2006). Liver transduction after intramuscular injection in non-transgenic mice was increased, compared to transduction in CD46 transgenic mice (Di Paolo *et al.*, 2006). There was also some lung accumulation in CD46 transgenic animals administered with Ad5/f35 by intramuscular injection (Di Paolo *et al.*, 2006).

In CD46-transgenic mice, intravenous administration of Ad5/f35 selectively targeted metastatic tumours, which had grown from cells engineered to express CD46 at a level comparable to human tumours (Ni *et al.*, 2006). This indicates that the transduction efficiency of Ad5/f35 depends on the CD46 expression density; since the cancer cells expressed more CD46, they were efficiently targeted.

Hemizygous and homozygous CD46 transgenic mice have been developed to investigate the differences in tropism by Ad35 (Sakurai *et al.*, 2006a). Intravenous administration of Ad35 produced increased transduction of liver, lung and kidney in CD46 transgenic mice, in comparison to non-transgenic mice, with no differences in transduction by Ad35 between the hemizygous and homozygous CD46 transgenic mice (Sakurai *et al.*, 2006a). Unfortunately, this study did not compare Ad5 and Ad35 transduction in CD46 transgenic mice. In a similar study, intravenous delivery of Ad35 into CD46 transgenic mice did not result in effective transduction of any organ when measured 24 hours after administration (Verhaagh *et al.*, 2006). However, 48 hours after administration, there were detectable levels of Ad35 in the lung (Verhaagh *et al.*, 2006). There was no Ad35 detected in the liver of the CD46 transgenic mice at either time point (Verhaagh *et al.*, 2006). When Ad35 was administered by intramuscular injection, the level of transduction produced was

comparable between non-transgenic and CD46 transgenic mice (Verhaagh *et al.*, 2006). In both of these studies in CD46 transgenic mice, there was no comparison made to gene transfer mediated by Ad5. Therefore, it is difficult to obtain an indication of the likely tropism in humans relative to the other previously tested vectors, for example, Ad5.

4.1.3.3 Studies in non-human primates

Non-human primates have a similar CD46 expression pattern to humans (Hsu *et al.*, 1997) with high homology in the short consensus repeats 1 and 2 regions, which are crucial for Ad35 binding (Fleischli *et al.*, 2005, Gaggar *et al.*, 2005, Sakurai *et al.*, 2006b). Non-human primates have been extensively used for studies with measles virus as it also uses CD46 as a receptor (Sakaguchi *et al.*, 1986, McChesney *et al.*, 1997, Premenko-Lanier *et al.*, 2003). In baboons, intravenous administration of Ad5 resulted in significantly increased levels of transduction in the liver, brain and stomach in comparison to the sub-species B pseudotype vectors Ad5/f11 and Ad5/f35 (Ni *et al.*, 2005). Interestingly, 5% of hepatocytes were transduced and areas of the arterial endothelium in the lung showed 100% transgene expression produced by Ad5 (Ni *et al.*, 2005), which was very different to previous findings where Ad5 usually demonstrates very high liver transduction. The toxicity of the vectors was also investigated with all vectors producing an increase in alanine aminotransferase (ALT), a marker of hepatocellular damage, one hour after administration (Ni *et al.*, 2005). The ALT level 72 hours post-administration was increased further in Ad5 treated animals, whereas 72 hours after delivery of Ad5/f11 and Ad5/f35, the ALT level had returned to normal (Ni *et al.*, 2005). Therefore, the sub-species B pseudotype vectors appear to possess a better safety profile than Ad5 in baboons but the levels of transduction by these pseudotype vectors are relatively low.

Experiments investigating the *in vivo* tropism of Ad35 after intravenous administration were reproduced in another non-human primate, the cynomolgus monkey (Sakurai *et al.*, 2008). Ad35 transduction mostly occurred in the liver, lung and kidney but all at substantially lower levels than transduction produced by Ad5 in these organs (Sakurai *et al.*, 2008). There was no difference in the blood-clearance

kinetics between Ad5 and Ad35 (Sakurai, 2008). However, Ad35 vectors remained associated with blood cells throughout the four days of study duration (Sakurai *et al.*, 2008). As the erythrocytes of the cynomolgus monkey express CD46 (Hsu *et al.*, 1999), this suggests that Ad35 may bind to blood cells or was taken up by blood cells after delivery of the vector, resulting in the increased association of this vector with blood cells over the course of the study and limiting bioavailability.

As Ad35 has relatively poor tissue transduction efficiency after systemic administration, this makes it a potential candidate for development into a targeted gene therapy vector. Targeting Ad35 by local delivery could potentially produce fewer side effects on non-target organs when Ad35 drains from the injection site into the bloodstream. Sakurai *et al*. administered Ad35 by direct injection into the liver of cynomolgus monkeys, which resulted in transgene expression only in those cells bordering the injection site (Sakurai *et al.*, 2009). Injection of Ad35 into skeletal muscle of cynomolgus monkey resulted in no transduction of muscle fibers (Sakurai *et al.*, 2009), in comparison to the transduction produced by this vector in both non-transgenic and CD46 transgenic mice (Sakurai *et al.*, 2003b, Verhaagh *et al.*, 2006). Renal tubular epithelial cells were transduced by Ad35 after local delivery to the kidney with some dispersion from the injection site (Sakurai *et al.*, 2009). Additionally, inflammatory cell infiltration was seen at many of the injection sites but there was no transduction observed in organs which were not injected (Sakurai *et al.*, 2009). However, this study did not compare the effects of local delivery of Ad35 to that of Ad5. Therefore, it is difficult to draw any firm conclusions on the efficiency of this vector.

As some non-human primates express CD46 on erythrocytes, whereas humans do not (Hsu *et al.*, 1999, Baker, 2007, Sakurai, 2008), this prevents their use as a truly relevant *in vivo* model. The sub-species B Ad vectors would have a reduced circulation time in these primates since the majority of the vector would bind to the available CD46 receptors on red blood cells rapidly after injection. Therefore, it is appropriate to use mice transgenic for human CD46 which display a similar expression profile to humans (Sakurai *et al.*, 2006a).

4.1.4 Interaction of sub-species B Ads with blood

Recent studies were designed to investigate the interaction(s) between blood and the sub-species B vectors in CD46 transgenic mice after it was shown that the Ad35 knob domain was sensitive to FIX binding (Shayakhmetov *et al.*, 2005b). After intravenous administration of Ad5 and Ad5/f35 into non-transgenic mice, both vectors produced similar levels of liver transduction (Shayakhmetov *et al.*, 2005b). Strikingly, *in vitro* Ad5/f35 produced significantly reduced transduction of hepatocytes compared to Ad5 (Shayakhmetov *et al.*, 2005b), suggesting an alternative CAR-independent, blood factor-dependent pathway exists for hepatocyte transduction *in vivo*. Liver transduction by Ad5/f35 was significantly reduced in an *in situ* perfusion model but the level of Ad5 transduction remained the same (Shayakhmetov *et al.*, 2005b). These experiments were performed in non-transgenic mice. Therefore, Ad5/f35 required the presence of the blood for efficient liver transduction due to the lack of its primary receptor in non-CD46 transgenic mice. However, when the blood was removed, Ad5 could still efficiently transduce the hepatocytes using a CAR-dependent pathway.

Intravenous infusion of heparinase I into mice before administration of the vectors significantly reduced liver transduction by both Ad5 and Ad5/f35 (Shayakhmetov *et al.*, 2005b). This indicates that in the presence of blood, both vectors use HSPGs as their cellular receptors. The presence of human FIX significantly enhanced *in vitro* transduction by Ad5/f35 (Shayakhmetov *et al.*, 2005b). *Ex vivo* liver perfusion in the presence of FIX also increased transduction by Ad5/f35 to levels comparable with Ad5, with a significant increase in accumulation of both vectors by Kupffer cells (Shayakhmetov *et al.*, 2005b). There was no significant difference in liver transduction by Ad5/f35 in control and FIX knockout mice (Shayakhmetov *et al.*, 2005b), suggesting an influence by other blood factors *in vivo*.

Ad5/f35 and Ad35 also interact with platelets *in vivo*. Early blood clearance kinetics were determined for Ad5, Ad5/f35 and Ad35 using a blood sample taken 10 minutes post-intravenous infusion of the vector (Stone *et al.*, 2007a). There was very little Ad35 remaining in the circulation 10 minutes after administration, whereas the level of both Ad5 and Ad5/f35 in the blood was higher (Stone *et al.*, 2007a). This

suggests that the interaction with the blood was not dependent on CD46 as Ad35 and Ad5/f35 both have the Ad35 fiber, which binds to CD46. Ad5/f35 and Ad35 have different levels of association with the blood indicating the involvement of other capsid proteins for the interaction with the blood. Six hours after systemic administration of the vectors, Ad5 and Ad35 expressed similar levels of liver transduction (contrary to reports 48-72 hours after administration (Verhaagh *et al.*, 2006)) with Ad35 producing significantly higher levels of transduction of the lung and spleen (Stone *et al.*, 2007a). Ad5, Ad5/f35 and Ad35 were shown to co-localise with platelets in hepatic sinusoids by co-staining for Ad hexon and the platelet marker CD41 (Stone *et al.*, 2007a). Ad5, Ad5/f35 and Ad35 also co-localised with platelets after sequestration in the marginal zone of the spleen (Stone *et al.*, 2007a). However, in the lung, there was no evidence of interaction between Ad35 and platelets, indicating that the Ad vector-platelet interaction was not required for lung tropism.

4.1.5 Interaction of sub-species B Ads with FX

Whilst the Ad5 hexon has been shown to reproducibly interact with FX (Kalyuzhniy *et al.*, 2008, Vigant *et al.*, 2008, Waddington *et al.*, 2008), the interaction of FX with Ad35 was controversial. Previously, it has been reported that FX bound to Ad35 as demonstrated by SPR with an equilibrium dissociation constant of $5.2x10^{-8}$ M (Waddington *et al.*, 2008). Conversely, Kalyuzhniy and colleagues (Kalyuzhniy *et al.*, 2008) reported no interaction between Ad35 and FX by SPR. There was also a difference between the reports for the sub-species B vector Ad50, which was either reported as a very strong FX binder (Waddington *et al.*, 2008) or no binding to FX was detected (Kalyuzhniy *et al.*, 2008). However, binding to FX by Ad16 was reported as strong by both groups (Kalyuzhniy *et al.*, 2008, Waddington *et al.*, 2008).

Based on the importance of virus capsid design in gene therapeutics, the aim of this study was to fully define the interaction and effect of FX on Ad35 and chimeric Ad5/Ad35 vectors *in vitro* and *in vivo*.

4.2 Results

4.2.1 Chimeric Ad5/Ad35 vectors

To fully define the interaction of FX with Ad35 vectors *in vitro* and *in vivo*, several chimeric vectors were used (Figure 4.2). In addition to Ad5 and Ad35 vectors, the following chimeric vectors used were: the pseudotype Ad5/f35, which contains the hexon and penton of Ad5 with the Ad35 fiber (f), Ad5/p35/f35, which has the hexon of Ad5 and the penton (p) and fiber of Ad35, and Ad35/f5, the reverse pseudotype (Figure 4.2).

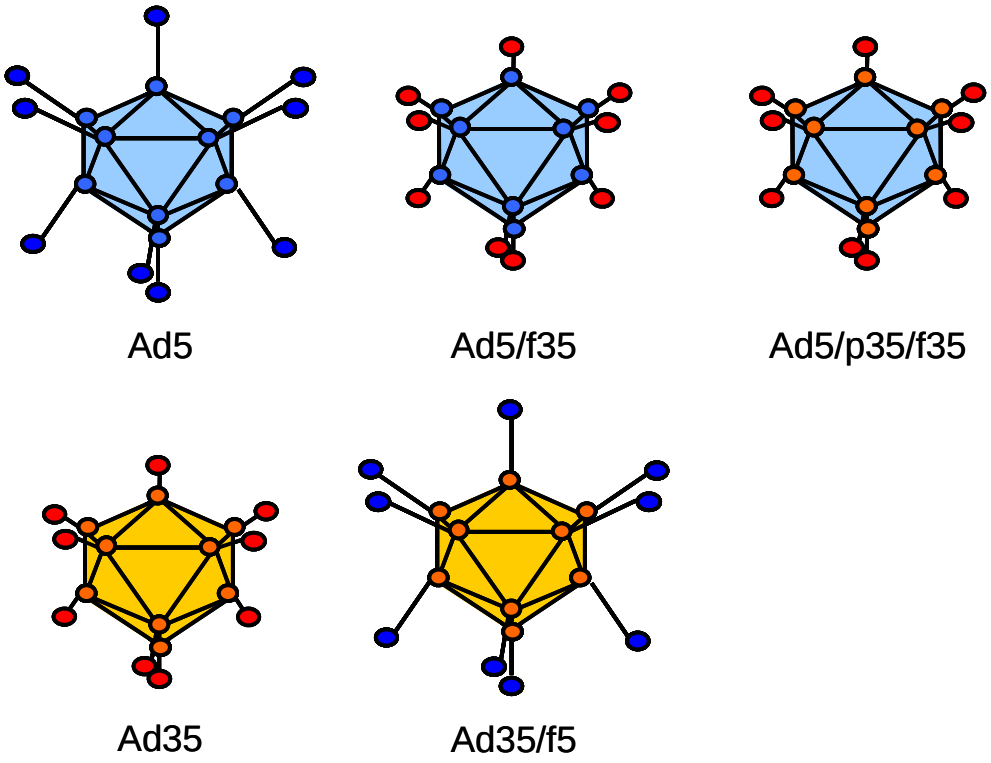

Figure 4.2 – Capsid configuration of Ad5, Ad35 and chimeric Ad5/Ad35 vectors.

Schematic to highlight the different vectors used in this study. Ad5 components are shown in blue and Ad35 components are shown in yellow/red. Ad5 and Ad35/f5 contain the long-shafted Ad5 fiber. Ad5/f35, Ad5/p35/f35 and Ad35 vectors all contain the short-shafted Ad35 fiber.

4.2.2 Affinity analysis of Ad5, Ad35 and chimeric Ad5/Ad35 vectors

The ability of Ad5, Ad35 and the chimeric Ad5/Ad35 vectors to bind the blood coagulation factor FX was analysed by SPR by Dr. J.H. McVey (Thrombosis Research Institute, London, UK). Following biotinylation of each vector, covalent linkage to a biosensor chip was performed and FX was injected over the chip at a flow rate of 30 µl/min. The presence of FX binding to the vectors was detected as a change in response units (RU) and kinetic analysis was performed post-hoc. SPR data was then compared to previous data characterising the Ad5:FX interaction (Waddington *et al.*, 2008).

SPR analysis revealed that Ad5, Ad35 and the chimeric Ad5/Ad35 vectors bound to FX and sensograms of the kinetic analysis for each vector are shown in Figure 4.3. The shape of the sensogram produced by each vector binding to FX was distinctly different depending on the capsid configuration. Ad5, Ad5/f35 and Ad5/p35/f35, which share the Ad5 hexon, had similar binding characteristics (Figure 4.3A, C, E). Conversely, Ad35 and Ad35/f5, which share the Ad35 hexon, have different binding characteristics (Figure 4.3B, D). The difference in binding characteristics was reflected in the kinetic analysis. Vectors containing the Ad5 hexon (Ad5, Ad5/f35 and Ad5/p35/f35) fitted to a 1:1 binding model with equilibrium dissociation constants of $2.7x10^{-9}$ M, $1.9x10^{-9}$ M and $1.0x10^{-9}$ M, respectively (Table 6), which is similar to previously reported findings for Ad5 (Waddington *et al.*, 2008). It should be noted that the biotinylated Ad5/p35/f35 bound much less FX than the other viruses, indicated by a lower change in RU (Figure 4.3E). In contrast, vectors containing the Ad35 hexon (Ad35 and Ad35/f5) fitted poorly to a 1:1 binding model but fitted to a heterogenous ligand model with equilibrium dissociation constants of $5.4x10^{-8}$ M and $3.5x10^{-9}$ M for Ad35 and $2.4x10^{-8}$ M and $6.6x10^{-9}$ M for Ad35/f5 (Table 6). Therefore, both the Ad5 and Ad35 pseudotypes have FX binding affinities akin to other vectors possessing the same hexon, with vectors containing the Ad5 hexon having an approximately ten-fold higher affinity for FX than those vectors containing the Ad35 hexon (Table 6).

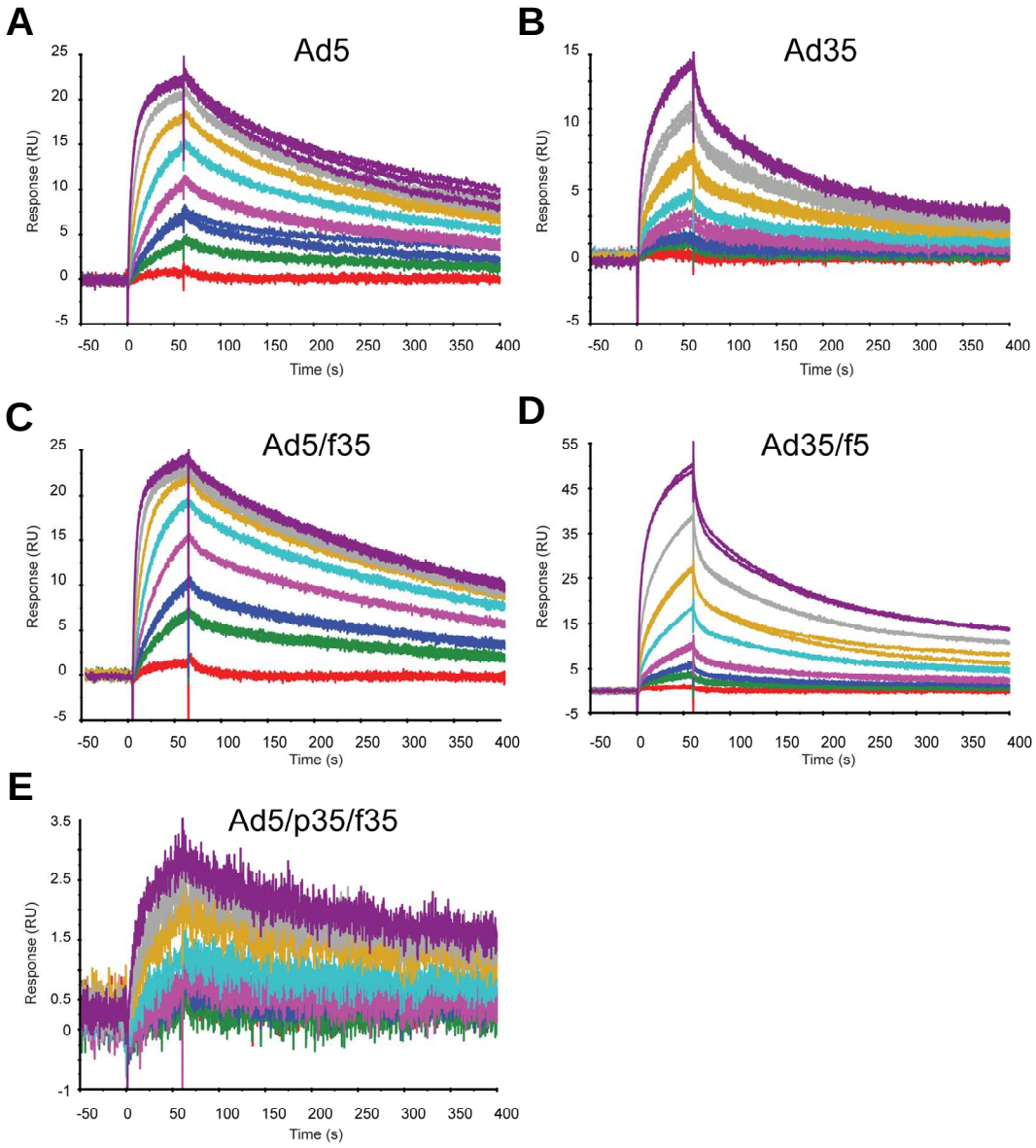

Figure 4.3 – Ad5, Ad35 and chimeric Ad5/Ad35 vectors bind FX.

Representative SPR sensograms for (A) Ad5, (B) Ad35, pseudotype vectors (C) Ad5/f35 and (D) Ad35/f5, and (E) chimeric vector Ad5/p35/f35. All vectors bind FX as shown by an increase in response units (RU).

	Ad5	Ad5/f35	Ad5/p35/f35	Ad35	Ad35/f5
ka1 (1/Ms)	$9.53x10^{5}$	$1.27x10^{6}$	$1.90x10^{6}$	$1.98x10^{5}$	$1.11x10^{10}$
kd1 (1/s)	$2.5x10^{-3}$	$2.4x10^{-3}$	$2.0x10^{-4}$	$1.1x10^{-2}$	269.7
K_D1 (M)	$2.7x10^{-9}$	$1.9x10^{-9}$	$1.0x10^{-9}$	$5.4x10^{-8}$	$2.4x10^{-8}$
Rmax1 (RU)	18.37	21.11	1.9	10.61	30.72
ka2 (1/Ms)				$2.09x10^{5}$	$2.29x10^{5}$
kd2 (1/s)				$7.42x10^{-4}$	$1.52x10^{-3}$
K_D2 (M)				$3.5x10^{-9}$	$6.6x10^{-9}$
Rmax2 (RU)				4.076	22.39

Table 6 – Ad5, Ad35 and chimeric Ad5/Ad35 vectors bind FX.

SPR kinetic analysis determined the calculated association rate (ka), dissociation rate (kd) and equilibrium dissociation constant (K_D) values for each vector.

4.2.3 Ad35 hexon binds to FX

CyroEM was performed by Dr. D. Bhella and Ms. R. Pink (MRC Virology Unit, University of Glasgow, UK) to further investigate the interaction between FX and Ad35. Ad35 virions were incubated overnight at 4°C in the presence of FX to allow FX to complex with the vector. Images of both the complexed and non-complexed vector and a composite image were resolved to 35Å resolution (Figure 4.4). The areas of green on the composite image indicate that FX bound to the Ad35 hexon with a clear density in the centre of the trimeric hexon proteins (Figure 4.4). Interestingly, in the presence of FX, the fibers of Ad35 are resolved (Figure 4.4). The Ad35 fibers are not usually present in cyroEM reconstructions due to the flexibility of the fiber (Saban *et al.*, 2005).

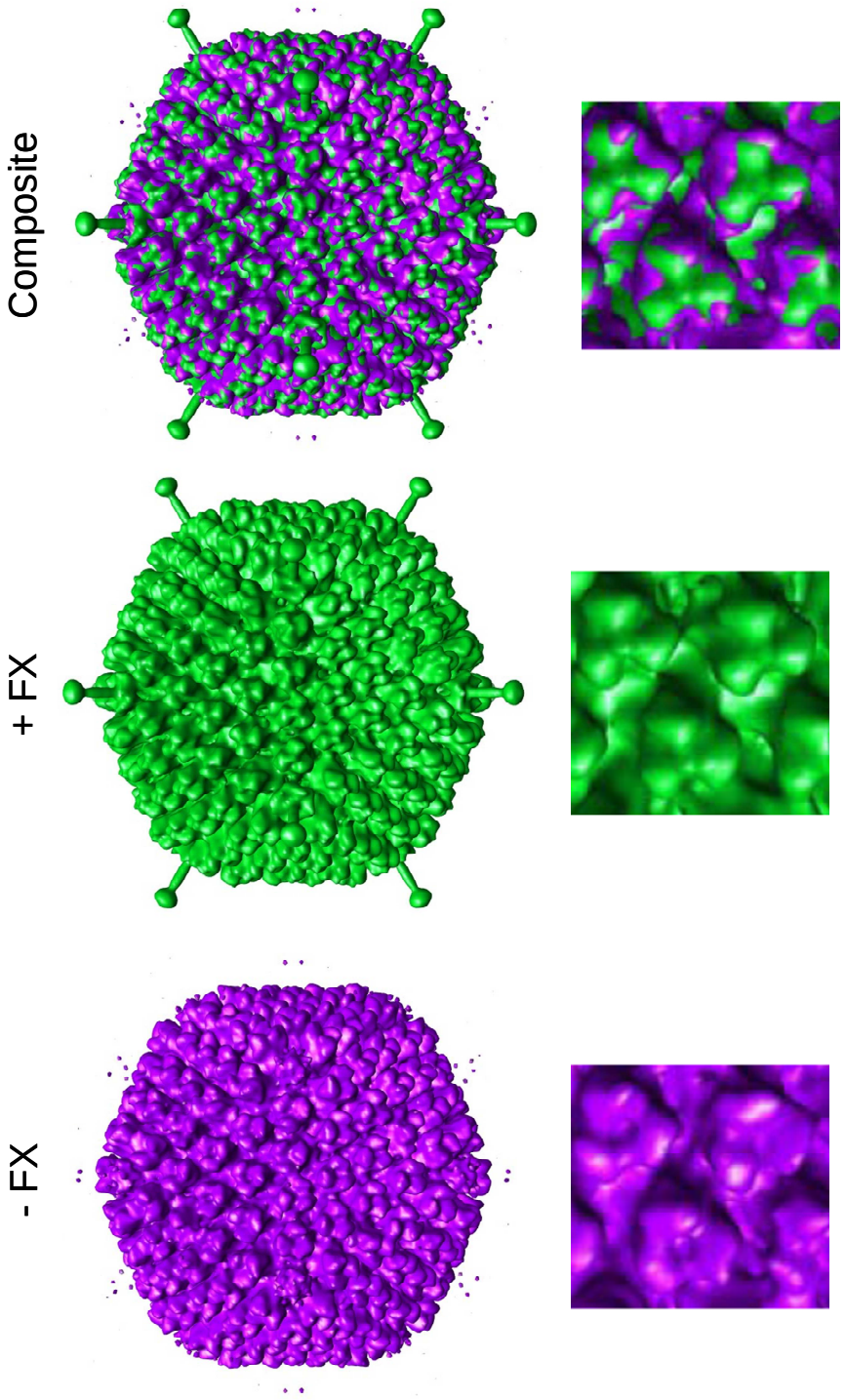

Figure 4.4 – FX binds to the Ad35 hexon.

Cryo-electron microscopic reconstruction of Ad35 in the presence and absence of FX. Composite image shows FX bound within a cavity formed by Ad35 trimeric hexon proteins.

4.2.4 CD46 expressing cell line

To investigate the effect of these interactions between Ad5, Ad35 and the chimeric Ad5/Ad35 vectors with FX *in vitro*, two cell lines were used. These were Chinese hamster ovary (CHO)-BC1 and CHO-WTR cells, obtained as a gift from Professor J. Atkinson (Washington University School of Medicine, St. Louis, MO, USA). The CHO-BC1 cell line stably expresses the BC1 isoform of the human membrane glycoprotein CD46, whereas the control CHO-WTR cells do not express CD46 as they were transfected with a control plasmid (Figure 4.5).

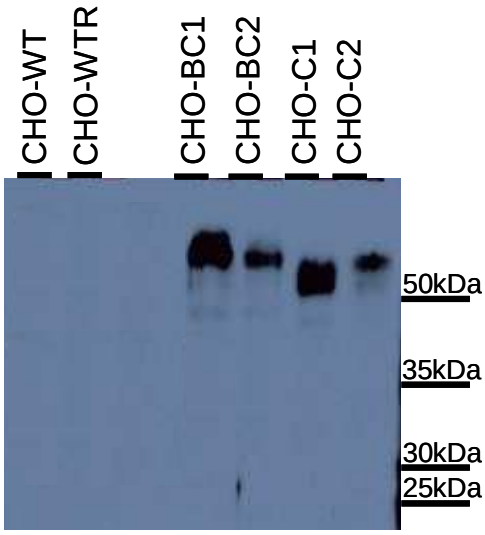

Figure 4.5 – Western blot for CD46 expression in CHO cell lines.

Anti-CD46 antibody probed membrane to detect relative levels of CD46 expression. Cells were cultured and lysed before determination of protein concentration by BCA assay. The same concentration of protein from each cell line was run on a 12% polyacrylamide gel with a rainbow ladder as a marker of protein size at 200 V for approximately 6 hours to achieve separation of the CD46 isoforms (56-66 kDa). CHO-WT, control CHO cells. CHO-WTR, transfected with a control plasmid. CHO-BC1, BC2, C1 and C2, cells stably expressing the BC1, BC2, C1 and C2 isoforms of CD46, respectively.

To confirm that gene transfer was mediated by CD46 in the CHO-BC1 cell line, the anti-CD46 antibody MEM258 was used (Figure 4.6). Transduction by the vectors in the presence of MEM258 was compared to transduction in the presence of control IgG (Figure 4.6). In CHO-WTR cells, which do not express CD46, transduction by Ad5, Ad5/f35, Ad5/p35/f35 and Ad35 was low and not effected by the presence of MEM258 (Figure 4.6A). The addition of MEM258 did not effect Ad5 transduction in CHO-BC1 cells (Figure 4.6B), where Ad5 produced a similar level of transduction in CHO-WTR cells (Figure 4.6A). In CHO-BC1 cells, the presence of MEM258 significantly reduced transduction by Ad5/f35, Ad5/p35/f35 and Ad35 by 6.7-, 14.2- and 22.6-fold, respectively (Figure 4.6B). Therefore, as MEM258 significantly reduced transduction by vectors possessing the Ad35 fiber (which is responsible for binding to CD46), CHO-BC1 cells stably express CD46 and gene transfer is mediated through this receptor for vectors with the Ad35 fiber.

4.2.5 Effect of FX on cell binding by Ad5, Ad35 and chimeric Ad5/Ad35 vectors in CHO-CD46 cells

The ability of the vectors to bind to CHO-BC1 and CHO-WTR cells in the presence and absence of FX was assessed by infecting the cell lines with the vectors at 4°C for one hour. Incubation with the vectors at 4°C allows binding by the vectors to the cell surface but not internalisation, which is energy-dependent and hence occurs at 37°C. After washing to remove unbound vectors, cells were collected, viral and total genomic DNA was isolated and qPCR was preformed to calculate the number of vector genomes per ng total DNA isolated.

The addition of physiological levels of FX significantly increased binding of Ad5 to both CHO-BC1 and CHO-WTR cells by 5.0- and 15.9-fold, respectively (Figure 4.7). This increase in binding in the presence of FX was significantly inhibited by the FX binding protein X-bp (Figure 4.7). X-bp is a 29 kDa protein isolated from *Deinagkistrodon acutus* (the hundred pace snake) which binds with high affinity to the Gla domain of human and murine FX (Atoda *et al.*, 1998), thus preventing the interaction between FX and the vector from occurring (Waddington *et al.*, 2008). Ad35/f5 showed a similar profile to Ad5 in both CHO-WTR and CHO-BC1 cells with a significant increase of 6.5- and 3.7-fold, respectively, in the presence of FX,

which was completely inhibited by the addition of X-bp (Figure 4.7A, B). In the absence of FX, binding of Ad5/f35, Ad5/p35/f35 and Ad35 was considerably higher in CHO-BC1 cells compared to binding in CHO-WTR cells (Figure 4.7). The addition of FX had no effect on CHO-BC1 cell binding mediated by Ad5/f35, Ad5/p35/f35 and Ad35 (Figure 4.7B) but enhanced binding in CHO-WTR cells by 7.3-, 3.6- and 2.0-fold, respectively (Figure 4.7A).

In summary, in CHO-WTR cells binding by Ad5, Ad5/f35, Ad5/p35/f35, Ad35 and Ad35/f5 was significantly increased in the presence of FX and blocked by X-bp, confirming the FX:Ad35 interaction. The interaction between the Ad35 fiber and CD46 in CHO-BC1 cells is very efficient and cannot be further enhanced by FX or blocked with X-bp. The presence of the Ad5 fiber on the Ad35 capsid in Ad35/f5 converts the binding profile back to one similar to Ad5. Thus, these data indicate the importance of both hexon and fiber in the cell binding process.

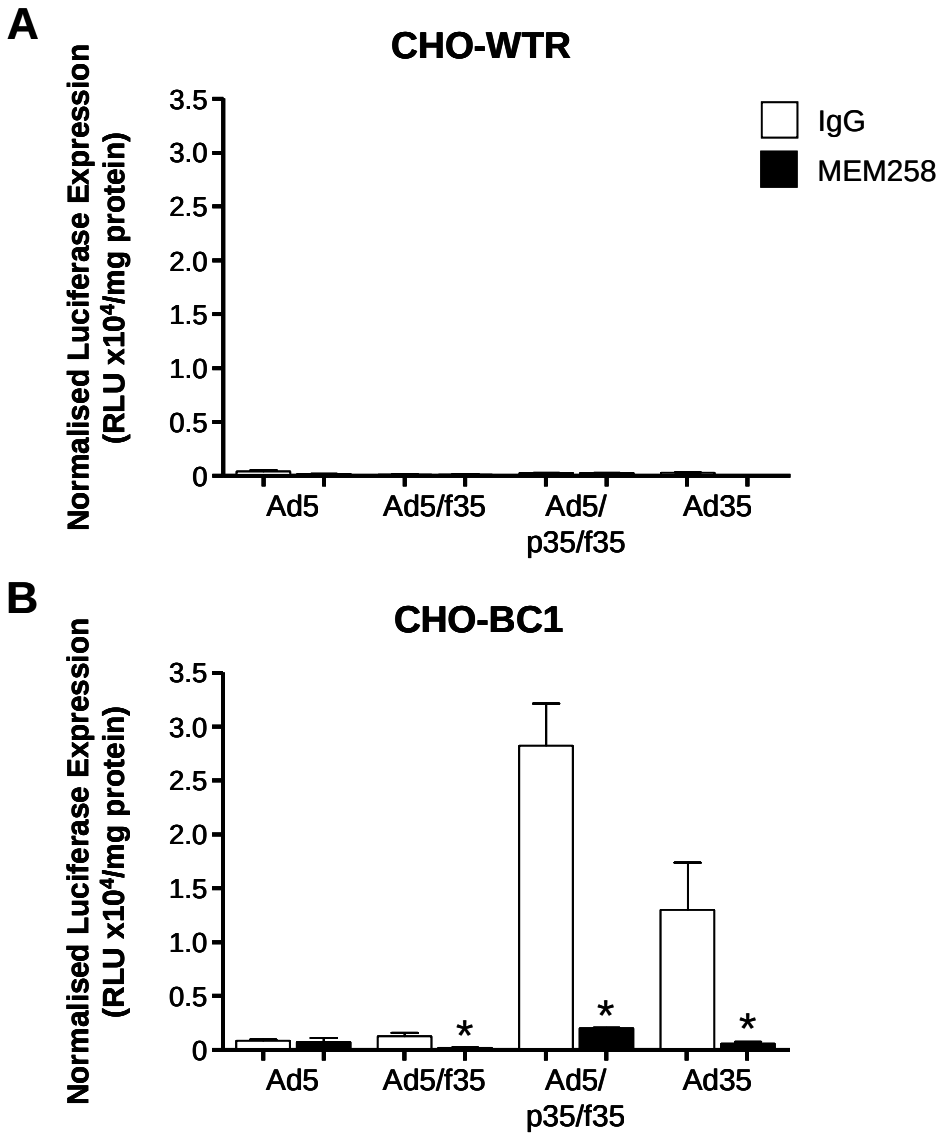

Figure 4.6 – Inhibition of transduction by Ad35 and chimeric Ad5/Ad35 vectors in CHO-WTR and CHO-CD46 cells in the presence of anti-CD46 antibody.

(A) CHO-WTR cells and (B) CHO-BC1 cells were exposed to each Ad vector at a concentration of 1000 VP/cell in the presence and absence of the anti-CD46 antibody MEM258 or IgG control for 3 hours at 37ºC. Cells were washed and maintained at 37°C for a further 72 hours before quantification of transgene expression by luciferase assay, normalised to total protein content determined by BCA assay. Error bars represent SEM (* $p < 0.05$ versus IgG control).

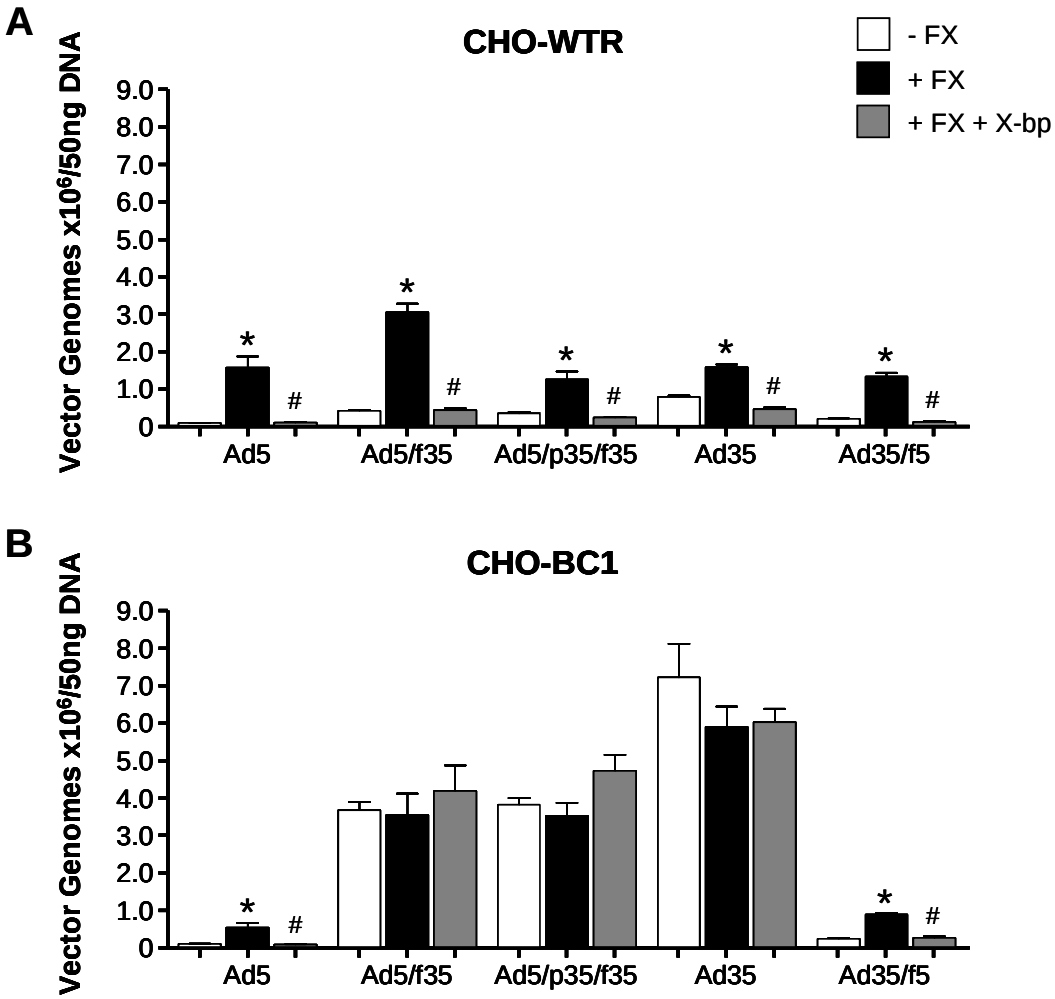

Figure 4.7 – Binding by Ad5, Ad35 and chimeric Ad5/Ad35 vectors in CHO-WTR and CHO-CD46 cells.

(A) CHO-WTR and (B) CHO-BC1 cells were exposed to each Ad vector at a concentration of 1000 VP/cell in the presence and absence of physiological FX levels and 15 μg/ml FX binding protein, X-bp, for 1 hour at 4ºC. Viral and total genomic DNA was extracted and the cell-bound adenovirus quantified by qPCR. Error bars represent SEM (* $p < 0.05$ versus absence of FX, # $p < 0.05$ versus presence of FX).

4.2.6 Effect of FX on cell internalisation by Ad5, Ad35 and chimeric Ad5/Ad35 vectors in CHO-CD46 cells

Previous reports have demonstrated differences in intracellular trafficking by vectors based on the sub-species B Ads in comparison to Ad5 (Miyazawa *et al.*, 1999, Shayakhmetov and Lieber, 2000, Shayakhmetov *et al.*, 2003, Shayakhmetov *et al.*, 2005a). These potentially very important differences in trafficking and the resulting differences in Ad genome localisation to the nucleus of infected cells could lead to a substantial difference in the level of transduction achieved by each vector. Therefore, the level of cellular internalisation mediated by Ad35 and the chimeric Ad5/Ad35 vectors was assessed through repetition of the binding experiment outlined above with an additional one hour incubation at 37°C (to allow internalisation) and concomitant removal of cell surface bound vector by washing with 0.2 M glycine, pH 2.2 (Figure 4.8).

Cell internalisation by all vectors was significantly enhanced by the addition of physiological levels of FX in CHO-WTR cells (Figure 4.8A). In the absence of FX all vectors likely use the low affinity HSPG pathway for cell entry (Tuve *et al.*, 2008). The addition of FX and resultant FX binding to both the Ad5 and Ad35 hexon possibly leads to all vectors being able to utilise the high affinity HSPG pathway for cell internalisation (Waddington *et al.*, 2008). The addition of FX significantly enhanced cell entry by vectors containing the Ad5 fiber (Ad5 and Ad35/f5) by 17.2- and 4.8-fold, respectively, in the CHO-BC1 cell line (Figure 4.8B). In the presence of FX, Ad5 and Ad35/f5 can utilise the HSPG pathway for enhanced internalisation. FX significantly increased cell internalisation by Ad35 by 1.8-fold in CHO-BC1 cells, indicating that FX and the resulting interaction of the Ad35:FX complex with the cellular receptor system (as yet undefined) can further enhance cell entry by Ad35 (Figure 4.8B).

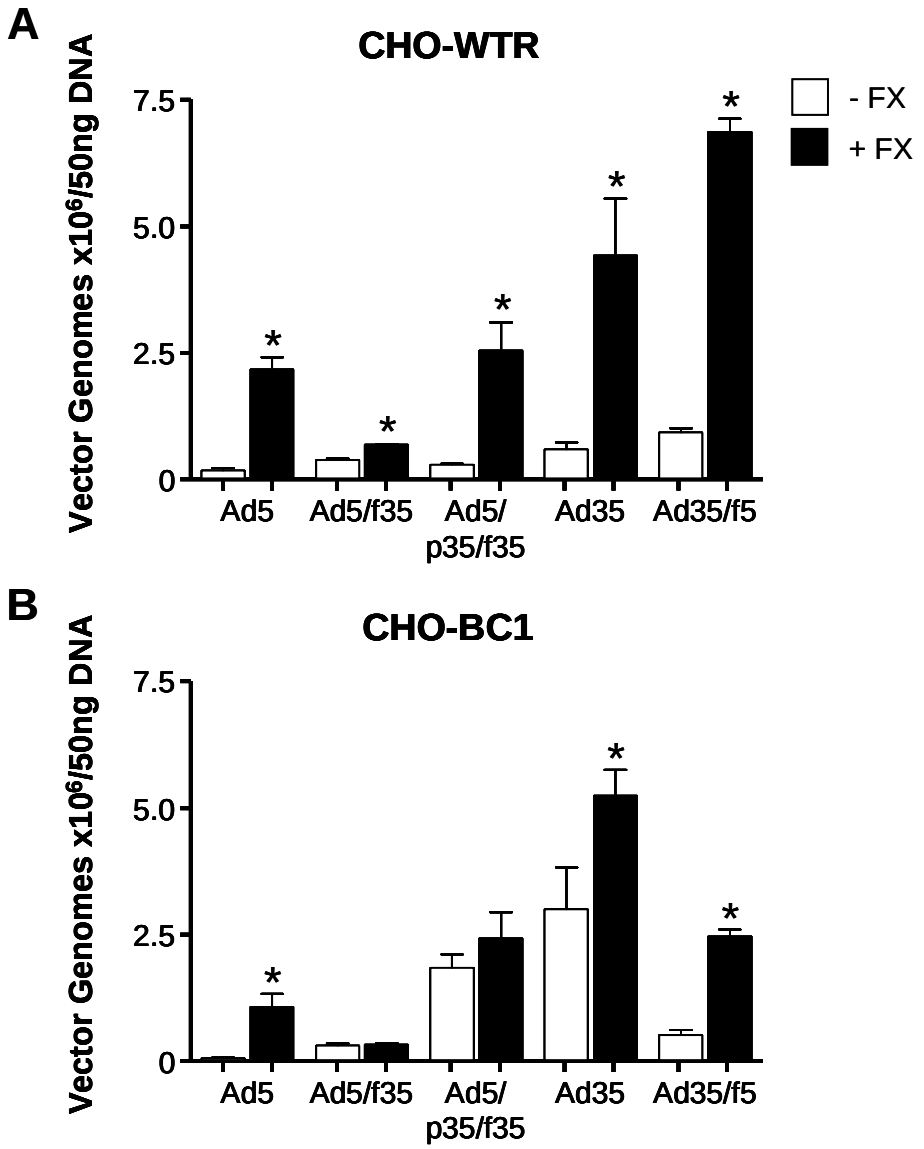

Figure 4.8 – Internalisation by Ad5, Ad35 and chimeric Ad5/Ad35 vectors in CHO-WTR and CHO-CD46 cells.

(A) CHO-WTR and (B) CHO-BC1 cells were exposed to each Ad vector at a concentration of 1000 VP/cell in the presence and absence of physiological FX levels for 1 hour at 4ºC, followed by 1 hour at 37°C. After washing with 0.2 M glycine, pH 2.2 to remove cell surface-bound vectors, viral and total genomic DNA was extracted and adenovirus quantified by qPCR. Error bars represent SEM (* $p < 0.05$ versus absence of FX).

4.2.7 FX limits cellular transduction by Ad35 and chimeric Ad5/Ad35 vectors containing the Ad35 fiber in CHO-CD46 cells

The recombinant Ad5, Ad35 and chimeric Ad5/Ad35 vectors express the luciferase reporter gene allowing transduction experiments to be performed and quantified by expression of the luciferase transgene after normalisation to the total protein content of the cells used in the experiment. In the presence of physiological levels of FX, the level of transgene expression mediated by Ad5 was significantly increased 3.6-fold in the CHO-BC1 cells and 38.6-fold in the CHO-WTR cells (Figure 4.9). In both cells lines, this enhancement in transduction produced by the addition of FX was entirely inhibited by X-bp (Figure 4.9).

In the presence of FX transduction by Ad5/f35, Ad5/p35/f35 and Ad35 in the CHO-BC1 cells was significantly inhibited by 2.7-, 1.9- and 2.2-fold, respectively (Figure 4.9B). Levels of expression were substantially lower for all three viruses in CHO-WTR cells, where FX significantly enhanced transduction by all vectors (Figure 4.9A).

Taken together, these data suggests that FX limits post-binding or post-internalisation mechanism(s) that leads to cellular transduction by viruses containing the Ad35 fiber (Ad5/f35, Ad5/p35/f35 and Ad35) in CHO-BC1 cells, where the high affinity interaction with CD46 is important. Such a limitation was not observed for Ad5 since strong potentiation of binding and transduction in the presence of FX was observed. Ad35/f5 also showed a significant increase in transduction in the presence of FX, which was inhibited by X-bp similar to Ad5 in both cell lines (Figure 4.9). However, in both CHO-BC1 and CHO-WTR cells, the level of transduction produced was very low (Figure 4.9).

The effect of FX on binding (attachment), internalisation and transduction (transgene expression) by Ad5, Ad35 and chimeric Ad5/Ad35 vectors in the CHO-BC1 and CHO-WTR cell lines is summarised in Table 7.

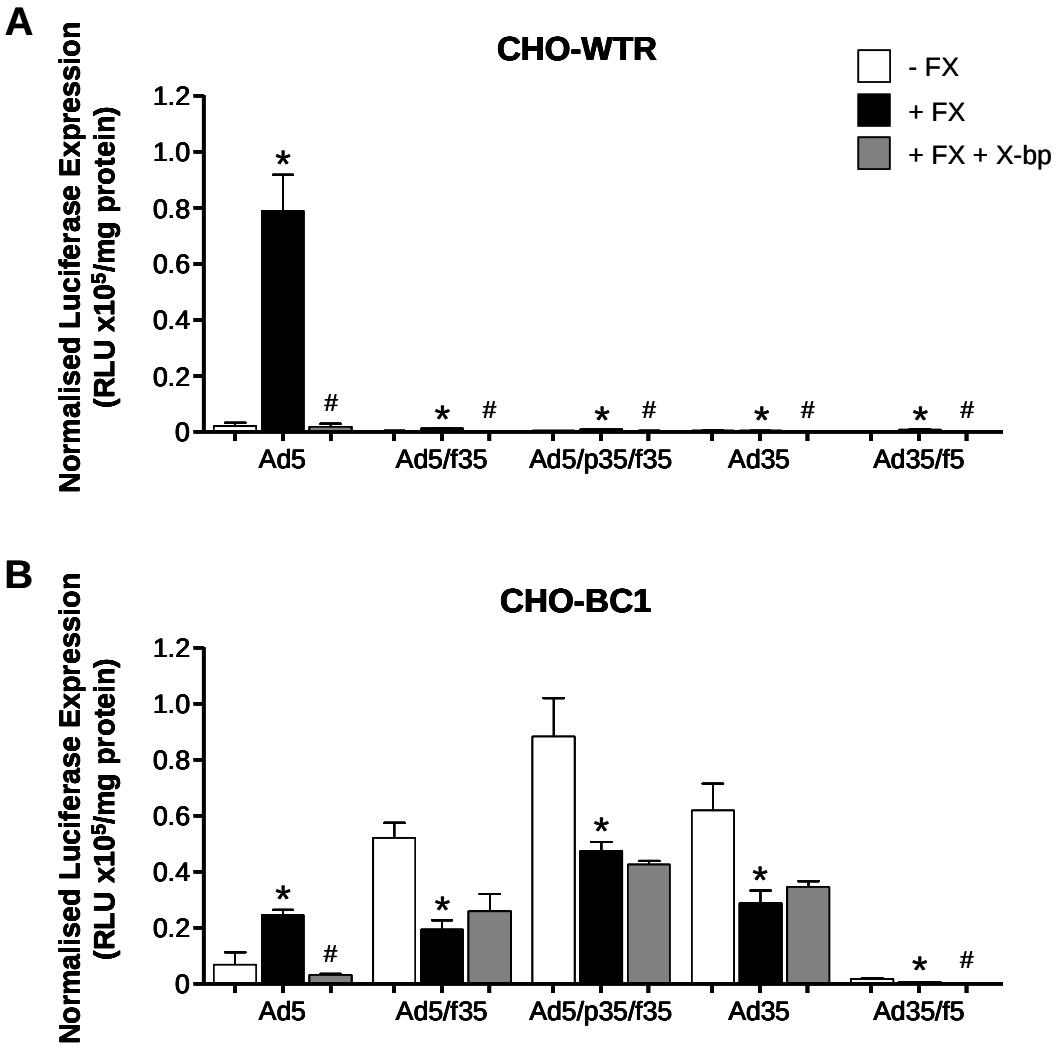

Figure 4.9 – Transduction by Ad5, Ad35 and chimeric Ad5/Ad35 vectors in CHO-WTR and CHO-CD46 cells.

(A) CHO-WTR and (B) CHO-BC1 cells were exposed to each Ad vector at a concentration of 1000 VP/cell in the presence and absence of physiological levels of FX and 15 μg/ml FX binding protein, X-bp, for 3 hours at 37ºC. Cells were washed and maintained at 37ºC for a further 72 hours before quantification of transgene expression by luciferase assay, normalised to total protein content determined by BCA assay. Error bars represent SEM (* $p < 0.05$ versus absence of FX, # $p < 0.05$ versus presence of FX).

Virus	CHO-BC1			CHO-WTR		
	Attachment	Internalisation	Transgene Expression	Attachment	Internalisation	Transgene Expression
Ad5	+	+	+	+	+	+
Ad5/f35	0	0	-	+	+	+
Ad5/p35/f35	0	0	-	+	+	+
Ad35	0	+	-	+	+	+
Ad35/f5	+	+	+	+	+	+

Table 7 – Effect of FX on attachment, internalisation and transgene expression by Ad5, Ad35 and chimeric Ad5/Ad35 vectors *in vitro*.

Summary of the effect of FX on attachment (binding), internalisation and transgene expression (transduction) by Ad5, Ad35 and chimeric Ad5/Ad35 vectors in CHO-BC1 and CHO-WTR cell lines. + indicates enhancement in the presence of FX, - indicates inhibition in the presence of FX and 0 indicates no effect of FX.

4.2.8 Effect of NAPc2 on Ad35 transduction in CHO-CD46 cells

To confirm the effect of FX on Ad35 transduction, *in vitro* transduction experiments were performed in the presence of increasing concentrations of NAPc2 (Figure 4.10). NAPc2 is nematode anticoagulant peptide which is a potent inhibitor of Ad5 transduction (Waddington *et al.*, 2008). NAPc2 binds to a putative heparin binding exosite in the FX serine protease domain with high affinity (Murakami *et al.*, 2007). Therefore, the presence of NAPc2 prevents the interaction between the Ad5:FX complex and (putatively) HSPGs, resulting in ablation of Ad5 transduction through blockade of receptor binding (Waddington *et al.*, 2008). As previously reported above, the addition of physiological levels of FX significantly increased transduction by Ad5 in both CHO-WTR and CHO-BC1 cell lines (Figure 4.10). The addition of 10 μg/ml NAPc2 completely ablated transduction by Ad5 by 574.4- and 341.5-fold in CHO-WTR and CHO-BC1 cells, respectively (Figure 4.10). This inhibition of transduction was concentration-dependent (Figure 4.10). Although 0.1 μg/ml NAPc2 produced a significant reduction in Ad5 transduction in CHO-WTR and CHO-BC1 cells, dilution of NAPc2 to a concentration of 0.01 μg/ml did not significantly reduce transduction by Ad5 in either cell line (Figure 4.10). This is similar to results previously reported in HepG2 cells (Waddington *et al.*, 2008).

Transduction by Ad35 was significantly inhibited 1.7-fold in the presence of FX in CHO-BC1 cells (Figure 4.10B), as previously shown. The addition of 1 and 10 μg/ml NAPc2 significantly reduced transduction further (Figure 4.10B). This suggests that the Ad35:FX complex also uses the HSPG pathway for transduction. In the presence of NAPc2, transduction by Ad35 was significantly inhibited, likely due to an inability to utilise HSPGs as cellular receptors for transduction. However, there was an indication that transduction by Ad35 in the presence of FX was not singularly dependent on HSPGs, in comparison to transduction by Ad5. Although NAPc2 produced a significant reduction in transduction by Ad35, this was not to the same degree as the inhibition of Ad5 transduction. This indicates that a modest level of transduction by Ad35 was still CD46-dependent. In CHO-WTR cells, Ad35 produced very low levels of transduction under all conditions (Figure 4.10A).

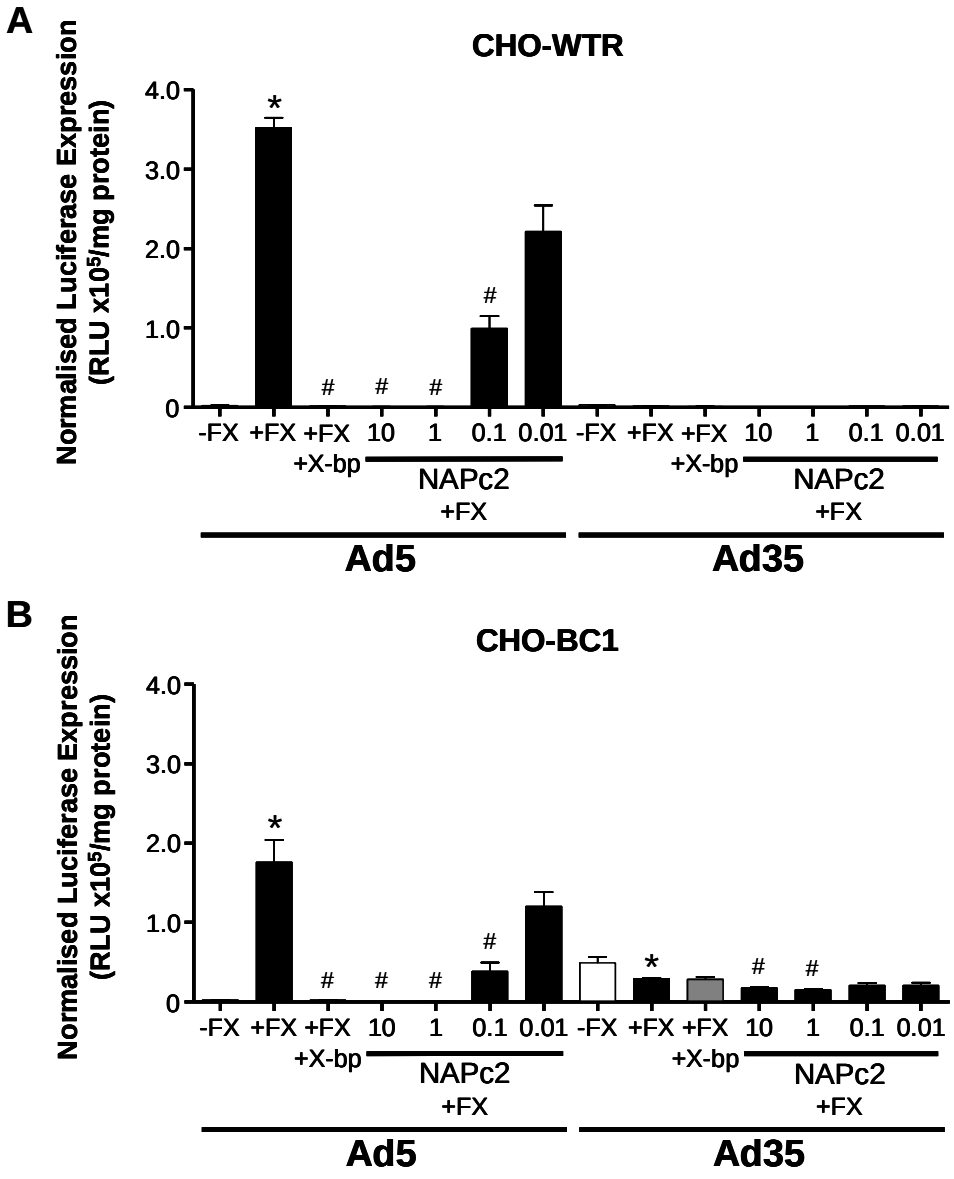

Figure 4.10 – Transduction by Ad5 and Ad35 vectors in CHO-WTR and CHO-CD46 cells in the presence of NAPc2.

(A) CHO-WTR and (B) CHO-BC1 cells were exposed to each Ad vector at a concentration of 1000 VP/cell in the presence and absence of physiological levels of FX and 0.01 – 10 μg/ml NAPc2 for 3 hours at 37ºC. Cells were washed and maintained at 37°C for a further 72 hours before quantification of transgene expression by luciferase assay, normalised to total protein content determined by BCA assay. Error bars represent SEM (* $p < 0.05$ versus absence of FX, # $p < 0.01$ versus presence of FX).

4.2.9 Effect of FX on cell binding and transduction by Ad5, Ad35 and chimeric Ad5/Ad35 vectors in human cancer cell lines

Vectors containing the Ad35 fiber are becoming increasing popular as gene therapy vectors, especially for use in cancer gene therapy. Therefore, the effect of FX on binding and transduction by Ad35 and the chimeric Ad5/Ad35 vectors was investigated in three cancer cell lines, MDA-MB-435, SKOV-3 and T-47D cells. These cell lines were selected from the NCI60 database (http://dtp.nci.nih.gov) as they expressed a range of CAR and CD46 levels determined by RNA level, RNA expression and normalised gene expression (Table 8). MDA-MB-435 cells have a low CAR and CD46 expression levels, SKOV-3 cells have moderate CAR expression and low CD46 expression and T-47D cells have high expression of both CAR and CD46 (Table 8).

Additionally, the relative expression of CAR and CD46 in these cancer cell lines was confirmed by TaqMan qPCR (Figures 4.11, 4.12) and by western blot for CD46 (Figure 4.13). A western blot was performed to detect the relative CAR expression level but the anti-CAR antibody (RmcB clone; Upstate, Lake Placid, NY, USA) did not perform to the standard required. MDA-MB-435 cells have also been previously reported to express very low levels of CAR by flow cytometry (Shayakhmetov *et al.*, 2002).

Cell Line	CAR			CD46		
	RNA Levels	RNA Expression	Normalised Gene Expression	RNA Levels	RNA Expression	Normalised Gene Expression
MDA-MB-435	5.0	-0.9	18.3	200.2	45.3	92.7
SKOV-3	79.8	44.3	83.5	401.2	-14.7	64.6
T-47D	226.1	108.7	274.1	1024.9	150.3	569.7

Table 8 – CAR and CD46 levels in human cancer cell lines.

CAR and CD46 RNA level, RNA expression and normalised gene expression data taken from the NCI60 database (http://dtp.nci.nih.gov).

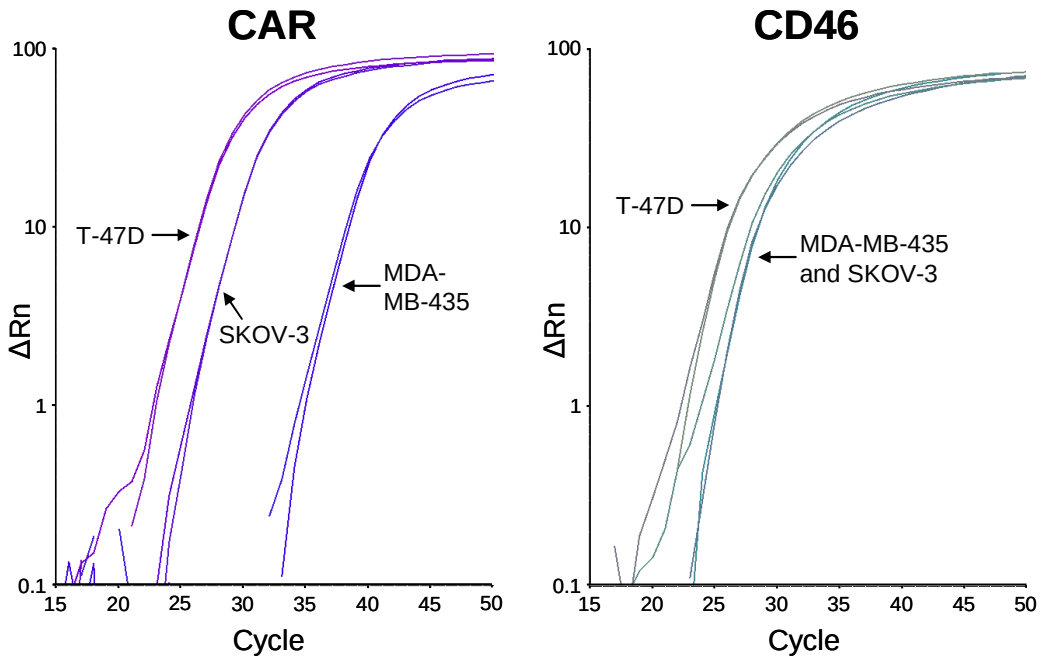

Figure 4.11 – Amplification plots from TaqMan qPCR for CAR and CD46 expression in human cancer cell lines.

RNA was extracted from each of the three cancer cell lines. cDNA was synthesised and amplified using primers specific for CAR and CD46 and TaqMan qPCR was performed using the Power SYBR Green detection system. The amount of fluorescence released during the amplification cycle is proportional to the amount of product generated in each cycle and these representative traces from qPCR show the relative CAR and CD46 expression levels in the three cancer cell lines.

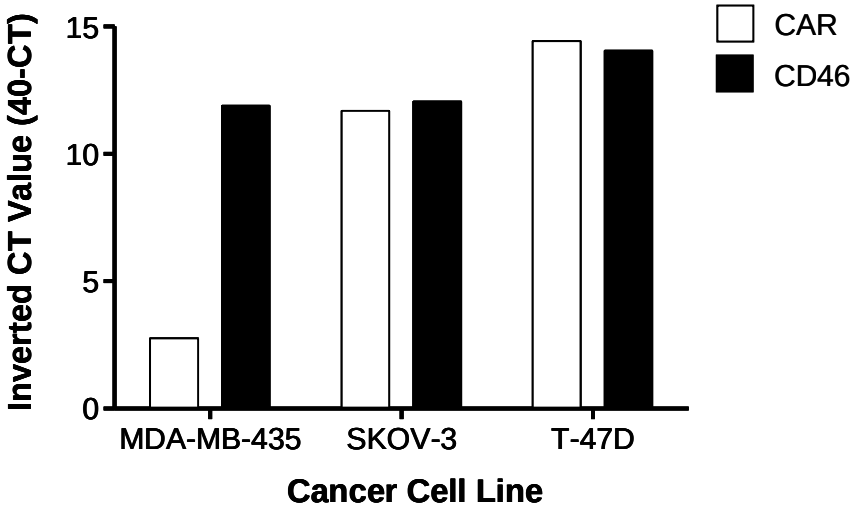

Figure 4.12 – TaqMan quantification of relative CAR and CD46 expression in cancer cell lines.

RNA was extracted from each of the three cancer cell lines. cDNA was synthesised and amplified using primers specific for CAR and CD46 and TaqMan qPCR was performed using the Power SYBR Green detection system. Acquisition of data occurs when PCR amplification is in the exponential stage. Data expressed as inverted CT value (40-CT) showing the relative CAR and CD46 expression levels in the three cancer cell lines.

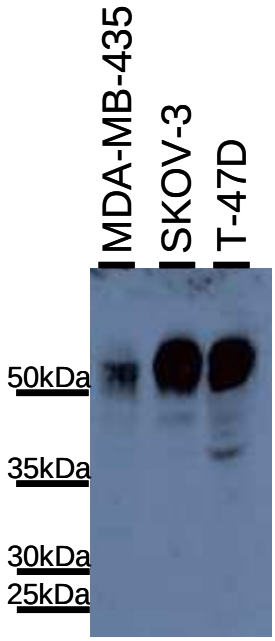

Figure 4.13 – Western blot for CD46 expression in human cancer cell lines.

Anti-CD46 (56-66 kDa) antibody probed membranes to detect relative levels of receptor expression in cancer cell lines. Cells were cultured and lysed before determination of protein concentration by BCA assay. The same concentration of protein from each cell line was run on a 12% polyacrylamide gel with a rainbow ladder as a marker of protein size at 200 V for approximately 6 hours to achieve separation of the CD46 isoforms.

4.2.9.1 Effect of FX on binding and transduction by Ad5, Ad35 and chimeric Ad5/Ad35 vectors in MDA-MB-435 cells

The addition of physiological levels of FX significantly enhanced binding by Ad5 and Ad35/f5 by 49.6- and 16.3-fold, respectively, in MDA-MB-435 cells (Figure 4.14A). Transduction by Ad5 and Ad35/f5 was also significantly enhanced in the presence of FX by 65.4- and 3.7-fold, respectively (Figure 4.14B). However, the level of transduction produced by Ad35/f5 was very low in this cell line (Figure

4.14B). The low CAR expression on MDA-MB-435 cells (Figure 4.12) results in low levels of binding by vectors with the Ad5 fiber in the absence of FX (Figure 4.14A). The addition of FX produces a significant enhancement in binding (Figure 4.14A).

The addition of FX had no effect on binding by Ad5/f35 and Ad5/p35/f35, possibly due the nature of the high affinity interaction between the Ad35 fiber and CD46, which could not be further enhanced by possible inclusion of binding to HSPGs in the presence of FX (Figure 4.14A). However, the presence of FX binding by Ad35 was significantly enhanced by 1.9-fold in the MDA-MB-435 cells (Figure 4.14A), indicating differences between vectors with the Ad35 fiber (Ad5/f35 and Ad5/p35/f35) and the complete Ad35 vector in binding to this cancer cell line.

The addition of FX significantly inhibited transduction by Ad5/p35/f35 and Ad35 by 1.8- and 1.9-fold, respectively, in MDA-MB-435 cells (Figure 4.14B). Ad5/f35 produced very low levels of transduction in this cancer cell line (Figure 4.14B). This adds further evidence to the hypothesis that FX limits a post-binding or post-internalisation mechanism(s) that leads to cellular transduction by vectors containing the Ad35 fiber (Ad5/p35/f35 and Ad35). Although Ad5/p35/f35 and Ad35 both demonstrated high levels of binding to the MDA-MB-435 cells, this did not translate to similar transduction levels in this cell line.

4.2.9.2 Effect of FX on binding and transduction by Ad5, Ad35 and chimeric Ad5/Ad35 vectors in T-47D cells

The addition of physiological levels of FX significantly increased binding by Ad5 and Ad35/f5 in the T-47D cell line by 2.84- and 4.6-fold, respectively (Figure 4.15A). However, the difference between binding in the presence and absence of FX was less in this cell line compared to MDA-MB-435 cells (Figure 4.15A). The T-47D cell line has high CAR expression (Figure 4.12) and, although binding can be significantly enhanced in the presence of FX, the difference was not so profound, likely due to increased binding by vectors with the Ad5 fiber in the absence of FX.

Binding by Ad5/f35 and Ad5/p35/f35 was significantly reduced in the presence of FX by 1.8- and 2.6- fold, respectively (Figure 4.15A). However, the addition of FX had no effect on binding by Ad35 (Figure 4.15A). This suggests that FX binding to the Ad5 hexon in the presence of the Ad35 fiber in both Ad5/f35 and Ad5/p35/f35 inhibits cell binding by these vectors (Figure 4.15A). Overall, the level of cell binding by all vectors in the T-47D cell line was enhanced compared to binding to MDA-MB-435 cells, likely due to the increased expression of both CAR and CD46 receptors on T-47D cells (Figure 4.12).

In T-47D cells, transduction by Ad5 was significantly enhanced by 1.9-fold in the presence of FX (Figure 4.15B). However, the addition of FX significantly inhibited transduction by Ad5/p35/f35 by 2.3-fold (Figure 4.15B), possibly due to the significantly reduced binding by this vector in the presence of FX (Figure 4.15A). FX had no effect on transduction by Ad35, in comparison to other cell lines where the presence of FX significantly inhibits transduction (Figures 4.9, 4.15). However, the level of transduction by Ad35 in T-47D cells was greater than in the other cell lines, likely due to the increased CD46 expression in this cell line (levels are similar or higher than in CHO-BC1 cells (Figures 4.5, 4.13, taken from the same western blot)). Ad5/f35 and Ad35/f5 both produced very low levels of transduction in T-47D cells (Figure 4.15B).

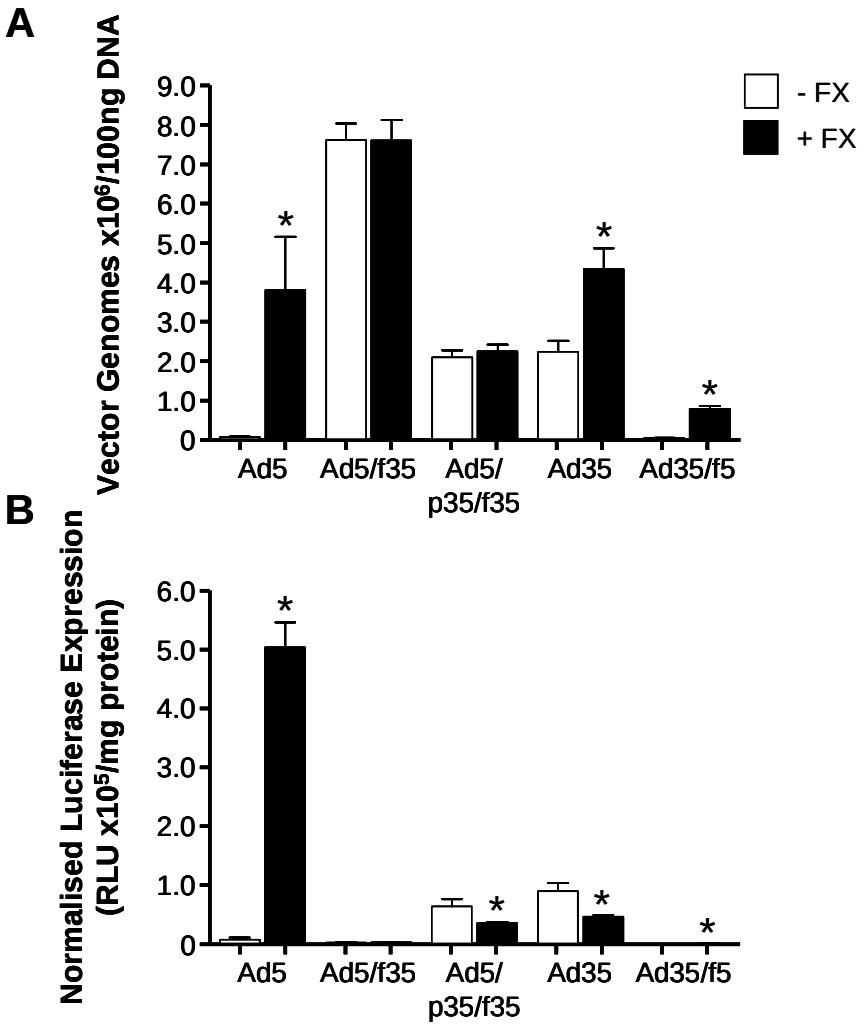

Figure 4.14 – Binding and transduction by Ad5, Ad35 and chimeric Ad5/Ad35 vectors in MDA-MB-435 cells.

(A) MDA-MB-435 cells were exposed to each Ad vector at a concentration of 1000 VP/cell in the presence and absence of physiological FX levels for 1 hour at 4ºC. Viral and total genomic DNA was extracted and the cell-bound adenovirus quantified by qPCR. Error bars represent SEM (* $p < 0.05$ versus absence of FX). (B) MDA-MB-435 cells were exposed to each Ad vector at a concentration of 1000 VP/cell in the presence and absence of physiological levels of FX for 3 hours at 37ºC. Cells were washed and maintained at 37°C for a further 72 hours before quantification of transgene expression by luciferase assay, normalised to total protein content determined by BCA assay. Error bars represent SEM (* $p < 0.05$ versus absence of FX).

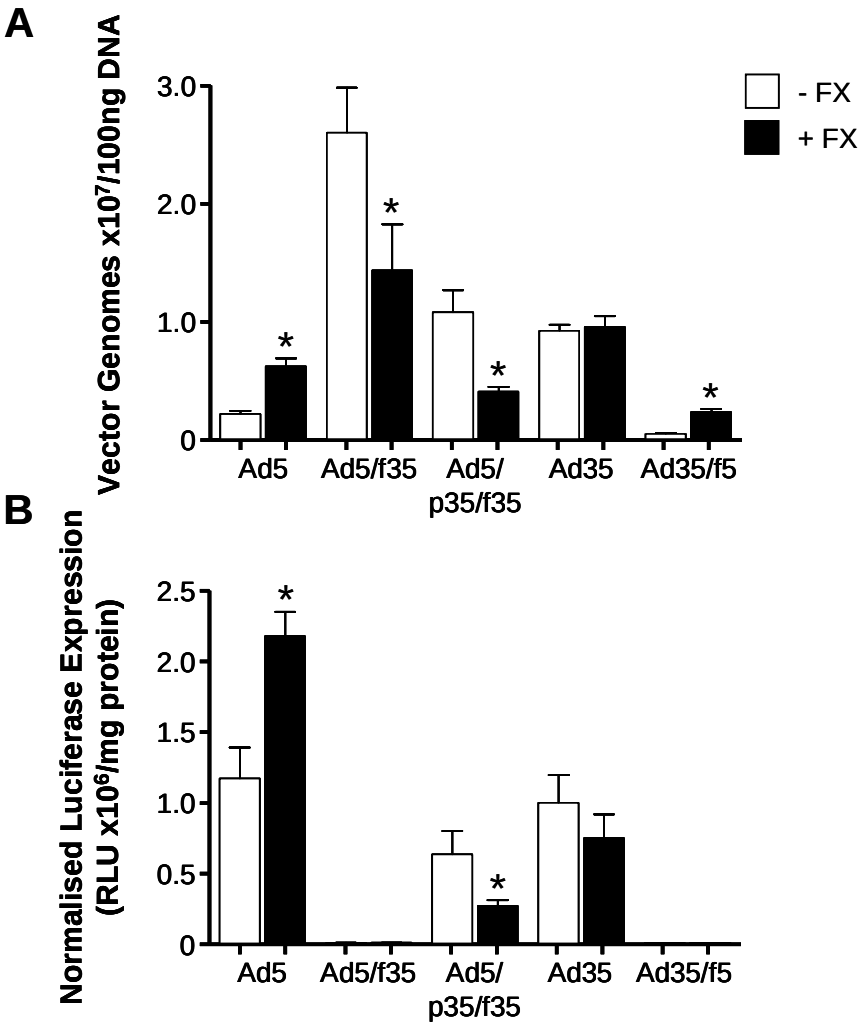

Figure 4.15 – Binding and transduction by Ad5, Ad35 and chimeric Ad5/Ad35 vectors in T-47D cells.

(A) T-47D cells were exposed to each Ad vector at a concentration of 1000 VP/cell in the presence and absence of physiological FX levels for 1 hour at 4ºC. Viral and total genomic DNA was extracted and the cell-bound adenovirus quantified by qPCR. Error bars represent SEM (* $p < 0.05$ versus absence of FX). (B) T-47D cells were exposed to each Ad vector at a concentration of 1000 VP/cell in the presence and absence of physiological levels of FX for 3 hours at 37ºC. Cells were washed and maintained at 37°C for a further 72 hours before quantification of transgene expression by luciferase assay, normalised to total protein content determined by BCA assay. Error bars represent SEM (* $p < 0.05$ versus absence of FX).

4.2.9.3 Effect of FX on binding and transduction by Ad5, Ad35 and chimeric Ad5/Ad35 vectors in SKOV-3 cells

The addition of physiological levels of FX significantly enhanced binding by Ad5, Ad5/f35, Ad35 and Ad35/f5 by 19.3-, 3.6-, 6.0- and 19.8-fold, respectively, in SKOV-3 cells (Figure 4.16A). For each of these vectors, the addition of X-bp significantly inhibited the enhancement in binding produced in the presence of FX (Figure 4.16A). SKOV-3 cells express a moderate level of CAR in comparison to the other two cancer cell lines (Figure 4.12). Thus, the fold change increase in binding by Ad5 and Ad35/f5 in the presence of FX was between that produced in the MDA-MB-435 and T-47D cells (Figures 4.14A, 4.15A, 4.16A). The addition of FX significantly enhances binding by Ad5/f35 and Ad35 (Figure 4.16A). This was likely due to SKOV-3 cells also having low CD46 expression (Figure 4.12). Therefore, FX binding to the Ad35 hexon and the subsequent use of alternative receptors (possibly HSPGs) produced an increase in binding.

The presence of FX has a very similar effect on transduction as on cell binding by each Ad vector in the SKOV-3 cells (Figure 4.16). Transduction by Ad5, Ad5/p35/f35, Ad35 and Ad35/f5 was significantly increased in the presence of FX by 51.9-, 2.6-, 1.8- and 10.2-fold, respectively (Figure 4.16B). The increase in transduction by these vectors was also significantly inhibited in the presence of X-bp (Figure 4.16B).

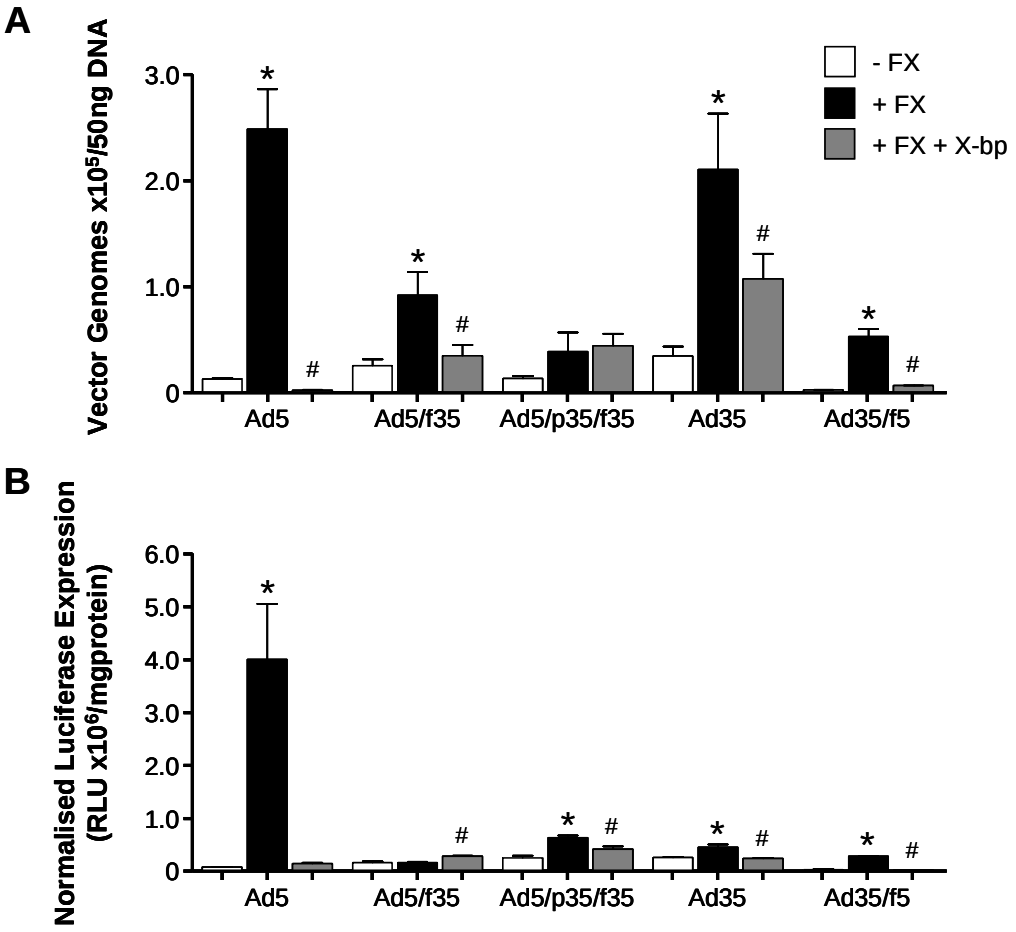

Figure 4.16 – Binding and transduction by Ad5, Ad35 and chimeric Ad5/Ad35 vectors in SKOV-3 cells.

(A) SKOV-3 cells were exposed to each Ad vector at a concentration of 1000 VP/cell in the presence and absence of physiological FX levels and 15 μg/ml FX binding protein, X-bp, for 1 hour at 4ºC. Viral and total genomic DNA was extracted and the cell-bound adenovirus quantified by qPCR. Error bars represent SEM (* $p < 0.05$ versus absence of FX, # $p < 0.05$ versus presence of FX). (B) SKOV-3 cells were exposed to each Ad vector at a concentration of 1000 VP/cell in the presence and absence of physiological levels of FX and 15 μg/ml FX binding protein, X-bp, for 3 hours at 37ºC. Cells were washed and maintained at 37°C for a further 72 hours before quantification of transgene expression by luciferase assay, normalised to total protein content determined by BCA assay. Error bars represent SEM (* $p < 0.05$ versus absence of FX, # $p < 0.05$ versus presence of FX).

To further investigate the effect of FX on Ad35 transduction in SKOV-3 cells, the transduction experiment was repeated in the presence of increasing concentrations of NAPc2 (Figure 4.17). As reported above (Figure 4.16), the addition of physiological levels of FX significantly increased transduction by Ad5 (Figure 4.17). The addition of 10, 1 and 0.1 μg/ml NAPc2 significantly reduced transduction by Ad5 by 138.1-, 105.8- and 1.3-fold, respectively, with the difference decreasing after each ten-fold dilution of NAPc2 (Figure 4.17). 0.01 μg/ml NAPc2 did not significantly inhibit transduction by Ad5 in the SKOV-3 cells (Figure 4.17). The addition of FX significantly increased transduction by Ad35 by 1.1-fold in SKOV-3 cells (Figure 4.17). Addition of 10 μg/ml and 1 μg/ml NAPc2 significantly inhibited transduction by Ad35 by 3.2- and 3.7-fold, respectively (Figure 4.17). However, the level of transduction produced by Ad35 was very low in all cases (Figure 4.17). This illustrates that in the SKOV-3 cancer cell line, the Ad35:FX complex also uses the putative HSPG pathway for transduction as transduction was significantly inhibited in the presence of NAPc2.

4.2.10 Effect of FX on cell trafficking by Ad5, Ad35 and chimeric Ad5/Ad35 vectors in SKOV-3 cells

To investigate the differences in intracellular trafficking between Ad5, Ad35 and the chimeric vectors Ad5/f35 and Ad5/p35/f35, the vectors were labelled with Alexa Fluor® 488 (Figures 4.18, 4.19, 4.20, 4.21). SKOV-3 cells were exposed to vectors in the presence and absence of physiological levels of FX for one hour at 4ºC to allow binding to occur. The cells were then either immediately fixed or fixed after incubation at 37°C for 15 minutes, one hour or three hours to allow vector internalisation. Images were taken after visualisation on a confocal microscope.

After one hour at 4°C (time 0), the labelled vectors were visualised bound to the cell surface as expected for Ad vectors (Figures 4.18, 4.19, 4.20, 4.21). Ad5 had reached the nucleus after one hour incubation at 37°C in both the presence and absence of FX, although the concentration of labelled Ad5 vectors was higher in the presence of FX (Figure 4.18). This correlates well with the enhanced transduction produced *in vitro* by the addition of FX in SKOV-3 cells (Figure 4.16). After three hours at 37°C, there was a higher concentration of labelled Ad5 in the perinuclear space (seen

by co-localisation with DAPI nuclear stain) and possibly indicating localisation of the vector with the microtubule organising centre (Figure 4.18). However, after the same incubation time Ad5/f35, Ad5/p35/f35 and Ad35 remained in the cytosol, indicating that vectors with the Ad35 fiber had inefficient intracellular trafficking (Figures 4.19, 4.20, 4.21, respectively). The intracellular trafficking for these vectors was similar in the presence and absence of FX (Figures 4.19, 4.20, 4.21). The lack of nuclear localisation after three hours (the time period the cells were exposed to the vector in the transduction experiments) by Ad35 and Ad35 fiber-containing vectors is one possible explanation for the lower levels of transduction produced by these vectors.

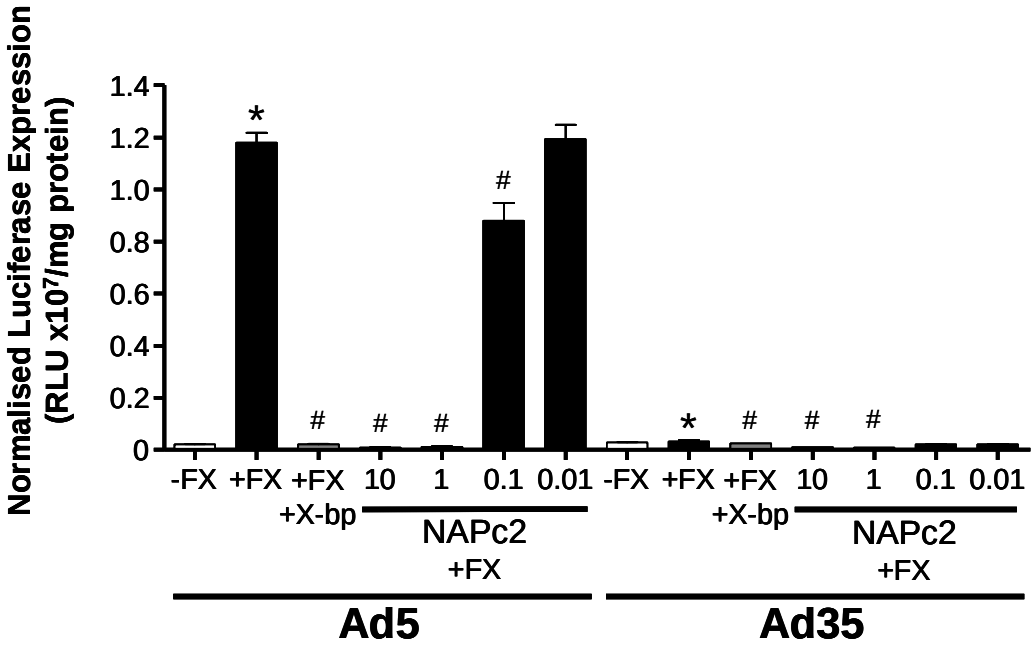

Figure 4.17 – Transduction by Ad5 and Ad35 vectors in SKOV-3 cells in the presence of NAPc2.

SKOV-3 cells were exposed to adenoviral vectors at a concentration of 1000 VP/cell in the presence and absence of physiological levels of FX and 0.01 – 10 μg/ml NAPc2 for 3 hours at 37ºC. Cells were washed and maintained at 37°C for a further 72 hours before quantification of transgene expression by luciferase assay, normalised to total protein content determined by BCA assay. Error bars represent SEM (* $p < 0.05$ versus absence of FX, # $p < 0.01$ versus presence of FX).

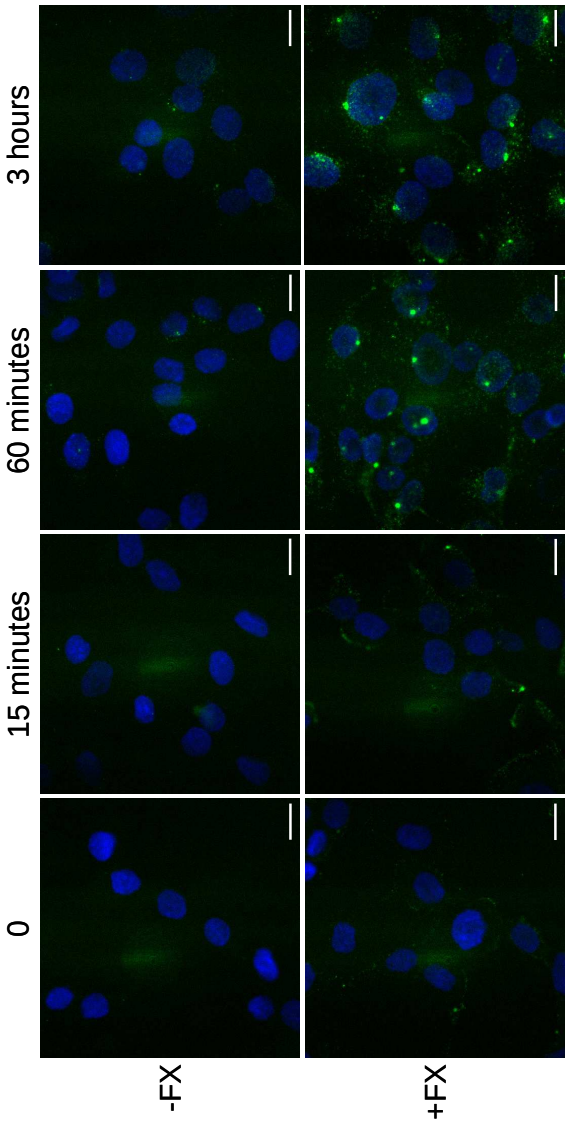

Figure 4.18 – Cell trafficking in SKOV-3 cells by Ad5.

Vectors were labelled with Alexa Fluor® 488 and the nuclei of SKOV-3 cells were counterstained with DAPI. SKOV-3 cells were exposed to 10000 VP/cell of labelled Ad5. Binding was allowed to occur for 1 hour at 4°C and cells were fixed either immediately or after incubation for 15 minutes, 1 hour or 3 hours at 37°C to allow vector internalisation in the absence or presence of FX. After 1 hour at 37°C, Ad5 had reached the nucleus of the cell. After 3 hours at 37°C, there was a higher concentration of Ad5 in the perinuclear space (co-localisation with DAPI). This possibly indicates localisation of Ad5 with the microtubule organising centre. Scale bar = 20 μm.

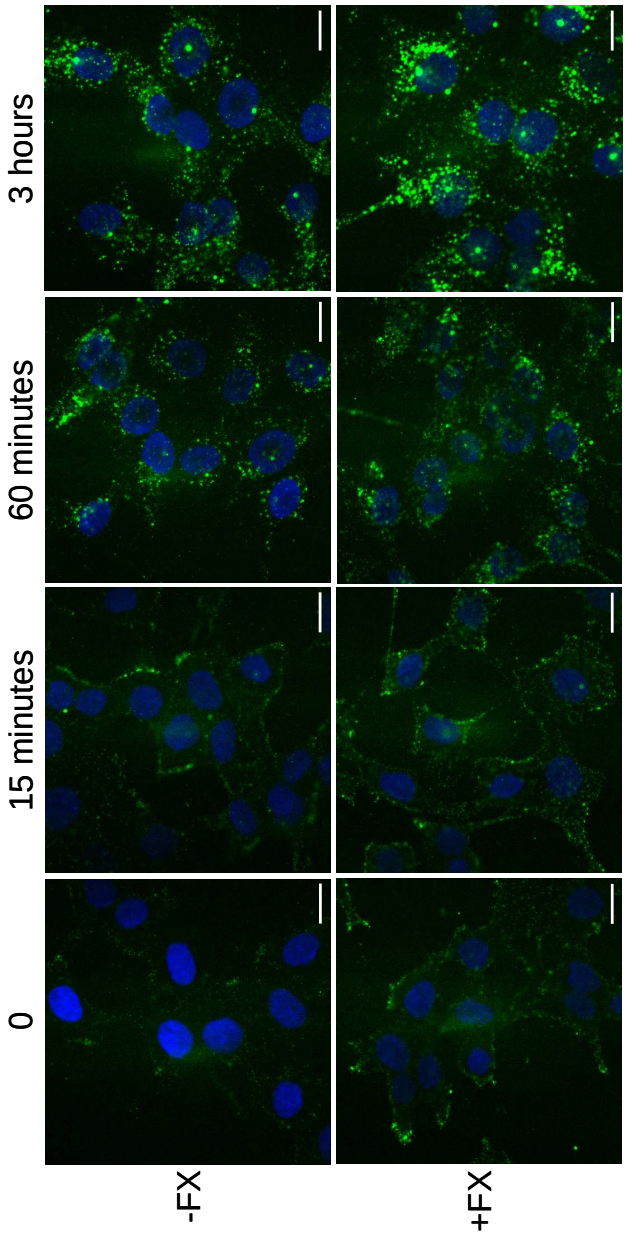

Figure 4.19 – Cell trafficking in SKOV-3 cells by Ad5/f35.

Vectors were labelled with Alexa Fluor® 488 and the nuclei of SKOV-3 cells were counterstained with DAPI. SKOV-3 cells were exposed to 10000 VP/cell of labelled Ad5/f35. Binding was allowed to occur for 1 hour at 4°C and cells were fixed either immediately or after incubation for 15 minutes, 1 hour or 3 hours at 37°C to allow vector internalisation in the absence or presence of FX. After 3 hours at 37°C, Ad5/f35 remained in the cytosol of the cells, indicating inefficient trafficking by this vector. Scale bar = 20 μm.

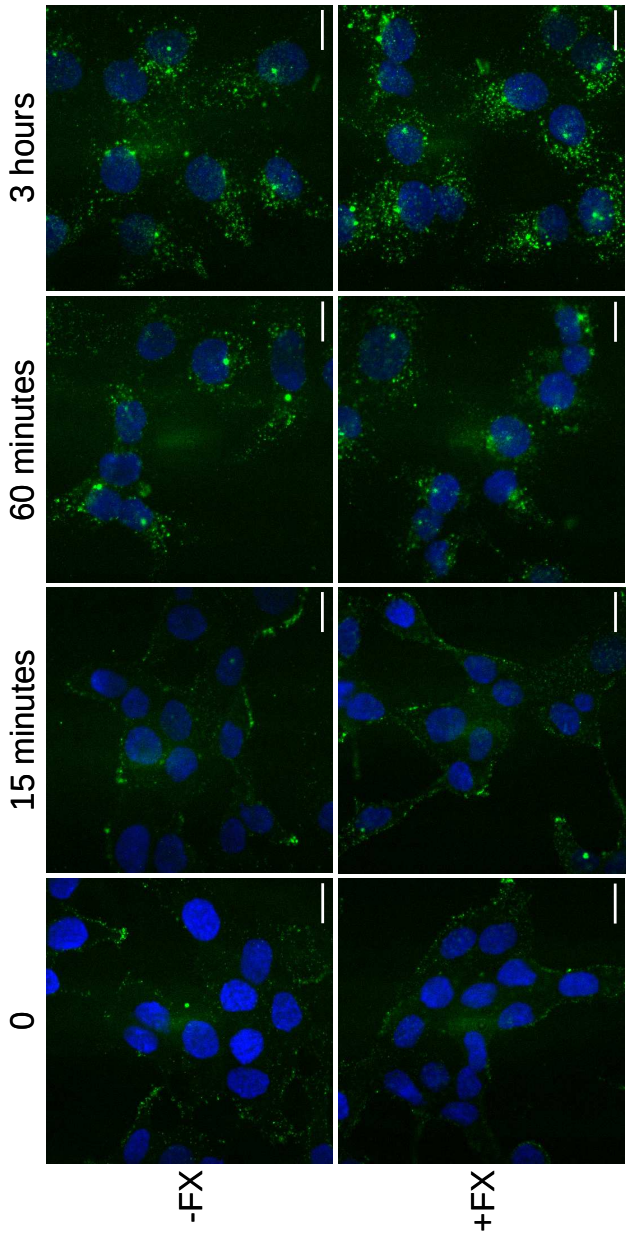

Figure 4.20 – Cell trafficking in SKOV-3 cells by Ad5/p35/f35.

Vectors were labelled with Alexa Fluor® 488 and the nuclei of SKOV-3 cells were counterstained with DAPI. SKOV-3 cells were exposed to 10000 VP/cell of labelled Ad5/p35/f35. Binding was allowed to occur for 1 hour at 4°C and cells were fixed either immediately or after incubation for 15 minutes, 1 hour or 3 hours at 37°C to allow vector internalisation in the absence or presence of FX. After 3 hours at 37°C, Ad5/p35/f35 remained in the cytosol of the cells, indicating inefficient trafficking by this vector. Scale bar = 20 μm.

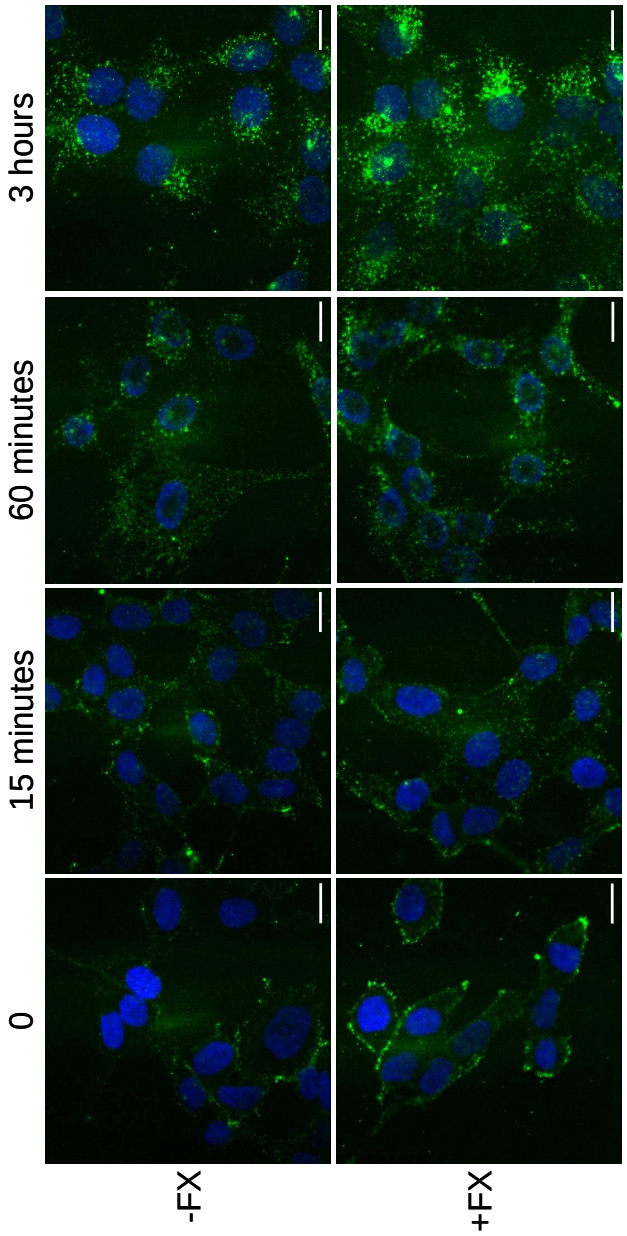

Figure 4.21 – Cell trafficking in SKOV-3 cells by Ad35.

Vectors were labelled with Alexa Fluor® 488 and the nuclei of SKOV-3 cells were counterstained with DAPI. SKOV-3 cells were exposed to 10000 VP/cell of labelled Ad35. Binding was allowed to occur for 1 hour at 4°C and cells were fixed either immediately or after incubation for 15 minutes, 1 hour or 3 hours at 37°C to allow vector internalisation in the absence or presence of FX. After 3 hours at 37°C, Ad35 remained in the cytosol of the cells, indicating inefficient trafficking by this vector. Scale bar = 20 μm.

4.2.11 In vivo *study with Ad5, Ad35 and chimeric Ad5/Ad35 vectors*

To assess the influence of FX interactions *in vivo*, CD46 transgenic mice were used. In rodents, CD46 expression is restricted to the testes, whereas CD46 is present on every nucleated cell in humans (Inoue *et al.*, 2003). Therefore, it was more appropriate for this study to produce an animal model with a similar CD46 expression profile as that in humans. The CD46 transgenic mice were generated by back-crossing an established CD46 transgenic line (Oldstone *et al.*, 1999) onto white MF1 mice to allow better bioluminescence images to be produced and these were used for all *in vivo* experiments. White MF1 non-transgenic mice were also used as a control.

Mice were injected intravenously with $5x10^{10}$ VP/mouse in the absence or presence of a pre-injection of X-bp 30 minutes beforehand. Luciferase transgene expression was visualised by whole-body bioluminescence imaging 48 hours after administration (Figure 4.22). Tissues were harvested 72 hours post-administration of the vectors and homogenates produced for quantification of luciferase transgene expression by luciferase assay normalised to total protein content. DNA was also extracted from tissue homogenates and vector genomes (VG) were quantified by qPCR.

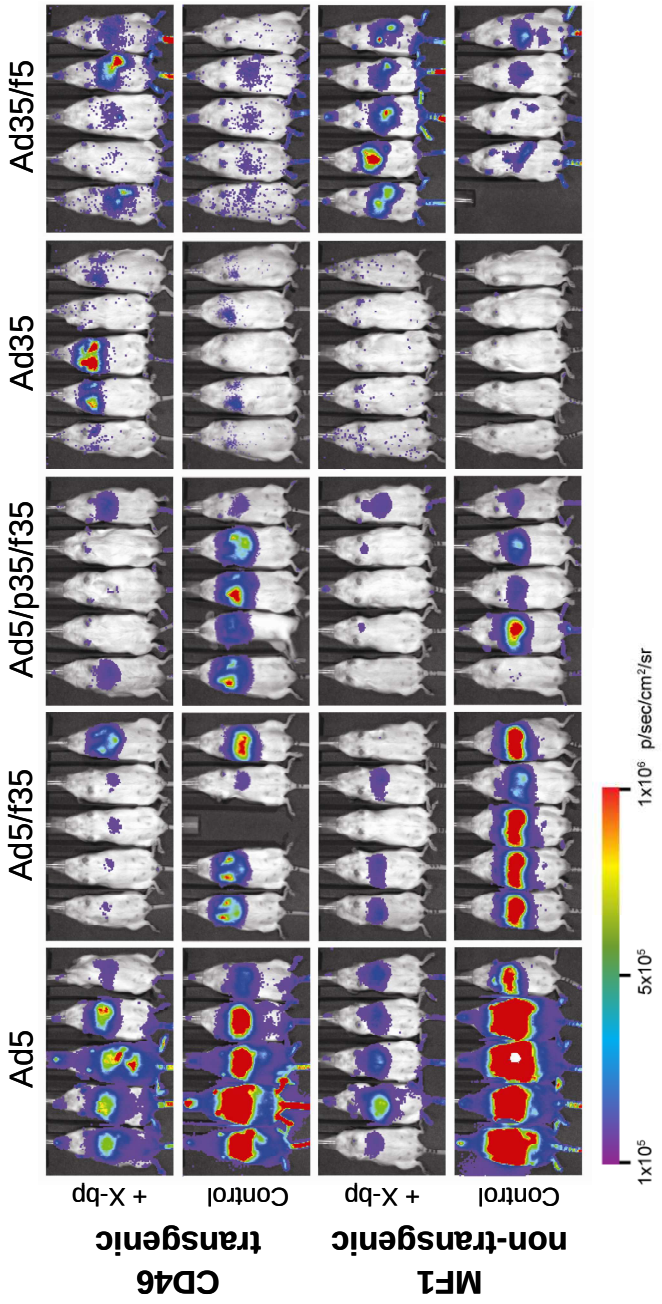

Figure 4.22 – Effect of FX on *in vivo* transduction by Ad5, Ad35 and chimeric Ad5/Ad35 vectors in CD46 transgenic and non-transgenic MF1 mice.

Luciferase expression visualised by whole-body bioluminescence imaging 48 hours after systemic administration of $5x10^{10}$ VP/mouse into CD46 transgenic or non-transgenic MF1 mice in the presence or absence of a pre-injection of FX binding protein X-bp, 30 minutes before administration of the vector.

4.2.12 Liver vector accumulation and transduction by Ad5, Ad35 and chimeric Ad5/Ad35 vectors in MF1 mice

Vector genome accumulation in liver homogenate samples from MF1 mice was determined by qPCR (Figure 4.23A). Ad5 selectively targeted the liver as expected and Ad5 vector accumulation was significantly inhibited by 9.3-fold in the presence of X-bp (Figure 4.23A). Liver accumulation by all other vectors was substantially lower than that for Ad5 and the presence of X-bp significantly further reduced liver vector accumulation by Ad5/p35/f35, Ad35 and Ad35/f5 (Figure 4.23A). This suggests that FX binding to both Ad5 and Ad35 hexons mediates liver accumulation and that this can be, at least partially, reduced by inhibition of the virus:FX interaction by X-bp. Additionally, it further reinforces the relative inefficiency of the CAR-dependent pathway for liver vector accumulation *in vivo* as vectors with the Ad5 fiber (Ad5 and Ad35/f5) produced low levels of transduction in the absence of FX. However, the presence of X-bp enhanced liver vector accumulation by Ad5/f35 by 1.6-fold (Figure 4.23A).

Luciferase assays were also performed to determine the level of liver transduction by each vector and to quantify the data obtained from the bioluminescent imaging (Figure 4.22, 4.23B). Liver transduction by Ad5 was substantially decreased by 89.1-fold after pre-injection of X-bp (Figure 4.23B). Levels of transgene expression by the other vectors in the liver were not sufficient to be quantified by luciferase expression assay (Figure 4.23B).

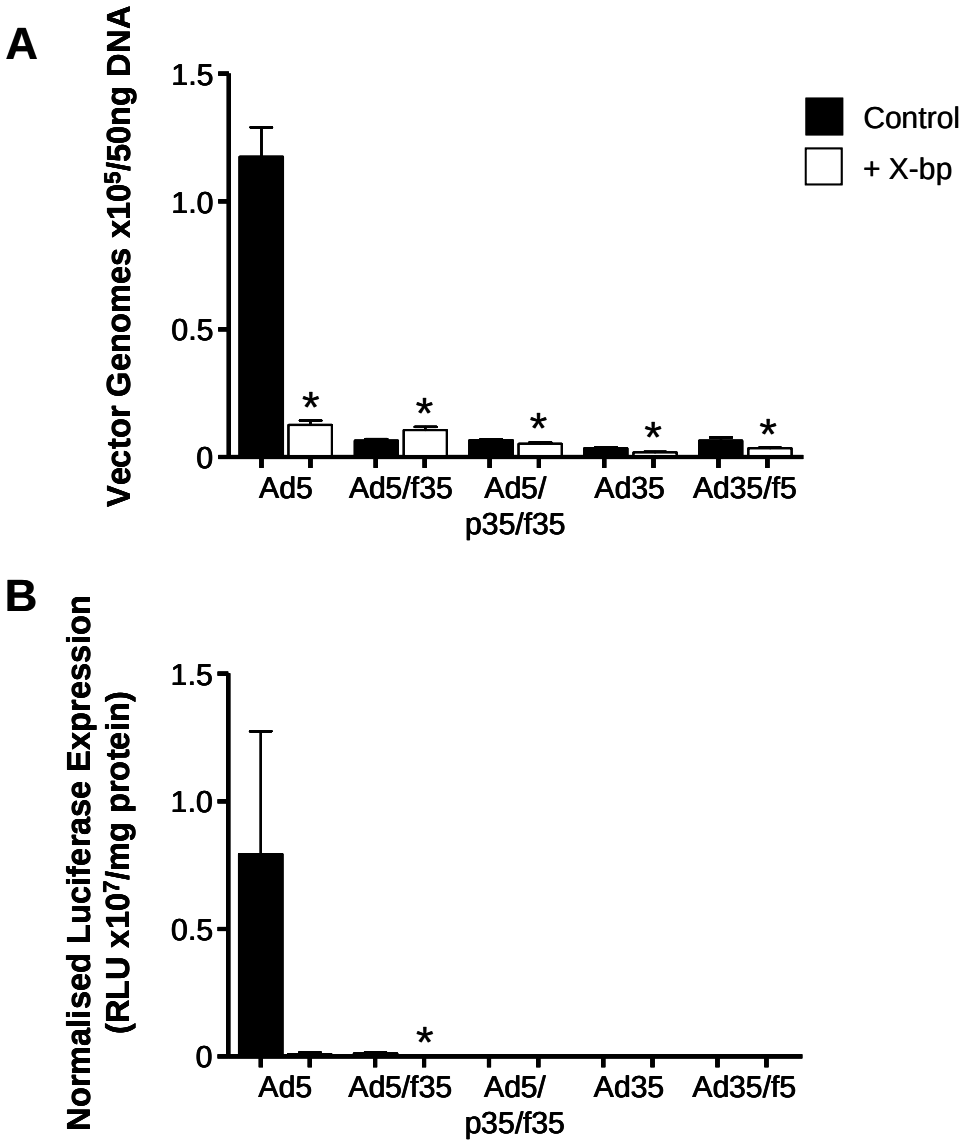

Figure 4.23 – Liver vector accumulation and transduction by Ad5, Ad35 and chimeric Ad5/Ad35 vectors in MF1 mice.

(A) Viral and total genomic DNA was extracted from liver samples taken 72 hours post-administration of vectors in the presence or absence of X-bp pre-injection 30 minutes before administration of each vector. Vector genome accumulation was quantified by qPCR. (B) Luciferase expression was quantified at 72 hours post-infection and normalised to total protein content determined by BCA assay. Error bars represent SEM (* $p < 0.05$, versus control).

4.2.13 Spleen vector accumulation and transduction by Ad5, Ad35 and chimeric Ad5/Ad35 vectors in MF1 mice

A similar level of vector genome accumulation was detected in the liver and spleen of the MF1 mice (Figures 4.23A, 4.24A). Increased vector accumulation was detected in the spleen for vectors with the Ad5 fiber, Ad5 and Ad35/f5, compared to vectors with the Ad35 fiber (Figure 4.24A). Additionally, vector accumulation by Ad5 and Ad35/f5 was not effected by the presence of X-bp (Figure 4.24A). This suggests that although the interaction with neither HSPGs (in the presence of FX) nor CAR (in the presence of X-bp) was responsible for accumulation of these vectors in the spleen, the increased accumulation by Ad5 and Ad35/f5 was fiber-dependent. Pre-administration of X-bp significantly enhanced vector accumulation by Ad5/p35/f35 by 4.4-fold but collectively the level of vector accumulation by vectors with the Ad35 fiber in the spleen was low (Figure 4.24A).

Transduction by Ad5 in the spleen was low in comparison to transduction by this vector in the liver (Figures 4.23B, 4.24B) and was substantially reduced in the presence of X-bp (Figure 4.24B). The levels of transgene expression by the other vectors in the spleen were not sufficient for quantification (Figure 4.24B).

4.2.14 Heart vector accumulation and transduction by Ad5, Ad35 and chimeric Ad5/Ad35 vectors in MF1 mice

Vector genome accumulation in the heart was low in MF1 mice, less than $2x10^4$ VG/50 ng DNA (Figure 4.25A). Accumulation by Ad5 in the heart was significantly reduced in the presence of X-bp by 3.6-fold (Figure 4.25A), indicating that heart transduction may be FX mediated. In contrast, pre-administration of X-bp significantly enhanced vector accumulation by Ad5/f35 and Ad35/f5 by 6.6- and 1.9-fold, respectively (Figure 4.25A). Ad5 produced the highest level of cardiac transduction in the MF1 mice (Figure 4.25B). Transduction of the heart by the other vectors was low and X-bp had no effect on transduction of the heart by any of the vectors (Figure 4.25B).

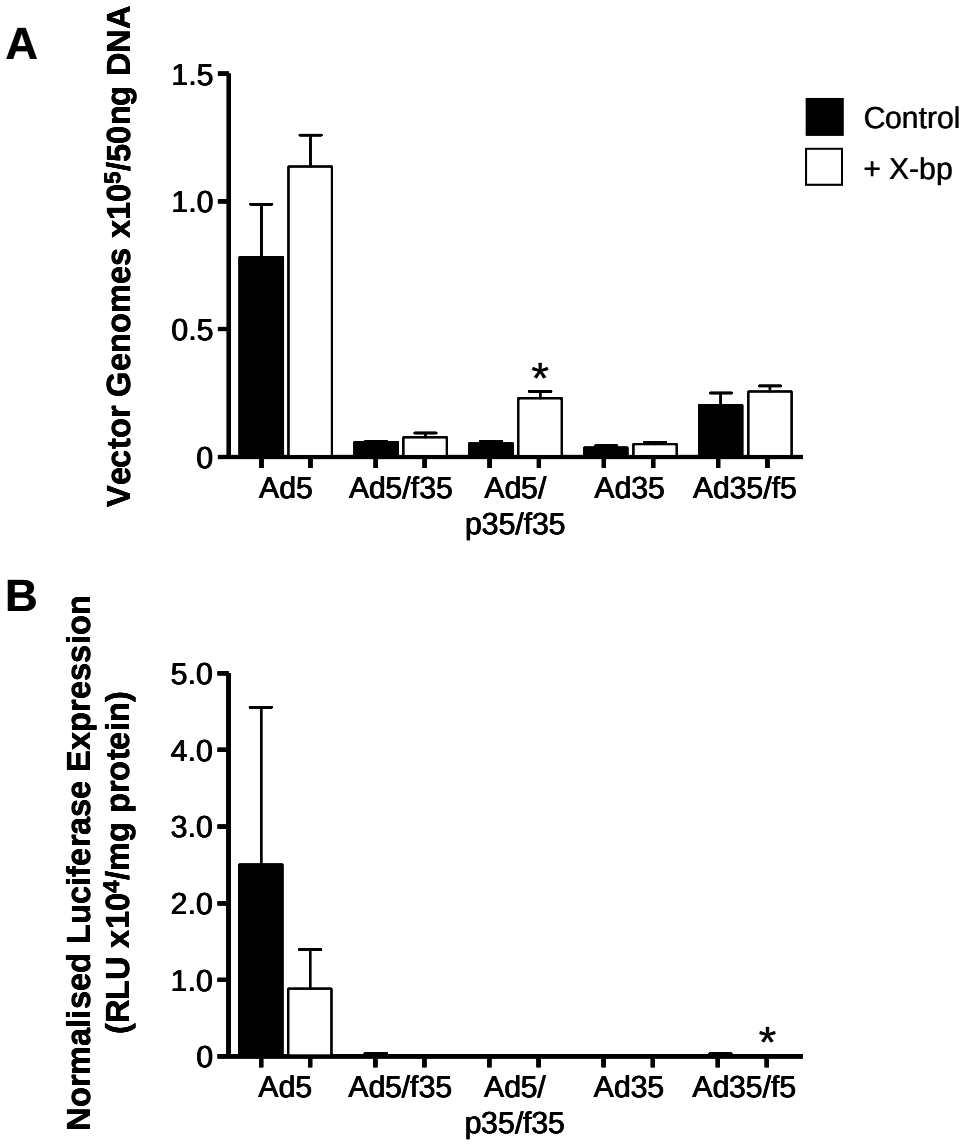

Figure 4.24 – Spleen vector accumulation and transduction by Ad5, Ad35 and chimeric Ad5/Ad35 vectors in MF1 mice.

(A) Viral and total genomic DNA was extracted from spleen samples taken 72 hours post-administration of vectors in the presence or absence of X-bp pre-injection 30 minutes before administration of each vector. Vector genome accumulation was quantified by qPCR. (B) Luciferase expression was quantified at 72 hours post-infection and normalised to total protein content determined by BCA assay. Error bars represent SEM (* $p < 0.05$, versus control).

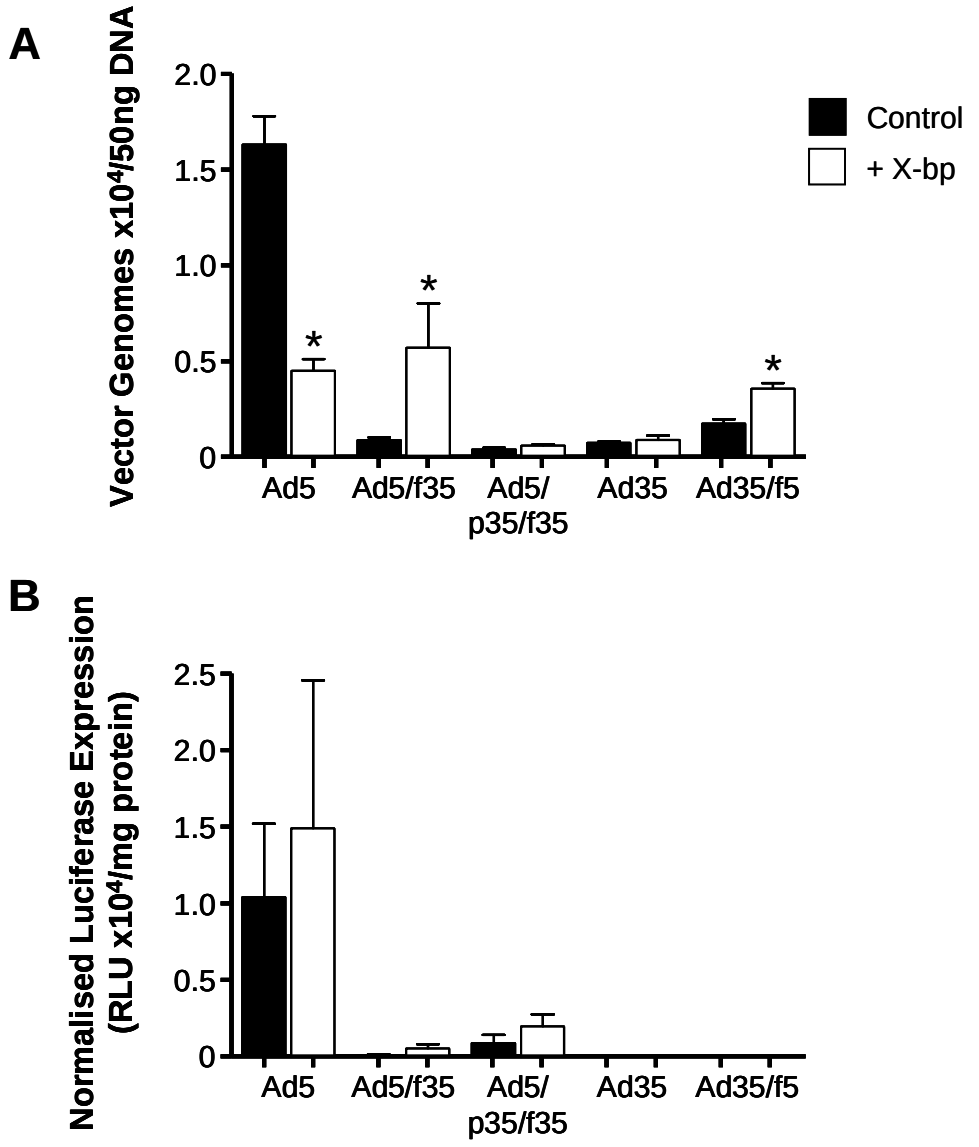

Figure 4.25 – Heart vector accumulation and transduction by Ad5, Ad35 and chimeric Ad5/Ad35 vectors in MF1 mice.

(A) Viral and total genomic DNA was extracted from heart samples taken 72 hours post-administration of vectors in the presence or absence of X-bp pre-injection 30 minutes before administration of each vector. Vector genome accumulation was quantified by qPCR. (B) Luciferase expression was quantified at 72 hours post-infection and normalised to total protein content determined by BCA assay. Error bars represent SEM (* $p < 0.05$, versus control).

4.2.15 Lung vector accumulation and transduction by Ad5, Ad35 and chimeric Ad5/Ad35 vectors in MF1 mice

Low levels of vector genome accumulation (less than $3x10^4$ VG/50 ng DNA) were present in the lungs of MF1 mice (Figure 4.26A). Ad5 vector accumulation was significantly reduced in the presence of X-bp (Figure 4.26A). However, in the presence of X-bp, vector accumulation by Ad5/f35, Ad5/p35/f35 and Ad35/f5 was significantly enhanced by 3.5-, 3.1- and 2.3-fold, respectively (Figure 4.26A). The level of lung transduction in the MF1 mice was also low (Figure 4.26B). The addition of X-bp substantially reduced transduction by Ad5 and had no effect on transduction by the other vectors (Figure 4.26B), confirming that lung transduction in MF1 mice by Ad5 was dependent on FX.

4.2.16 Liver vector accumulation and transduction by Ad5, Ad35 and chimeric Ad5/Ad35 vectors in CD46 transgenic mice

The liver vector accumulation and transduction by each of the vectors in CD46 transgenic mice demonstrated a very similar pattern to that observed in the MF1 mice (Figures 4.23, 4.27). Ad5 selectively targeted to the liver as expected in the CD46 transgenic mice, an effect that was significantly inhibited in the presence of X-bp by 5.6-fold (Figure 4.27A). Liver accumulation by all other vectors was substantially lower than that for Ad5 and X-bp significantly further reduced the liver vector accumulation by Ad5/f35, Ad5/p35/f35, Ad35 and Ad35/f5 by 2.3-, 4.3-, 1.6- and 1.4-fold, respectively (Figure 4.27A). This suggests that FX binding to both Ad5 and Ad35 hexon mediates liver accumulation in the CD46 transgenic mice as well as in MF1 mice and that accumulation can be, at least partially, reduced by inhibition of the virus:FX interaction by X-bp.

Liver transduction by Ad5 was substantially decreased after pre-injection of X-bp by 17.1-fold but the levels of transgene expression by the other vectors in the liver were not sufficient to be quantified by luciferase expression assay (Figure 4.27B).

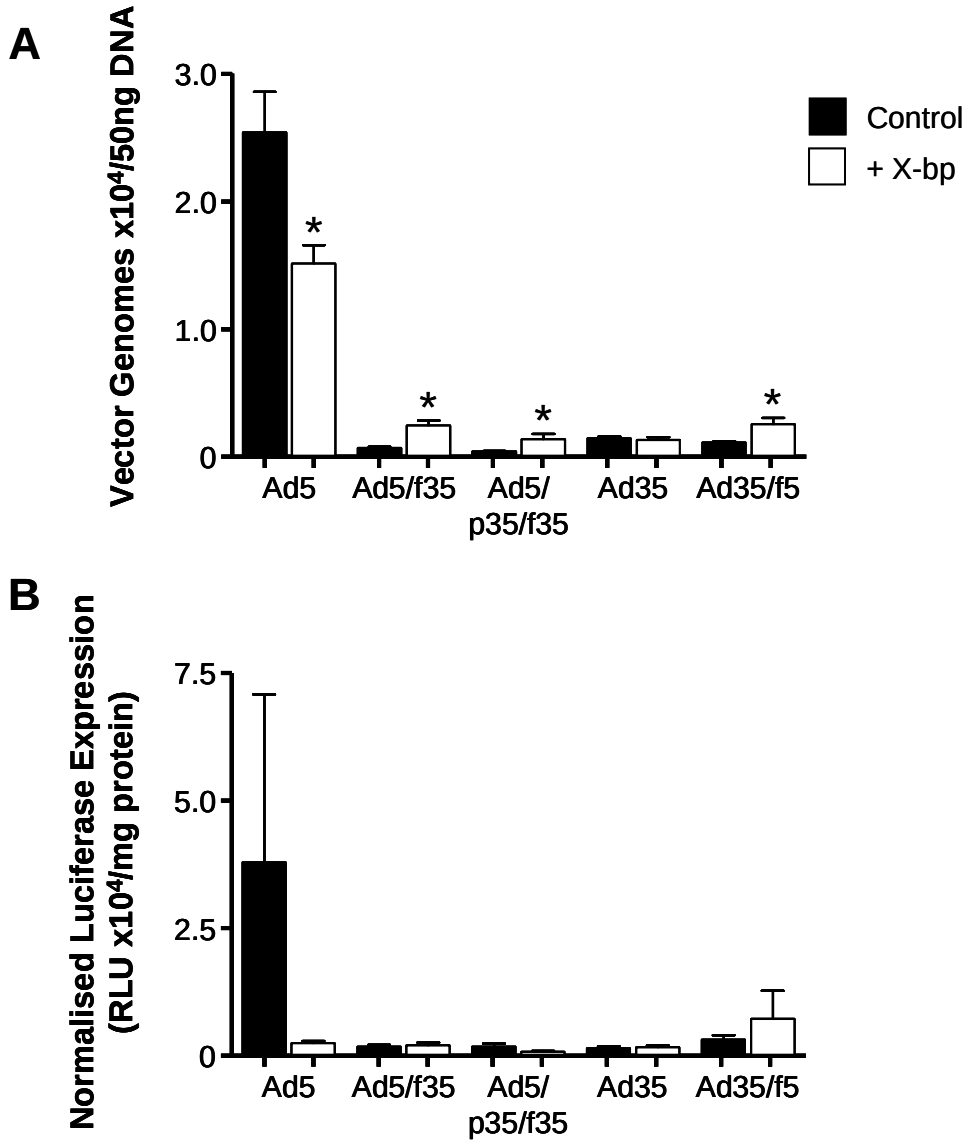

Figure 4.26 – Lung vector accumulation and transduction by Ad5, Ad35 and chimeric Ad5/Ad35 vectors in MF1 mice.

(A) Viral and total genomic DNA was extracted from lung samples taken 72 hours post-administration of vectors in the presence or absence of X-bp pre-injection 30 minutes before administration of each vector. Vector genome accumulation was quantified by qPCR. (B) Luciferase expression was quantified at 72 hours post-infection and normalised to total protein content determined by BCA assay. Error bars represent SEM (* $p < 0.05$, versus control).

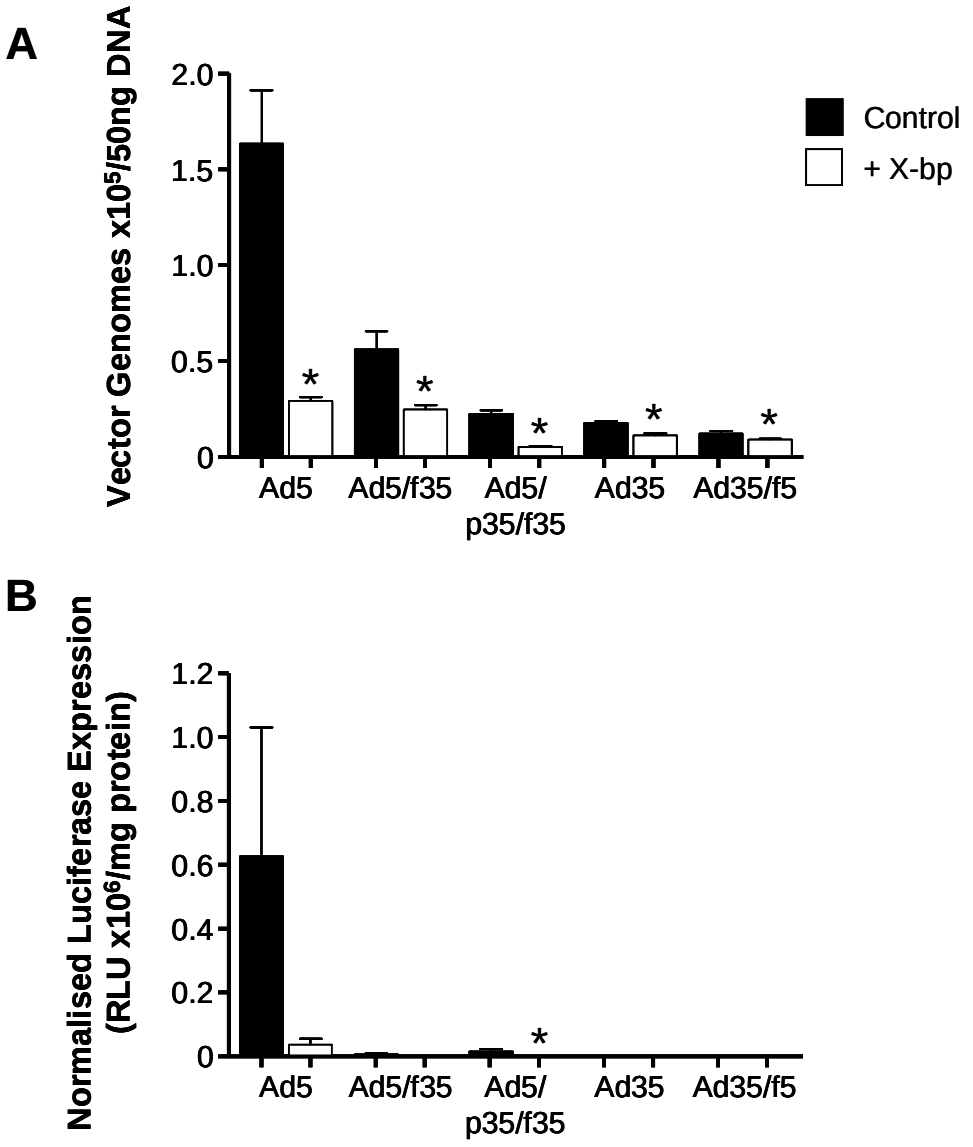

Figure 4.27 – Liver vector accumulation and transduction by Ad5, Ad35 and chimeric Ad5/Ad35 vectors in CD46 transgenic mice.

(A) Viral and total genomic DNA was extracted from liver samples taken 72 hours post-administration of vectors in the presence or absence of X-bp pre-injection 30 minutes before administration of each vector. Vector genome accumulation was quantified by qPCR. (B) Luciferase expression was quantified at 72 hours post-infection and normalised to total protein content determined by BCA assay. Error bars represent SEM (* $p < 0.05$, versus control).

4.2.17 Spleen vector accumulation and transduction by Ad5, Ad35 and chimeric Ad5/Ad35 vectors in CD46 transgenic mice

Vector genomes were detected in the spleen of the CD46 transgenic mice at a similar level to vector accumulation in the liver (Figures 4.27A, 4.28A). The vector accumulation in the spleen was higher for vectors with the Ad5 hexon, compared to vectors with the Ad35 hexon (Figure 4.28A). This suggests that vector accumulation in the spleen was enhanced by the presence of the Ad5 hexon. Only accumulation by Ad5/f35 was significantly decreased in the presence of X-bp (Figure 4.28A). However, the reduced level of Ad5/f35 vector genomes detected in the spleen in the presence of X-bp remained greater than Ad35 and Ad35/f5 vector accumulation levels (Figure 4.28A). This indicates that vector accumulation in the spleen was not dependent on FX and was more likely due to the innate action of splenic macrophages to clear the blood of pathogens.

However, in the presence of FX, Ad5 efficiently transduced the cells of the spleen, an effect completely abolished in the presence of X-bp (Figure 4.28B), thus suggesting that FX mediates transduction in the spleen by Ad5. Transduction by Ad5/f35, Ad5/p35/f35, Ad35 and Ad35/f5 in the spleen was very low (Figure 4.28B). The degree of transduction by the vectors did not correlate well with vector accumulation in the spleen (Figure 4.28), indicating the importance of the spleen to remove viruses from the circulation while preventing transduction of this organ.

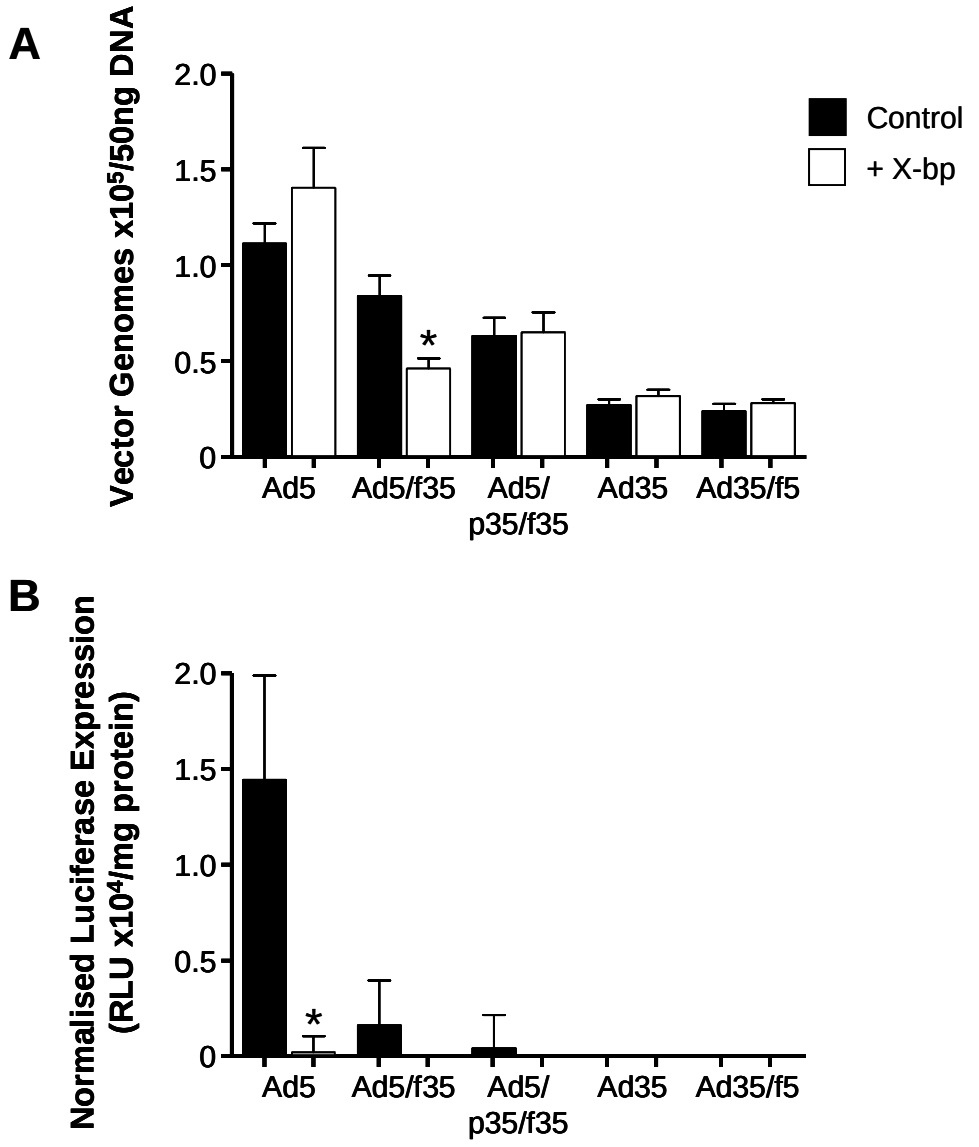

Figure 4.28 – Spleen vector accumulation and transduction by Ad5, Ad35 and chimeric Ad5/Ad35 vectors in CD46 transgenic mice.

(A) Viral and total genomic DNA was extracted from spleen samples taken 72 hours post-administration of vectors in the presence or absence of X-bp pre-injection 30 minutes before administration of each vector. Vector genome accumulation was quantified by qPCR. (B) Luciferase expression was quantified at 72 hours post-infection and normalised to total protein content determined by BCA assay. Error bars represent SEM (* $p < 0.05$, versus control).

4.2.18 Heart vector accumulation and transduction by Ad5, Ad35 and chimeric Ad5/Ad35 vectors in CD46 transgenic mice

Unexpectedly, vector genomes were detected in the heart at similar levels detected in the spleen at approximately $1x10^5$ VG/50 ng DNA (Figure 4.29A). Vector accumulation by Ad5 in the heart was modestly, yet significantly inhibited in the presence of X-bp (Figure 4.29A). However, transduction by Ad5 in the heart was significantly enhanced by 8.8-fold after the addition of X-bp (Figure 4.29B). This suggests that in CD46 transgenic mice, FX either effects transduction directly by blocking a native infective pathway for Ad5 in the heart or indirectly by reducing bioavailability of the vector.

Vector accumulation in the heart was higher for vectors with the Ad35 fiber, compared to vectors with the Ad5 fiber (Figure 4.29A). In the presence of X-bp, vector accumulation by Ad5/f35 and Ad5/p35/f35 was significantly reduced by 2.7- and 4.9-fold, respectively (Figure 4.29A). This suggests that the presence of FX enhances vector accumulation in the heart by these vectors. Pre-administration of X-bp significantly enhanced Ad35 vector accumulation by 2.3-fold in the heart (Figure 4.29), suggesting that in the absence of the FX interaction, Ad35 can efficiently utilise the interaction of the Ad35 fiber with CD46 for vector accumulation in the heart. However, Ad5/f35, Ad5/p35/f35, Ad35 and Ad35/f5 all produced extremely low levels of transduction in the heart (Figure 4.29B).

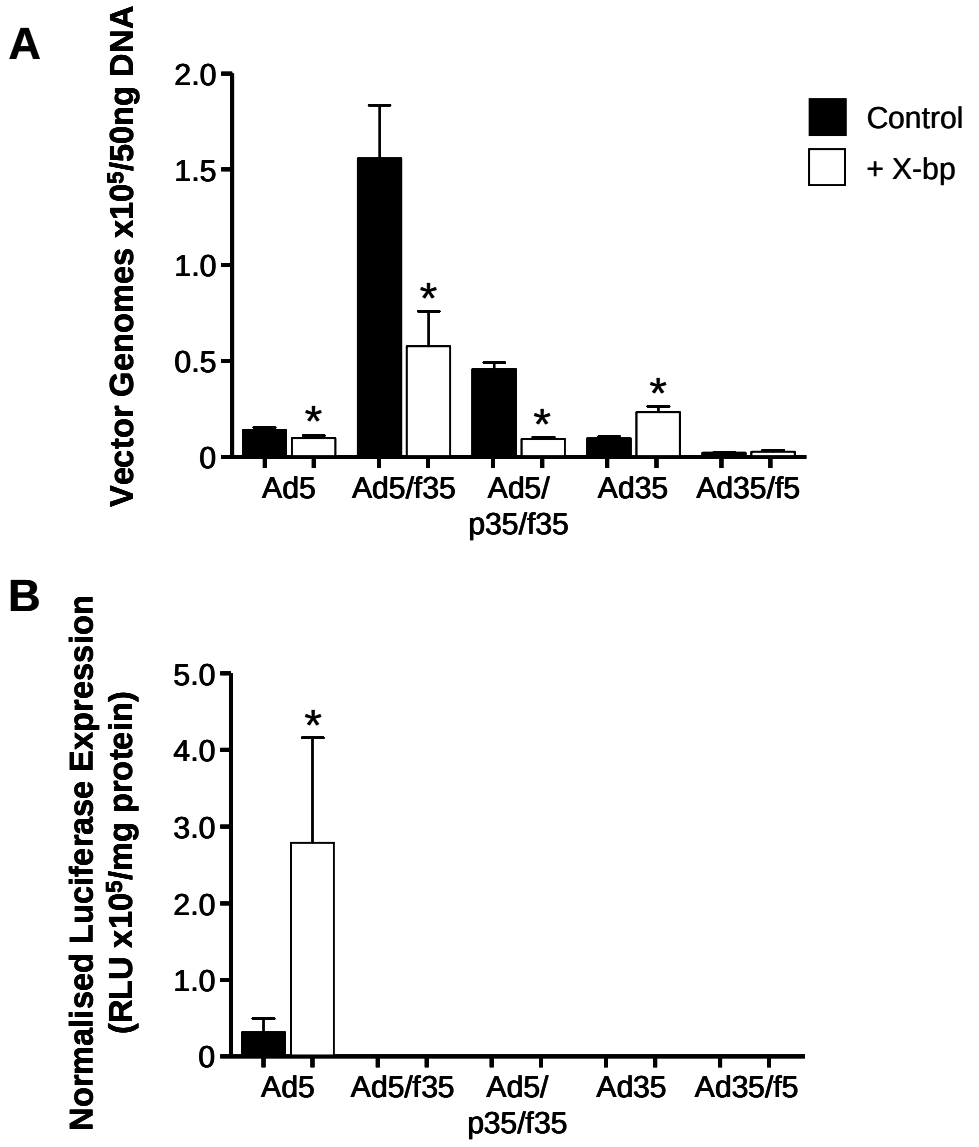

Figure 4.29 – Heart vector accumulation and transduction by Ad5, Ad35 and chimeric Ad5/Ad35 vectors in CD46 transgenic mice.

(A) Viral and total genomic DNA was extracted from heart samples taken 72 hours post-administration of vectors in the presence or absence of X-bp pre-injection 30 minutes before administration of each vector. Vector genome accumulation was quantified by qPCR. (B) Luciferase expression was quantified at 72 hours post-infection and normalised to total protein content determined by BCA assay. Error bars represent SEM (* $p < 0.05$, versus control).

4.2.19 Lung vector accumulation and transduction by Ad5, Ad35 and chimeric Ad5/Ad35 vectors in CD46 transgenic mice

It has previously been reported that vectors containing the Ad35 fiber possess the capacity to transduce the lungs of CD46 transgenic mice (Sakurai *et al.*, 2006a, Verhaagh *et al.*, 2006, Stone *et al.*, 2007a). *In vivo* bioluminescent imaging appeared to confirm this finding (Figure 4.22). Vectors with an Ad35 fiber, Ad5/f35 and Ad5/p35/f35, exhibited significantly higher levels of lung vector accumulation compared to Ad5 with $5.6x10^5$ and $5.7x10^5$ VG/50 ng of total DNA isolated in the absence of X-bp, respectively (Figure 4.30A). Pre-administration of X-bp significantly reduced genome accumulation in the lung by Ad5/f35 and Ad5/p35/f35 1.9- and 6.6-fold, respectively (Figure 4.30A). Lung transduction by Ad5/f35 and Ad5/p35/f35 exhibited the same pattern as vector genome accumulation in the lung, with high levels of transgene expression by these vectors being significantly reduced 51.9- and 5.9-fold in the presence of X-bp, respectively (Figure 4.30B). This suggests that FX enhances vector accumulation in the lung mediated by these vectors, potentially via additive effects of CD46:Ad35 fiber interactions and the high affinity Ad5 hexon:FX:HSPG interaction.

Lung accumulation for Ad35 was lower than Ad5/f35 and Ad5/p35/f35 and modestly, but significantly enhanced by X-bp (Figure 4.30A). Levels of transgene expression were modest yet detectable and selective for the lung in the presence of X-bp (Figure 4.22, 4.30B). This suggests that Ad35 was efficient at utilising CD46 for delivery *in vivo* and that targeting was most efficient and selective when FX binding to the Ad35 hexon was ablated by X-bp.

In the presence or absence of X-bp, Ad5 showed low level vector accumulation in the lung (Figure 4.30A) and no luciferase transgene expression (Figure 4.30B). Similarly, Ad35/f5, which also possesses the Ad5 fiber showed negligible vector accumulation in the lung (Figure 4.30A). However, transgene expression by Ad35/f5 was substantially enhanced in the presence of X-bp, in the same manner as transduction by Ad35 (Figure 4.30B).

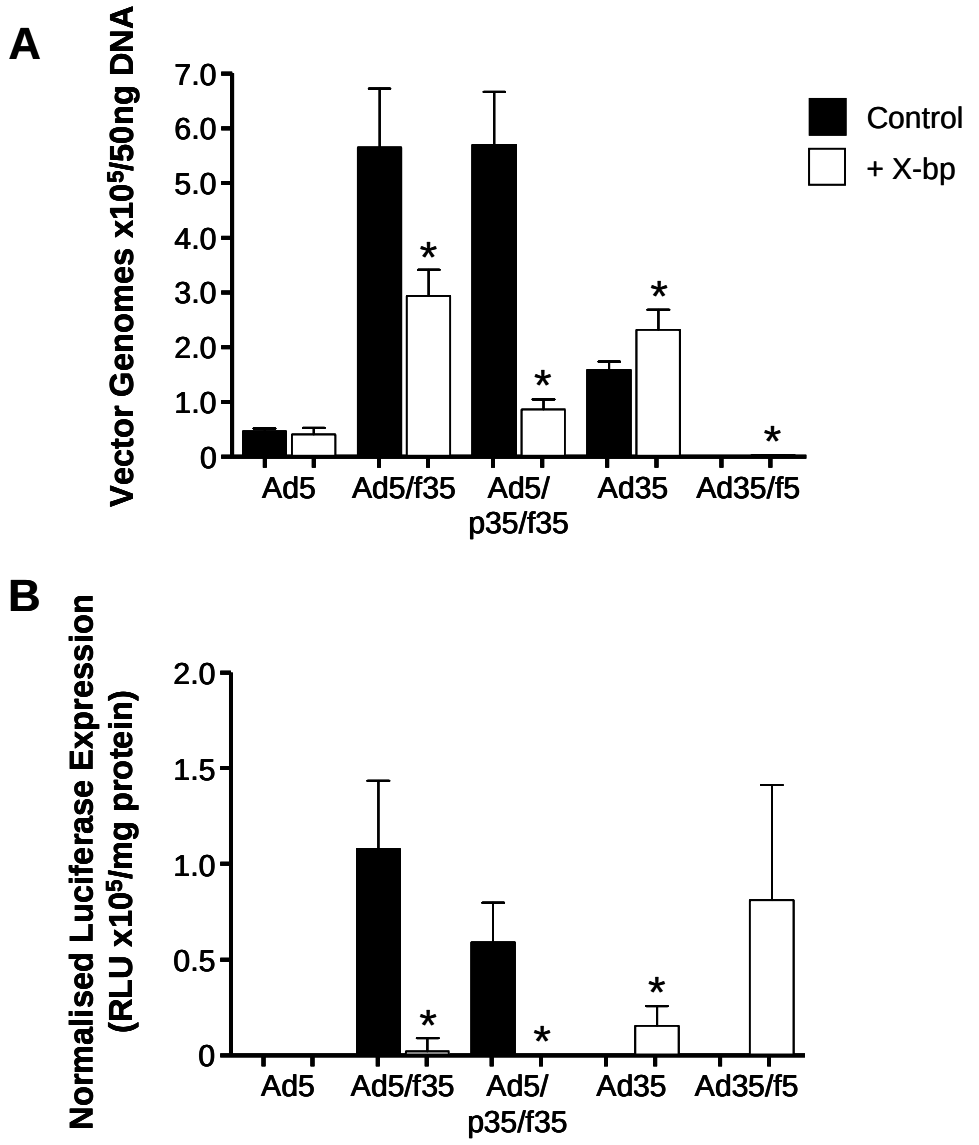

Figure 4.30 – Lung vector accumulation and transduction by Ad5, Ad35 and chimeric Ad5/Ad35 vectors in CD46 transgenic mice.

(A) Viral and total genomic DNA was extracted from lung samples taken 72 hours post-administration of vectors in the presence or absence of X-bp pre-injection 30 minutes before administration of each vector. Vector genome accumulation was quantified by qPCR. (B) Luciferase expression was quantified at 72 hours post-infection and normalised to total protein content determined by BCA assay. Error bars represent SEM (* $p < 0.05$, versus control).

4.2.20 Effect of FX on retargeting of Ad5, Ad35 and chimeric Ad5/Ad35 vectors in CD46 transgenic mice

The lung:liver ratio of vector genome accumulation for each of the vectors in the CD46 transgenic mice was calculated to determine the degree of retargeting which occurred in the presence of X-bp (Figure 4.31). The lung:liver ratio produced by Ad5/f35 was the same in the presence and absence of X-bp (Figure 4.31), indicating that the addition of X-bp had no effect on retargeting Ad5/f35. Although the levels of vector accumulation in both the liver and lung were significantly reduced in the presence of X-bp (Figures 4.27, 4.30), the ratio of vector genomes present in these organs remains the same (Figure 4.31). In contrast, Ad5/p35/f35 had a reduced lung:liver ratio in the presence of X-bp (Figure 4.31). This suggests some level of retargeting away from the lung through the interaction of the Ad5 hexon with FX. Importantly, Ad35 had an increased lung:liver ratio in the presence of X-bp (Figure 4.31), indicating retargeting of this vector to the lung after the addition of X-bp. The vectors possessing an Ad5 fiber (Ad5 and Ad35/f5) both had a very low lung:liver ratio, further emphasising the degree of liver targeting possessed by these vectors (Figure 4.31).

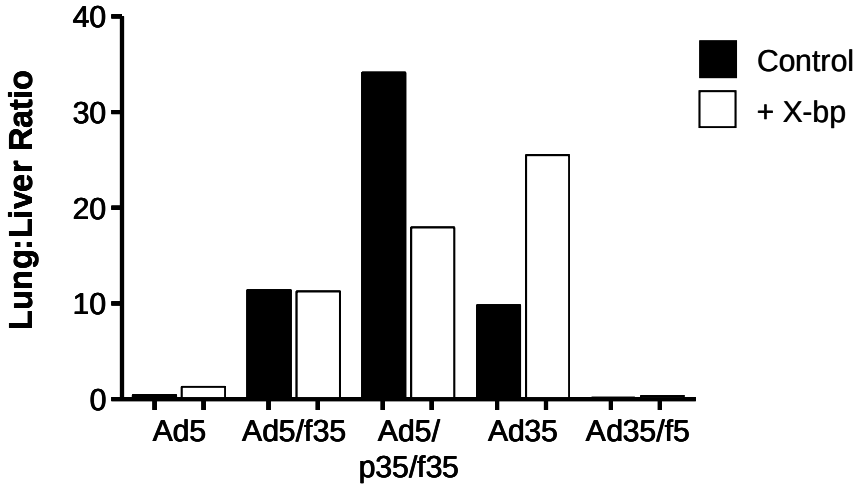

Figure 4.31 – Lung:liver ratio of vector genome accumulation in CD46 transgenic mice.

The lung:liver ratio of vector genome accumulation/50 ng DNA was calculated to determine the degree of retargeting by the vectors in CD46 transgenic mice after the addition of X-bp.

4.2.21 Immunohistochemical analysis of transduction by Ad5, Ad5/f35 and Ad35 in CD46 transgenic mice

To further investigate the selectivity of lung transduction by vectors possessing the Ad35 fiber in CD46 transgenic mice, the *in vivo* experiments were repeated with Ad5, Ad5/f35 and Ad35 vectors which expressed an enhanced green fluorescent protein (eGFP) transgene. Mice were again injected intravenously with $5x10^{10}$ VP/mouse in the absence or presence of a pre-injection of X-bp 30 minutes beforehand. Tissues were harvested 72 hours post-administration of the vectors. Sections were analysed for native eGFP expression and by immunohistochemistry (IHC) using an anti-GFP antibody and images were taken by confocal microscopy.

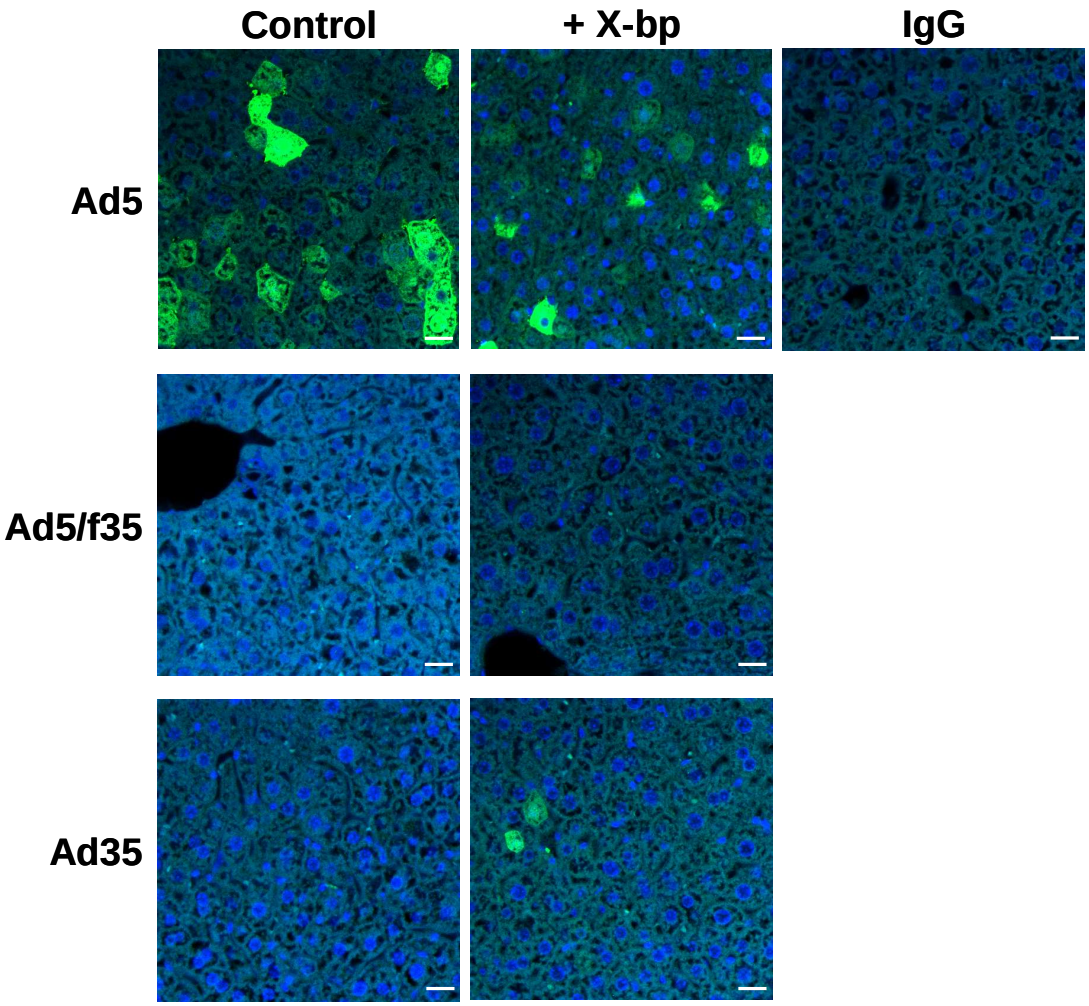

Figure 4.32 – Immunohistochemistical analysis of liver transduction by Ad5, Ad5/f35 and Ad35 in CD46 transgenic mice.

Anti-GFP antibody localisation and native eGFP expression on sections of liver tissue from CD46 transgenic mice injected with eGFP expressing Ad5, Ad5/f35 and Ad35 vectors. Scale bar = 20 μm.

IHC on liver sections taken from CD46 transgenic mice administered with Ad5, Ad5/f35 and Ad35 demonstrated very similar results to the relative levels of vector genome accumulation and transduction by the vectors, as seen by qPCR and luciferase assay, respectively (Figures 4.27, 4.32). Liver sections from animals injected with Ad5.eGFP showed high levels of native eGFP expression and anti-GFP staining (detected with an Alexa Fluor® 488 (green) secondary antibody) with individual hepatocytes depicted due to very high levels of transgene expression (Figure 4.32). The staining was reduced in the presence of X-bp (Figure 4.32). Very few hepatocytes showed eGFP transgene expression in animals administered with Ad5/f35 and Ad35 (Figure 4.32), similar to the low levels of vector genome accumulation and luciferase expression by these vectors (Figure 4.27).

Due to the very high levels of lung accumulation and transduction by the Ad5/f35 and Ad35 vectors, IHC was also performed on lung sections to investigate which cells were transduced by the vectors. By examination of a whole lung taken from a CD46 transgenic mouse administered with Ad35.eGFP, it was observed that the majority of eGFP expression was in the outer surface of the lung (Figure 4.33A). When the lung was cross-sectioned, eGFP expression was around the periphery of the lung with no expression seen in the large airways (Figure 4.33B). IHC on lung sections produced a level of green staining (due to a combination of native eGFP expression and the anti-GFP antibody) relative to the levels of lung vector accumulation and transduction for each of the vectors (Figures 4.30, 4.34). Ad5/f35 transduction was significantly inhibited in the presence of X-bp (Figure 4.34), as previously determined by vector genome accumulation and transgene expression quantification (Figure 4.30).

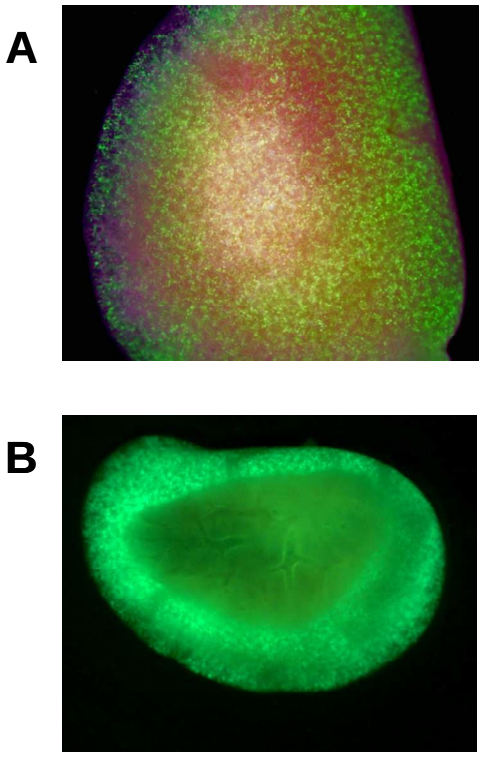

Figure 4.33 – Fluorescent imaging of lung transduction by Ad35 in CD46 transgenic mice.

(A) eGFP expression on outer surface of the lung and (B) cross-section of lung taken from a CD46 transgenic mouse injected with an Ad35 vector containing the eGFP transgene.

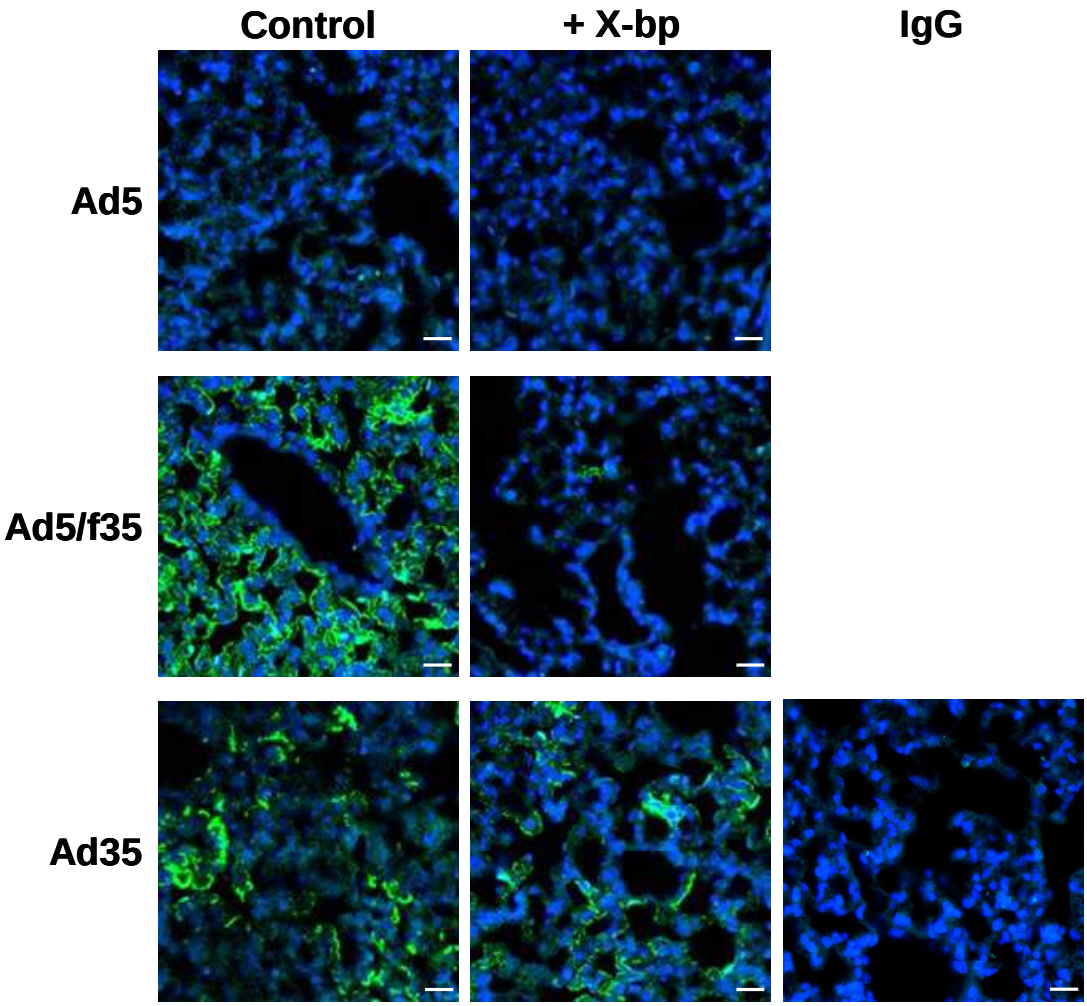

Figure 4.34 – Immunohistochemistical analysis of lung transduction by Ad5, Ad5/f35 and Ad35 in CD46 transgenic mice.

Anti-GFP antibody localisation and native eGFP expression on sections of lung tissue from CD46 transgenic mice injected with Ad5, Ad5/f35 and Ad35 vectors containing the eGFP transgene. Scale bar = 20 μm.

4.3 Discussion

This study has utilised Ad35 and chimeric Ad5/Ad35 vectors to determine the importance of the interaction of these vectors with FX. FX was shown to bind directly to the Ad35 hexon, in a similar manner to Ad5, by cryoEM and SPR. *In vitro*, the presence of FX does not further enhance binding to cells by vectors containing the Ad35 fiber. However, FX can enhance binding by vectors with an Ad5 fiber, independent of capsid. Ad35 internalisation in CHO-CD46 cells was enhanced by FX but FX significantly inhibited transduction by all vectors with the Ad35 fiber. In cells which did not express CD46, binding, internalisation and transduction by vectors containing the Ad35 fiber demonstrated a similar profile to vectors with the Ad5 fiber. The presence of FX significantly enhanced binding, internalisation and transduction by all vectors in CHO-WTR cells.

In control MF1 mice, vectors with either the Ad35 fiber or hexon proteins demonstrated significantly lower levels of liver and spleen vector accumulation and transduction compared to Ad5. In the presence of X-bp, vector accumulation in the heart and lungs by the chimeric vectors was significantly enhanced in MF1 mice. In CD46 transgenic mice, liver vector accumulation and transduction by Ad5/f35, Ad5/p35/f35, Ad35 and Ad35/f5 was significantly reduced compared to Ad5 and the presence of X-bp further significantly reduced accumulation in the liver. Accumulation of vector genomes in the spleen was detected at similar levels to accumulation in the liver of the CD46 transgenic mice but the levels of splenic transduction were very low for all vectors except Ad5. Vector genome accumulation in the heart and lungs of the CD46 transgenic mice exhibited a very similar profile but transduction in the lung was significantly increased. In the lung, vectors with the Ad35 fiber exhibited significantly higher levels of lung vector accumulation than Ad5. The presence of X-bp significantly reduced vector accumulation in the lung by Ad5/f35 and Ad5/p35/f35 but enhanced Ad35 lung accumulation. Calculation of the lung:liver ratio showed that in the presence of X-bp, Ad5/p35/f35 was retargeted away from the lung, whereas Ad35 was targeted to the lung.

Contrary to previous reports (Kalyuzhniy *et al.*, 2008) but consistent with our previous findings (Waddington *et al.*, 2008), this study has demonstrated that FX

binds directly to Ad35. Kalyuzhniy *et al*. used SPR to determine the affinity of the FX interaction with several human Ad serotypes and reported that Ad35 does not bind to FX (Kalyuzhniy *et al.*, 2008). However, SPR data presented here demonstrates that the Ad35:FX interaction fitted to a heterogenous ligand model with equilibrium dissociation constants of $5.4x10^{-8}$ M and $3.5x10^{-9}$ M, confirming that Ad35 binds to FX with approximately ten-fold lower affinity than the Ad5:FX interaction. The Ad35 hexon was also shown to bind FX in the context of the pseudotype vector Ad35/f5, as has been previously shown for Ad5 pseudotype vectors (Parker *et al.*, 2007). By cryoEM, it was observed as Ad5, binding was via the hexon protein with FX density in the centre of the trimeric hexon proteins. It remains to be determined which Ad35 HVRs and specific loops mediate this interaction in a similar manner to the reported interaction of FX with Ad5 HVRs 5 and 7 (Waddington *et al.*, 2008, Alba *et al.*, 2009) as the crystal structure of Ad35 has not yet been resolved.

Although FX was shown to bind to the Ad35 hexon, FX had no effect on binding by Ad35 to CHO-CD46 cells *in vitro*. The presence of FX had no effect on any of the vectors containing the Ad35 fiber (Ad5/f35, Ad5/p35/f35 and Ad35) due to the high affinity interaction between the Ad35 fiber and its primary cellular receptor, the membrane glycoprotein CD46 (Gaggar *et al.*, 2003, Tuve *et al.*, 2006). However, in the CHO-WTR cell line, FX significantly increased binding by all vectors. In the absence of CD46 expression in this cell line, Ad5/f35, Ad5/p35/f35 and Ad35 use a low affinity interaction with HSPGs for binding (Tuve *et al.*, 2008). Ad35 has been shown to interact with the sulphated regions of HSPGs but not via the fiber knob domain (Tuve *et al.*, 2008). In the presence of FX, binding was enhanced by all vectors possibly due to incorporation of the high affinity HSPG pathway used by vectors with the Ad5 hexon in the presence of FX (Waddington *et al.*, 2008). FX can significantly enhance binding by vectors with an Ad5 fiber, independent of capsid type, indicating the importance of both hexon and fiber in the cell binding process. This has important implications in the design of future gene therapy vectors, as pseudotyping may not be sufficient to increase binding to a specific cell type due to interactions with blood coagulation factors following intravenous administration.

Cell internalisation by all vectors was significantly enhanced in the presence of FX in the CHO-WTR cell line. In the absence of FX, vectors have been shown to bind to HSPGs with low affinity (Tuve *et al.*, 2008) and the addition of FX results in utilisation of a high affinity interaction with HSPGs (Waddington *et al.*, 2008). Therefore, these data suggest that in the absence of the primary receptors for the Ad5 and Ad35 fibers, vectors bind and internalise through a low affinity HSPG pathway and the addition of FX causes an increase in binding and internalisation through a high affinity HSPG pathway. Cell internalisation by Ad5, Ad35 and Ad35/f5 was significantly enhanced by the presence of FX in CHO-CD46 cells. This indicates that FX has the potential to increase cell entry by Ad35 due to the interaction with HSPGs, in addition to binding to CD46, in a similar manner to vectors with the Ad5 fiber.

In CHO-CD46 cells, the presence of FX significantly inhibited transduction by vectors possessing the Ad35 fiber; an effect which was reversed by the addition of X-bp. However, the addition of FX enhanced transduction by all vectors in CHO-WTR cells. This suggests that the presence of FX, and the resulting recruitment of HSPGs for internalisation, possibly leads to inhibition of a post-internalisation intracellular trafficking pathway for vectors with the Ad35 fiber compared to transduction through the CD46-dependent pathway. In the absence of the CD46-dependent pathway in CHO-WTR cells, the conversion from the HSPG pathway used in the absence of FX to the high affinity HSPG pathway used in the presence of FX, results in significantly enhanced transduction.

The interaction between Ad35 and the chimeric Ad5/Ad35 vectors and FX was also investigated in three human cancer cell lines as CD46 expression is up-regulated in many cancers (Kinugasa *et al.*, 1999, Murray *et al.*, 2000, Ni *et al.*, 2006), making sub-species B Ads attractive candidates for cancer gene therapy applications. The level of binding by vectors with the Ad35 fiber was high but resulted in much lower transduction levels in the cancer cell lines. There was variability in the influence of FX on binding and transduction by Ad5/f35, Ad5/p35/f35 and Ad35 across the three cancer cell lines and the relative expression level of CD46 appeared to have no influence on the pattern of binding and transduction.

Binding by Ad5/f35 was high in the three cancer cell lines and varying effects were produced in the presence of FX; FX enhanced binding in the SKOV-3 cells, inhibited binding in T-47D cells and had no effect on binding by Ad5/f35 in MDA-MD-435 cells. In the three cancer cell lines, the high level of binding by Ad5/f35 did not translate to high levels of transduction. This suggests that Ad5/f35 vector inefficiently traffics to the nucleus of the cell, resulting in low transgene expression. However, Ad5/f35 has been previously shown to efficiently transduce MDA-MB-435 cells but at a substantially increased concentration of vector was used (Shayakhmetov *et al.*, 2002). This inefficiency in transduction was not seen for Ad5/p35/f35, suggesting that transduction was enhanced by the presence of the Ad35 penton. In contrast to Ad5/f35, Ad35 demonstrated moderate levels of binding to MDA-MB-435 and T-47D cells and high binding to SKOV-3 cells and this correlated into efficient transduction of the three cancer cell lines. Ad35 was also influenced differentially by FX in MDA-MB-435 and SKOV-3 cells but the presence of FX had no effect on either binding or transduction in T-47D cells, possibly as binding and transduction could not be further enhanced in the T-47D cells by incorporation of the high affinity HSPG pathway due to the high expression of CD46. Overall, the influence of FX on binding and transduction by Ad35 and the chimeric Ad5/Ad35 vectors varies greatly between the MDA-MB-435, SKOV-3 and T-47D cell lines. This is likely due to the relative CAR and CD46 expression levels, which have been previously shown to correlate strongly with levels of transduction in primary cancer cells (Ni *et al.*, 2006, Suominen *et al.*, 2006, Brouwer *et al.*, 2007).

Ad5 and Ad35/f5 reproducibly demonstrated enhanced binding and transduction in the presence of FX in all three cancer cell lines. Additionally, the degree of enhancement which occurred in the presence of FX correlated well with the level of CAR expression in the cancer cells; the presence of FX produced a substantial enhancement in binding and transduction in cells with low CAR expression due to recruitment of HSPGs, compared to cells with high CAR expression which resulted in a lesser enhancement in binding and transduction in the presence of FX. The level of transduction produced by Ad35/f5 was very low in all cases, indicating that its gene transfer ability was diminished compared to either parent vector Ad5 or Ad35.

The findings *in vitro* indicate the complexity of the FX interaction as the presence of FX can change the way in which binding, internalisation and intracellular trafficking by the vectors possessing the Ad35 fiber occurs. In the absence of FX, vectors with an Ad35 fiber bind to CD46, which allows internalisation of the vectors. The intracellular trafficking pathways of the sub-species B Ads have been previously studied (Miyazawa *et al.*, 1999, Shayakhmetov *et al.*, 2003). Despite high levels of cellular binding by vectors with fibers from sub-species B Ads, these vectors take significantly longer than Ad5 to reach the nucleus of the cell in SKOV-3 cells despite no obvious difference in internalisation kinetics (Miyazawa *et al.*, 1999). Sub-species B Ads remain in late endosomes or lysosomes for long periods after infection and use these intracellular organelles for localisation with the nucleus (Shayakhmetov *et al.*, 2003). However, this continued presence of vectors with the Ad35 fiber in late endosomes and lysosomes can lead to recycling of the vectors to the cell surface, resulting in reduced transduction by these vectors (Shayakhmetov *et al.*, 2003). This is in contrast to Ad5 which rapidly escapes from endosomes into the cytosol three to 15 minutes after internalisation, allowing efficient transduction (Greber *et al.*, 1993, Greber *et al.*, 1996, Leopold *et al.*, 1998, Miyazawa *et al.*, 1999). The presence of FX allows the utilisation of an alternative pathway for transduction by vectors with the Ad35 hexon. In the absence of FX, Ad35 uses two pathways for transduction, the high affinity CD46 pathway and low affinity HSPG pathway (Tuve *et al.*, 2008). In the presence of FX, there are three pathways that can be used; the CD46-dependent pathway and high and low affinity HSPG pathways (Tuve *et al.*, 2008, Waddington *et al.*, 2008). Therefore, as the addition of FX causes an inhibition of transduction by Ad35 hexon-containing vectors, this could possibly be due to a further hindrance in intracellular trafficking after internalisation through the high affinity HSPG pathway. Taken together this suggests that the absolute levels of CAR, CD46 and HSPGs on the surface of target cells define the importance of FX in modulating cell binding and transduction mediated by Ad5, Ad35 and the chimeric Ad5/Ad35 vectors. Therefore, heparinase I pre-treatment before administration of CD46 binding ablated vectors, in the presence and absence of FX, could be used to further dissect the role of each receptor and subsequent intracellular trafficking pathway for transduction.

Vectors with the Ad35 hexon demonstrated lower levels of liver vector genome accumulation *in vivo*, in both MF1 and CD46 transgenic mice, compared to vectors possessing the Ad5 hexon. FX binding to the hexon of Ad5 results in increased liver vector accumulation, compared to in the presence of X-bp (Waddington *et al.*, 2008). Therefore, liver accumulation by Ad35 hexon-containing vectors may be reduced due to the lower affinity interaction between the Ad35 hexon protein and FX. Liver vector accumulation was significantly reduced by all vectors, indicating that FX binding was an important feature mediating liver uptake of Ad5- and Ad35-based vectors. However, there was also a significant influence of the Ad35 fiber on liver vector accumulation as Ad5/f35 and Ad5/p35/f35 both have the Ad5 hexon but demonstrated significantly reduced liver accumulation than Ad5. This reduced liver tropism by Ad5/f35 has been previously reported in non-CD46 transgenic mice (Shayakhmetov *et al.*, 2002, Bernt *et al.*, 2003, Sakurai *et al.*, 2003b) and rats (Shinozaki *et al.*, 2006). As X-bp could further reduce liver accumulation by Ad5/f35 and Ad5/p35/f35, this suggests that the interaction with FX targets these vectors to the liver and removal of this interaction could allow retargeting of these vectors to other organs.

Low level vector genome accumulation and transduction by Ad35 was detected in the liver of CD46 transgenic mice in this study, in comparison to a previous study which reported no detectable levels of Ad35 in the liver (Verhaagh *et al.*, 2006). Additionally, vector accumulation and especially transduction in the spleen of CD46 transgenic mice by Ad35 was very low compared to Ad5. This is in contrast to another study performed in CD46 transgenic mice where Ad5 and Ad35 expressed similar levels of liver transduction and Ad35 produced significantly higher levels of transduction in the spleen (Stone *et al.*, 2007a). Vector accumulation and transduction in the spleen by Ad5/f35, Ad5/p35/f35 and Ad35 was increased in the CD46 transgenic mice, compared to the MF1 mice. This suggests that accumulation and transduction in the spleen was, at least in part, mediated by the Ad35 fiber:CD46 interaction. Additionally, vectors with the Ad5 hexon showed increased vector accumulation and transduction of the spleen in the CD46 transgenic mice, in comparison to Ad35 hexon-containing vectors. This indicates a possible involvement of the Ad5 hexon in splenic targeting.

Previously, Ad5/f35 showed no retargeting away from the liver in non-CD46 transgenic mice (Shayakhmetov *et al.*, 2002). However, in this study pre-administration of X-bp clearly retargeted Ad5/f35 and Ad35/f5 to the heart and Ad5/f35, Ad5/p35/f35 and Ad35/f5 to the lungs in MF1 mice as vector accumulation was significantly reduced in the liver and increased in the heart and lungs. This suggests that this retargeting to specific organs by each of the vectors was not fiber-dependent as the receptor for the Ad35 fiber, CD46, was not present in these organs of MF1 mice.

It has previously been reported that vectors containing the Ad35 fiber transduce the lungs of CD46 transgenic mice (Sakurai *et al.*, 2006a, Verhaagh *et al.*, 2006, Stone *et al.*, 2007a). This study showed that levels of transduction in the lung by Ad35 were significantly increased compared to Ad5, in agreement with Stone *et al*. (Stone *et al.*, 2007a). Interestingly, the data in this study is similar to a previous study of sub-species B Ad vectors in non-transgenic mice, where transduction in the spleen, heart and lung by Ad35 was lower than transduction by Ad5/f35 (Sakurai *et al.*, 2003b). Therefore, the differences in the transduction efficiency by Ad5/f35 and Ad35 were due to the interaction of the Ad5 and Ad35 hexons, respectively, with FX as a similar pattern of transduction was seen in a study which did not involve the Ad35 fiber:CD46 interaction. This suggests that FX binding to the Ad35 hexon inhibited an intracellular pathway leading to transduction *in vivo*, as well as previously seen *in vitro*. The high affinity of the Ad35 fiber for CD46 partially overcomes the Ad5 hexon:FX interaction as the level of lung transduction in CD46 transgenic mice administered with Ad5/f35 and Ad5/p35/f35 was significantly higher compared to Ad5. However, both vector genome accumulation and transduction by Ad5/f35 and Ad5/p35/f35 was significantly inhibited in the presence of X-bp. Determination of the lung:liver ratio of vector accumulation produced by Ad5/f35 and Ad5/p35/f35 found that pre-administration of X-bp had no effect on retargeting Ad5/f35 as the lung:liver ratio remained constant. Conversely, the lung:liver ratio for Ad5/p35/f35 was significantly reduced in the presence of X-bp indicating retargeting away from the lung. This suggests that a certain degree of lung targeting by Ad5/p35/f35 was determined by the interaction of this vector with FX. Therefore, Ad5/f35 and Ad5/p35/f35 demonstrated the highest levels of

selective lung targeting in the presence of FX, causing them to be good candidates for development into gene therapy vectors.

Lung vector genome accumulation and transduction by Ad35 was lower than that by Ad5/f35 and Ad5/p35/f35. However, in contrast to the vectors containing the Ad5 hexon, Ad35 produced increased lung accumulation and transduction in the presence of X-bp. Additionally, *in vivo* Ad35 had an increased lung:liver ratio in the presence of X-bp, indicating enhanced accumulation of this vector in the lung after the removal of the FX interaction. Therefore, due to its selective lung targeting ability and low seroprevalence development of a vector based on Ad35, which had been modified to ablate the interaction with FX, would be a highly useful tool to selectively target CD46 and tumours *in vivo* by intravascular administration.

The addition of X-bp had very similar effects on vector genome accumulation by the vectors in the heart of CD46 transgenic mice as in the lung, suggesting that FX was involved in retargeting away from the liver and not targeting of the vectors to another specific organ. However, no transduction by Ad5/f35, Ad5/p35/f35 and Ad35 was detected in the heart. Pre-administration of X-bp significantly decreased vector accumulation in the heart of both MF1 and CD46 transgenic mice by Ad5. Surprisingly, the presence of X-bp substantially enhanced cardiac transduction in the absence of FX either by a direct effect on transduction by blockade of a native infective pathway for Ad5 in the heart or indirectly by reducing bioavailability of the vector.

The use of a variety of *in vitro* techniques and *in vivo* administration of Ad35 and chimeric Ad35-based vectors has investigated the interaction between these vectors and the blood coagulation FX. This study has increased understanding of the requirements needed for the generation of a successfully targeted Ad35 vector.

CHAPTER 5

General Discussion

This thesis has focussed on identifying novel techniques which may impact on treatment of disease via targeting. A novel *in vivo* targeting strategy was developed to enhance delivery of the anti-oxidant peptide gp91ds (Rey *et al.*, 2001) to sites of oxidative stress in the vasculature, to reduce SO production and subsequent endothelial dysfunction. By targeting defined cells *in vivo*, this anti-oxidant has increased potential efficacy compared to alternative anti-oxidant therapies. Additionally, administration of a variety of Ad35-based vectors has led to increased understanding of the requirements needed for the generation of a successfully targeted Ad35 vector, which has relevance primarily to the treatment of cancer as the primary cellular receptor for the Ad35 fiber is up-regulated in many cancers (Kinugasa *et al.*, 1999, Murray *et al.*, 2000, Ni *et al.*, 2006).

Previously, the gp91ds anti-oxidant peptide has been used in a non-targeted approach by linkage to the HIV-tat peptide to allow internalisation of the anti-oxidant peptide into every cell (Rey *et al.*, 2001, Jacobson *et al.*, 2003, Zhou *et al.*, 2006). Co-infusion of angiotensin II and gp91ds-tat significantly attenuated angiotensin II-induced hypertension in mice (Rey *et al.*, 2001). However, *in vivo* administration of gp91ds-tat into salt-induced hypertensive rats did not significantly reduced systolic BP (Zhou *et al.*, 2006). The gp91ds-tat did reduce the production of aortic SO and inhibited the development of endothelial dysfunction in the aorta of these inducibly-hypertensive animals but this was not sufficient to produce a reduction in systolic BP (Zhou *et al.*, 2006). Additionally, gp91ds-tat did not reduce systolic BP in the normotensive Sprague-Dawley rat (Jacobson *et al.*, 2003), suggesting that the SO production in these animals was not excessive. In this study, and similar to the previous studies in rats (Jacobson *et al.*, 2003, Zhou *et al.*, 2006), administration of the non-targeted HIV-tat-gp91ds in the SHRSP had no effect on systolic BP. However, in contrast to the study performed in Dahl salt-sensitive rats (Zhou *et al.*, 2006), HIV-tat-gp91ds did not have a significant effect on SO production in the aorta as determined by the reduced aortic response to the NAD(P)H oxidase inhibitor apocynin. The HIV-tat-gp91ds peptide did produce a significant reduction in SO production in whole blood, indicating that the HIV-tat peptide was effective at delivering the anti-oxidant peptide. However, the lack of targeting capacity by this peptide meant that it was not successful in conveying the

anti-oxidant peptide to sites of oxidative stress, where it could produce significant effects on BP and endothelial function.

Evaluation of a vascular targeting anti-oxidant therapy in the SHRSP, a model of human essential hypertension, has potential clinical implications. As a significant reduction in systolic BP was achieved in animals treated with CRPPR-gp91ds, this indicates that selective inhibition of vascular NAD(P)H oxidase has potential as a future target for drug development. Additionally, SHRSP administered with CRPPR-gp91ds demonstrated significantly improved NO bioavailability in functional studies by large vessel myography, indicating reduced endothelial dysfunction. Endothelial dysfunction is an important risk factor for cardiovascular adverse events (Cai and Harrison, 2000, Schachinger *et al.*, 2000, Suwaidi *et al.*, 2000, Halcox *et al.*, 2002). Indeed, the commonly prescribed family of drugs, the statins, partly exert their beneficial effects by inactivation of endothelial NAD(P)H oxidase and, thereby, maintenance of endothelial function (Wassmann *et al.*, 2002, Liao and Laufs, 2005). Therefore, selectively targeting vascular NAD(P)H oxidase has clinical relevance.

Importantly, patients with auto-immune diseases and organ transplant recipients bear an increased risk of coronary vascular dysfunction (Frostegard, 2002). Calcineurin inhibitors CsA and FK506 are immunosuppressive drugs which have been shown to increase endothelial SO production in HUVECs, an effect which could be selectively inhibited by gp91ds-tat (Krotz *et al.*, 2007). This suggests that these drugs are activating endothelial NAD(P)H oxidase, increasing production of SO, which could be contributing to endothelial dysfunction. Therefore, immunosuppressive medications to enable treatment of one condition could be leading to the development of another serious condition. However, the immunosuppressive drugs rapamycin and mycophenolate acid did not alter and attenuated endothelial SO release, respectively (Krotz *et al.*, 2007). Therefore, not only does this suggest the inhibition of vascular NAD(P)H oxidase by gp91ds is a viable treatment option but careful consideration is needed before the use of drugs which effect oxidative stress and endothelial function.

Administration of the vascular targeting anti-oxidant peptide to patients is not a viable treatment option as it would require vast quantities of peptides most likely delivered daily by subcutaneous injection, which would result in inflammation at the injection and possibly systemic immune reactions. Therefore, an alternative method of delivering the anti-oxidant peptide to the vasculature would be required. One possibility is intravenous administration of a vascular targeting Ad vector, which is capable of delivering the anti-oxidant peptide. Previous studies have shown that insertion of a targeting peptide sequence into the HI loop in the fiber protein of the Ad5 capsid allows effective targeting by several Ad vectors to either ECs (Nicklin *et al.*, 2001, Nicklin *et al.*, 2004) or VSMCs (Work *et al.*, 2004) *in vitro*. However, after systemic administration, these vectors retained profound liver tropism (Nicklin *et al.*, 2001), characteristic of Ad5 (Huard *et al.*, 1995, Connelly, 1999, Parker *et al.*, 2006, Waddington *et al.*, 2007, Kalyuzhniy *et al.*, 2008, Waddington *et al.*, 2008), due to the interaction with FX (Parker *et al.*, 2006, Waddington *et al.*, 2008). By high resolution cryo-EM, it was determined that HVR 5 and 7 were crucial for FX binding (Kalyuzhniy *et al.*, 2008, Waddington *et al.*, 2008). This enabled the development of vectors based on Ad5 with an ablated interaction with FX (Alba *et al.*, 2009). Therefore, there is now the potential to develop selectively vascular-targeting vectors by insertion of the CRPPR peptide into the HI loop of a FX-binding ablated vector. Ablation of the FX interaction should prevent the liver tropism seen in previous studies investigating targeting *in vivo*.

Vectors containing the Ad35 fiber have become popular for gene therapy applications for use in cell types (for example, vascular cells and cancer cell lines) which are relatively refractory to infection by Ad5. This thesis has shown that Ad5/f35, Ad5/p35/f35 and Ad35 selectively transduce the lungs in CD46 transgenic mice and the degree of lung targeting was dependent on the interaction with FX. Gene therapy vectors containing the Ad35 fiber may afford many benefits compared to Ad5. There is a possibility that a reduced dose of gene therapy vectors based on Ad35 would be required for treatment, thus impacting on dose limiting toxicities. Vectors possessing the Ad35 shaft, but not the fiber knob, produced significantly impaired Kupffer cell depletion compared to Ad5 (Smith *et al.*, 2008). This was independent of vector clearance rate from the blood as Ad5 and pseudotype vectors have approximately similar clearance kinetics (Alemany *et al.*, 2000, Kanerva *et al.*,

2002, Koizumi *et al.*, 2003, Sakurai *et al.*, 2003b). Studies have also shown significant differences in vector accumulation in Kupffer cells by Ad5 and Ad35 fiber-containing vectors, although the reason for such differences is presently unclear. Kupffer cell accumulation for Ad5 and vectors containing the Ad35 fiber were shown to be similar in two studies (Shayakhmetov *et al.*, 2005b, Smith *et al.*, 2008). However, other studies have shown reduced accumulation in Kupffer cells by Ad5/f35 (Bernt *et al.*, 2003, Shayakhmetov *et al.*, 2004). As Ad5/f35 and Ad35 have been shown to interact with platelets (Stone *et al.*, 2007b), inhibition of Kupffer cell death by Ad35 fiber-containing vectors could result in reduced adverse effects of Ad35-based gene therapy, in comparison to Ad5, as Kupffer cells are required to clear aggregated platelets produced by interaction with blood-borne vectors. Also reduced accumulation of these vectors in Kupffer cells would increase the bioavailability of the administered dose, enabling a lower dose of Ad35 fiber-containing vectors with correspondingly reduced toxicity issues.

The differences in Kupffer cell accumulation after administration of Ad5 or Ad35 fiber-containing vectors was shown to be due to deficiencies in intracellular trafficking by vectors with the Ad35 fiber shaft (Smith *et al.*, 2008). Ad5 and vectors with the Ad35 fiber have been shown to use different intracellular trafficking pathways (Miyazawa *et al.*, 1999, Shayakhmetov *et al.*, 2003). This was also seen in SKOV-3 cells in this study where Ad5/f35, Ad5/p35/f35 and Ad35 took substantially longer than Ad5 to reach the nucleus of the cell. Studies into the interactions with vectors and Kupffer cells were performed in non-CD46 transgenic mice (Bernt *et al.*, 2003, Shayakhmetov *et al.*, 2004, Shayakhmetov *et al.*, 2005b, Smith *et al.*, 2008). This suggests that the Kupffer cell interaction with Ad35 fiber-containing vectors was not CD46-dependent. It is possible that the inhibition of Kupffer cell depletion, seen with vectors possessing the Ad35 fiber shaft, is FX-dependent as FX significantly inhibits a post-internalisation mechanism leading to transduction *in vitro*. The inhibition of transduction by FX was seen in CD46 expressing cells but could potentially occur *in vivo* in non-CD46 transgenic animals as Ads are internalised into Kupffer cells by endocytosis (Zsengeller *et al.*, 2000) in large numbers (Manickan *et al.*, 2006). If FX was bound to the vector containing the Ad35 fiber before internalisation, the presence of FX could inhibit subsequent intracellular trafficking mechanisms. Sub-species B Ads remain in late endosomes

or lysosomes for long periods after infection and use these intracellular organelles for localisation with the nucleus (Shayakhmetov *et al.*, 2003), unlike Ad5 which rapidly lyses the endosomal membrane and escapes into the cytosol (Seth, 1994b, Miyazawa *et al.*, 2001). As membrane-lytic activity is also required for Kupffer cell death (Smith *et al.*, 2008), it is possible that it is the ability to lyse membranes which is reduced in Ad35 fiber-containing vectors. Time lapse trafficking experiments and co-localisation with antibodies directed against a variety of intracellular organelles are required to fully investigate the differences in intracellular trafficking by vectors possessing the Ad35 fiber, in both the presence and absence of FX. Additionally, it is currently unknown how long FX remains bound to either the Ad5 or Ad35 hexon. Therefore, trafficking experiments should also be performed with labelled FX to determine whether FX is internalised with the vectors and, if so, where in the intracellular pathways FX dissociates.

In this study and others, vectors possessing the Ad35 fiber (Ad5/f35, Ad5/p35/f35 and Ad35) showed lung transduction in CD46 transgenic mice but at varying levels (Sakurai *et al.*, 2006a, Verhaagh *et al.*, 2006, Stone *et al.*, 2007a). The CD46 transgenic mice expressed both BC and C isoforms of CD46 (Sakurai *et al.*, 2006a, Verhaagh *et al.*, 2006, Stone *et al.*, 2007a). Another study showed much lower levels of lung transduction by Ad5/f35 (Ni *et al.*, 2006). The CD46 transgenic mice used only expressed the C1 isoform of CD46 (Ni *et al.*, 2006), possibly suggesting that the interaction between the Ad35 fiber and the BC1 isoform results in enhanced lung transduction. However, the mechanism of lung infection by vectors with the Ad35 fiber remains unclear. Human CD46 is primarily expressed on the basolateral surface of polarised epithelial cells (Ichida *et al.*, 1994, Maisner *et al.*, 1997). Therefore, vectors which use CD46 as their receptor need to surmount anatomical barriers, such as tight junctions between cells and the extracellular matrix. Further investigation into the mechanism of Ad35 infection is required, in both the presence and absence of FX.

Sub-species B Ads are primarily in development for cancer gene therapy as CD46 is up-regulated in many cancers (Kinugasa *et al.*, 1999, Murray *et al.*, 2000, Ni *et al.*, 2006). Ad5/f35 has been previously shown to selectively target liver metastases *in vivo* (Bernt *et al.*, 2003). However, the complex structure of tumours provides

another anatomical barrier which limits the accessibility of vectors. In particular, many tumours have a basement membrane which forms a network through the extracellular matrix. Ad35-based vectors could provide a dual approach to cancer gene therapy as they have not only shown tumour targeting but the Ad35 knob protein also binds to ECs of tumour feeding blood vessels but not to blood vessels present in non-malignant tissues (Ni *et al.*, 2006). This can occur due to the expression of different surface markers in neoangiogenic vasculature compared to tissue blood vessels (Arap *et al.*, 2002).

The interaction with FX could play a significant role in the design of future gene therapy vectors. This study suggests that a certain degree of lung targeting by Ad5/p35/f35 in CD46 transgenic mice was determined by the interaction of this vector with FX as the lung:liver ratio for Ad5/p35/f35 was reduced in the presence of X-bp. Although the lung:liver ratio produced by Ad5/f35 was the same in the presence and absence of X-bp, indicating that the addition of X-bp had no effect on retargeting Ad5/f35. Ad5/f35 and Ad5/p35/f35 demonstrated the highest levels of selective lung targeting in the presence of FX, causing them to be good candidates for development into gene therapy vectors. However, as both Ad5/f35 and Ad5/p35/f35 possess the Ad5 hexon, these vectors will be susceptible to anti-Ad5 antibodies which are present in a high percentage of the population (Christ *et al.*, 1997, Seshidhar Reddy *et al.*, 2003, Sprangers *et al.*, 2003, Vogels *et al.*, 2003, Sumida *et al.*, 2005, Abbink *et al.*, 2007, Parker *et al.*, 2009). The resulting neutralisation of these vectors *in vivo* would lead to very low levels of transduction after systemic administration and hinder their use as gene therapy vectors.

Importantly, Ad35 had an increased lung:liver ratio in the presence of X-bp, indicating retargeting of this vector to the lung in the absence of the interaction with FX. X-bp could be replaced by a small molecule screen which is more pharmaceutically and therapeutically relevant. Vectors based on Ad35 have the potential for reduced immune reactions. Even though the sub-species B Ads have been isolated frequently from immunocompromised patients (De Jong *et al.*, 1999) and though the immune system is suppressed in cancer patients, only 31% of Dutch cancer patients possessed neutralising antibodies against Ad35 (Brouwer *et al.*, 2007). Other studies have shown that the typical seroprevalence of neutralising

antibodies to Ad35 is between zero (Vogels *et al.*, 2003) and 17% (Abbink *et al.*, 2007). This is significantly lower than the Ad5 seroprevalence, which ranges from 66% of cancer patients having neutralising antibodies to Ad5 (Brouwer *et al.*, 2007), to nearly 80% of healthy people (Vogels *et al.*, 2003), to 100% of the population (Abbink *et al.*, 2007). This suggests that vectors based on the Ad35 hexon would induce fewer immune reactions after gene therapy. To overcome the significant problem of the high seroprevalence of Ad neutralising antibodies, there are many Ads from other species (Jager and Ehrhardt, 2007). These viruses could be developed into gene vectors which have relevance to human gene therapy and especially vaccine development.

In summary, this thesis has shown that the selective targeting of an anti-oxidant peptide to the vasculature has led to a significant enhancement in the efficacy and verified that inhibition of vascular NAD(P)H oxidase is a clinically relevant target. Administration of a variety of Ad35-based vectors has led to increased understanding of the requirements needed for the generation of a successfully targeted vector based on Ad35, which has potential as a vector for cancer gene therapy. Currently in the UK, there is an approved phase I clinical trial for cancer gene therapy using intravenous delivery of Ad5/f35 at high doses (http://www.dh.gov.uk/ab/GTAC/index.htm). However, the work presented here suggests important issues which may impact on the effectiveness of this strategy.

List of References

ABBINK, P., LEMCKERT, A. A., EWALD, B. A., *et al.* (2007) Comparative seroprevalence and immunogenicity of six rare serotype recombinant adenovirus vaccine vectors from subgroups B and D. *J Virol,* 81**,** 4654-63.

ACEVEDO, L. M., BARILLAS, S., WEIS, S. M., GOTHERT, J. R. and CHERESH, D. A. (2008) Semaphorin 3A suppresses VEGF-mediated angiogenesis yet acts as a vascular permeability factor. *Blood,* 111**,** 2674-80.

ALBA, R., BRADSHAW, A. C., PARKER, A. L., *et al.* (2009) Identification of coagulation factor (F)X binding sites on the adenovirus serotype 5 hexon: effect of mutagenesis on FX interactions and gene transfer. *Blood.*

ALEMANY, R. and CURIEL, D. T. (2001) CAR-binding ablation does not change biodistribution and toxicity of adenoviral vectors. *Gene Ther,* 8**,** 1347-53.

ALEMANY, R., SUZUKI, K. and CURIEL, D. T. (2000) Blood clearance rates of adenovirus type 5 in mice. *J Gen Virol,* 81**,** 2605-9.

ALEXANDER, M. Y., BROSNAN, M. J., HAMILTON, C. A., *et al.* (1999) Gene transfer of endothelial nitric oxide synthase improves nitric oxide-dependent endothelial function in a hypertensive rat model. *Cardiovasc Res,* 43**,** 798-807.

ALEXANDER, M. Y., BROSNAN, M. J., HAMILTON, C. A., *et al.* (2000) Gene transfer of endothelial nitric oxide synthase but not Cu/Zn superoxide dismutase restores nitric oxide availability in the SHRSP. *Cardiovasc Res,* 47**,** 609-17.

ARAP, W., KOLONIN, M. G., TREPEL, M., *et al.* (2002) Steps toward mapping the human vasculature by phage display. *Nat Med,* 8**,** 121-7.

ATODA, H., ISHIKAWA, M., MIZUNO, H. and MORITA, T. (1998) Coagulation factor X-binding protein from Deinagkistrodon acutus venom is a Gla domain-binding protein. *Biochemistry,* 37**,** 17361-70.

BAI, M., HARFE, B. and FREIMUTH, P. (1993) Mutations that alter an Arg-Gly-Asp (RGD) sequence in the adenovirus type 2 penton base protein abolish its cell-rounding activity and delay virus reproduction in flat cells. *J Virol,* 67**,** 5198-205.

BAILEY, C. J., CRYSTAL, R. G. and LEOPOLD, P. L. (2003) Association of adenovirus with the microtubule organizing center. *J Virol,* 77**,** 13275-87.

BAKER, A. H. (2007) Shedding light on tumor targeting by adenovirus. *Mol Ther,* 15**,** 841-2.

BAUERSACHS, J., BOULOUMIE, A., FRACCAROLLO, D., HU, K., BUSSE, R. and ERTL, G. (1999) Endothelial dysfunction in chronic myocardial infarction despite increased vascular endothelial nitric oxide synthase and soluble guanylate cyclase expression: role of enhanced vascular superoxide production. *Circulation,* 100**,** 292-8.

BAYO-PUXAN, N., CASCALLO, M., GROS, A., HUCH, M., FILLAT, C. and ALEMANY, R. (2006) Role of the putative heparan sulfate glycosaminoglycan-binding site of the adenovirus type 5 fiber shaft on liver detargeting and knob-mediated retargeting. *J Gen Virol,* 87**,** 2487-95.

BECKER, P. M., WALTENBERGER, J., YACHECHKO, R., *et al.* (2005) Neuropilin-1 regulates vascular endothelial growth factor-mediated endothelial permeability. *Circ Res,* 96**,** 1257-65.

BENDALL, J. K., RINZE, R., ADLAM, D., *et al.* (2007) Endothelial Nox2 overexpression potentiates vascular oxidative stress and hemodynamic response to angiotensin II: studies in endothelial-targeted Nox2 transgenic mice. *Circ Res,* 100**,** 1016-25.

BERGELSON, J. M., CUNNINGHAM, J. A., DROGUETT, G., *et al.* (1997) Isolation of a common receptor for Coxsackie B viruses and adenoviruses 2 and 5. *Science,* 275**,** 1320-3.

BERGELSON, J. M., KRITHIVAS, A., CELI, L., *et al.* (1998) The murine CAR homolog is a receptor for coxsackie B viruses and adenoviruses. *J Virol,* 72**,** 415-9.

BERNT, K. M., NI, S., GAGGAR, A., LI, Z. Y., SHAYAKHMETOV, D. M. and LIEBER, A. (2003) The effect of sequestration by nontarget tissues on anti-tumor efficacy of systemically applied, conditionally replicating adenovirus vectors. *Mol Ther,* 8**,** 746-55.

BERRY, C., BROSNAN, M. J., FENNELL, J., HAMILTON, C. A. and DOMINICZAK, A. F. (2001) Oxidative stress and vascular damage in hypertension. *Curr Opin Nephrol Hypertens,* 10**,** 247-55.

BERRY, C., HAMILTON, C. A., BROSNAN, M. J., *et al.* (2000) Investigation into the sources of superoxide in human blood vessels: angiotensin II increases superoxide production in human internal mammary arteries. *Circulation,* 101**,** 2206-12.

BOAZ, M., SMETANA, S., WEINSTEIN, T., *et al.* (2000) Secondary prevention with antioxidants of cardiovascular disease in endstage renal disease (SPACE): randomised placebo-controlled trial. *Lancet,* 356**,** 1213-8.

BRIGELIUS-FLOHE, R. and TRABER, M. G. (1999) Vitamin E: function and metabolism. *FASEB J,* 13**,** 1145-55.

BROUWER, E., HAVENGA, M. J., OPHORST, O., *et al.* (2007) Human adenovirus type 35 vector for gene therapy of brain cancer: improved transduction and bypass of pre-existing anti-vector immunity in cancer patients. *Cancer Gene Ther,* 14**,** 211-9.

BURTON, G. W. and INGOLD, K. U. (1984) beta-Carotene: an unusual type of lipid antioxidant. *Science,* 224**,** 569-73.

CAI, H. and HARRISON, D. G. (2000) Endothelial dysfunction in cardiovascular diseases: the role of oxidant stress. *Circ Res,* 87**,** 840-4.

CANDOTTI, F., JOHNSTON, J. A., PUCK, J. M., SUGAMURA, K., O'SHEA, J. J. and BLAESE, R. M. (1996) Retroviral-mediated gene correction for X-linked severe combined immunodeficiency. *Blood,* 87**,** 3097-102.

CARDARELLI, F., SERRESI, M., BIZZARRI, R., GIACCA, M. and BELTRAM, F. (2007) In Vivo Study of HIV-1 Tat Arginine-rich Motif Unveils Its Transport Properties. *Mol Ther,* 15**,** 1313-22.

CARLISLE, R. C., DI, Y., CERNY, A. M., *et al.* (2009) Human erythrocytes bind and inactivate type 5 adenovirus by presenting Coxsackie virus-adenovirus receptor and complement receptor 1. *Blood,* 113**,** 1909-18.

CARRETERO, O. A. and OPARIL, S. (2000) Essential hypertension. Part I: definition and etiology. *Circulation,* 101**,** 329-35.

CAVAZZANA-CALVO, M., HACEIN-BEY, S., DE SAINT BASILE, G., *et al.* (1996) Role of interleukin-2 (IL-2), IL-7, and IL-15 in natural killer cell differentiation from cord blood hematopoietic progenitor cells and from gamma c transduced severe combined immunodeficiency X1 bone marrow cells. *Blood,* 88**,** 3901-9.

CAVAZZANA-CALVO, M., HACEIN-BEY, S., DE SAINT BASILE, G., *et al.* (2000) Gene therapy of human severe combined immunodeficiency (SCID)-X1 disease. *Science,* 288**,** 669-72.

CAVAZZANA-CALVO, M., LAGRESLE, C., HACEIN-BEY-ABINA, S. and FISCHER, A. (2005) Gene therapy for severe combined immunodeficiency. *Annu Rev Med,* 56**,** 585-602.

CHAKRABARTI, S., COLLINGHAM, K. E., FEGAN, C. D., PILLAY, D. and MILLIGAN, D. W. (2000) Adenovirus infections following haematopoietic cell transplantation: is there a role for adoptive immunotherapy? *Bone Marrow Transplant,* 26**,** 305-7.

CHIU, C. Y., WU, E., BROWN, S. L., VON SEGGERN, D. J., NEMEROW, G. R. and STEWART, P. L. (2001) Structural analysis of a fiber-pseudotyped adenovirus with ocular tropism suggests differential modes of cell receptor interactions. *J Virol,* 75**,** 5375-80.

CHRIST, M., LUSKY, M., STOECKEL, F., *et al.* (1997) Gene therapy with recombinant adenovirus vectors: evaluation of the host immune response. *Immunol Lett,* 57**,** 19-25.

CLARK, J. S., JEFFS, B., DAVIDSON, A. O., *et al.* (1996) Quantitative trait loci in genetically hypertensive rats. Possible sex specificity. *Hypertension,* 28**,** 898-906.

COHEN, C. J., SHIEH, J. T., PICKLES, R. J., OKEGAWA, T., HSIEH, J. T. and BERGELSON, J. M. (2001) The coxsackievirus and adenovirus receptor is a transmembrane component of the tight junction. *Proc Natl Acad Sci U S A,* 98**,** 15191-6.

CONNELLY, S. (1999) Adenoviral vectors for liver-directed gene therapy. *Curr Opin Mol Ther,* 1**,** 565-72.

CRAWFORD-MIKSZA, L. and SCHNURR, D. P. (1996) Analysis of 15 adenovirus hexon proteins reveals the location and structure of seven hypervariable regions containing serotype-specific residues. *J Virol,* 70**,** 1836-44.

CROYLE, M. A., LE, H. T., LINSE, K. D., *et al.* (2005) PEGylated helper-dependent adenoviral vectors: highly efficient vectors with an enhanced safety profile. *Gene Ther,* 12**,** 579-87.

DAVIDSON, A. O., SCHORK, N., JAQUES, B. C., *et al.* (1995) Blood pressure in genetically hypertensive rats. Influence of the Y chromosome. *Hypertension,* 26**,** 452-9.

DE JONG, J. C., WERMENBOL, A. G., VERWEIJ-UIJTERWAAL, M. W., *et al.* (1999) Adenoviruses from human immunodeficiency virus-infected individuals, including two strains that represent new candidate serotypes Ad50 and Ad51 of species B1 and D, respectively. *J Clin Microbiol,* 37**,** 3940-5.

DECHECCHI, M. C., MELOTTI, P., BONIZZATO, A., SANTACATTERINA, M., CHILOSI, M. and CABRINI, G. (2001) Heparan sulfate glycosaminoglycans are receptors sufficient to mediate the initial binding of adenovirus types 2 and 5. *J Virol,* 75**,** 8772-80.

DECHECCHI, M. C., TAMANINI, A., BONIZZATO, A. and CABRINI, G. (2000) Heparan sulfate glycosaminoglycans are involved in adenovirus type 5 and 2-host cell interactions. *Virology,* 268**,** 382-90.

DEFER, C., BELIN, M. T., CAILLET-BOUDIN, M. L. and BOULANGER, P. (1990) Human adenovirus-host cell interactions: comparative study with members of subgroups B and C. *J Virol,* 64**,** 3661-73.

DELEO, F. R. and QUINN, M. T. (1996) Assembly of the phagocyte NADPH oxidase: molecular interaction of oxidase proteins. *J Leukoc Biol,* 60**,** 677-91.

DELEO, F. R., YU, L., BURRITT, J. B., *et al.* (1995) Mapping sites of interaction of p47-phox and flavocytochrome b with random-sequence peptide phage display libraries. *Proc Natl Acad Sci U S A,* 92**,** 7110-4.

DENBY, L., WORK, L. M., GRAHAM, D., *et al.* (2004) Adenoviral serotype 5 vectors pseudotyped with fibers from subgroup D show modified tropism in vitro and in vivo. *Hum Gene Ther,* 15**,** 1054-64.

DENBY, L., WORK, L. M., SEGGERN, D. J., *et al.* (2007) Development of Renal-targeted Vectors Through Combined In Vivo Phage Display and Capsid Engineering of Adenoviral Fibers From Serotype 19p. *Mol Ther,* 15**,** 1647-54.

DI PAOLO, N., NI, S., GAGGAR, A., *et al.* (2006) Evaluation of adenovirus vectors containing serotype 35 fibers for vaccination. *Mol Ther,* 13**,** 756-65.

DI PAOLO, N. C., MIAO, E. A., IWAKURA, Y., *et al.* (2009a) Virus binding to a plasma membrane receptor triggers interleukin-1 alpha-mediated proinflammatory macrophage response in vivo. *Immunity,* 31**,** 110-21.

DI PAOLO, N. C., VAN ROOIJEN, N. and SHAYAKHMETOV, D. M. (2009b) Redundant and synergistic mechanisms control the sequestration of blood-born adenovirus in the liver. *Mol Ther,* 17**,** 675-84.

DI WANG, H., HOPE, S., DU, Y., *et al.* (1999) Paracrine role of adventitial superoxide anion in mediating spontaneous tone of the isolated rat aorta in angiotensin II-induced hypertension. *Hypertension,* 33**,** 1225-32.

DMITRIEV, I., KRASNYKH, V., MILLER, C. R., *et al.* (1998) An adenovirus vector with genetically modified fibers demonstrates expanded tropism via utilization of a coxsackievirus and adenovirus receptor-independent cell entry mechanism. *J Virol,* 72**,** 9706-13.

DOMINICZAK, A. F., DEVLIN, A. M., LEE, W. K., ANDERSON, N. H., BOHR, D. F. and REID, J. L. (1996) Vascular smooth muscle polyploidy and cardiac hypertrophy in genetic hypertension. *Hypertension,* 27**,** 752-9.

DOMINICZAK, A. F., MCLAREN, Y., KUSEL, J. R., *et al.* (1993) Lateral diffusion and fatty acid composition in vascular smooth muscle membrane from stroke-prone spontaneously hypertensive rats. *Am J Hypertens,* 6**,** 1003-8.

DOWELL, F. J., MARTIN, W., DOMINICZAK, A. F. and HAMILTON, C. A. (1999) Decreased basal despite enhanced agonist-stimulated effects of nitric oxide in 12-week-old stroke-prone spontaneously hypertensive rat. *Eur J Pharmacol,* 379**,** 175-82.

ECHAVARRIA, M., FORMAN, M., VAN TOL, M. J., VOSSEN, J. M., CHARACHE, P. and KROES, A. C. (2001) Prediction of severe disseminated adenovirus infection by serum PCR. *Lancet,* 358**,** 384-5.

EINFELD, D. A., SCHROEDER, R., ROELVINK, P. W., *et al.* (2001) Reducing the native tropism of adenovirus vectors requires removal of both CAR and integrin interactions. *J Virol,* 75**,** 11284-91.

ESSLER, M. and RUOSLAHTI, E. (2002) Molecular specialization of breast vasculature: a breast-homing phage-displayed peptide binds to aminopeptidase P in breast vasculature. *Proc Natl Acad Sci U S A,* 99**,** 2252-7.

ETO, Y., GAO, J. Q., SEKIGUCHI, F., *et al.* (2005) PEGylated adenovirus vectors containing RGD peptides on the tip of PEG show high transduction efficiency and antibody evasion ability. *J Gene Med,* 7**,** 604-12.

FARMER, C., MORTON, P. E., SNIPPE, M., SANTIS, G. and PARSONS, M. (2009) Coxsackie adenovirus receptor (CAR) regulates integrin function through activation of p44/42 MAPK. *Exp Cell Res,* 315**,** 2637-47.

FAWELL, S., SEERY, J., DAIKH, Y., *et al.* (1994) Tat-mediated delivery of heterologous proteins into cells. *Proc Natl Acad Sci U S A,* 91**,** 664-8.

FENNELL, J. P., BROSNAN, M. J., FRATER, A. J., *et al.* (2002) Adenovirus-mediated overexpression of extracellular superoxide dismutase improves endothelial dysfunction in a rat model of hypertension. *Gene Ther,* 9**,** 110-7.

FLEISCHLI, C., VERHAAGH, S., HAVENGA, M., *et al.* (2005) The distal short consensus repeats 1 and 2 of the membrane cofactor protein CD46 and their distance from the cell membrane determine productive entry of species B adenovirus serotype 35. *J Virol,* 79**,** 10013-22.

FLOMENBERG, P., BABBITT, J., DROBYSKI, W. R., *et al.* (1994) Increasing incidence of adenovirus disease in bone marrow transplant recipients. *J Infect Dis,* 169**,** 775-81.

FRANKEL, A. D. and PABO, C. O. (1988) Cellular uptake of the tat protein from human immunodeficiency virus. *Cell,* 55**,** 1189-93.

FRAZIER, D. P., WILSON, A., DOUGHERTY, C. J., LI, H., BISHOPRIC, N. H. and WEBSTER, K. A. (2007) PKC-alpha and TAK-1 are intermediates in the activation of c-Jun NH2-terminal kinase by hypoxia-reoxygenation. *Am J Physiol Heart Circ Physiol,* 292**,** H1675-84.

FREIMUTH, P., SPRINGER, K., BERARD, C., HAINFELD, J., BEWLEY, M. and FLANAGAN, J. (1999) Coxsackievirus and adenovirus receptor amino-terminal immunoglobulin V-related domain binds adenovirus type 2 and fiber knob from adenovirus type 12. *J Virol,* 73**,** 1392-8.

FROSTEGARD, J. (2002) Autoimmunity, oxidized LDL and cardiovascular disease. *Autoimmun Rev,* 1**,** 233-7.

GAGGAR, A., SHAYAKHMETOV, D. M. and LIEBER, A. (2003) CD46 is a cellular receptor for group B adenoviruses. *Nat Med,* 9**,** 1408-12.

GAGGAR, A., SHAYAKHMETOV, D. M., LISZEWSKI, M. K., ATKINSON, J. P. and LIEBER, A. (2005) Localization of regions in CD46 that interact with adenovirus. *J Virol,* 79**,** 7503-13.

GALL, J., KASS-EISLER, A., LEINWAND, L. and FALCK-PEDERSEN, E. (1996) Adenovirus type 5 and 7 capsid chimera: fiber replacement alters receptor tropism without affecting primary immune neutralization epitopes. *J Virol,* 70**,** 2116-23.

GARLANDA, C. and DEJANA, E. (1997) Heterogeneity of endothelial cells. Specific markers. *Arterioscler Thromb Vasc Biol,* 17**,** 1193-202.

GASPAR, H. B., PARSLEY, K. L., HOWE, S., *et al.* (2004) Gene therapy of X-linked severe combined immunodeficiency by use of a pseudotyped gammaretroviral vector. *Lancet,* 364**,** 2181-7.

GHITESCU, L. D., CRINE, P. and JACOBSON, B. S. (1997) Antibodies specific to the plasma membrane of rat lung microvascular endothelium. *Exp Cell Res,* 232**,** 47-55.

GOKCE, N., KEANEY, J. F., JR., FREI, B., *et al.* (1999) Long-term ascorbic acid administration reverses endothelial vasomotor dysfunction in patients with coronary artery disease. *Circulation,* 99**,** 3234-40.

GOKCE, N., KEANEY, J. F., JR., HUNTER, L. M., WATKINS, M. T., MENZOIAN, J. O. and VITA, J. A. (2002) Risk stratification for postoperative cardiovascular events via noninvasive assessment of endothelial function: a prospective study. *Circulation,* 105**,** 1567-72.

GOMEZ, K. and MCVEY, J. H. (2006) Tissue factor initiated blood coagulation. *Front Biosci,* 11**,** 1349-59.

GORLACH, A., BRANDES, R. P., NGUYEN, K., AMIDI, M., DEHGHANI, F. and BUSSE, R. (2000) A gp91phox containing NADPH oxidase selectively expressed in endothelial cells is a major source of oxygen radical generation in the arterial wall. *Circ Res,* 87**,** 26-32.

GRAHAM, D., HUYNH, N. N., HAMILTON, C. A., *et al.* (2009) Mitochondria-targeted antioxidant MitoQ10 improves endothelial function and attenuates cardiac hypertrophy. *Hypertension,* 54**,** 322-8.

GRATTON, J. A., SAUTER, A., RUDIN, M., *et al.* (1998) Susceptibility to cerebral infarction in the stroke-prone spontaneously hypertensive rat is inherited as a dominant trait. *Stroke,* 29**,** 690-4.

GREBER, U. F., SUOMALAINEN, M., STIDWILL, R. P., BOUCKE, K., EBERSOLD, M. W. and HELENIUS, A. (1997) The role of the nuclear pore complex in adenovirus DNA entry. *Embo J,* 16**,** 5998-6007.

GREBER, U. F., WEBSTER, P., WEBER, J. and HELENIUS, A. (1996) The role of the adenovirus protease on virus entry into cells. *Embo J,* 15**,** 1766-77.

GREBER, U. F., WILLETTS, M., WEBSTER, P. and HELENIUS, A. (1993) Stepwise dismantling of adenovirus 2 during entry into cells. *Cell,* 75**,** 477-86.

GREEN, M. and LOEWENSTEIN, P. M. (1988) Autonomous functional domains of chemically synthesized human immunodeficiency virus tat trans-activator protein. *Cell,* 55**,** 1179-88.

GRIENDLING, K. K., MINIERI, C. A., OLLERENSHAW, J. D. and ALEXANDER, R. W. (1994) Angiotensin II stimulates NADH and NADPH oxidase activity in cultured vascular smooth muscle cells. *Circ Res,* 74**,** 1141-8.

GRIENDLING, K. K., SORESCU, D. and USHIO-FUKAI, M. (2000) NAD(P)H oxidase: role in cardiovascular biology and disease. *Circ Res,* 86**,** 494-501.

GROMOVA, I., GROMOV, P. and CELIS, J. E. (2002) bc10: A novel human bladder cancer-associated protein with a conserved genomic structure downregulated in invasive cancer. *Int J Cancer,* 98**,** 539-46.

HACEIN-BEY-ABINA, S., VON KALLE, C., SCHMIDT, M., *et al.* (2003) LMO2-associated clonal T cell proliferation in two patients after gene therapy for SCID-X1. *Science,* 302**,** 415-9.

HACEIN-BEY, H., CAVAZZANA-CALVO, M., LE DEIST, F., *et al.* (1996) gamma-c gene transfer into SCID X1 patients' B-cell lines restores normal high-affinity interleukin-2 receptor expression and function. *Blood,* 87**,** 3108-16.

HACEIN-BEY, S., BASILE, G. D., LEMERLE, J., FISCHER, A. and CAVAZZANA-CALVO, M. (1998) gammac gene transfer in the presence of stem cell factor, FLT-3L, interleukin-7 (IL-7), IL-1, and IL-15 cytokines restores T-cell differentiation from gammac(-) X-linked severe combined immunodeficiency hematopoietic progenitor cells in murine fetal thymic organ cultures. *Blood,* 92**,** 4090-7.

HALCOX, J. P., SCHENKE, W. H., ZALOS, G., *et al.* (2002) Prognostic value of coronary vascular endothelial dysfunction. *Circulation,* 106**,** 653-8.

HAMILTON, C. A., BROSNAN, M. J., AL-BENNA, S., BERG, G. and DOMINICZAK, A. F. (2002) NAD(P)H oxidase inhibition improves endothelial function in rat and human blood vessels. *Hypertension,* 40**,** 755-62.

HARRIS, S. L. and LEVINE, A. J. (2005) The p53 pathway: positive and negative feedback loops. *Oncogene,* 24**,** 2899-908.

HARRISON, D. G. (1997) Endothelial function and oxidant stress. *Clin Cardiol,* 20**,** II-11-7.

HAVENGA, M. J., LEMCKERT, A. A., GRIMBERGEN, J. M., *et al.* (2001) Improved adenovirus vectors for infection of cardiovascular tissues. *J Virol,* 75**,** 3335-42.

HAVENGA, M. J., LEMCKERT, A. A., OPHORST, O. J., *et al.* (2002) Exploiting the natural diversity in adenovirus tropism for therapy and prevention of disease. *J Virol,* 76**,** 4612-20.

HEINECKE, J. W. (2001) Is the emperor wearing clothes? Clinical trials of vitamin E and the LDL oxidation hypothesis. *Arterioscler Thromb Vasc Biol,* 21**,** 1261-4.

HEITZER, T., SCHLINZIG, T., KROHN, K., MEINERTZ, T. and MUNZEL, T. (2001) Endothelial dysfunction, oxidative stress, and risk of cardiovascular events in patients with coronary artery disease. *Circulation,* 104**,** 2673-8.

HENRY, L. J., XIA, D., WILKE, M. E., DEISENHOFER, J. and GERARD, R. D. (1994) Characterization of the knob domain of the adenovirus type 5 fiber protein expressed in Escherichia coli. *J Virol,* 68**,** 5239-46.

HEUMULLER, S., WIND, S., BARBOSA-SICARD, E., *et al.* (2008) Apocynin is not an inhibitor of vascular NADPH oxidases but an antioxidant. *Hypertension,* 51**,** 211-7.

HIERHOLZER, J. C. (1992) Adenoviruses in the immunocompromised host. *Clin Microbiol Rev,* 5**,** 262-74.

HIGASHI, Y., NOMA, K., YOSHIZUMI, M. and KIHARA, Y. (2009) Endothelial function and oxidative stress in cardiovascular diseases. *Circ J,* 73**,** 411-8.

HOFHERR, S. E., MOK, H., GUSHIKEN, F. C., LOPEZ, J. A. and BARRY, M. A. (2007) Polyethylene glycol modification of adenovirus reduces platelet

activation, endothelial cell activation, and thrombocytopenia. *Hum Gene Ther,* 18**,** 837-48.

HONDA, T., SAITOH, H., MASUKO, M., *et al.* (2000) The coxsackievirus-adenovirus receptor protein as a cell adhesion molecule in the developing mouse brain. *Brain Res Mol Brain Res,* 77**,** 19-28.

HORNIG, B. (2002) Vitamins, antioxidants and endothelial function in coronary artery disease. *Cardiovasc Drugs Ther,* 16**,** 401-9.

HOWE, S. J., MANSOUR, M. R., SCHWARZWAELDER, K., *et al.* (2008) Insertional mutagenesis combined with acquired somatic mutations causes leukemogenesis following gene therapy of SCID-X1 patients. *J Clin Invest,* 118**,** 3143-50.

HSU, E. C., DORIG, R. E., SARANGI, F., MARCIL, A., IORIO, C. and RICHARDSON, C. D. (1997) Artificial mutations and natural variations in the CD46 molecules from human and monkey cells define regions important for measles virus binding. *J Virol,* 71**,** 6144-54.

HSU, E. C., SABATINOS, S., HOEDEMAEKER, F. J., ROSE, D. R. and RICHARDSON, C. D. (1999) Use of site-specific mutagenesis and monoclonal antibodies to map regions of CD46 that interact with measles virus H protein. *Virology,* 258**,** 314-26.

HUARD, J., LOCHMULLER, H., ACSADI, G., JANI, A., MASSIE, B. and KARPATI, G. (1995) The route of administration is a major determinant of the transduction efficiency of rat tissues by adenoviral recombinants. *Gene Ther,* 2**,** 107-15.

HUTNICK, N. A., CARNATHAN, D. G., DUBEY, S. A., *et al.* (2009) Baseline Ad5 serostatus does not predict Ad5 HIV vaccine-induced expansion of adenovirus-specific CD4+ T cells. *Nat Med,* 15**,** 876-8.

ICHIDA, S., YUZAWA, Y., OKADA, H., YOSHIOKA, K. and MATSUO, S. (1994) Localization of the complement regulatory proteins in the normal human kidney. *Kidney Int,* 46**,** 89-96.

INOUE, N., IKAWA, M., NAKANISHI, T., *et al.* (2003) Disruption of mouse CD46 causes an accelerated spontaneous acrosome reaction in sperm. *Mol Cell Biol,* 23**,** 2614-22.

JACOBSON, G. M., DOURRON, H. M., LIU, J., *et al.* (2003) Novel NAD(P)H oxidase inhibitor suppresses angioplasty-induced superoxide and neointimal hyperplasia of rat carotid artery. *Circ Res,* 92**,** 637-43.

JAGER, L. and EHRHARDT, A. (2007) Emerging adenoviral vectors for stable correction of genetic disorders. *Curr Gene Ther,* 7**,** 272-83.

JAKUBCZAK, J. L., ROLLENCE, M. L., STEWART, D. A., *et al.* (2001) Adenovirus type 5 viral particles pseudotyped with mutagenized fiber proteins show diminished infectivity of coxsackie B-adenovirus receptor-bearing cells. *J Virol,* 75**,** 2972-81.

JANEWAY, C. A., JR. and MEDZHITOV, R. (2002) Innate immune recognition. *Annu Rev Immunol,* 20**,** 197-216.

JEFFS, B., CLARK, J. S., ANDERSON, N. H., *et al.* (1997) Sensitivity to cerebral ischaemic insult in a rat model of stroke is determined by a single genetic locus. *Nat Genet,* 16**,** 364-7.

JIA, H., LOHR, M., JEZEQUEL, S., *et al.* (2001) Cysteine-rich and basic domain HIV-1 Tat peptides inhibit angiogenesis and induce endothelial cell apoptosis. *Biochem Biophys Res Commun,* 283**,** 469-79.

JIANG, H., WANG, Z., SERRA, D., FRANK, M. M. and AMALFITANO, A. (2004) Recombinant adenovirus vectors activate the alternative complement pathway, leading to the binding of human complement protein C3 independent of anti-ad antibodies. *Mol Ther,* 10**,** 1140-2.

KALYUZHNIY, O., DI PAOLO, N. C., SILVESTRY, M., *et al.* (2008) Adenovirus serotype 5 hexon is critical for virus infection of hepatocytes in vivo. *Proc Natl Acad Sci U S A,* 105**,** 5483-8.

KANERVA, A., WANG, M., BAUERSCHMITZ, G. J., *et al.* (2002) Gene transfer to ovarian cancer versus normal tissues with fiber-modified adenoviruses. *Mol Ther,* 5**,** 695-704.

KELKAR, S. A., PFISTER, K. K., CRYSTAL, R. G. and LEOPOLD, P. L. (2004) Cytoplasmic dynein mediates adenovirus binding to microtubules. *J Virol,* 78**,** 10122-32.

KEMPER, C., LEUNG, M., STEPHENSEN, C. B., *et al.* (2001) Membrane cofactor protein (MCP; CD46) expression in transgenic mice. *Clin Exp Immunol,* 124**,** 180-9.

KERR, S., BROSNAN, M. J., MCINTYRE, M., REID, J. L., DOMINICZAK, A. F. and HAMILTON, C. A. (1999) Superoxide anion production is increased in a model of genetic hypertension: role of the endothelium. *Hypertension,* 33**,** 1353-8.

KIANG, A., HARTMAN, Z. C., EVERETT, R. S., *et al.* (2006) Multiple innate inflammatory responses induced after systemic adenovirus vector delivery depend on a functional complement system. *Mol Ther,* 14**,** 588-98.

KIM, D. T., MITCHELL, D. J., BROCKSTEDT, D. G., *et al.* (1997) Introduction of soluble proteins into the MHC class I pathway by conjugation to an HIV tat peptide. *J Immunol,* 159**,** 1666-8.

KINUGASA, N., HIGASHI, T., NOUSO, K., *et al.* (1999) Expression of membrane cofactor protein (MCP, CD46) in human liver diseases. *Br J Cancer,* 80**,** 1820-5.

KIRBY, I., DAVISON, E., BEAVIL, A. J., *et al.* (2000) Identification of contact residues and definition of the CAR-binding site of adenovirus type 5 fiber protein. *J Virol,* 74**,** 2804-13.

KIRBY, I., LORD, R., DAVISON, E., *et al.* (2001) Adenovirus type 9 fiber knob binds to the coxsackie B virus-adenovirus receptor (CAR) with lower affinity than fiber knobs of other CAR-binding adenovirus serotypes. *J Virol,* 75**,** 7210-4.

KOBORI, M., YOSHIDA, M., OHNISHI-KAMEYAMA, M. and SHINMOTO, H. (2007) Ergosterol peroxide from an edible mushroom suppresses inflammatory responses in RAW264.7 macrophages and growth of HT29 colon adenocarcinoma cells. *Br J Pharmacol,* 150**,** 209-19.

KOIZUMI, N., MIZUGUCHI, H., SAKURAI, F., YAMAGUCHI, T., WATANABE, Y. and HAYAKAWA, T. (2003) Reduction of natural adenovirus tropism to mouse liver by fiber-shaft exchange in combination with both CAR- and alphav integrin-binding ablation. *J Virol,* 77**,** 13062-72.

KOLONIN, M. G., SAHA, P. K., CHAN, L., PASQUALINI, R. and ARAP, W. (2004) Reversal of obesity by targeted ablation of adipose tissue. *Nat Med,* 10**,** 625-32.

KRITZ, A. B., NICOL, C. G., DISHART, K. L., *et al.* (2007) Adenovirus 5 fibers mutated at the putative HSPG-binding site show restricted retargeting with targeting peptides in the HI loop. *Mol Ther,* 15**,** 741-9.

KROTZ, F., KELLER, M., DERFLINGER, S., *et al.* (2007) Mycophenolate acid inhibits endothelial NAD(P)H oxidase activity and superoxide formation by a Rac1-dependent mechanism. *Hypertension,* 49**,** 201-8.

KURIYAMA, S., TOMINAGA, K., KIKUKAWA, M., *et al.* (1998) Inhibitory effects of human sera on adenovirus-mediated gene transfer into rat liver. *Anticancer Res,* 18**,** 2345-51.

KUZKAYA, N., WEISSMANN, N., HARRISON, D. G. and DIKALOV, S. (2003) Interactions of peroxynitrite, tetrahydrobiopterin, ascorbic acid, and thiols: implications for uncoupling endothelial nitric-oxide synthase. *J Biol Chem,* 278**,** 22546-54.

LA ROSA, A. M., CHAMPLIN, R. E., MIRZA, N., *et al.* (2001) Adenovirus infections in adult recipients of blood and marrow transplants. *Clin Infect Dis,* 32**,** 871-6.

LANKESTER, A. C., VAN TOL, M. J., CLAAS, E. C., VOSSEN, J. M. and KROES, A. C. (2002) Quantification of adenovirus DNA in plasma for management of infection in stem cell graft recipients. *Clin Infect Dis,* 34**,** 864-7.

LAURSEN, J. B., RAJAGOPALAN, S., GALIS, Z., TARPEY, M., FREEMAN, B. A. and HARRISON, D. G. (1997) Role of superoxide in angiotensin II-induced but not catecholamine-induced hypertension. *Circulation,* 95**,** 588-93.

LAURSEN, J. B., SOMERS, M., KURZ, S., *et al.* (2001) Endothelial regulation of vasomotion in apoE-deficient mice: implications for interactions between peroxynitrite and tetrahydrobiopterin. *Circulation,* 103**,** 1282-8.

LEGRAND, F., BERREBI, D., HOUHOU, N., *et al.* (2001) Early diagnosis of adenovirus infection and treatment with cidofovir after bone marrow transplantation in children. *Bone Marrow Transplant,* 27**,** 621-6.

LEOPOLD, P. L., FERRIS, B., GRINBERG, I., WORGALL, S., HACKETT, N. R. and CRYSTAL, R. G. (1998) Fluorescent virions: dynamic tracking of the pathway of adenoviral gene transfer vectors in living cells. *Hum Gene Ther,* 9**,** 367-78.

LEOPOLD, P. L., KREITZER, G., MIYAZAWA, N., *et al.* (2000) Dynein- and microtubule-mediated translocation of adenovirus serotype 5 occurs after endosomal lysis. *Hum Gene Ther,* 11**,** 151-65.

LEVINE, G. N., FREI, B., KOULOURIS, S. N., GERHARD, M. D., KEANEY, J. F., JR. and VITA, J. A. (1996) Ascorbic acid reverses endothelial vasomotor dysfunction in patients with coronary artery disease. *Circulation,* 93**,** 1107-13.

LI, J., LAD, S., YANG, G., *et al.* (2006) Adenovirus fiber shaft contains a trimerization element that supports peptide fusion for targeted gene delivery. *J Virol,* 80**,** 12324-31.

LI, Y., PONG, R. C., BERGELSON, J. M., *et al.* (1999) Loss of adenoviral receptor expression in human bladder cancer cells: a potential impact on the efficacy of gene therapy. *Cancer Res,* 59**,** 325-30.

LIAO, J. K. and LAUFS, U. (2005) Pleiotropic effects of statins. *Annu Rev Pharmacol Toxicol,* 45**,** 89-118.

LIEBER, A., HE, C. Y., MEUSE, L., *et al.* (1997) The role of Kupffer cell activation and viral gene expression in early liver toxicity after infusion of recombinant adenovirus vectors. *J Virol,* 71**,** 8798-807.

LION, T., BAUMGARTINGER, R., WATZINGER, F., *et al.* (2003) Molecular monitoring of adenovirus in peripheral blood after allogeneic bone marrow transplantation permits early diagnosis of disseminated disease. *Blood,* 102**,** 1114-20.

LJUNGMAN, P. (1997) Respiratory virus infections in bone marrow transplant recipients: the European perspective. *Am J Med,* 102**,** 44-7.

LO, M., BLOOM, M. L., IMADA, K., *et al.* (1999) Restoration of lymphoid populations in a murine model of X-linked severe combined immunodeficiency by a gene-therapy approach. *Blood,* 94**,** 3027-36.

LOZIER, J. N., CSAKO, G., MONDORO, T. H., *et al.* (2002) Toxicity of a first-generation adenoviral vector in rhesus macaques. *Hum Gene Ther,* 13**,** 113-24.

LYONS, M., ONION, D., GREEN, N. K., *et al.* (2006) Adenovirus type 5 interactions with human blood cells may compromise systemic delivery. *Mol Ther,* 14**,** 118-28.

MABIT, H., NAKANO, M. Y., PRANK, U., *et al.* (2002) Intact microtubules support adenovirus and herpes simplex virus infections. *J Virol,* 76**,** 9962-71.

MADAMANCHI, N. R., HAKIM, Z. S. and RUNGE, M. S. (2005a) Oxidative stress in atherogenesis and arterial thrombosis: the disconnect between cellular studies and clinical outcomes. *J Thromb Haemost,* 3**,** 254-67.

MADAMANCHI, N. R., VENDROV, A. and RUNGE, M. S. (2005b) Oxidative stress and vascular disease. *Arterioscler Thromb Vasc Biol,* 25**,** 29-38.

MADISCH, I., HARSTE, G., POMMER, H. and HEIM, A. (2005) Phylogenetic analysis of the main neutralization and hemagglutination determinants of all human adenovirus prototypes as a basis for molecular classification and taxonomy. *J Virol,* 79**,** 15265-76.

MAISNER, A., ZIMMER, G., LISZEWSKI, M. K., LUBLIN, D. M., ATKINSON, J. P. and HERRLER, G. (1997) Membrane cofactor protein (CD46) is a basolateral protein that is not endocytosed. Importance of the tetrapeptide FTSL at the carboxyl terminus. *J Biol Chem,* 272**,** 20793-9.

MAMLUK, R., KLAGSBRUN, M., DETMAR, M. and BIELENBERG, D. R. (2005) Soluble neuropilin targeted to the skin inhibits vascular permeability. *Angiogenesis,* 8**,** 217-27.

MANCHESTER, M., LISZEWSKI, M. K., ATKINSON, J. P. and OLDSTONE, M. B. (1994) Multiple isoforms of CD46 (membrane cofactor protein) serve as receptors for measles virus. *Proc Natl Acad Sci U S A,* 91**,** 2161-5.

MANICKAN, E., SMITH, J. S., TIAN, J., *et al.* (2006) Rapid Kupffer cell death after intravenous injection of adenovirus vectors. *Mol Ther,* 13**,** 108-17.

MARTIN-FERNANDEZ, M., LONGSHAW, S. V., KIRBY, I., *et al.* (2004) Adenovirus type-5 entry and disassembly followed in living cells by FRET, fluorescence anisotropy, and FLIM. *Biophys J,* 87**,** 1316-27.

MARTIN, K., BRIE, A., SAULNIER, P., PERRICAUDET, M., YEH, P. and VIGNE, E. (2003) Simultaneous CAR- and alpha V integrin-binding ablation fails to reduce Ad5 liver tropism. *Mol Ther,* 8**,** 485-94.

MAXFIELD, F. R. and MCGRAW, T. E. (2004) Endocytic recycling. *Nat Rev Mol Cell Biol,* 5**,** 121-32.

MCBRIDE, M. W., BROSNAN, M. J., MATHERS, J., *et al.* (2005) Reduction of Gstm1 expression in the stroke-prone spontaneously hypertension rat contributes to increased oxidative stress. *Hypertension,* 45**,** 786-92.

MCBRIDE, M. W., CARR, F. J., GRAHAM, D., *et al.* (2003) Microarray analysis of rat chromosome 2 congenic strains. *Hypertension,* 41**,** 847-53.

MCCHESNEY, M. B., MILLER, C. J., ROTA, P. A., *et al.* (1997) Experimental measles. I. Pathogenesis in the normal and the immunized host. *Virology,* 233**,** 74-84.

MEDINA-KAUWE, L. K. (2003) Endocytosis of adenovirus and adenovirus capsid proteins. *Adv Drug Deliv Rev,* 55**,** 1485-96.

MILLER, C. R., BUCHSBAUM, D. J., REYNOLDS, P. N., *et al.* (1998) Differential susceptibility of primary and established human glioma cells to adenovirus infection: targeting via the epidermal growth factor receptor achieves fiber receptor-independent gene transfer. *Cancer Res,* 58**,** 5738-48.

MILLER, W. H., BROSNAN, M. J., GRAHAM, D., *et al.* (2005) Targeting endothelial cells with adenovirus expressing nitric oxide synthase prevents elevation of blood pressure in stroke-prone spontaneously hypertensive rats. *Mol Ther,* 12**,** 321-7.

MINOR, R. L., JR., MYERS, P. R., GUERRA, R., JR., BATES, J. N. and HARRISON, D. G. (1990) Diet-induced atherosclerosis increases the release of nitrogen oxides from rabbit aorta. *J Clin Invest,* 86**,** 2109-16.

MIYAZAWA, N., CRYSTAL, R. G. and LEOPOLD, P. L. (2001) Adenovirus serotype 7 retention in a late endosomal compartment prior to cytosol escape is modulated by fiber protein. *J Virol,* 75**,** 1387-400.

MIYAZAWA, N., LEOPOLD, P. L., HACKETT, N. R., *et al.* (1999) Fiber swap between adenovirus subgroups B and C alters intracellular trafficking of adenovirus gene transfer vectors. *J Virol,* 73**,** 6056-65.

MOK, H., PALMER, D. J., NG, P. and BARRY, M. A. (2005) Evaluation of polyethylene glycol modification of first-generation and helper-dependent adenoviral vectors to reduce innate immune responses. *Mol Ther,* 11**,** 66-79.

MOLLNAU, H., WENDT, M., SZOCS, K., *et al.* (2002) Effects of angiotensin II infusion on the expression and function of NAD(P)H oxidase and components of nitric oxide/cGMP signaling. *Circ Res,* 90**,** E58-65.

MORRAL, N., MCEVOY, R., DONG, H., *et al.* (2002) Adenovirus-mediated expression of glucokinase in the liver as an adjuvant treatment for type 1 diabetes. *Hum Gene Ther,* 13**,** 1561-70.

MORSY, M. A., ZHAO, J. Z., NGO, T. T., *et al.* (1996) Patient selection may affect gene therapy success. Dominant negative effects observed for ornithine transcarbamylase in mouse and human hepatocytes. *J Clin Invest,* 97**,** 826-32.

MRKIC, B., PAVLOVIC, J., RULICKE, T., *et al.* (1998) Measles virus spread and pathogenesis in genetically modified mice. *J Virol,* 72**,** 7420-7.

MUGGE, A., ELWELL, J. H., PETERSON, T. E., HOFMEYER, T. G., HEISTAD, D. D. and HARRISON, D. G. (1991) Chronic treatment with polyethylene-glycolated superoxide dismutase partially restores endothelium-dependent vascular relaxations in cholesterol-fed rabbits. *Circ Res,* 69**,** 1293-300.

MULLBACHER, A., BELLETT, A. J. and HLA, R. T. (1989) The murine cellular immune response to adenovirus type 5. *Immunol Cell Biol,* 67 (Pt 1)**,** 31-9.

MURAKAMI, M. T., RIOS-STEINER, J., WEAVER, S. E., TULINSKY, A., GEIGER, J. H. and ARNI, R. K. (2007) Intermolecular interactions and characterization of the novel factor Xa exosite involved in macromolecular recognition and inhibition: crystal structure of human Gla-domainless factor Xa complexed with the anticoagulant protein NAPc2 from the hematophagous nematode Ancylostoma caninum. *J Mol Biol,* 366**,** 602-10.

MURRAY, K. P., MATHURE, S., KAUL, R., *et al.* (2000) Expression of complement regulatory proteins-CD 35, CD 46, CD 55, and CD 59-in benign and malignant endometrial tissue. *Gynecol Oncol,* 76**,** 176-82.

MUUL, L. M., TUSCHONG, L. M., SOENEN, S. L., *et al.* (2003) Persistence and expression of the adenosine deaminase gene for 12 years and immune reaction to gene transfer components: long-term results of the first clinical gene therapy trial. *Blood,* 101**,** 2563-9.

NEUNTEUFL, T., HEHER, S., KATZENSCHLAGER, R., *et al.* (2000) Late prognostic value of flow-mediated dilation in the brachial artery of patients with chest pain. *Am J Cardiol,* 86**,** 207-10.

NI, S., BERNT, K., GAGGAR, A., LI, Z. Y., KIEM, H. P. and LIEBER, A. (2005) Evaluation of biodistribution and safety of adenovirus vectors containing group B fibers after intravenous injection into baboons. *Hum Gene Ther,* 16**,** 664-77.

NI, S., GAGGAR, A., DI PAOLO, N., *et al.* (2006) Evaluation of adenovirus vectors containing serotype 35 fibers for tumor targeting. *Cancer Gene Ther,* 13**,** 1072-81.

NICKLIN, S. A., VON SEGGERN, D. J., WORK, L. M., *et al.* (2001) Ablating adenovirus type 5 fiber-CAR binding and HI loop insertion of the SIGYPLP

peptide generate an endothelial cell-selective adenovirus. *Mol Ther,* 4**,** 534-42.

NICKLIN, S. A., WHITE, S. J., NICOL, C. G., VON SEGGERN, D. J. and BAKER, A. H. (2004) In vitro and in vivo characterisation of endothelial cell selective adenoviral vectors. *J Gene Med,* 6**,** 300-8.

NICKLIN, S. A., WHITE, S. J., WATKINS, S. J., HAWKINS, R. E. and BAKER, A. H. (2000) Selective targeting of gene transfer to vascular endothelial cells by use of peptides isolated by phage display. *Circulation,* 102**,** 231-7.

NICKLIN, S. A., WU, E., NEMEROW, G. R. and BAKER, A. H. (2005) The influence of adenovirus fiber structure and function on vector development for gene therapy. *Mol Ther,* 12**,** 384-93.

NICOL, C. G., DENBY, L., LOPEZ-FRANCO, O., *et al.* (2009) Use of in vivo phage display to engineer novel adenoviruses for targeted delivery to the cardiac vasculature. *FEBS Lett,* 583**,** 2100-7.

NICOL, C. G., GRAHAM, D., MILLER, W. H., *et al.* (2004) Effect of adenovirus serotype 5 fiber and penton modifications on in vivo tropism in rats. *Mol Ther,* 10**,** 344-54.

NORRBY, E. (1969) The structural and functional diversity of Adenovirus capsid components. *J Gen Virol,* 5**,** 221-36.

NUNES, F. A., FURTH, E. E., WILSON, J. M. and RAPER, S. E. (1999) Gene transfer into the liver of nonhuman primates with E1-deleted recombinant adenoviral vectors: safety of readministration. *Hum Gene Ther,* 10**,** 2515-26.

O'BRIEN, K. L., LIU, J., KING, S. L., *et al.* (2009) Adenovirus-specific immunity after immunization with an Ad5 HIV-1 vaccine candidate in humans. *Nat Med,* 15**,** 873-5.

OH, P., LI, Y., YU, J., *et al.* (2004) Subtractive proteomic mapping of the endothelial surface in lung and solid tumours for tissue-specific therapy. *Nature,* 429**,** 629-35.

OKAMOTO, K. and AOKI, K. (1963) Development of a strain of spontaneously hypertensive rats. *Jpn Circ J,* 27**,** 282-93.

OKEGAWA, T., LI, Y., PONG, R. C., BERGELSON, J. M., ZHOU, J. and HSIEH, J. T. (2000) The dual impact of coxsackie and adenovirus receptor expression on human prostate cancer gene therapy. *Cancer Res,* 60**,** 5031-6.

OLDSTONE, M. B., LEWICKI, H., THOMAS, D., *et al.* (1999) Measles virus infection in a transgenic model: virus-induced immunosuppression and central nervous system disease. *Cell,* 98**,** 629-40.

OPARIL, S., ZAMAN, M. A. and CALHOUN, D. A. (2003) Pathogenesis of hypertension. *Ann Intern Med,* 139**,** 761-76.

OSTAPCHUK, P. and HEARING, P. (2001) Pseudopackaging of adenovirus type 5 genomes into capsids containing the hexon proteins of adenovirus serotypes B, D, or E. *J Virol,* 75**,** 45-51.

OTHMAN, M., LABELLE, A., MAZZETTI, I., ELBATARNY, H. S. and LILLICRAP, D. (2007) Adenovirus-induced thrombocytopenia: the role of von Willebrand factor and P-selectin in mediating accelerated platelet clearance. *Blood,* 109**,** 2832-9.

PARKER, A. L., MCVEY, J. H., DOCTOR, J. H., *et al.* (2007) Influence of coagulation factor zymogens on the infectivity of adenoviruses pseudotyped with fibers from subgroup D. *J Virol,* 81**,** 3627-31.

PARKER, A. L., WADDINGTON, S. N., BUCKLEY, S. M., *et al.* (2009) Effect of neutralizing sera on factor x-mediated adenovirus serotype 5 gene transfer. *J Virol,* 83**,** 479-83.

PARKER, A. L., WADDINGTON, S. N., NICOL, C. G., *et al.* (2006) Multiple vitamin K-dependent coagulation zymogens promote adenovirus-mediated gene delivery to hepatocytes. *Blood,* 108**,** 2554-61.

PERREAU, M., PANTALEO, G. and KREMER, E. J. (2008) Activation of a dendritic cell-T cell axis by Ad5 immune complexes creates an improved environment for replication of HIV in T cells. *J Exp Med,* 205**,** 2717-25.

PIEPER, G. M., LANGENSTROER, P. and SIEBENEICH, W. (1997) Diabetic-induced endothelial dysfunction in rat aorta: role of hydroxyl radicals. *Cardiovasc Res,* 34**,** 145-56.

PODMORE, I. D., GRIFFITHS, H. R., HERBERT, K. E., MISTRY, N., MISTRY, P. and LUNEC, J. (1998) Vitamin C exhibits pro-oxidant properties. *Nature,* 392**,** 559.

PREMENKO-LANIER, M., ROTA, P. A., RHODES, G., *et al.* (2003) DNA vaccination of infants in the presence of maternal antibody: a measles model in the primate. *Virology,* 307**,** 67-75.

RAJAGOPALAN, S., KURZ, S., MUNZEL, T., *et al.* (1996) Angiotensin II-mediated hypertension in the rat increases vascular superoxide production via membrane NADH/NADPH oxidase activation. Contribution to alterations of vasomotor tone. *J Clin Invest,* 97**,** 1916-23.

RAJOTTE, D. and RUOSLAHTI, E. (1999) Membrane dipeptidase is the receptor for a lung-targeting peptide identified by in vivo phage display. *J Biol Chem,* 274**,** 11593-8.

RAPER, S. E., CHIRMULE, N., LEE, F. S., *et al.* (2003) Fatal systemic inflammatory response syndrome in a ornithine transcarbamylase deficient patient following adenoviral gene transfer. *Mol Genet Metab,* 80**,** 148-58.

RAPER, S. E., YUDKOFF, M., CHIRMULE, N., *et al.* (2002) A pilot study of in vivo liver-directed gene transfer with an adenoviral vector in partial ornithine transcarbamylase deficiency. *Hum Gene Ther,* 13**,** 163-75.

RAPOLA, J. M., VIRTAMO, J., RIPATTI, S., *et al.* (1997) Randomised trial of alpha-tocopherol and beta-carotene supplements on incidence of major coronary events in men with previous myocardial infarction. *Lancet,* 349**,** 1715-20.

REY, F. E., CIFUENTES, M. E., KIARASH, A., QUINN, M. T. and PAGANO, P. J. (2001) Novel competitive inhibitor of NAD(P)H oxidase assembly attenuates vascular O(2)(-) and systolic blood pressure in mice. *Circ Res,* 89**,** 408-14.

REY, F. E., LI, X. C., CARRETERO, O. A., GARVIN, J. L. and PAGANO, P. J. (2002) Perivascular superoxide anion contributes to impairment of endothelium-dependent relaxation: role of gp91(phox). *Circulation,* 106**,** 2497-502.

RIBATTI, D., NICO, B., VACCA, A., RONCALI, L. and DAMMACCO, F. (2002) Endothelial cell heterogeneity and organ specificity. *J Hematother Stem Cell Res,* 11**,** 81-90.

RIGANTI, C., GAZZANO, E., POLIMENI, M., COSTAMAGNA, C., BOSIA, A. and GHIGO, D. (2004) Diphenyleneiodonium inhibits the cell redox metabolism and induces oxidative stress. *J Biol Chem,* 279**,** 47726-31.

RIOU, P., VANDROMME, M. and GAZZOLO, L. (2001) Human T-cell leukemia virus type 1 tax protein inhibits the expression of the basic helix-loop-helix

transcription factor MyoD in muscle cells: maintenance of proliferation and repression of differentiation. *Cell Growth Differ,* 12**,** 613-22.

ROBERTS, D. M., NANDA, A., HAVENGA, M. J., *et al.* (2006) Hexon-chimaeric adenovirus serotype 5 vectors circumvent pre-existing anti-vector immunity. *Nature,* 441**,** 239-43.

ROELVINK, P. W., MI LEE, G., EINFELD, D. A., KOVESDI, I. and WICKHAM, T. J. (1999) Identification of a conserved receptor-binding site on the fiber proteins of CAR-recognizing adenoviridae. *Science,* 286**,** 1568-71.

RUNDE, V., ROSS, S., TRENSCHEL, R., *et al.* (2001) Adenoviral infection after allogeneic stem cell transplantation (SCT): report on 130 patients from a single SCT unit involved in a prospective multi center surveillance study. *Bone Marrow Transplant,* 28**,** 51-7.

RUOSLAHTI, E. and RAJOTTE, D. (2000) An address system in the vasculature of normal tissues and tumors. *Annu Rev Immunol,* 18**,** 813-27.

RUSSELL, W. C. (2000) Update on adenovirus and its vectors. *J Gen Virol,* 81**,** 2573-604.

RUSSELL, W. C. (2009) Adenoviruses: update on structure and function. *J Gen Virol,* 90**,** 1-20.

SABAN, S. D., NEPOMUCENO, R. R., GRITTON, L. D., NEMEROW, G. R. and STEWART, P. L. (2005) CryoEM structure at 9A resolution of an adenovirus vector targeted to hematopoietic cells. *J Mol Biol,* 349**,** 526-37.

SAKAGUCHI, M., YOSHIKAWA, Y., YAMANOUCHI, K., SATA, T., NAGASHIMA, K. and TAKEDA, K. (1986) Growth of measles virus in epithelial and lymphoid tissues of cynomolgus monkeys. *Microbiol Immunol,* 30**,** 1067-73.

SAKURAI, F. (2008) Development and evaluation of a novel gene delivery vehicle composed of adenovirus serotype 35. *Biol Pharm Bull,* 31**,** 1819-25.

SAKURAI, F., KAWABATA, K., KOIZUMI, N., *et al.* (2006a) Adenovirus serotype 35 vector-mediated transduction into human CD46-transgenic mice. *Gene Ther,* 13**,** 1118-26.

SAKURAI, F., MIZUGUCHI, H. and HAYAKAWA, T. (2003a) Efficient gene transfer into human CD34+ cells by an adenovirus type 35 vector. *Gene Ther,* 10**,** 1041-8.

SAKURAI, F., MIZUGUCHI, H., YAMAGUCHI, T. and HAYAKAWA, T. (2003b) Characterization of in vitro and in vivo gene transfer properties of adenovirus serotype 35 vector. *Mol Ther,* 8**,** 813-21.

SAKURAI, F., MURAKAMI, S., KAWABATA, K., *et al.* (2006b) The short consensus repeats 1 and 2, not the cytoplasmic domain, of human CD46 are crucial for infection of subgroup B adenovirus serotype 35. *J Control Release,* 113**,** 271-8.

SAKURAI, F., NAKAMURA, S., AKITOMO, K., *et al.* (2008) Transduction properties of adenovirus serotype 35 vectors after intravenous administration into nonhuman primates. *Mol Ther,* 16**,** 726-33.

SAKURAI, F., NAKAMURA, S. I., AKITOMO, K., *et al.* (2009) Adenovirus serotype 35 vector-mediated transduction following direct administration into organs of nonhuman primates. *Gene Ther,* 16**,** 297-302.

SAMOYLOVA, T. I. and SMITH, B. F. (1999) Elucidation of muscle-binding peptides by phage display screening. *Muscle Nerve,* 22**,** 460-6.

SCHACHINGER, V., BRITTEN, M. B. and ZEIHER, A. M. (2000) Prognostic impact of coronary vasodilator dysfunction on adverse long-term outcome of coronary heart disease. *Circulation,* 101**,** 1899-906.

SCHIEDNER, G., BLOCH, W., HERTEL, S., *et al.* (2003) A hemodynamic response to intravenous adenovirus vector particles is caused by systemic Kupffer cell-mediated activation of endothelial cells. *Hum Gene Ther,* 14**,** 1631-41.

SCHNELL, M. A., ZHANG, Y., TAZELAAR, J., *et al.* (2001) Activation of innate immunity in nonhuman primates following intraportal administration of adenoviral vectors. *Mol Ther,* 3**,** 708-22.

SEGERMAN, A., ARNBERG, N., ERIKSON, A., LINDMAN, K. and WADELL, G. (2003a) There are two different species B adenovirus receptors: sBAR, common to species B1 and B2 adenoviruses, and sB2AR, exclusively used by species B2 adenoviruses. *J Virol,* 77**,** 1157-62.

SEGERMAN, A., ATKINSON, J. P., MARTTILA, M., DENNERQUIST, V., WADELL, G. and ARNBERG, N. (2003b) Adenovirus type 11 uses CD46 as a cellular receptor. *J Virol,* 77**,** 9183-91.

SESHIDHAR REDDY, P., GANESH, S., LIMBACH, M. P., *et al.* (2003) Development of adenovirus serotype 35 as a gene transfer vector. *Virology,* 311**,** 384-93.

SETH, P. (1994a) Adenovirus-dependent release of choline from plasma membrane vesicles at an acidic pH is mediated by the penton base protein. *J Virol,* 68**,** 1204-6.

SETH, P. (1994b) Mechanism of adenovirus-mediated endosome lysis: role of the intact adenovirus capsid structure. *Biochem Biophys Res Commun,* 205**,** 1318-24.

SHAYAKHMETOV, D. M., EBERLY, A. M., LI, Z. Y. and LIEBER, A. (2005a) Deletion of penton RGD motifs affects the efficiency of both the internalization and the endosome escape of viral particles containing adenovirus serotype 5 or 35 fiber knobs. *J Virol,* 79**,** 1053-61.

SHAYAKHMETOV, D. M., GAGGAR, A., NI, S., LI, Z. Y. and LIEBER, A. (2005b) Adenovirus binding to blood factors results in liver cell infection and hepatotoxicity. *J Virol,* 79**,** 7478-91.

SHAYAKHMETOV, D. M., LI, Z. Y., NI, S. and LIEBER, A. (2002) Targeting of adenovirus vectors to tumor cells does not enable efficient transduction of breast cancer metastases. *Cancer Res,* 62**,** 1063-8.

SHAYAKHMETOV, D. M., LI, Z. Y., NI, S. and LIEBER, A. (2004) Analysis of adenovirus sequestration in the liver, transduction of hepatic cells, and innate toxicity after injection of fiber-modified vectors. *J Virol,* 78**,** 5368-81.

SHAYAKHMETOV, D. M., LI, Z. Y., TERNOVOI, V., GAGGAR, A., GHARWAN, H. and LIEBER, A. (2003) The interaction between the fiber knob domain and the cellular attachment receptor determines the intracellular trafficking route of adenoviruses. *J Virol,* 77**,** 3712-23.

SHAYAKHMETOV, D. M. and LIEBER, A. (2000) Dependence of adenovirus infectivity on length of the fiber shaft domain. *J Virol,* 74**,** 10274-86.

SHAYAKHMETOV, D. M., PAPAYANNOPOULOU, T., STAMATOYANNOPOULOS, G. and LIEBER, A. (2000) Efficient gene transfer into human CD34(+) cells by a retargeted adenovirus vector. *J Virol,* 74**,** 2567-83.

SHINOZAKI, K., SUOMINEN, E., CARRICK, F., *et al.* (2006) Efficient infection of tumor endothelial cells by a capsid-modified adenovirus. *Gene Ther,* 13**,** 52-9.

SHIRLEY, R. (2008) Development of targeted gene delivery vectors to assess cardiac overexpression of ACE2 in vivo. *PhD Thesis*.

SIMONS, J. M., HART, B. A., IP VAI CHING, T. R., VAN DIJK, H. and LABADIE, R. P. (1990) Metabolic activation of natural phenols into selective oxidative burst agonists by activated human neutrophils. *Free Radic Biol Med,* 8**,** 251-8.

SIRENA, D., LILIENFELD, B., EISENHUT, M., *et al.* (2004) The human membrane cofactor CD46 is a receptor for species B adenovirus serotype 3. *J Virol,* 78**,** 4454-62.

SMITH, J. S., XU, Z., TIAN, J., STEVENSON, S. C. and BYRNES, A. P. (2008) Interaction of systemically delivered adenovirus vectors with Kupffer cells in mouse liver. *Hum Gene Ther,* 19**,** 547-54.

SMITH, T., IDAMAKANTI, N., KYLEFJORD, H., *et al.* (2002) In vivo hepatic adenoviral gene delivery occurs independently of the coxsackievirus-adenovirus receptor. *Mol Ther,* 5**,** 770-9.

SMITH, T. A., IDAMAKANTI, N., MARSHALL-NEFF, J., *et al.* (2003a) Receptor interactions involved in adenoviral-mediated gene delivery after systemic administration in non-human primates. *Hum Gene Ther,* 14**,** 1595-604.

SMITH, T. A., IDAMAKANTI, N., ROLLENCE, M. L., *et al.* (2003b) Adenovirus serotype 5 fiber shaft influences in vivo gene transfer in mice. *Hum Gene Ther,* 14**,** 777-87.

SOUDAIS, C., SHIHO, T., SHARARA, L. I., *et al.* (2000) Stable and functional lymphoid reconstitution of common cytokine receptor gamma chain deficient mice by retroviral-mediated gene transfer. *Blood,* 95**,** 3071-7.

SPRANGERS, M. C., LAKHAI, W., KOUDSTAAL, W., *et al.* (2003) Quantifying adenovirus-neutralizing antibodies by luciferase transgene detection: addressing preexisting immunity to vaccine and gene therapy vectors. *J Clin Microbiol,* 41**,** 5046-52.

STALLWOOD, Y., FISHER, K. D., GALLIMORE, P. H. and MAUTNER, V. (2000) Neutralisation of adenovirus infectivity by ascitic fluid from ovarian cancer patients. *Gene Ther,* 7**,** 637-43.

STEPHAN, V., WAHN, V., LE DEIST, F., *et al.* (1996) Atypical X-linked severe combined immunodeficiency due to possible spontaneous reversion of the genetic defect in T cells. *N Engl J Med,* 335**,** 1563-7.

STEPHENS, N. G., PARSONS, A., SCHOFIELD, P. M., KELLY, F., CHEESEMAN, K. and MITCHINSON, M. J. (1996) Randomised controlled trial of vitamin E in patients with coronary disease: Cambridge Heart Antioxidant Study (CHAOS). *Lancet,* 347**,** 781-6.

STONE, D., LIU, Y., LI, Z. Y., TUVE, S., STRAUSS, R. and LIEBER, A. (2007a) Comparison of adenoviruses from species B, C, E, and F after intravenous delivery. *Mol Ther,* 15**,** 2146-53.

STONE, D., LIU, Y., SHAYAKHMETOV, D., LI, Z. Y., NI, S. and LIEBER, A. (2007b) Adenovirus-platelet interaction in blood causes virus sequestration to the reticuloendothelial system of the liver. *J Virol,* 81**,** 4866-71.

SU, C. C., LIN, J. G., LI, T. M., *et al.* (2006) Curcumin-induced apoptosis of human colon cancer colo 205 cells through the production of ROS, Ca2+ and the activation of caspase-3. *Anticancer Res,* 26**,** 4379-89.

SUBR, V., KOSTKA, L., SELBY-MILIC, T., *et al.* (2009) Coating of adenovirus type 5 with polymers containing quaternary amines prevents binding to blood components. *J Control Release,* 135**,** 152-8.

SUMIDA, S. M., TRUITT, D. M., LEMCKERT, A. A., *et al.* (2005) Neutralizing antibodies to adenovirus serotype 5 vaccine vectors are directed primarily against the adenovirus hexon protein. *J Immunol,* 174**,** 7179-85.

SUOMALAINEN, M., NAKANO, M. Y., BOUCKE, K., KELLER, S. and GREBER, U. F. (2001) Adenovirus-activated PKA and p38/MAPK pathways boost microtubule-mediated nuclear targeting of virus. *Embo J,* 20**,** 1310-9.

SUOMALAINEN, M., NAKANO, M. Y., KELLER, S., BOUCKE, K., STIDWILL, R. P. and GREBER, U. F. (1999) Microtubule-dependent plus- and minus end-directed motilities are competing processes for nuclear targeting of adenovirus. *J Cell Biol,* 144**,** 657-72.

SUOMINEN, E., TOIVONEN, R., GRENMAN, R. and SAVONTAUS, M. (2006) Head and neck cancer cells are efficiently infected by Ad5/35 hybrid virus. *J Gene Med,* 8**,** 1223-31.

SUWAIDI, J. A., HAMASAKI, S., HIGANO, S. T., NISHIMURA, R. A., HOLMES, D. R., JR. and LERMAN, A. (2000) Long-term follow-up of

patients with mild coronary artery disease and endothelial dysfunction. *Circulation,* 101**,** 948-54.

TADDEI, S., VIRDIS, A., GHIADONI, L., MAGAGNA, A. and SALVETTI, A. (1998) Vitamin C improves endothelium-dependent vasodilation by restoring nitric oxide activity in essential hypertension. *Circulation,* 97**,** 2222-9.

TAYLOR, N., URIBE, L., SMITH, S., JAHN, T., KOHN, D. B. and WEINBERG, K. (1996) Correction of interleukin-2 receptor function in X-SCID lymphoblastoid cells by retrovirally mediated transfer of the gamma-c gene. *Blood,* 87**,** 3103-7.

TEESALU, T., SUGAHARA, K. N., KOTAMRAJU, V. R. and RUOSLAHTI, E. (2009) C-end Rule: Peptides with C-terminal arginine mediate neuropilin-1 dependent cell, vascular and tissue penetration. *Proc Natl Acad Sci U S A.*

THOMSON, L., TRUJILLO, M., TELLERI, R. and RADI, R. (1995) Kinetics of cytochrome c2+ oxidation by peroxynitrite: implications for superoxide measurements in nitric oxide-producing biological systems. *Arch Biochem Biophys,* 319**,** 491-7.

THORIN, E. and SHREEVE, S. M. (1998) Heterogeneity of vascular endothelial cells in normal and disease states. *Pharmacol Ther,* 78**,** 155-66.

TING, H. H., TIMIMI, F. K., HALEY, E. A., RODDY, M. A., GANZ, P. and CREAGER, M. A. (1997) Vitamin C improves endothelium-dependent vasodilation in forearm resistance vessels of humans with hypercholesterolemia. *Circulation,* 95**,** 2617-22.

TOMKO, R. P., XU, R. and PHILIPSON, L. (1997) HCAR and MCAR: the human and mouse cellular receptors for subgroup C adenoviruses and group B coxsackieviruses. *Proc Natl Acad Sci U S A,* 94**,** 3352-6.

TROTMAN, L. C., MOSBERGER, N., FORNEROD, M., STIDWILL, R. P. and GREBER, U. F. (2001) Import of adenovirus DNA involves the nuclear pore complex receptor CAN/Nup214 and histone H1. *Nat Cell Biol,* 3**,** 1092-100.

TUVE, S., WANG, H., JACOBS, J. D., YUMUL, R. C., SMITH, D. F. and LIEBER, A. (2008) Role of cellular heparan sulfate proteoglycans in infection of human adenovirus serotype 3 and 35. *PLoS Pathog,* 4**,** e1000189.

TUVE, S., WANG, H., WARE, C., *et al.* (2006) A new group B adenovirus receptor is expressed at high levels on human stem and tumor cells. *J Virol,* 80**,** 12109-20.

VAN HAM, M., CROES, H., SCHEPENS, J., FRANSEN, J., WIERINGA, B. and HENDRIKS, W. (2003) Cloning and characterization of mCRIP2, a mouse LIM-only protein that interacts with PDZ domain IV of PTP-BL. *Genes Cells,* 8**,** 631-44.

VAN RAAIJ, M. J., CHOUIN, E., VAN DER ZANDT, H., BERGELSON, J. M. and CUSACK, S. (2000) Dimeric structure of the coxsackievirus and adenovirus receptor D1 domain at 1.7 A resolution. *Structure,* 8**,** 1147-55.

VERHAAGH, S., DE JONG, E., GOUDSMIT, J., *et al.* (2006) Human CD46-transgenic mice in studies involving replication-incompetent adenoviral type 35 vectors. *J Gen Virol,* 87**,** 255-65.

VIGANT, F., DESCAMPS, D., JULLIENNE, B., *et al.* (2008) Substitution of hexon hypervariable region 5 of adenovirus serotype 5 abrogates blood factor binding and limits gene transfer to liver. *Mol Ther,* 16**,** 1474-80.

VIGNE, E., MAHFOUZ, I., DEDIEU, J. F., BRIE, A., PERRICAUDET, M. and YEH, P. (1999) RGD inclusion in the hexon monomer provides adenovirus type 5-based vectors with a fiber knob-independent pathway for infection. *J Virol,* 73**,** 5156-61.

VOGELS, R., ZUIJDGEEST, D., VAN RIJNSOEVER, R., *et al.* (2003) Replication-deficient human adenovirus type 35 vectors for gene transfer and vaccination: efficient human cell infection and bypass of preexisting adenovirus immunity. *J Virol,* 77**,** 8263-71.

VON SEGGERN, D. J., CHIU, C. Y., FLECK, S. K., STEWART, P. L. and NEMEROW, G. R. (1999) A helper-independent adenovirus vector with E1, E3, and fiber deleted: structure and infectivity of fiberless particles. *J Virol,* 73**,** 1601-8.

VON SEGGERN, D. J., KEHLER, J., ENDO, R. I. and NEMEROW, G. R. (1998) Complementation of a fibre mutant adenovirus by packaging cell lines stably expressing the adenovirus type 5 fibre protein. *J Gen Virol,* 79 (Pt 6)**,** 1461-8.

VON WRONSKI, M. A., RAJU, N., PILLAI, R., *et al.* (2006) Tuftsin binds neuropilin-1 through a sequence similar to that encoded by exon 8 of vascular endothelial growth factor. *J Biol Chem,* 281**,** 5702-10.

WADDINGTON, S. N., MCVEY, J. H., BHELLA, D., *et al.* (2008) Adenovirus serotype 5 hexon mediates liver gene transfer. *Cell,* 132**,** 397-409.

WADDINGTON, S. N., PARKER, A. L., HAVENGA, M., *et al.* (2007) Targeting of adenovirus serotype 5 (Ad5) and 5/47 pseudotyped vectors in vivo: fundamental involvement of coagulation factors and redundancy of CAR binding by Ad5. *J Virol,* 81**,** 9568-71.

WADELL, G., HAMMARSKJOLD, M. L., WINBERG, G., VARSANYI, T. M. and SUNDELL, G. (1980) Genetic variability of adenoviruses. *Ann N Y Acad Sci,* 354**,** 16-42.

WANG, H., LIU, Y., LI, Z., *et al.* (2008a) In vitro and in vivo properties of adenovirus vectors with increased affinity to CD46. *J Virol.*

WANG, H., LIU, Y., LI, Z., *et al.* (2008b) In vitro and in vivo properties of adenovirus vectors with increased affinity to CD46. *J Virol,* 82**,** 10567-79.

WANG, H. D., PAGANO, P. J., DU, Y., *et al.* (1998a) Superoxide anion from the adventitia of the rat thoracic aorta inactivates nitric oxide. *Circ Res,* 82**,** 810-8.

WANG, H. D., XU, S., JOHNS, D. G., *et al.* (2001) Role of NADPH oxidase in the vascular hypertrophic and oxidative stress response to angiotensin II in mice. *Circ Res,* 88**,** 947-53.

WANG, K., HUANG, S., KAPOOR-MUNSHI, A. and NEMEROW, G. (1998b) Adenovirus internalization and infection require dynamin. *J Virol,* 72**,** 3455-8.

WANG, X. and BERGELSON, J. M. (1999) Coxsackievirus and adenovirus receptor cytoplasmic and transmembrane domains are not essential for coxsackievirus and adenovirus infection. *J Virol,* 73**,** 2559-62.

WANG, Y., HU, J. K., KROL, A., LI, Y. P., LI, C. Y. and YUAN, F. (2003) Systemic dissemination of viral vectors during intratumoral injection. *Mol Cancer Ther,* 2**,** 1233-42.

WASSMANN, S., LAUFS, U., MULLER, K., *et al.* (2002) Cellular antioxidant effects of atorvastatin in vitro and in vivo. *Arterioscler Thromb Vasc Biol,* 22**,** 300-5.

WHITWAM, T., HASKINS, M. E., HENTHORN, P. S., *et al.* (1998) Retroviral marking of canine bone marrow: long-term, high-level expression of human interleukin-2 receptor common gamma chain in canine lymphocytes. *Blood,* 92**,** 1565-75.

WICKHAM, T. J., MATHIAS, P., CHERESH, D. A. and NEMEROW, G. R. (1993) Integrins alpha v beta 3 and alpha v beta 5 promote adenovirus internalization but not virus attachment. *Cell,* 73**,** 309-19.

WORGALL, S., WOLFF, G., FALCK-PEDERSEN, E. and CRYSTAL, R. G. (1997) Innate immune mechanisms dominate elimination of adenoviral vectors following in vivo administration. *Hum Gene Ther,* 8**,** 37-44.

WORK, L. M., NICKLIN, S. A., BRAIN, N. J., *et al.* (2004) Development of efficient viral vectors selective for vascular smooth muscle cells. *Mol Ther,* 9**,** 198-208.

YANG, Y., NUNES, F. A., BERENCSI, K., FURTH, E. E., GONCZOL, E. and WILSON, J. M. (1994) Cellular immunity to viral antigens limits E1-deleted adenoviruses for gene therapy. *Proc Natl Acad Sci U S A,* 91**,** 4407-11.

YE, X., ROBINSON, M. B., BATSHAW, M. L., FURTH, E. E., SMITH, I. and WILSON, J. M. (1996) Prolonged metabolic correction in adult ornithine transcarbamylase-deficient mice with adenoviral vectors. *J Biol Chem,* 271**,** 3639-46.

YE, X., ROBINSON, M. B., PABIN, C., *et al.* (1997) Adenovirus-mediated in vivo gene transfer rapidly protects ornithine transcarbamylase-deficient mice from an ammonium challenge. *Pediatr Res,* 41**,** 527-34.

YU, T. S., MOCTEZUMA-ANAYA, M., KUBO, A., KELLER, G. and ROBERTSON, S. (2002) The heart LIM protein gene (Hlp), expressed in the developing and adult heart, defines a new tissue-specific LIM-only protein family. *Mech Dev,* 116**,** 187-92.

ZHANG, L., HOFFMAN, J. A. and RUOSLAHTI, E. (2005) Molecular profiling of heart endothelial cells. *Circulation,* 112**,** 1601-11.

ZHOU, M. S., HERNANDEZ SCHULMAN, I., PAGANO, P. J., JAIMES, E. A. and RAIJ, L. (2006) Reduced NAD(P)H oxidase in low renin hypertension: link among angiotensin II, atherogenesis, and blood pressure. *Hypertension,* 47**,** 81-6.

ZINN, K. R., SZALAI, A. J., STARGEL, A., KRASNYKH, V. and CHAUDHURI, T. R. (2004) Bioluminescence imaging reveals a significant role for complement in liver transduction following intravenous delivery of adenovirus. *Gene Ther,* 11**,** 1482-6.

ZIVELIN, A., RAO, L. V. and RAPAPORT, S. I. (1993) Mechanism of the anticoagulant effect of warfarin as evaluated in rabbits by selective depression of individual procoagulant vitamin K-dependent clotting factors. *J Clin Invest,* 92**,** 2131-40.

ZSENGELLER, Z., OTAKE, K., HOSSAIN, S. A., BERCLAZ, P. Y. and TRAPNELL, B. C. (2000) Internalization of adenovirus by alveolar macrophages initiates early proinflammatory signaling during acute respiratory tract infection. *J Virol,* 74**,** 9655-67.

Appendices

Appendix 1

J.A. Greig, S.M.K. Buckley, S.N. Waddington, A.L. Parker, D. Bhella, R. Pink, A.A. Rahim, T. Morita, S.A. Nicklin, J.H. McVey and A.H. Baker (2009) Influence of Coagulation Factor X on *In Vitro* and *In Vivo* Gene Delivery by Adenovirus (Ad) 5, Ad35, and Chimeric Ad5/Ad35 Vectors. *Molecular Therapy*, **17**, 1683-91

Appendix 2

S.N. Waddington, J.H. McVey, D. Bhella, A.L. Parker, K. Barker, H. Atoda, R. Pink, S.M.K. Buckley, **J.A. Greig**, L. Denby, J. Custers, T. Morita, I.M.B. Francischetti, R.Q. Monteiro, D.H. Barouch, N. van Rooijen, C. Napoli, M.J.E. Havenga, S.A. Nicklin and A.H. Baker (2008) Adenovirus Serotype 5 Hexon Mediates Liver Gene Transfer. *Cell*, **132**, 397-409